frontiers | Research Topics

The effect of muscle pathogenesis on avian physiology, animal welfare, and quality of muscle as a food

Edited by
Wei Guo, Sandra G. Velleman and Gale M. Strasburg

Published in
Frontiers in Physiology

ISSN 1664-8714
ISBN 978-2-8325-6153-9
DOI 10.3389/978-2-8325-6153-9

About Frontiers

Frontiers is more than just an open access publisher of scholarly articles: it is a pioneering approach to the world of academia, radically improving the way scholarly research is managed. The grand vision of Frontiers is a world where all people have an equal opportunity to seek, share and generate knowledge. Frontiers provides immediate and permanent online open access to all its publications, but this alone is not enough to realize our grand goals.

Frontiers journal series

The Frontiers journal series is a multi-tier and interdisciplinary set of open-access, online journals, promising a paradigm shift from the current review, selection and dissemination processes in academic publishing. All Frontiers journals are driven by researchers for researchers; therefore, they constitute a service to the scholarly community. At the same time, the *Frontiers journal series* operates on a revolutionary invention, the tiered publishing system, initially addressing specific communities of scholars, and gradually climbing up to broader public understanding, thus serving the interests of the lay society, too.

Dedication to quality

Each Frontiers article is a landmark of the highest quality, thanks to genuinely collaborative interactions between authors and review editors, who include some of the world's best academicians. Research must be certified by peers before entering a stream of knowledge that may eventually reach the public - and shape society; therefore, Frontiers only applies the most rigorous and unbiased reviews. Frontiers revolutionizes research publishing by freely delivering the most outstanding research, evaluated with no bias from both the academic and social point of view. By applying the most advanced information technologies, Frontiers is catapulting scholarly publishing into a new generation.

What are Frontiers Research Topics?

Frontiers Research Topics are very popular trademarks of the *Frontiers journals series*: they are collections of at least ten articles, all centered on a particular subject. With their unique mix of varied contributions from Original Research to Review Articles, Frontiers Research Topics unify the most influential researchers, the latest key findings and historical advances in a hot research area.

Find out more on how to host your own Frontiers Research Topic or contribute to one as an author by contacting the Frontiers editorial office: frontiersin.org/about/contact

The effect of muscle pathogenesis on avian physiology, animal welfare, and quality of muscle as a food

Topic editors

Wei Guo — University of Wisconsin-Madison, United States

Sandra G. Velleman — The Ohio State University, United States

Gale M. Strasburg — Michigan State University, United States

Citation

Guo, W., Velleman, S. G., Strasburg, G. M., eds. (2025). *The effect of muscle pathogenesis on avian physiology, animal welfare, and quality of muscle as a food*. Lausanne: Frontiers Media SA. doi: 10.3389/978-2-8325-6153-9

Table of contents

frontiers | Frontiers in Physiology

TYPE Editorial
PUBLISHED 10 March 2025
DOI 10.3389/fphys.2025.1577465

OPEN ACCESS

EDITED AND REVIEWED BY
Krystyna Pierzchała-Koziec,
University of Agriculture in Krakow, Poland

*CORRESPONDENCE
Sandra G. Velleman,
✉ Velleman.1@osu.edu

RECEIVED 15 February 2025
ACCEPTED 17 February 2025
PUBLISHED 10 March 2025

CITATION
Velleman SG, Guo W and Strasburg GM (2025) Editorial: The effect of muscle pathogenesis on avian physiology, animal welfare, and quality of muscle as a food.
Front. Physiol. 16:1577465.
doi: 10.3389/fphys.2025.1577465

Editorial: The effect of muscle pathogenesis on avian physiology, animal welfare, and quality of muscle as a food

Sandra G. Velleman[1]*, Wei Guo[2] and Gale M. Strasburg[3]

[1]Department of Animal Sciences, The Ohio State University, Wooster, OH, United States, [2]Department of Animal and Dairy Sciences, University of Wisconsin-Madison, Madison, WI, United States, [3]Department of Food Science and Human Nutrition, Michigan State University, East Lansing, MI, United States

KEYWORDS

metabolomics, muscle physiology, myopathy, spaghetti meat, wooden breast, welfare

Editorial on the Research Topic
The effect of muscle pathogenesis on avian physiology, animal welfare, and quality of muscle as a food

Introduction

The effect of muscle pathogenesis on avian physiology, animal welfare, and quality of muscle as a food Research Topic was aimed at highlighting research focused on the physiological mechanisms of muscle pathogenesis in poultry, which can alter bird survival and the quality of muscle as food. A total of 11 submissions were accepted for publication, covering the areas of wooden breast and spaghetti meat, meat quality and welfare, immune system function and fibroadipogenic progenitors, and the merging of modern omics research with hypothesis-based research.

Wooden breast and spaghetti meat

Six manuscripts within the Research Topic are devoted to wooden breast and spaghetti meat myopathies. Rimmer and Zumbaugh provided a review of the current status of wooden breast, with attention paid to biochemical pathways involved in the conversion of muscle to meat. Alteration of these pathways may result in the high ultimate pH found in wooden breast meat. They suggested altered mitochondria function may exist in wooden breast-affected muscle. Supporting evidence comes from an original research study by Greene et al., who compared mitochondria isolated from wooden breast muscle with that of hypoxic chicken myoblasts and found Ca^{2+} overload and other features of mitochondrial dysfunction. Their results suggest that aberrant Ca^{2+} signaling associated with chronic local hypoxia may be a primary contributor to the etiology of the wooden breast myopathy. Two original research contributions by Pejšková et al. focused on extracellular matrix remodeling and the expression of transmembrane heparan sulfate proteoglycans, the syndecans. Since syndecans are transmembrane proteoglycans, they form a bridge between the external

extracellular matrix and the internal cellular environment. Syndecan-4 plays a significant role in muscle regeneration by regulating the proliferation of muscle satellite cells. They reported decreased syndecan-4 expression and increased shedding of the ectodomain, leading to decreased cell proliferation affecting the regeneration of damaged muscle fibers. Furthermore, expression and oligomerization patterns of syndecans-1 through 3 also changed with wooden breast, affecting key cellular signal transduction pathways like MAPK, AKT, and Wnt.

Che and Hall and Choi et al. contributed an Opinion paper and original research contribution, respectively, comparing spaghetti meat to wooden breast. Both spaghetti meat and wooden breast are two myopathies resulting in economic losses for the poultry industry by affecting the broiler breast meat quality. Spaghetti meat results in the separation of muscle fibers, leading to a spaghetti-type phenotype, whereas wooden breast is characterized by a hard breast muscle. Che and Hall highlighted that the differences in heritability and processing factors require multifaceted approaches, including genetic selection, management practices, and processing methods. Choi et al. utilized a comparative metabolomic analysis to identify similarities and differences between wooden breast and spaghetti meat. In their study, they identified 3,090 metabolites in the chicken breast. In wooden breast, 850 metabolites are affected, whereas in spaghetti meat, 617 metabolites are differential. There were differences in the differential metabolites between the two myopathies, with cellular homeostasis and lipid metabolism both being affected in wooden breast and spaghetti meat. For example, purine metabolism was upregulated, and folic acid was decreased. They suggested that dietary supplementation of appropriate nutrients like folic acid may be a strategy to reduce the incidence or severity of wooden breast and spaghetti meat.

Meat quality and welfare

Maynard et al. reported on the effects of *in ovo* nicotinamide riboside feeding of high-yield Cobb 700 broilers for growth and meat quality. Nicotinamide riboside is a vitamin B3 analog that may protect against muscle degeneration. In general, nicotinamide ribose dosing increased pectoralis major and minor weights coupled with increased muscle fiber numbers. Despite the increase in weight and muscle fibers, myopathy scores and incidence of wooden breast were minimally affected. Anthney et al. reviewed bacterial chondronecrosis with osteomyelitis lameness and its effects on broiler welfare and meat quality. As a welfare issue, bacterial chondronecrosis leads to lameness which is considered painful to the bird but also results in the loss of product from culls and condemnations. Frequently, birds with bacterial chondronecrosis will be targets of aggression from more dominant littermates. Meat quality is a concern due to possible microbial contamination, especially in birds whose internal lesions have not been detected during carcass processing.

Immune system and fibroadipogenic progenitors

Song et al. conducted a comparative transcriptomic analysis of organs affected by Marek's disease virus and found cytokine–cytokine receptor interactions and cellular development were affected by Marek's disease. Lesions in wooden breast and white striping are characterized by the replacement of healthy tissue with fibrous and fatty tissue deposits. Fibroadipogenic progenitors are interstitial muscle mesenchymal stem cells and differentiate into both adipocytes and fibroblasts. To date, fibroadipogenic progenitors have been identified in myopathies in mice and humans. Jung et al. reviewed evidence that the fibroadipogenic population of cells may be a novel cell type and new target to direct research in chickens to reduce the incidence of breast muscle myopathies.

Merging of modern omics research with hypothesis-based research

Guo et al. provided an Opinion paper exploring how we have shifted to new omics technologies scientifically that have moved us to hypothesis-generating research. Traditionally, science made incremental advances through hypothesis-based research. The authors discuss how a balance and integration of both strategies is needed to translate new molecular discoveries into biological mechanistic insights and applications.

Author contributions

SV: conceptualization, writing–original draft, and writing–review and editing. WG: conceptualization and writing–review and editing. GS: conceptualization and writing–review and editing.

Funding

The author(s) declare that no financial support was received for the research, authorship, and/or publication of this article.

Conflict of interest

The authors declare that the research was conducted in the absence of any commercial or financial relationships that could be construed as a potential conflict of interest.

The author(s) declared that they were an editorial board member of Frontiers, at the time of submission. This had no impact on the peer review process and the final decision.

Generative AI statement

The author(s) declare that no Generative AI was used in the creation of this manuscript.

Publisher's note

frontiers | Frontiers in Physiology

TYPE Original Research
PUBLISHED 05 December 2023
DOI 10.3389/fphys.2023.1301804

OPEN ACCESS

EDITED BY
Sandra G. Velleman,
The Ohio State University, United States

REVIEWED BY
Wei Guo,
University of Wisconsin-Madison, United States
Francesca Soglia,
University of Bologna, Italy

*CORRESPONDENCE
Lucie Pejšková,
lucie.pejskova@nofima.no

RECEIVED 25 September 2023
ACCEPTED 06 November 2023
PUBLISHED 05 December 2023

CITATION
Pejšková L, Rønning SB, Kent MP, Solberg NT, Høst V, Thu-Hien T, Wold JP, Lunde M, Mosleth E, Pisconti A, Kolset SO, Carlson CR and Pedersen ME (2023), Characterization of wooden breast myopathy: a focus on syndecans and ECM remodeling.
Front. Physiol. 14:1301804.
doi: 10.3389/fphys.2023.1301804

Characterization of wooden breast myopathy: a focus on syndecans and ECM remodeling

Lucie Pejšková[1]*, Sissel Beate Rønning[1], Matthew Peter Kent[2], Nina Therese Solberg[1], Vibeke Høst[1], To Thu-Hien[2], Jens Petter Wold[1], Marianne Lunde[3], Ellen Mosleth[1], Addolorata Pisconti[4], Svein Olav Kolset[5], Cathrine Rein Carlson[3] and Mona Elisabeth Pedersen[1]

[1]Raw Materials and Optimization, Nofima AS, Ås, Norway, [2]Center for Integrative Genetics, Department of Animal and Aquacultural Sciences, Faculty of Biosciences (BIOVIT), Norwegian University of Life Sciences (NMBU), Ås, Norway, [3]Institute for Experimental Medical Research, Oslo University Hospital and University of Oslo, Oslo, Norway, [4]Department of Biochemistry and Cell Biology, Stony Brook, NY, United States, [5]Department of Nutrition, Institute of Basic Medical Science, University of Oslo, Oslo, Norway

Introduction: The skeletal muscle deformity of commercial chickens *(Gallus gallus)*, known as the wooden breast (WB), is associated with fibrotic myopathy of unknown etiology. For future breeding strategies and genetic improvements, it is essential to identify the molecular mechanisms underlying the phenotype. The pathophysiological hallmarks of WB include severe skeletal muscle fibrosis, inflammation, myofiber necrosis, and multifocal degeneration of muscle tissue. The transmembrane proteoglycans syndecans have a wide spectrum of biological functions and are master regulators of tissue homeostasis. They are upregulated and shed (cleaved) as a regulatory mechanism during tissue repair and regeneration. During the last decades, it has become clear that the syndecan family also has critical functions in skeletal muscle growth, however, their potential involvement in WB pathogenesis is unknown.

Methods: In this study, we have categorized four groups of WB myopathy in broiler chickens and performed a comprehensive characterization of the molecular and histological profiles of two of them, with a special focus on the role of the syndecans and remodeling of the extracellular matrix (ECM).

Results and discussion: Our findings reveal differential expression and shedding of the four syndecan family members and increased matrix metalloproteinase activity. Additionally, we identified alterations in key signaling pathways such as MAPK, AKT, and Wnt. Our work provides novel insights into a deeper understanding of WB pathogenesis and suggests potential therapeutic targets for this condition.

KEYWORDS

wooden breast, myopathy, syndecans, extracellular matrix, broiler chicken

1 Introduction

The chicken skeletal myopathy, commonly known as the wooden breast (WB), is a condition that affects the breast muscles (*Pectoralis major*) of fast-growing broilers selected for meat production purposes. It is characterized by the hardening and stiffness of the breast muscles, resulting in poor meat quality and sensory traits (Mudalal et al., 2015; Petracci and Berri, 2017; Xing et al., 2020; Oliveira et al., 2021). WB has been reported in the *Pectoralis major* muscle in predominantly fast-growing broiler lines (Sihvo et al., 2014) and is thought to be caused by the intensive genetic selection and feeding optimization that have resulted in faster growth rates and increased breast meat yields recorded worldwide over the past few decades (Petracci et al., 2015). However, the etiology of WB myopathy is unknown, and investigating the mechanisms underlying this muscle disorder is challenging. Different production regimes and feeding strategies have been tested to ameliorate the outcome of WB, but with limited success (Kuttappan et al., 2021). An especially intriguing, unanswered question is why some animals from the same breed, feeding regime, and production conditions develop WB, whereas others do not. Identifying molecular mechanisms and signaling systems involved in WB pathogenesis is important to designing future breeding strategies and could even identify therapeutic targets in modern agricultural production.

The pathophysiological hallmarks of WB include severe skeletal muscle fibrosis, inflammation, myofiber necrosis, and multifocal degeneration of muscle tissue. Fibrosis, in general, is characterized by extensive extracellular matrix (ECM) remodeling and increased depositions of ECM, especially of collagens, fibronectin 1, and small leucine-rich proteoglycans (SLRPs) (Sihvo et al., 2014). In WB myopathy, the SLRP decorin is involved in collagen organization and crosslinking (Velleman et al., 2017; Velleman, 2020). The main trigger of fibrosis, transforming growth factor-beta 2 (TGF-β2) and its SMAD signaling pathway, is upregulated in WB (Xing et al., 2021b); however, the potential involvement of other signaling pathways is still unknown.

Syndecans are key regulators of the TGF-β/Smad signaling pathway (Cui et al., 2020). The syndecan family includes four members (syndecan-1, -2, -3, and -4) that are differentially expressed in various tissues and cell types (Lambaerts et al., 2009; Velleman, 2012). Syndecans play critical roles in cell adhesion, proliferation, differentiation, migration, and survival (Couchman et al., 2015) and are important for skeletal muscle growth, health, and aging (Pisconti et al., 2012; Rønning et al., 2015; Pisconti et al., 2016; Velleman and Song, 2017; Rønning et al., 2020; Sztretye et al., 2023). They also play a role in ECM remodeling and can act as co-receptors for growth factors, chemokines, and extracellular matrix molecules (Xian et al., 2009; Couchman, 2010; Lunde et al., 2016). Syndecans are composed of an extracellular domain (ectodomain), a well-characterized transmembrane region, and a highly conserved short cytoplasmic domain. The ectodomains of all syndecans harbor heparan sulfate (HS) chains, and in the case of syndecan-1 and -3, they also harbor chondroitin sulfate (CS) chains. Syndecans are remarkable due to their ability to regulate multiple biological activities at multiple levels: i) extracellularly, through both the glycosaminoglycan (GAG) chains and the core protein that interacts with matrix components and growth factors; ii) at the transmembrane level, via dimerization and intramembrane cleavage; iii) at the intracellular level, via interaction with cytoskeleton proteins and various intracellular signaling transducers (Couchman et al., 2015); and iv) systemically, through shedding and release of the extracellular domain by matrix metalloproteinases (MMPs) and A disintegrin and metalloproteinase with thrombospondin (ADAMTS) motifs, which can act both at the autocrine and paracrine levels as well as systemically through the bloodstream. Syndecan shedding is a physiological process; however, under different pathological conditions, shedding is increased (Manon-Jensen et al., 2010). The soluble ectodomains of syndecans can function both as promoters of signaling and as competitive inhibitors, depending on the circumstances (Manon-Jensen et al., 2010), often depending on the activity of the protein partners attached to the HS chains (Pap and Bertrand, 2013). Dysregulation of syndecan expression and shedding has been linked to various diseases, including cancer, fibrosis, and neurodegeneration (Choi et al., 2011; Gopal, 2020). MMPs and sheddases, in general, are activated by the cleavage of an inactive pro-form and can degrade ECM proteins through the cleavage of specific peptide bonds (Hrabia et al., 2019). Their activities are further regulated by tissue inhibitors of metalloproteinases (TIMPs), which can bind to the active site of MMPs, preventing their catalytic activity and the degradation of ECM proteins and shedding processes.

Few studies have addressed ECM remodeling or the involvement of syndecan family in WB myopathy, and thus, syndecans' potential involvement in skeletal muscle fibrosis in WB is at present unknown. Importantly, transcription analysis of WB myopathy has shown upregulation of MMPs, but their protein or activity levels have not been investigated (Xing et al., 2021b). In this study, we report a thorough characterization of WB-associated fibrosis and ECM remodeling, with a particular focus on syndecans and their shedding during WB myopathy.

2 Materials and methods

2.1 Animal sampling and sample preparation

Male Ross 308 broiler chickens (*Gallus gallus*) were fed an *ad libitum* diet of pelleted wheat/maize from 10 days of age. The broiler chickens were housed in 2.4 × 0.95 m pens on wood shavings in a room with 6 h of light and 18 h of darkness and a temperature gradually reduced from 28°C to 21°C. To identify individuals with or without WB, a veterinary inspection of the hardness of breast muscle of 60 36-day post-hatching male Ross 308 broiler chickens was performed (from a larger flock n = 2,000, approximately 10% developed WB). Palpation of the breast muscle (*Pectoralis major*) after slaughtering was included in this pre-evaluation to confirm the grouping of affected and non-affected chickens. Further grouping of samples was performed by histology and near-infrared (NIR) spectroscopy, as described in the following section. Samples for quantitative polymerase chain reaction (qPCR), RNA sequencing (RNA-seq), Western blotting, and zymography were excised immediately after slaughter, snap-frozen in liquid nitrogen, and stored at −80°C until further analysis. For the microscopy analysis, tissue samples measuring approximately 8 mm × 8 mm × 2 mm were cut from the outer layer in the upper part of *Pectoralis major* of

all animals after slaughtering and fixed in IHC Zinc Fixative (#550523, BD Pharmingen, New Jersey, United States) for 24 h before dehydrating and paraffin embedding. All animals were first sorted by palpation and then classified by histology and NIR spectroscopy. The muscle tissues used are extracted from already slaughtered chickens (Ross 308 breed, NMBU, Norway). These chickens are in line with common regulatory roles of food production, and therefore do not require REC or NSD approval. In compliance with Norwegian law regulations concerning the experimental use of animals (FOR-2015-06-18-761 §2a), ethical approval is not necessary when samples are collected from slaughtered animals/non-experimental agriculture and aquaculture. This is also confirmed by direct communication with the Norwegian Food Safety Authority (Mattilsynet).

2.2 Histology and immunohistochemistry

To perform histological evaluation, 3-µm-thick sections of fixed, paraffin-embedded samples were cut on a microtome (Leica RM 2165, Leica Biosystems Nussloch GmbH, Germany), mounted on poly-L-lysine-coated glass-slides, and all 60 samples were stained with hematoxylin and eosin (H&E) according to standard procedures. All slides were scanned using Aperio CS2 (Leica Biosystems Nussloch GmbH, Buffalo Grove, IL, United States), and digital images were taken using ImageScope 64 (Leica Biosystems Nussloch GmbH, Buffalo Grove, IL, United States). Picrosirius red staining was performed according to the protocol (#25901 Polysciences, Inc., PA, United States). Slides were examined using a Leica light microscope (DM6000 B, Leica Biosystems Nussloch GmbH, Germany), and images were captured with or without a polarization filter using the Leica Application Suite and DMC 4500 (Leica Microsystems, Leica Biosystems Nussloch GmbH, Germany). The H&E staining was used to classify the samples according to the severity of fibrosis into mild (n = 13), moderate (n = 22), severe (n = 12), and fatty (n = 13).

To perform immunohistochemistry analyses, tissue sections of severe and mild WB samples (n = 3 for each group) were fixed with 4% PFA for 10 min and washed three times in PBS–Tween (PBS–T), followed by permeabilization with 0.1% Triton X-100 for 10 min. Samples were blocked in 1x blocking buffer (#ab126587, Abcam, United Kingdom) in PBS–T for 30 min and then stained using NucBlue Live Cell Stain Ready Probe (Hoechst 33342, Invitrogen, MA, United States) and wheat germ agglutinin (WGA) (Alexa Fluor™ 488 conjugate) (#A32723, 1:200, Thermo Fisher Scientific, MA, United States) for 2 h at room temperature (RT). The samples were washed once with PBS before being transferred onto a microscope slide and mounted using the fluorescent mounting medium (#S3023, DAKO, Denmark). The sections were examined by fluorescence microscopy analysis (ZEISS Axio Observer Z1 microscope, Jena, Germany), and images were processed using ImageJ software (NIH, MD, United States).

2.3 Near-infrared spectroscopy

NIR spectroscopy is a rapid and non-destructive technique that can be used to grade the severity of the WB syndrome in chicken breasts. The method provides a detailed measure of the amount of protein and the degree of water binding in the breast tissue, well known to be markers of WB (Wold et al., 2017; Wold et al., 2019). The degree of water binding is constituted by a shift in the absorption peak of water at approximately 980 nm. This is the dominant variation component in spectra from chickens with large variation in the degree of WB and can easily be quantified by principal component analysis (PCA). A prototype spectroscopic instrument (Wold et al., 2020) was used to collect near-infrared spectra measured in the interactance mode. Interactance ensures measurement in the depth of the chicken breasts, typically 10–12 mm deep, which is important for proper grading of WB. A halogen light source of 50 W was used to illuminate the sample in two rectangular regions of approximately 2 mm × 20 mm. The distance between the two illuminated regions was 24 mm. Between the two illumination regions, there was a 4 × 4 mm field of view that was measured using a spectrometer, as described in detail by Wold et al. (2020). The spectra consisted of 20 evenly spaced wavelengths in the region of 761–1081 nm. For all samples (n = 60), one spectrum was collected in the rostral breast region after cooling to 4°C. Each measurement took 1 s and was done without contact with the sample.

2.4 RNA sequencing and analysis

Total RNA was extracted from muscle samples from all the individuals (n = 60) and stored at −80°C using the RNAdvance Tissue Kit (Beckman Coulter, IN, United States) according to the manufacturer's instructions. RNA purity and concentration were assessed for all samples using a NanoDrop spectrophotometer (Thermo Fisher Scientific, MA, United States), and the integrity of nine random samples was assessed using a 4150 TapeStation with RNA ScreenTape (Agilent, CA, United States). Extracted RNA (1.5–4.5 µg) was sent to a commercial sequencing provider (Novogene, United Kingdom), where quality was re-assessed (lowest RIN = 9.1). Sequencing libraries were prepared using NEBNext Ultra Directional RNA Library Prep Kits (NEB, MA, United States) and sequenced (PE150) on NovoSeq 6000 instruments using S4 flow cells (Illumina, CA, United States). FastQC (Andrews, 2010) was used to assess read quality, and raw reads were trimmed using fastp (Chen et al., 2018) to remove the adapter sequence. Gene expression levels were calculated by quantifying transcript expression with Salmon (Patro et al., 2017) (using the GRCg7b reference genome from NCBI) and then summarized into gene-level data. After obtaining read counts for each gene on each sample, DESeq2 (Love et al., 2014) was used to analyze differentially expressed genes between affected and normal groups. Gene Ontology (GO) and Kyoto Encyclopedia of Genes and Genomes (KEGG) pathway enrichment analyses were estimated using the R package clusterProfiler (Yu et al., 2012; Wu et al., 2021) for upregulated and downregulated gene sets separately.

2.5 RNA extraction and real-time quantitative PCR

Total RNA was extracted from eight chickens classified with severe WB and eight classified with mild WB using the RNeasy

10.3389/fphys.2023.1301804

TABLE 1 Gene target and TaqMan® primer/probe assays.

Gene target	TaqMan® primer/probe assays
EEF2	Gg03339740
TLR4	Gg03354643
DCN	Gg03355063
LUM	Gg03325844
BGN	Gg07177841
LOX	Gg03340182
TGF-β1	Gg07156069
COL1A1	Gg07167955
COL3A1	Gg03325764
SDC-1	Gg07175697
SDC-2	Gg03345644
SDC-3	Gg03339851
SDC-4	Gg03370419
MMP2	Gg03365277
MMP9	Gg03338324
TIMP2	Gg07157666
PDGFRβ	Gg07165531
ACTA2	Gg03352404

Midi Kit (#75144, Qiagen, Germany) according to the manufacturer's instructions. Approximately 100 mg of tissue was homogenized in RLT buffer containing 0.04 M DTT using the Precellys Lysing Kit (#P000911-LYSKO-A.0, Bertin Technologies, France), 4 × 20 s at 6,000 rpm with a 10-s break between shakes, followed by a 10-min spin at 5,000 g. Samples were incubated with proteinase K (#19131, Qiagen, Germany) according to the manufacturer's instructions. cDNA was generated from 2 µg of total RNA using TaqMan reverse transcription reagents (#N8080234, Thermo Fisher Scientific, MA, United States) in a 40 µL reaction volume with random hexamers according to the manufacturer's protocol. Real-time quantitative polymerase chain reaction (RT-qPCR) analysis was carried out using the TaqMan Gene Expression Master Mix (#4369510, Life Technologies, Thermo Fisher Scientific) and the QuantStudio 5 PCR System (Applied Biosystems, Foster City, CA, United States). The amplification protocol was initiated at 50°C for 2 min, followed by denaturation at 95°C for 10 min, 40 cycles of denaturation at 95°C for 15 min, and annealing of TaqMan probes and amplification at 60°C for 1 min. RT-qPCR analyses were performed with three technical replicates from each sample. The relative gene expression (RQ) was calculated using the comparative $2^{-\Delta Ct}$ method (Schmittgen and Livak, 2008). Normalization was performed against the *EEF2* reference gene for each sample and subsequently related to the average gene expression of the mild samples for each gene analyzed. All TaqMan® primers and probes are listed in Table 1.

2.6 Peptide synthesis, epitope mapping, and specificity testing with blocking peptides

Syndecan-1 to syndecan-4 cytoplasmic parts (mouse/chicken) were synthesized as overlapping 20-mer peptides on a cellulose membrane using a MultiPep automated peptide synthesizer, as previously described by Frank and Overwin (1996). The peptide arrays were blocked for 1 h at RT in 1% casein and thereafter overlaid with chicken syndecan-1 to syndecan-4 antibodies (1:1000) in 1% casein overnight at 4°C, washed three times for 5 min in TBS-T before incubation with anti-rabbit IgG conjugated with horseradish peroxidase (HRP) (#NA934V, Cytiva, GE Healthcare Life Sciences, MA, United States) for 1 h at RT. After further three washes in TBST-T, the signal was developed using ECL Prime (RPN 2236, GE Healthcare, IL, United States). The blocking peptides specific for each of the four chicken syndecan antibodies were synthesized to >80% purity by GenScript Corporation (United States) (syndecan-1: NGGYQKPHKQE; syndecan-2: RKPSSAAYQKAPTK; syndecan-3: KQANVTYQKPDKQE; and syndecan-4: DLGKKPIYKKAPTN).

2.7 Western blotting

For Western blotting, proteins were isolated from 50–100 mg of tissue samples. Protein extracts were prepared using the Precellys Lysing Kit CK28 (#P000911-LYSKO-A.0, Bertin Technologies, France) with 1 mL of Tris–EDTA lysis buffer (50 mM Tris and 10 mM EDTA, pH 8.3) supplemented with phosphatase inhibitor cocktail 2 (#P5726, Sigma-Aldrich, Merck) and AEBSF protease inhibitor (#78431, Thermo Fisher Scientific, United States). Tissue samples were homogenized two times for 20 s with a 5-s break at 6,000 rpm using the Precellys Evolution homogenizer (Bertin Technologies, France). The homogenized sample was mixed in a 1:1 ratio with 2x treatment buffer without DTT (0.125 M Tris, pH 6.8, 4% SDS, and 20% glycerol), heated for 20 min at 50°C, and centrifuged at 13,000 g for 30 min at 4°C. The supernatant, containing soluble proteins, was collected and stored at −80°C until analysis. The protein concentration was determined using DC (#5000112, Bio-Rad, CA, United States) or the Micro BCA Protein Assay Kit (#23235, Thermo Fisher Scientific, MA, United States).

Samples were prepared for Western blotting according to the NuPAGE reagent kit's protocol (Invitrogen, Massachusetts, United States) with deviation from the official protocol of boiling samples for 5 min at 80°C. In some experiments, the samples were mixed with 4x sample buffer, containing SDS and DTT, and boiled at 95°C. The 4%–15% Criterion TG Precast Gel (#5671084, Bio-Rad) was loaded in equal amounts with 40 or 60 µg of proteins per well. Standard molecular weights used were either ECL Plex Rainbow (#RPN851E, Cytiva, GE Healthcare Life Sciences, MA, United States), Dual Xtra Standards (#1610377, Bio-Rad), Precision Plus Protein All Blue (#1610373, Bio-Rad), or Dual Color (#1610374, Bio-Rad). The gels were blotted onto PVDF membranes (#1704157, Trans-Blot Turbo Transfer Pack, Bio-Rad) using the Trans-Blot Turbo system (Bio-Rad). The PVDF membranes

TABLE 2 Primary antibodies for Western blotting.

Antibody	Cat. no.	Producer	Dilution
pThr202/Tyr204-ERK1/2	#4695	Cell Signaling	1:1000
ERK1/2 total	#9272	Cell Signaling	1:1000
pSer240/244-rpS6	#2215	Cell Signaling	1:1000
rpS6	#2217	Cell Signaling	1:1000
AKT total	#9101	Cell Signaling	1:1000
pSer473-AKT	#4060	Cell Signaling	1:2000
Syndecan-1		GenScript	1:1000
Syndecan-2		GenScript	1:1000
Syndecan-3		GenScript	1:1000
Syndecan-4		GenScript	1:1000
TLR4	LSC756	LSBio	1:500
TIMP2	MBS9610370	MyBioSource	1:1000
TIMP1	sc-5538	Santa Cruz	1:200
MMP2	ab37150	Abcam	1:200
MMP9	NBP1-57940	Novus Biologicals	1:1000
Wnt7a	ab1000792		1:1000
Wnt4	ab91226		1:1000
β-catenin	#610153		1:1000
β-catenin non-phospho (active) Ser33/37/Thr41	#8814		1:1000
Dact1	#24768		1:1000

were blocked in 1% casein (Western Blocking Reagent, #11921681001, Sigma Merck), BSA (#805090, Norsk Labex, Norway), 1x blocking solution (Roche), or 2% ECL blocking buffer (#RPN2125, Cytiva, GE Healthcare Life Sciences, MA, United States) in TBS-T for 60 min at RT, followed by incubation with primary antibodies (Table 2) overnight at 4°C. Membranes were washed three times for 10 min each in TBS-T before being incubated with either secondary antibodies (Amersham ECL Plex Cy3 (#PA45011, anti-mouse, Cytiva, GE Healthcare Life Sciences, MA, United States) and Cy5 (#PA43009, anti-rabbit, Cytiva, GE Healthcare Life Sciences, MA, United States)) diluted at 1:2500 in TBS-T and incubated in the dark at RT for 1 h or with horseradish-peroxidase-conjugated secondary antibodies (anti-mouse IgG, NA931V, or anti-rabbit, NA934V, both from Cytiva) diluted at 1: 3000 in TBS-T, followed by another three rounds of 10-min washes in TBS-T. Blots were developed using G:BOX (Syngene International Ltd., United Kingdom) for fluorescence secondary antibodies and ECL Prime (#RPN2232/2236, GE Healthcare, IL, United States) for chemiluminescence signal detection. The chemiluminescence signals were detected using Las 4000 (GE Healthcare Life Sciences, MA, United States) or Azure Biosystems (CA, United States). To compare phosphorylated and total protein, the membranes were re-probed after stripping using the Restore Western blot Stripping buffer for 5 min at RT (#21063, Thermo Fisher Scientific, MA, United States) and washed 3 × 15 min in TBS-T before blocking. Quantification of Western bands was done using ImageQuant (Cytiva, GE Healthcare Life Sciences, MA, United States). For the blocking experiment, the blocking peptides (GenScript) were pre-incubated with the respective chicken syndecan-1–4 antibodies overnight at 4°C prior to blotting of the membranes for 2 h at room temperature.

2.8 Zymography

Gelatinase activity was measured using gelatin zymography. Samples (approximately 300 mg) were homogenized in 2-mL tubes with ceramic beads (Precellys CK28, Bertin Technologies) and 1 mL cold buffer containing 50 mM Tris and 10 mM EDTA. Samples were kept on ice all the time. The homogenate was centrifuged, and the supernatant was collected and stored at −80°C until further analysis. Prior to electrophoresis, equal volumes of samples were mixed with the 2x Tris-Glycine sample buffer (#LC2645, Invitrogen, MA, United States). The samples were loaded on Novex® 10% Zymogram gelatin gels (#ZY00100BOX, Invitrogen, MA, United States) and run at 125 V for 100 min using the Tris-glycine running buffer (#LC2646, Invitrogen, MA, United States). The gels were washed for 30 min in the Novex™ Zymogram Renaturing Buffer (#LC2670, Invitrogen,

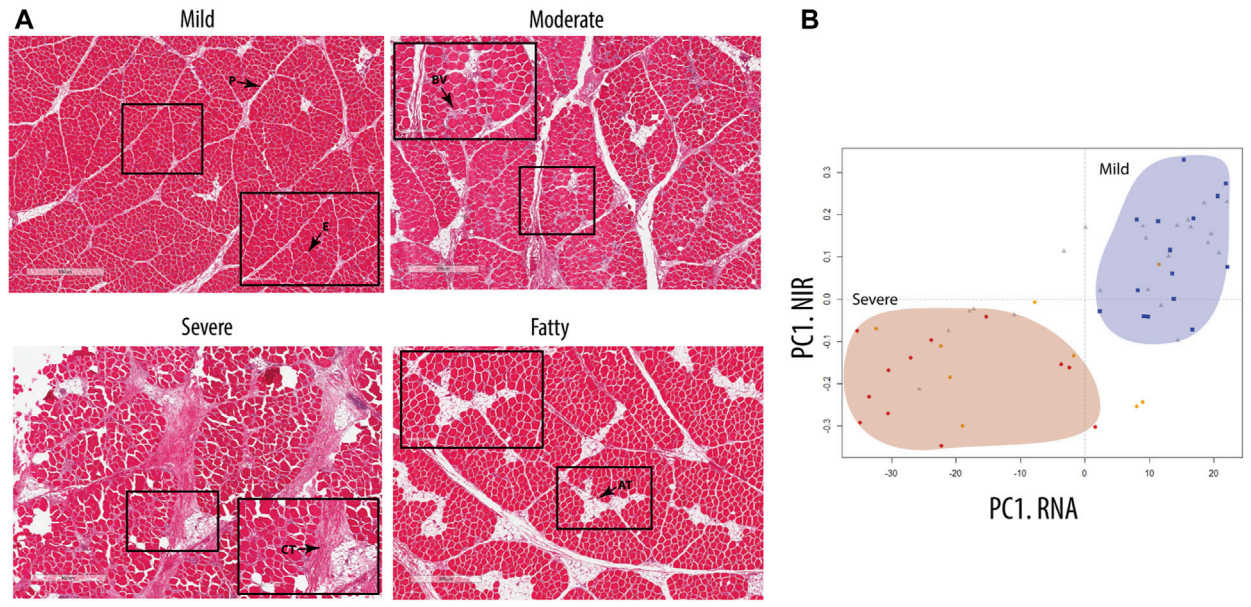

FIGURE 1
Classification of the groups. **(A)** Hematoxylin- and eosin-stained nuclei (a purplish blue) and eosin-stained extracellular matrix and cytoplasm (pink). E, epimysium; P, perimysium; CT, connective tissue; AT, adipose tissue; BV, blood vessel. **(B)** Score plot model based on RNA-seq data of chicken samples, showing group distribution comparable to data obtained from NIR spectra of cold chicken fillets measuring the amount of protein and the degree of water binding in the breast tissue. Visible separation of mild samples (blue square) and severe samples (red circle), with the moderate sample (gray triangles) distributed between them. Fatty samples (orange circle) are separated over the groups with a tendency toward the severe group.

MA, United States) and 30 min in the Novex™ Developing Buffer (#LC2671, Invitrogen, MA, United States) at RT; subsequently, they were incubated overnight at 37°C with a change to a new incubating buffer. The next day, gels were washed three times for 5 min each in distilled water, stained with SimplyBlue™ SafeStain (#LC6060, Invitrogen, MA, United States) for 1 h, and destained in distilled water overnight. Images of the gels were scanned using an Epson Perfection 4990 Photo Scanner (Epson America Inc., CA, United States). The bands were quantified using ImageQuantTL v 10.2-499 (Cytiva, GE Healthcare Life Sciences, MA, US).

2.9 ELISA

Competitive ELISA for heparan sulfate detection was performed in a 96-well on undiluted chicken serum collected after slaughtering, following the protocol of the heparan sulfate (MyBioSource, #MBS7217332) and syndecan-4 ELISA kits (MyBioSource, #MBS2514381). Subsequently, we determined the optical density at 450 nm using a microplate reader immediately after adding the stop solution.

2.10 Statistical analysis

All data of Western blots were expressed as mean ± SEM (standard error of mean, n = 6–8). For quantification of Western blots and zymography, ImageQuantTL v 10.2-499 (Cytiva, GE Healthcare Life Sciences, MA, US) was used with the background method of a rolling ball (radius 2). The statistical analyses of qPCR (n = 8) and Western blots were performed in GraphPad Prism version 8.0.1 (GraphPad Software, La Jolla, CA, United States), using a nested t-test for qPCR and a t-test with Welsh correction for Western blots. Statistical significance was considered at p-values <0.05 indicated in each figure. Explorative multivariate analysis by PCA was performed on all RNA-seq data and the collagens from the RNA-seq data. PCA was also applied to the NIR spectroscopic data to extract and quantify the spectral component related to WB.

3 Results

3.1 Histology classification, NIR spectroscopy, and RNA-seq analysis

All chicken samples (n = 60) were classified based on the severity of WB using H&E staining and NIR spectroscopy, grouping the samples into the following pathological categories: mild, moderate, and severe. Histology showed that the distribution of collagen-rich areas and adipose infiltrations in the perimysium varied in the WB-severe groups (Figure 1A). According to histology, a fourth group was observed, characterized by extensive adipose infiltration as well as a thinner perimysium (Figure 1A, bottom). Further investigation by RNA-seq showed a similar grouping to that achieved through NIR spectroscopy, with a clear separation between mild and severe groups (Figure 1B). The scores of the first principal components from NIR spectroscopy (Y-axis) and RNA-seq (X-axis), respectively, were combined into one plot in Figure 1B, showing a clear separation between the mild group (blue squares) and severe

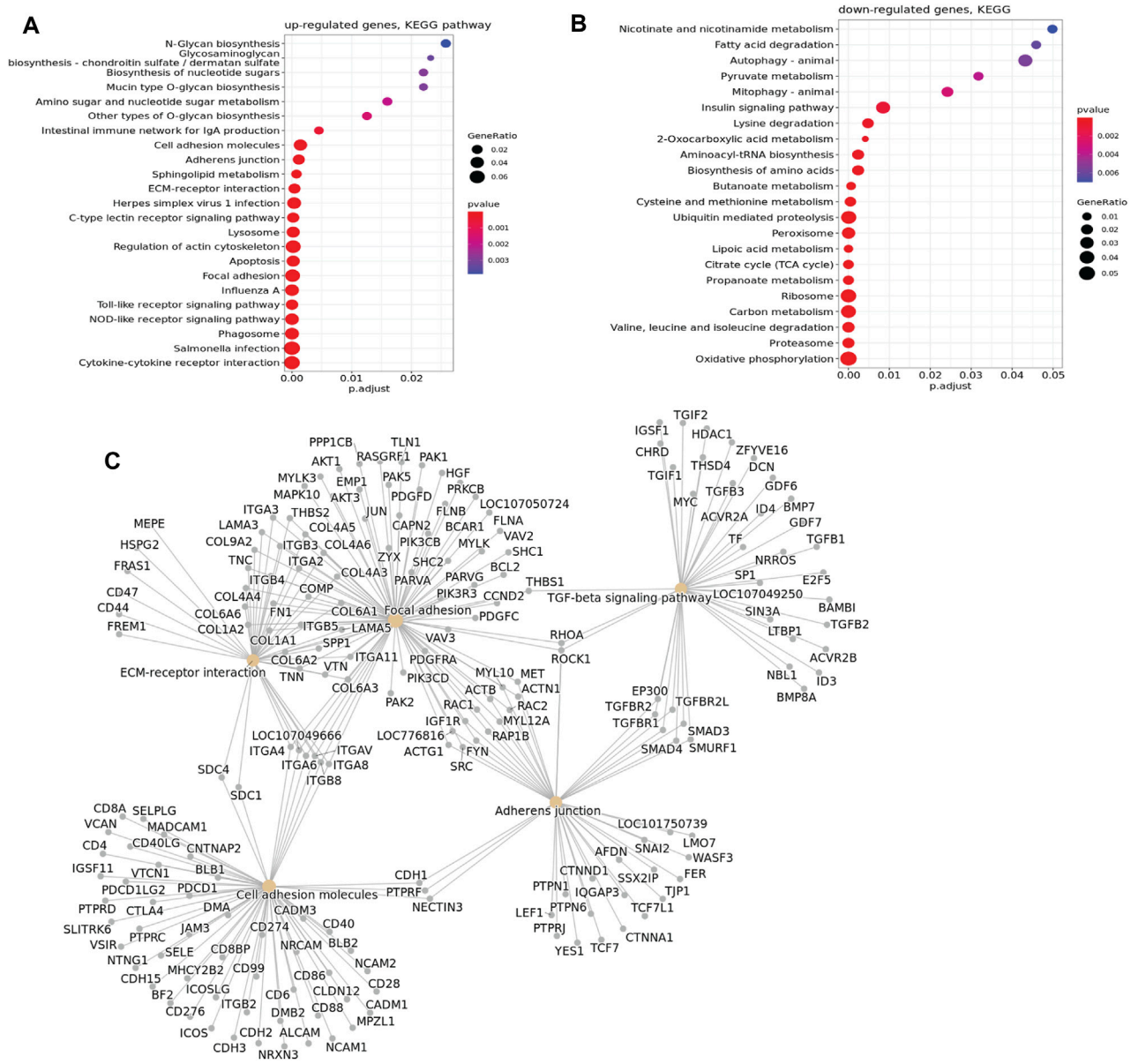

FIGURE 2
KEGG pathway enrichment bubble plot. **(A)** Upregulated genes according to KEGG pathway analysis. **(B)** Downregulated genes according to KEGG pathway analysis. In the graph, a larger dot size corresponds to more proteins in a given pathway. Additionally, a higher ratio of pathway proteins to the total proteins in the graph indicates a more significant difference in protein concentration within that pathway, suggesting a greater number of genes involved. **(C)** Cluster of upregulated genes in selected KEGG pathways associated with ECM remodeling, showing upregulation of SDC-1, SDC-4, and several other molecules studied.

group (red dots), whereas the moderate group (gray triangles) was spread along the first principal component (PC). The corresponding observation by NIR revealed low water binding in the samples with severe WB compared to the mild samples. The PCA of NIR measurements also, to some extent, discriminated between samples with high- and low-fat content (data not shown), which also corresponded to samples showing low- and high-fat deposits by histology. Since the main focus of this study was to examine ECM remodeling and fibrosis, the remaining analyses were, therefore, performed on the most separated groups, the mild and severe groups, excluding the medium and fatty groups.

The RNA-seq revealed major changes in several signaling pathways and processes between mild and severe WB cases; many of these changes are important for ECM remodeling and fibrosis. Altogether, 4,324 genes were observed to be upregulated in the severe group *versus* the mild group, whereas 4,934 genes were downregulated. The difference in the gene expression pattern between mild and moderate groups was minor, with only 21 genes upregulated and 286 genes downregulated (data not shown). Functional enrichment analysis of genes upregulated in severe cases compared with mild cases revealed molecular fingerprints of receptors and signaling pathways involved in

10.3389/fphys.2023.1301804

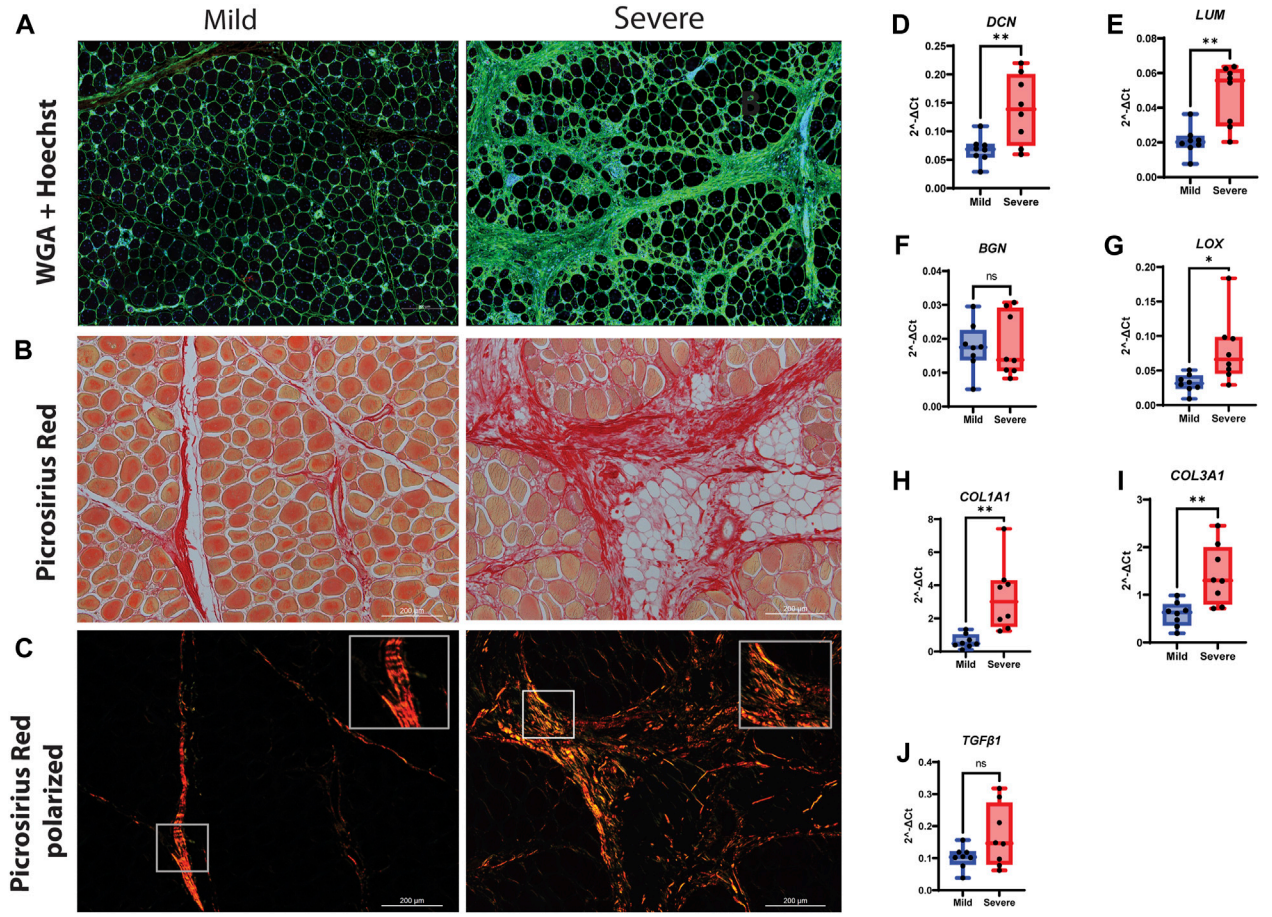

FIGURE 3
Production of connective tissue and collagen during WB. **(A)** Immunofluorescence staining of tissue by WGA shows an increased amount of connective tissue (green) in the severe group compared to the mild group. Nuclei are stained by Hoechst (Blue). **(B)** Picrosirius red visual and **(C)** polarization method. Polarized light shows the amount of new (green/yellow) and mature (red) collagen I and III and their structural differences between the two groups. **(D)** *DCN* and **(E)** *LUM* are highly upregulated in severe WB compared to the mild group. **(F)** *BGN* was shown without change. **(G)** *LOX* is upregulated in severe samples. Two types of collagens, **(H)** *COL1A1* and **(I)** *COL3A1*, are upregulated in severe samples. **(J)** *TGF-β1* shows no change between mild and severe groups. The data are presented as the fold change average relative to the mean of mild WB, ± SEM. Comparisons between the groups were analyzed using a t-test with Brown–Forsythe and Welsh correction; an asterisk indicates significant differences (ns, non-significant; *p < 0.05, **$p < 0.01$).

inflammatory processes and apoptosis, glycosaminoglycan biosynthesis, ECM–receptor interactions, cell adhesion molecules, focal adhesion, and adherent junctions (Figure 2A). In contrast, downregulated genes are prevalently linked to metabolic functions such as protein and fat metabolism, especially various catabolic degradation pathways (Figure 2B). Bioinformatic cluster analysis of selected KEGG pathways connected to ECM remodeling, including pathways of cell adhesion, focal adhesion, TGF-β signaling, and adherent junctions, identified several molecules, such as *SDC-1* and *SDC-4*, together with several collagen types, integrins, *FN1* (Fibronectin 1), *TGF-β1*, *TGF-β2*, and *DCN* (decorin) (Figure 2C). In addition, RNA-seq data showed upregulation of several genes of collagen crosslinking enzymes and SLRP members, such as *LOX* and *LUM* and *FMOD* (Supplementary Table S1). Moreover, we observed increased expression of fibrillar *COL1A1* and *COL3A1* in severe samples compared to mild samples. In addition, other collagen types, including fibrillar (*COL5*), fibril-associated collagens (*COL12* and *COL16*), and network-forming collagens (*COL6*), were found to be upregulated in the severe samples (Supplementary Table S1). We also investigated the change in gene expression for inflammatory markers by RNA-seq, and we observed a significant upregulation of *TLR4*, *IL-1β*, and *IL-6* in severe compared with mild samples (Supplementary Table S1). Moreover, *TLR4* gene expression by qPCR and protein expression of splicing of TLR4 (smTLR4) were elevated in WB samples compared to mild samples (Supplementary Figure S1).

3.2 Structural changes and ECM

To further characterize relevant components of the extracellular matrix in more detail, we stained for sialic acid and *N*-acetylglucosaminyl residues using WGA. We observed strong staining in the endomysium surrounding each muscle fiber and in

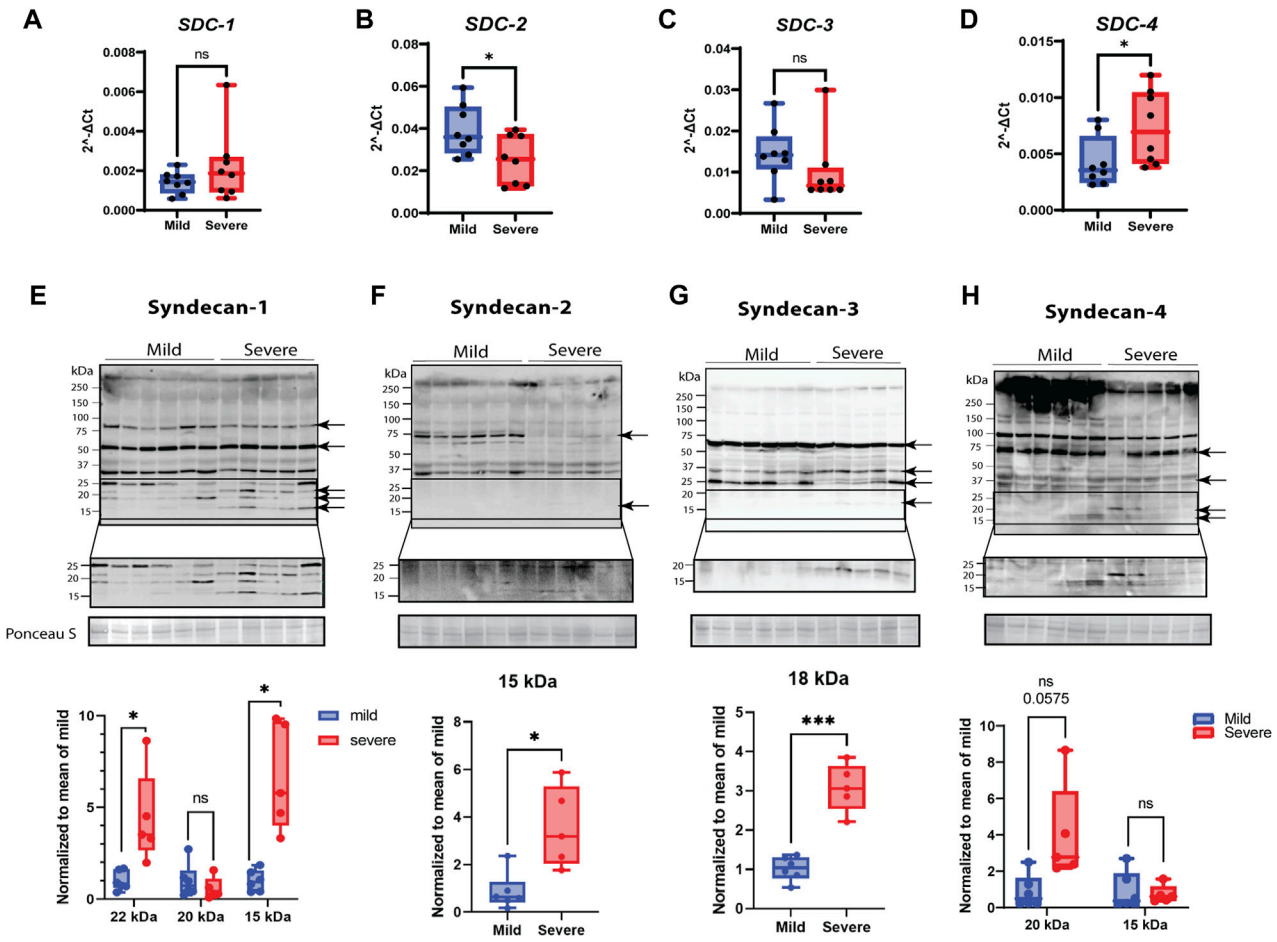

FIGURE 4
Gene and protein expression of syndecans and their shedding. **(A–D)** Gene expression monitored by RT-qPCR. Gene expression of **(A)** *SDC-1* by qPCR shows variety between samples. **(B)** *SDC-2* qPCR data shows downregulation in severe groups, and **(C)** *SDC-3* gene expression was insignificant between groups. **(D)** *SDC-4* qPCR data show significantly elevated gene expression in severe samples. **(E–H)** Protein expression of syndecans and their shedding. The specific bands are highlighted by arrows (confirmed by blocking experiments in Supplementary Figure S4). The lower part of the pictures shows increased signal intensity of the syndecan C-terminal domain after shedding. **(E)** Syndecan-1 shows extensive shedding between 15 and 25 kDa in severe samples. **(F)** Syndecan-2 is mainly present as a protein band of 75 kDa in mild samples and shows a weak, significant 15-kDa shed fragment in the severe group. **(G)** A shed fragment of 15 kDa of syndecan-3 was detected in severe samples. **(H)** Syndecan-4 shows a decreased amount of protein in the higher-molecular-weight area (>250 kDa) and shows several increased shed fragments of approximately 20 kDa (tendency). The qPCR data are presented as the fold change average relative to the mean of mild WB, ± SEM. Comparisons between the groups were analyzed using a nested t-test with Brown–Forsythe and Welsh correction (, $*p < 0.05$). Shedding of syndecans was normalized to the mean of the mild group and analyzed using an unpaired t-test with Brown–Forsythe and Welsh correction; asterisks indicate significant differences (ns, non-significant; $*p < 0.05$, $***p < 0.001$).

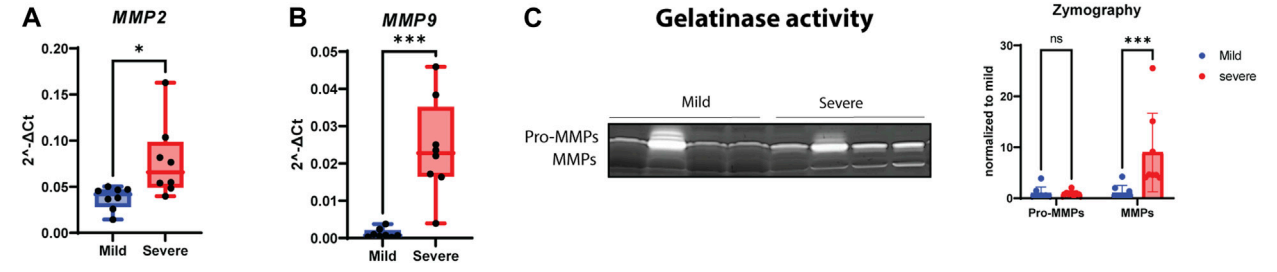

FIGURE 5
Increasing activity of MMPs in WB. Gene expressions of **(A)** *MMP2* and **(B)** *MMP9* show significant upregulation in severe WB. **(C)** A representative gelatin zymogram for measurement of pro-MMP and MMP activity in mild and severe WB samples and the quantified activity of MMP activity ($n = 8$ in each group). Comparisons between the groups (mean ± SEM, $n = 8$) were analyzed using a t-test with Brown–Forsythe and Welsh correction; asterisks indicate significant differences (ns, non-significant; $*p < 0.05$, $**p < 0.01$, $***p < 0.001$).

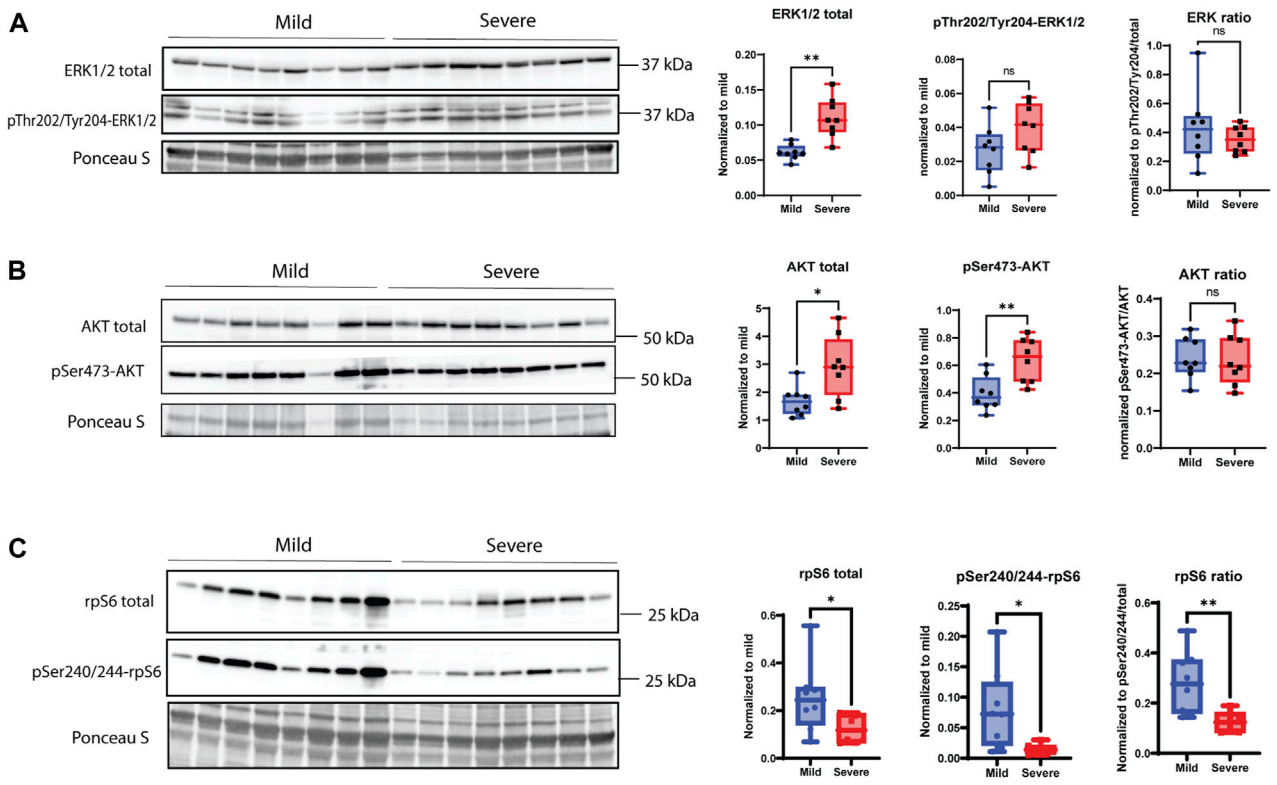

FIGURE 6
MAPK signaling pathway. **(A)** Total ERK1/2 is significantly upregulated in severe WB samples; however, pThr202/pTyr204-ERK1/2 shows no change between groups, and the overall ratio is not significant between mild and severe samples. **(B)** pSer473-AKT and total AKT are significantly increased in severe WB samples, but the overall ratio is not significant between groups. **(C)** pSer240/244-rpS6 and total rpS6 are downregulated in severe samples, and the total ratio is decreased in mild WB samples. Blots for phosphorylated version of proteins were reused for the detection of total version of proteins. Comparisons between the groups (mean ± SEM, n = 8) were analyzed using a t-test with Brown–Forsythe and Welsh correction; asterisks indicate significant differences (ns, non-significant; *$p < 0.05$, **$p < 0.01$).

the perimysium (Figure 3A), indicating extensive ECM deposition. To investigate the structural organization and possible changes in collagen I and III organization, picrosirius red staining was used combined with light microscopy in a bright field (Figure 3B) and polarized light (Figure 3C). In the bright-field mode, the severe samples showed denser matrix structures than the mild samples. In polarized light, the perimysium in mild WB samples appeared as a compact and continuous red string, indicating that the collagen bundles were even-sized, aligned in parallels, and tightly packed, which is consistent with previous studies (Sanden et al., 2021). In contrast, samples from severely affected tissues had more yellow/orange areas, suggesting the production of new collagen in a more disordered structure (Figure 3C).

Using RT-qPCR to validate the RNA-seq data, our results showed an upregulation of the SLRPs, *DCN* and *LUM*, in severe samples compared with mild samples (Figures 3D, E). No difference in gene expression was observed for biglycan (*BGN*) (Figure 3F), while the expression level of the collagen crosslinking enzyme lysyl oxidase (*LOX*) was increased in severe WB compared to mild WB (Figure 3G). Likewise, the gene expression of *COL1A1* and *COL3A1* was increased (Figures 3H, I). The pro-fibrotic cytokine *TGF-β1* showed upregulation in severe samples when analyzed by RNA-seq analysis (Supplementary Table S1) and showed an increasing trend (not significant) when analyzed by RT-qPCR (Figure 3J). No differences in the gene expression of myofibroblast markers, *PDGFRβ* and *ACTA2*, between the groups were observed (Supplementary Figures S2A, B). Furthermore, no differences in α-smooth muscle actin (α-SMA) protein expression were observed when analyzed by Western blotting (Supplementary Figure S2C).

3.3 Syndecan expression

Since transcriptomic analysis demonstrated that genes involved in cell adhesion were upregulated in muscles from severely affected animals (Figure 2A, KEGG pathway analysis, Supplementary Table S1), we sought to inspect in more detail key players of cell adhesion, with a focus on the syndecan family. RT-qPCR analysis of relative gene expression of *SDC-1* and *-3* showed no significant changes between the mild and severe groups (Figures 4A, C). In contrast, *SDC-2* was downregulated in severely affected muscles compared with mildly affected muscles (Figure 4B), while *SDC-4* was upregulated (Figure 4D).

When examining protein expression by Western blotting using custom-made chicken-specific antibodies generated against the cytoplasmic domain of the four syndecans (Supplementary Figure S3, epitope mapping), we observed numerous protein bands (Figures 4E–H). To determine the bands specific to

10.3389/fphys.2023.1301804

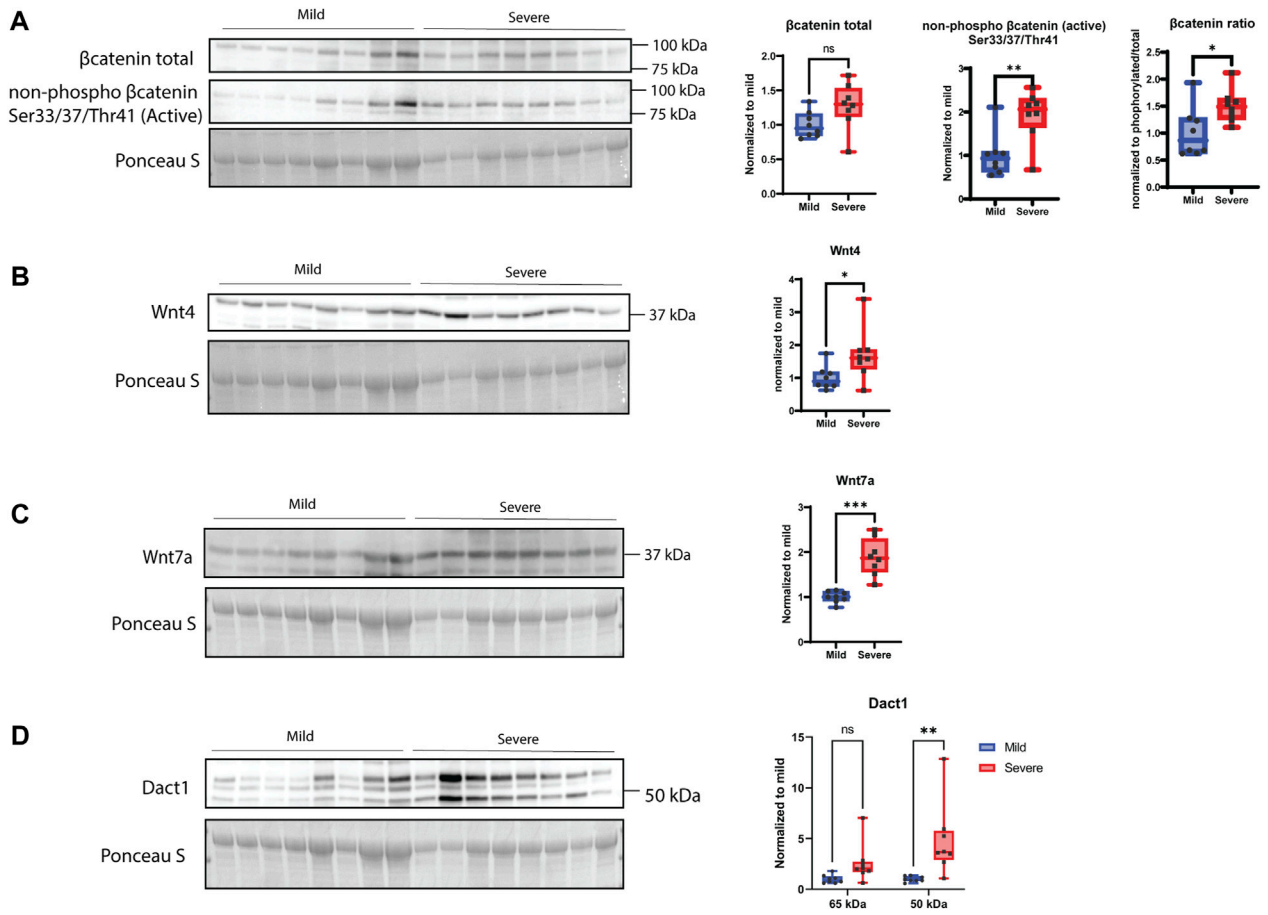

FIGURE 7
Wnt signaling. **(A)** β-catenin shows no significant difference between mild and severe groups, and its active non-phosphorylated version is upregulated in severe WB samples. The ratio is increased in severe WB. **(B)** Wnt4 and **(C)** Wnt7 are significantly upregulated in severe WB samples. **(D)** Dact1 was mainly detected as two bands (50 kDa and 65 kDa) and shows an increase of the 65 kDa band in severe samples. Blot was reused for both versions of β-catenin and Wnt4, and another blot was used for Wnt7 and Dact1. Comparisons between the groups (mean ± SEM, $n = 8$) were analyzed using a t-test with Brown–Forsythe and Welsh correction; asterisks indicate significant differences (ns, non-significant; *$p < 0.05$, **$p < 0.01$, ***$p < 0.001$).

syndecan-1–4, we performed blocking experiments using specific peptides containing the epitope for each of the four developed chicken syndecan antibodies (Supplementary Figure S4). The syndecan-1–4-specific bands, as verified by the peptide blocking experiments, ranged from 15 to 90 (syndecan-1), 15 to 75 (syndecan-2), 15 to 60 (syndecan-3), and 15 to 250 (syndecan-4) kDa (Figures 4E–H, indicated with arrows). It is possible that these higher-molecular-weight bands are SDS-resistant homo- or perhaps hetero-oligomers of syndecans. We could observe similar levels of a possible syndecan-1 oligomer of 80 kDa in the mild and severe groups; however, a possible syndecan-2 oligomer of 70 kDa was only observed in the mildly affected group. For syndecan-3, we observed a possible oligomer of 60 kDa at a similar level in both groups. The very-high-molecular-weight (HMW) bands observed in all four Western blots (>250 kDa) were prominently reduced for syndecan-4 in the severe group vs. mild group. Interestingly, we could also observe a distinct pattern of smaller fragments (<25 kDa) for all the syndecans in the severe group (Figures 4E–H, see increased contrast of the lowermost panels). These bands are likely the remaining transmembrane and cytoplasmic parts of the syndecans after shedding. Syndecan-1 exhibited several smaller fragments, probably reflecting a strong degree of shedding of ectodomains, but smaller fragments were also observed for syndecan-2, -3, and -4 (quantified in the lower panels in Figures 4E–H). We were unable to detect shed syndecan-4 in blood serum using commercial ELISA kits (data not shown); however, ELISA for HS chains demonstrated significantly reduced concentrations of HS in severe samples compared to mild samples (Supplementary Figure S4). Notably, the relative gene expression of heparanase was upregulated in severe WB (Supplementary Table S1).

3.4 MMP activity

To investigate whether MMPs were involved in WB pathogenesis, we analyzed *MMP2* and *MMP9* gene expression using RT-qPCR, assessed protein expression using Western blotting, and examined their gelatinase activity. Although both *MMP2* and *MMP9* gene expression levels were upregulated in severe samples (Figures 5A, B), their protein levels were

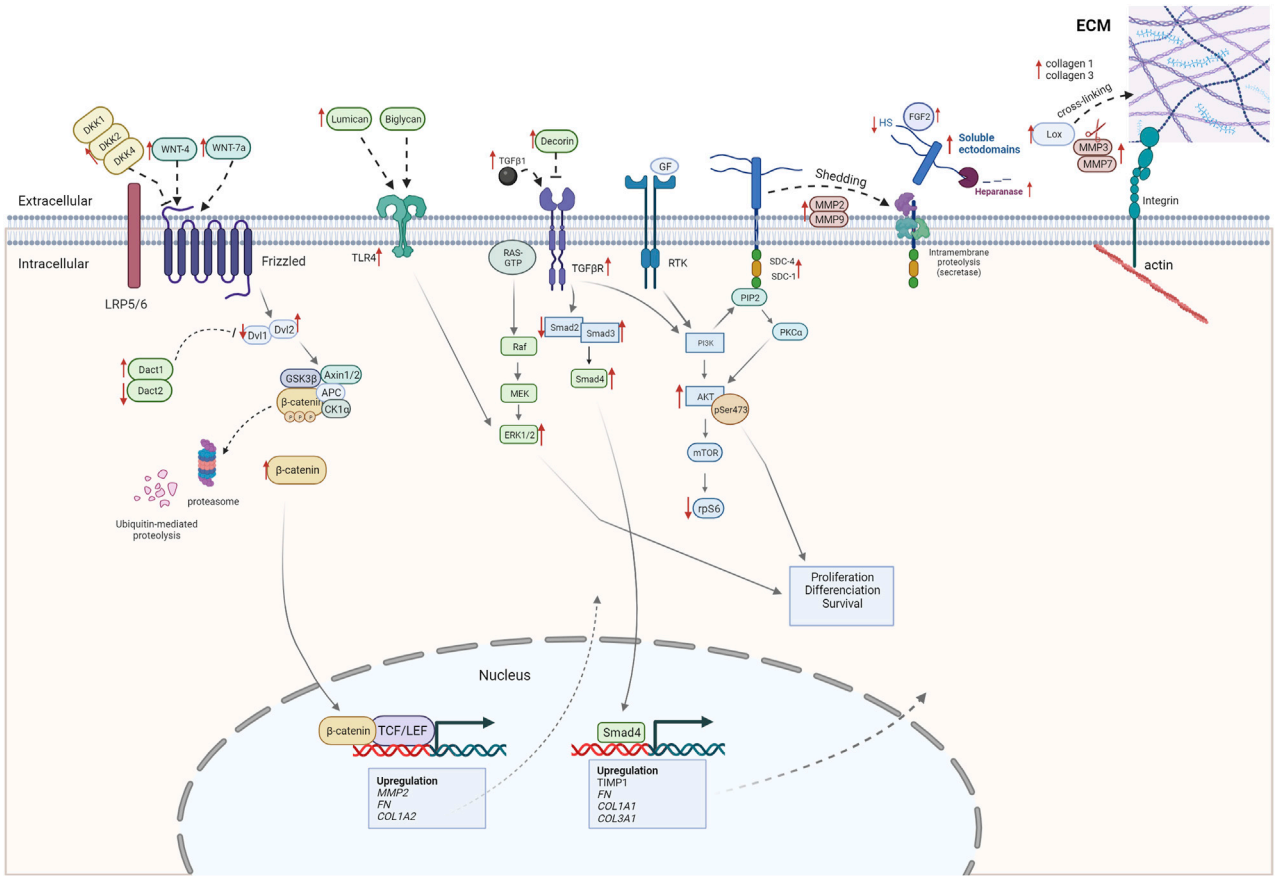

FIGURE 8
Alterations observed in severe WB myopathy (this study). The figure shows alterations observed in severe WB myopathy by RNA-seq, RT-qPCR, and Western blotting.

downregulated in severe compared to mild samples (Supplementary Figures S5A, B). In contrast, the MMPs had increased activity in severe WB samples (Figure 5C). Notably, the pro-form of MMPs was unchanged between groups (Figure 5C). The analysis of protein expression of MMP inhibitors, specifically, TIMP-1 and TIMP-2, through Western blotting showed no differences in their protein levels (Supplementary Figures S5C, D); however, the *TIMP2* gene level showed a tendency to be upregulated in severe WB (Supplementary Figure S5E).

3.5 MAPK, AKT, and Wnt signaling

According to the RNA-seq data (Supplementary Table S1), genes belonging to signaling pathways responsible for ECM remodeling, cell receptor signaling, and focal adhesions were significantly upregulated in WB pathogenesis. Increased levels of the total extracellular signal-regulated kinase 1/2 (ERK1/2) and its phosphorylated version (Thr202/Tyr204, tendency), which are parts of the MAPK signaling pathway, showed an increase in severe WB myopathy (Figure 6A). Increased levels were also observed for protein kinase B (AKT) and pSer473-AKT (Figure 6B). Surprisingly, ribosomal protein S6 (rpS6) and the phosphorylation of its serine residues 240 and 244 (pSer240/244), which is a downstream target of the AKT/mTOR signaling pathway, were both downregulated in severe samples (Figure 6C).

When examining players of the Wnt signaling pathway, including members of the canonical and non-canonical pathways, we could observe an increase in the active form of *ß*-catenin and a tendency for increased production of total *ß*-catenin in severe WB samples (Figure 7A). Moreover, Wnt-4 and Wnt-7a proteins were also found to be upregulated in severe cases of WB (Figures 7B, C). Furthermore, Dact1 (disheveled binding antagonist of *ß*-catenin 1) of 50 kDa showed no significant change between groups, whereas a 65-kDa form was found to be elevated in the severe group (Figure 7D).

4 Discussion

4.1 Extracellular matrix undergoes extensive remodeling during wooden breast pathogenesis

In the present study, we investigated the histological and molecular profiles of fibrosis, as this is a hallmark of WB pathogenesis. To classify the severity of WB, we used NIR, an established method for the measurement of WB severity

(Wold et al., 2017; Wold et al., 2019), together with the histology of connective tissue distribution. Histological analyses demonstrated that all the chickens had some signs of WB; hence, they were classified as mild, moderate, and severe. Previously, NIR spectral information displayed up to 97.5% accuracy in the classification of wooden breast samples (Geronimo et al., 2019). Consistently, in our NIR analysis, the severely affected WB samples were easily separated from the mild samples, while the moderate samples were identified both within and between the mild and severe groups. Notably, RNA-seq data and histology analyses resulted in a similar classification to the NIR analysis, separating the severe group with heavy fibrosis from the mild group with minimal signs of fibrosis.

The severe WB group showed a huge variation in gene expression levels compared with mild WB. Our RNA-seq data identified glycosaminoglycan biosynthesis, ECM–receptor interactions, focal adhesions, cell adhesion molecules, toll-like receptor signaling pathways, and apoptosis as the most prominent upregulated genes in severe WB. Syndecan family members, especially syndecan-4, were found upregulated in severe WB with increased shedding of their ectodomains. In line with previous reports (Papah et al., 2018; Brothers et al., 2019; Malila et al., 2021), ECM components such as SLRPs, different collagen types, and the collagen crosslinking enzyme *LOX* were upregulated. The increased *LOX* level probably resulted from the increased inflammatory response observed in severe WB. Inflammation has been shown to induce LOX and lysyl hydroxylase expression *via* the hypoxia-inducible factor 1α (Hofbauer et al., 2003). Moreover, disruption of focal adhesion signaling has been reported to be accompanied by defective ECM, insufficient angiogenesis, poorer tissue oxygenation, impaired wound healing, aberrant depositions of ECM proteins, and, ultimately, fibrosis in mice (Koivisto et al., 2013).

Fibrosis-induced tissue hardness is affected by both the extent and structure of fibrillar collagens (Xing et al., 2020). In our study, we observed both increased collagen depositions and rearrangement of collagen fibrillary structure in severe WB, reflecting extensive ECM remodeling, in line with previous findings by us and others (Velleman and Clark, 2015; Griffin et al., 2018; Praud et al., 2020; Sanden et al., 2021). Fibrillar collagen types I and III are the dominant collagen types in muscle (Deshmukh et al., 2016), and our gene expression analysis demonstrated the upregulation of both types in severe WB. In addition, several other collagen types, such as fibrillar (collagen type V), fibril-associated collagens (collagen types XII and XVI), and network-forming collagens (collagen VI), were upregulated. Fibrillar collagens can be cross-linked with other ECM molecules, such as fibronectin (upregulated in our dataset), to form stable networks that provide mechanical support to the tissue. Fibrillar collagens are also crosslinked by LOX. LOX contributes to increasing collagen fibril diameter and tissue hardness (Xing et al., 2021a). SLRPs, including LUM, BGN, and DCN, are all crosslinking regulators and are shown to play a role in ECM remodeling and fibrosis in different mouse models of muscular and cardiovascular diseases (Mohammadzadeh et al., 2019). Only DCN has previously been investigated in WB in relation to collagen organization and crosslinking (Velleman et al., 2017; Velleman, 2020). DCN binds to collagens and TGF-β, and its level has been found to correlate with increased fibrosis in different muscular dystrophies (Zanotti et al., 2005). Our study identified the upregulation of both *LUM* and *DCN* in severe WB samples, and both expression levels were found to be similar to those previously reported in different muscle dystrophies (Zanotti et al., 2005; Velleman, 2015; Velleman et al., 2017; Xing et al., 2020). LUM is known to play a crucial role in maintaining the integrity of cardiac ECM and is involved in tissue inflammation by regulating immune cell recruitment in different mouse models (Wu et al., 2007; Mohammadzadeh et al., 2019). On the other hand, BGN, which is an important pro-inflammatory factor acting as an endogenous ligand of TLR-4, has been found to be highly upregulated in different types of fibrosis (Schaefer et al., 2005). However, no changes were observed in the *BGN* gene expression level in our study of WB myopathy. Taken together, the upregulation of *DCN* and *LUM* in severe WB, along with the upregulation of TLR signaling pathways, suggests an involvement of DCN and LUM, but not BGN, in the inflammatory responses of WB.

4.2 Syndecans as key players in WB pathogenesis

Syndecans play a major role in focal adhesion regulation, as well as in ECM–receptor interactions and cell adhesion regulation (Couchman, 2010)—all of which constitute some of the most upregulated genes observed in our RNA-seq data sets. To the best of our knowledge, expression and shedding levels of the syndecan family in WB myopathy have not been previously investigated. The altered syndecan expression and shedding levels support the notion that these cell surface receptors are involved in WB skeletal myopathy, adding to their importance as skeletal muscle regulators and molecular players in ECM-tissue homeostasis. Syndecans and their role in fibrosis have primarily been studied in relation to cancer (Cheng et al., 2016), cardiac (Lunde et al., 2016; Herum et al., 2020), and lung fibrosis (Parimon et al., 2019) and skeletal muscle aging in mice (Pisconti et al., 2016). The upregulation of *SDC-1* (tendency) and *SDC-4* gene expression in severe WB, coupled with the downregulation of *SDC-2* gene expression, suggests different and specific roles for the different syndecans. In tissue regeneration, syndecan-2 plays a major role in vascularization, regulating cell adhesion, and promoting spreading (Noguer et al., 2009). In line with the reduced expression of *SDC-2*, reduced vascularization has been demonstrated in WB (Luque et al., 1995), and it is suggested to induce muscle cell necrosis and tissue damage (Reine et al., 2014; Velleman and Clark, 2015). Syndecan-1 regulates cardiac fibroblast physiology through TGF-β signaling and is revealed as a pro-fibrotic molecule (Schellings et al., 2010). Syndecan-4 plays a major role in focal adhesions and migration of fibroblasts (Li and Chaikof, 2002; Herum et al., 2013) and is involved in cardiac myofibroblast differentiation and collagen production (Herum et al., 2015). Consistent with a role for syndecan-4 in fibrosis, we have previously observed increased gene expression levels of *DCN*, *COL1A1*, *COL3A1*, *FMOD*, *BGN*, and *LOX* in skeletal muscle (*tibialis anterior*) from *SDC-4* KO mice (Rønning et al., 2020). Moreover, cardiac syndecan-4 expression is upregulated by pro-inflammatory stimuli such as TNFα and IL-1β (Strand et al., 2013a). Although we detected elevated gene expression levels of *IL-1β*, *IL-6*, and *TGF-β1* in severe WB, no differences in the inflammation markers, *VCAM1* and *IL-10*, were observed. This

observation can be explained by the fact that inflammation markers are time-sensitive and depend on whether the injury is acute or chronic. Additionally, we studied α-smooth muscle actin (α-SMA and *ACTA*), which is a marker for myofibroblast differentiation and linked to syndecan-4 function (Herum et al., 2015). To our surprise, we did not detect any differences in α-SMA, neither at the gene nor protein level. In addition, the myofibroblast marker *PDGFR* was unchanged. These observations are in line with previous reports showing that α-SMA is not a functional marker of fibrogenic cells in skeletal muscle fibrosis associated with muscular dystrophy (Zhao et al., 2018). Notably, since endothelial cells also express α-SMA and reduced angiogenesis and vascular endothelial dysfunction are associated with WB (Abasht et al., 2021), a potential increase in α-SMA expression by fibrogenic cells might be zeroed out by lower α-SMA expression from endothelial cells.

Moreover, our study indicated altered oligomerization patterns of the syndecans in relation to WB pathogenesis. Syndecans form non-covalently linked homodimers through a highly conserved transmembrane domain, which contains the ubiquitously conserved GxxxG motif (Lambaerts et al., 2009). The syndecan family is also reported to have the ability to heterodimerize (Choi et al., 2015). Even in the presence of a strong anionic detergent, like sodium dodecyl sulfate (SDS), the syndecans can form dimers, a property known as SDS-resistant dimerization (Choi et al., 2015). Homo- and hetero-oligomerization properties appear essential for the function of syndecan-2 and syndecan-4 as cytoskeletal organizers and mediators for migration and adhesion (Choi et al., 2005; Choi et al., 2008; Choi et al., 2015).

The shedding of the syndecan ectodomain, containing the HS GAG chains, is a mechanism through which cell-bound HS is turned into a soluble effector molecule; this process may affect the inflammatory process (Strand et al., 2013b) and could cause fibrosis. In our study, we investigated the shedding of the syndecans using specific antibodies directed against the cytoplasmic part (C-terminus) of all four chicken syndecans. The exact shedding sites in chickens and the amounts and types of GAGs attached to different chicken syndecans are unknown. Studies have shown that the shedding of syndecan core proteins can be accelerated by pathological events and various stimuli, leading to increased expression of pro-inflammatory molecules and NF-κβ activation (Lambaerts et al., 2009). Our data using specific antibodies against the syndecan-1 to -4 cytoplasmic parts identified smaller syndecan fragments of 15–35 kDa, suggesting the shedding sites to be near the transmembrane domain and likely also within the N-terminus. Increased shedding of syndecan-4 was observed in severe WB, and consistently, a decreased amount of HMW syndecan-4 on the top of the SDS/PAGE gel, probably corresponding to the intact proteoglycan form, was also observed. The short cytoplasmic tail of syndecans regulates signaling, while their extracellular part, modified with glycosaminoglycan chains, binds to a range of extracellular matrix molecules involved in fibrosis and immune cell adhesion proteins (Lunde et al., 2016). The detailed investigation of GAG-attachment and their sulfation pattern was not the aim of this study. However, it is worth noting that the functions of syndecans depend largely on the sulfation level and pattern of the heparan/chondroitin sulfate chains, the rate of ectodomain shedding, the solubility of the ectodomains, and the different partner molecules binding to the ectodomain (Gopal, 2020). Interestingly, investigation of HS chain concentration in chicken serum showed degradation of HS in severe WB samples compared to mild samples. Consistently, we observed significant upregulation of gene expression of *HPSE* (heparanase) in WB samples (Supplementary Table S1). This is in line with data from Ozkok et al. (2018) who found that increased inflammation is associated with elevated heparanase activity, which might cause degradation of HS chains attached to soluble ectodomains in serum. Elevated shedding of syndecans is mediated by MMPs (Manon-Jensen et al., 2013), and in our study, we found that both *MMP2* and *MMP9* were increased at the transcript levels in severe WB samples, along with increased gelatinase activity. The upregulation of MMPs correlates with the inflammatory process in muscular dystrophies and inflammatory myopathies, suggesting a potential contribution to muscle regeneration (Kherif et al., 1999; Miyazaki et al., 2011). TIMPs function exclusively as endogenous inhibitors of MMPs, thereby modulating ECM degradation and remodeling (Alameddine and Morgan, 2016). Thus, the balance between MMP and TIMP levels modulates ECM homeostasis. Perturbation of this balance occurs in various physiological and pathological remodeling situations, including different muscular dystrophies, neuromuscular diseases, and inflammatory myopathies (Alameddine, 2012). In this study, RNA-seq analysis identified increased levels of *TIMP2* in severe WB, and there was a tendency of increase observed by qPCR. However, no changes in TIMP2 were observed at the protein level.

4.3 Signaling mechanisms in wooden breast fibrosis

Syndecans are involved in several signaling pathways, including ERK/MAPK (Hara et al., 2021), AKT/mTOR/S6K1, and Wnt signaling (Luyten et al., 2008; Jones et al., 2020; Hara et al., 2021; Johnson de Sousa Brito et al., 2021; Jones et al., 2022); however, none of them have previously been investigated in the context of WB myopathy.

The ERK1/2 signaling cascade is a crucial pathway that integrates extracellular signals from cell surface receptors to regulate gene expression and multiple cellular proteins. Ligand binding activates several intracellular proteins, including Ras, Raf, MEK, and, finally, ERK1/2, through a cascade of phosphorylation events (Foglia et al., 2019), affecting cell proliferation, differentiation, adhesion, migration, and survival (Foglia et al., 2019). Our results showed upregulation of total ERK1/2 and its phosphorylated pThr202/Tyr204 form in severe WB. We also found elevated amounts of AKT and pSer473-AKT, which are involved in muscle growth and hypertrophy (Lai et al., 2004). In contrast, phosphorylation of the downstream target Ser240/244-rpS6 was downregulated in severe WB. Previous studies have shown that ablation of syndecan-4 leads to the activation of the AKT/mTOR/S6K1 pathway in skeletal and cardiac muscle from female mice (Rønning et al., 2020; Støle et al., 2022). On the contrary, the ablation of syndecan-4 in endothelial cells is reported to result in decreased AKT activation (Partovian et al., 2008). In contrast, we observed upregulation of both syndecan-4 and AKT activity in severe WB. The disparities in results might be explained by differences in species, tissue, or perhaps sex.

It has already been shown that Wnt signaling is essential for normal heart valve development during chicken embryogenesis (Brade et al., 2006), and it has several times been linked to skeletal muscle hypertrophy (Armstrong and Esser, 2005; Steelman et al., 2006). We found alterations in both canonical and non-canonical Wnt signaling in WB myopathy, both at the gene and protein levels. In particular, active *ß*-catenin, Dact1, Wnt-4, and Wnt-7a were all upregulated in severe WB. Furthermore, RNA-seq data showed alterations in several genes involved in Wnt signaling, such as *APC*, *DACT1*, *DKK2*, *DVL2*, and *WNT4* (Supplementary Table S1), emphasizing an important role for Wnt signaling in WB myopathy.

5 Conclusion

In conclusion, our study has focused on characterizing WB myopathy and its ECM remodeling, with a special emphasis on the syndecan family and signaling pathways involved in fibrosis. A summary of our findings obtained from RNA-seq, RT-qPCR, and Western blotting analyses is depicted in Figure 8. In brief, several collagens, SLRPs, LOX, expression of syndecan-4, shedding of all the syndecans, MMPs, heparanase activity, TLR4, and ERK/MAPK, AKT, and Wnt signaling pathways all appeared to be increased in severe WB (Figure 8). Further study of the mechanisms underlying WB myopathy is warranted.

Data availability statement

The original contributions presented in the study are publicly available. This data can be found here: https://www.ebi.ac.uk/ena/browser/view/PRJEB66500.

Ethics statement

Ethical approval was not required for the study involving animals in accordance with the local legislation and institutional requirements because the muscle tissue used are extracted from already slaughtered chickens (Ross 308 breed, NMBU, Norway). These chickens are in line with common regulatory roles of food production and, therefore, do not require REC or NSD approval. In compliance with Norwegian law regulations concerning experimental use of animals (FOR-2015-06-18-761 §2a), ethical approval is not necessary when samples are collected from slaughter animals/non-experimental agriculture and aquaculture. This is also confirmed by direct communication with the Norwegian Food Safety Authority (Mattilsynet).

Author contributions

LP: data curation, formal analysis, investigation, methodology, visualization, and writing–original draft. SR: conceptualization, funding acquisition, methodology, supervision, and writing–review and editing. MK: methodology and writing–review and editing. NS: data curation, formal analysis, methodology, and writing–review and editing. VH: data curation, formal analysis, methodology, and writing–review and editing. TT-H: methodology and writing–review and editing. JPW: data curation, formal analysis, methodology, and writing–review and editing. ML: data curation, formal analysis, methodology, and writing–review and editing. EM: writing–review and editing. AP: writing–review and editing. SK: writing–review and editing. CC: conceptualization, funding acquisition, supervision, and writing–review and editing. MP: conceptualization, funding acquisition, project administration, supervision, and writing–review and editing.

Funding

The author(s) declare that financial support was received for the research, authorship, and/or publication of this article. Funding from the Norwegian Research Council ("ChickenHealth," no. 323939) is acknowledged. This work was supported by a grant from the Research Council of Norway (NFR 323939).

Acknowledgments

The authors would like to acknowledge Birger Svihus at the Norwegian University of Life Sciences for assistance in planning the chicken feeding trial and the Livestock Production Research Center for technical assistance. The authors would also like to thank Atle Løvland from Nortura for assistance in planning and sampling and Karen Sanden and Lene Øverby from Nofima for technical assistance during sampling.

Conflict of interest

The authors declare that the research was conducted in the absence of any commercial or financial relationships that could be construed as a potential conflict of interest.

Publisher's note

Supplementary material

The Supplementary Material for this article can be found online at: https://www.frontiersin.org/articles/10.3389/fphys.2023.1301804/full#supplementary-material

References

Abasht, B., Papah, M. B., and Qiu, J. (2021). Evidence of vascular endothelial dysfunction in Wooden Breast disorder in chickens: insights through gene expression analysis, ultra-structural evaluation and supervised machine learning methods. *PLoS One* 16 (1), e0243983. doi:10.1371/journal.pone.0243983

Alameddine, H. S. (2012). Matrix metalloproteinases in skeletal muscles: friends or foes? *Neurobiol. Dis.* 48 (3), 508–518. doi:10.1016/j.nbd.2012.07.023

Alameddine, H. S., and Morgan, J. E. (2016). Matrix metalloproteinases and tissue inhibitor of metalloproteinases in inflammation and fibrosis of skeletal muscles. *J. Neuromuscul. Dis.* 3 (4), 455–473. doi:10.3233/JND-160183

Andrews, S. (2010). "FastQC: a quality control tool for high throughput sequence data," in *Babraham bioinformatics* (Cambridge, United Kingdom: Babraham Institute).

Brothers, B., Zhuo, Z., Papah, M. B., and Abasht, B. (2019). RNA-seq analysis reveals spatial and sex differences in pectoralis major muscle of broiler chickens contributing to difference in susceptibility to wooden breast disease. *Front. Physiol.* 10, 764. doi:10.3389/fphys.2019.00764

Chen, S., Zhou, Y., Chen, Y., and Gu, J. (2018). fastp: an ultra-fast all-in-one FASTQ preprocessor. *Bioinformatics* 34 (17), i884–i890. doi:10.1093/bioinformatics/bty560

Cheng, B., Montmasson, M., Terradot, L., and Rousselle, P. (2016). Syndecans as cell surface receptors in cancer Biology. A focus on their interaction with pdz domain proteins. *Front. Pharmacol.* 7, 10. doi:10.3389/fphar.2016.00010

Choi, S., Lee, E., Kwon, S., Park, H., Yi, J. Y., Kim, S., et al. (2005). Transmembrane domain-induced oligomerization is crucial for the functions of syndecan-2 and syndecan-4. *J. Biol. Chem.* 280 (52), 42573–42579. doi:10.1074/jbc.M509238200

Choi, Y., Chung, H., Jung, H., Couchman, J. R., and Oh, E.-S. (2011). Syndecans as cell surface receptors: unique structure equates with functional diversity. *Matrix Biol.* 30 (2), 93–99. doi:10.1016/j.matbio.2010.10.006

Choi, Y., Kim, S., Lee, J., Ko, S. G., Lee, W., Han, I. O., et al. (2008). The oligomeric status of syndecan-4 regulates syndecan-4 interaction with alpha-actinin. *Eur. J. Cell Biol.* 87 (10), 807–815. doi:10.1016/j.ejcb.2008.04.005

Choi, Y., Kwon, M. J., Lim, Y., Yun, J. H., Lee, W., and Oh, E. S. (2015). Trans-regulation of syndecan functions by hetero-oligomerization. *J. Biol. Chem.* 290 (27), 16943–16953. doi:10.1074/jbc.M114.611798

Couchman, J. R. (2010). Transmembrane signaling proteoglycans. *Annu. Rev. Cell Dev. Biol.* 26, 89–114. doi:10.1146/annurev-cellbio-100109-104126

Couchman, J. R., Gopal, S., Lim, H. C., Nørgaard, S., and Multhaupt, H. A. B. (2015). Fell-Muir Lecture: syndecans: from peripheral coreceptors to mainstream regulators of cell behaviour. *Int. J. Exp. pathology* 96 (1), 1–10. doi:10.1111/iep.12112

Cui, J., Jin, S., Jin, C., and Jin, Z. (2020). Syndecan-1 regulates extracellular matrix expression in keloid fibroblasts via TGF-β1/Smad and MAPK signaling pathways. *Life Sci.* 254, 117326. doi:10.1016/j.lfs.2020.117326

Deshmukh, S. N., Dive, A. M., Moharil, R., and Munde, P. (2016). Enigmatic insight into collagen. *J. oral Maxillofac. pathology JOMFP* 20 (2), 276–283. doi:10.4103/0973-029x.185932

Foglia, B., Cannito, S., Bocca, C., Parola, M., and Novo, E. (2019). ERK pathway in activated, myofibroblast-like, hepatic stellate cells: a critical signaling crossroad sustaining liver fibrosis. *Int. J. Mol. Sci.* 20 (11), 2700. doi:10.3390/ijms20112700

Frank, R., and Overwin, H. (1996). SPOT synthesis. Epitope analysis with arrays of synthetic peptides prepared on cellulose membranes. *Methods Mol. Biol.* 66, 149–169. doi:10.1385/0-89603-375-9:149

Geronimo, B. C., Mastelini, S. M., Carvalho, R. H., Barbon Júnior, S., Barbin, D. F., Shimokomaki, M., et al. (2019). Computer vision system and near-infrared spectroscopy for identification and classification of chicken with wooden breast, and physicochemical and technological characterization. *Infrared Phys. Technol.* 96, 303–310. doi:10.1016/j.infrared.2018.11.036

Gopal, S. (2020). Syndecans in inflammation at a glance. *Front. Immunol.* 11, 227. doi:10.3389/fimmu.2020.00227

Griffin, J. R., Moraes, L., Wick, M., and Lilburn, M. S. (2018). Onset of white striping and progression into wooden breast as defined by myopathic changes underlying Pectoralis major growth. Estimation of growth parameters as predictors for stage of myopathy progression. *Avian Pathol.* 47 (1), 2–13. doi:10.1080/03079457.2017.1356908

Hara, T., Sato, A., Yamamoto, C., and Kaji, T. (2021). Syndecan-1 downregulates syndecan-4 expression by suppressing the ERK1/2 and p38 MAPK signaling pathways in cultured vascular endothelial cells. *Biochem. biophysics Rep.* 26, 101001. doi:10.1016/j.bbrep.2021.101001

Herum, K. M., Lunde, I. G., Skrbic, B., Florholmen, G., Behmen, D., Sjaastad, I., et al. (2013). Syndecan-4 signaling via NFAT regulates extracellular matrix production and cardiac myofibroblast differentiation in response to mechanical stress. *J. Mol. Cell Cardiol.* 54, 73–81. doi:10.1016/j.yjmcc.2012.11.006

Herum, K. M., Lunde, I. G., Skrbic, B., Louch, W. E., Hasic, A., Boye, S., et al. (2015). Syndecan-4 is a key determinant of collagen cross-linking and passive myocardial stiffness in the pressure-overloaded heart. *Cardiovasc Res.* 106 (2), 217–226. doi:10.1093/cvr/cvv002

Herum, K. M., Romaine, A., Wang, A., Melleby, A. O., Strand, M. E., Pacheco, J., et al. (2020). Syndecan-4 protects the heart from the profibrotic effects of thrombin-cleaved osteopontin. *J. Am. Heart Assoc.* 9 (3), e013518. doi:10.1161/jaha.119.013518

Hofbauer, K.-H., Gess, B., Lohaus, C., Meyer, H. E., Katschinski, D., and Kurtz, A. (2003). Oxygen tension regulates the expression of a group of procollagen hydroxylases. *Eur. J. Biochem.* 270 (22), 4515–4522. doi:10.1046/j.1432-1033.2003.03846.x

Hrabia, A., Wolak, D., Kwaśniewska, M., Kieronska, A., Socha, J. K., and Sechman, A. (2019). Expression of gelatinases (MMP-2 and MMP-9) and tissue inhibitors of metalloproteinases (TIMP-2 and TIMP-3) in the chicken ovary in relation to follicle development and atresia. *Theriogenology* 125, 268–276. doi:10.1016/j.theriogenology.2018.11.017

Johnson de Sousa Brito, F. M., Butcher, A., Pisconti, A., Poulet, B., Prior, A., Charlesworth, G., et al. (2021). Syndecan-3 enhances anabolic bone formation through WNT signaling. *Faseb J.* 35 (4), e21246. doi:10.1096/fj.202002024R

Jones, F. K., Phillips, A. M., Jones, A. R., and Pisconti, A. (2022). The INSR/AKT/mTOR pathway regulates the pace of myogenesis in a syndecan-3-dependent manner. *Matrix Biol.* 113, 61–82. doi:10.1016/j.matbio.2022.09.004

Jones, F. K., Stefan, A., Kay, A. G., Hyland, M., Morgan, R., Forsyth, N. R., et al. (2020). Syndecan-3 regulates MSC adhesion, ERK and AKT signalling *in vitro* and its deletion enhances MSC efficacy in a model of inflammatory arthritis *in vivo*. *Sci. Rep.* 10 (1), 20487. doi:10.1038/s41598-020-77514-z

Kherif, S., Lafuma, C., Dehaupas, M., Lachkar, S., Fournier, J. G., Verdière-Sahuqué, M., et al. (1999). Expression of matrix metalloproteinases 2 and 9 in regenerating skeletal muscle: a study in experimentally injured and mdx muscles. *Dev. Biol.* 205 (1), 158–170. doi:10.1006/dbio.1998.9107

Koivisto, L., Heino, J., Häkkinen, L., and Larjava, H. (2013). Integrins in wound healing. *Adv. Wound Care* 3 (12), 762–783. doi:10.1089/wound.2013.0436

Kuttappan, V. A., Manangi, M., Bekker, M., Chen, J., and Vazquez-Anon, M. (2021). Nutritional intervention strategies using dietary antioxidants and organic trace minerals to reduce the incidence of wooden breast and other carcass quality defects in broiler birds. *Front. Physiology* 12, 663409. doi:10.3389/fphys.2021.663409

Lai, K.-M. V., Gonzalez, M., Poueymirou, W. T., Kline, W. O., Na, E., Zlotchenko, E., et al. (2004). Conditional activation of akt in adult skeletal muscle induces rapid hypertrophy. *Mol. Cell. Biol.* 24 (21), 9295–9304. doi:10.1128/MCB.24.21.9295-9304.2004

Lambaerts, K., Wilcox-Adelman, S. A., and Zimmermann, P. (2009). The signaling mechanisms of syndecan heparan sulfate proteoglycans. *Curr. Opin. Cell Biol.* 21 (5), 662–669. doi:10.1016/j.ceb.2009.05.002

Li, L., and Chaikof, E. L. (2002). Mechanical stress regulates syndecan-4 expression and redistribution in vascular smooth muscle cells. *Arterioscler. Thromb. Vasc. Biol.* 22 (1), 61–68. doi:10.1161/hq0102.100314

Love, M. I., Huber, W., and Anders, S. (2014). Moderated estimation of fold change and dispersion for RNA-seq data with DESeq2. *Genome Biol.* 15 (12), 550. doi:10.1186/s13059-014-0550-8

Lunde, I. G., Herum, K. M., Carlson, C. C., and Christensen, G. (2016). Syndecans in heart fibrosis. *Cell Tissue Res.* 365 (3), 539–552. doi:10.1007/s00441-016-2454-2

Luque, E., Peña, J., Martin, P., Jimena, I., and Vaamonde, R. (1995). Capillary supply during development of individual regenerating muscle fibers. *Anat. Histol. Embryol.* 24 (2), 87–89. doi:10.1111/j.1439-0264.1995.tb00016.x

Luyten, A., Mortier, E., Van Campenhout, C., Taelman, V., Degeest, G., Wuytens, G., et al. (2008). The postsynaptic density 95/disc-large/zona occludens protein syntenin directly interacts with frizzled 7 and supports noncanonical Wnt signaling. *Mol. Biol. Cell* 19 (4), 1594–1604. doi:10.1091/mbc.e07-08-0832

Malila, Y., Uengwetwanit, T., Thanatsang, K. V., Arayamethakorn, S., Srimarut, Y., Petracci, M., et al. (2021). Insights into transcriptome profiles associated with wooden breast myopathy in broilers slaughtered at the age of 6 or 7 weeks. *Front. Physiol.* 12, 691194. doi:10.3389/fphys.2021.691194

Manon-Jensen, T., Itoh, Y., and Couchman, J. R. (2010). Proteoglycans in health and disease: the multiple roles of syndecan shedding. *FEBS J.* 277 (19), 3876–3889. doi:10.1111/j.1742-4658.2010.07798.x

Manon-Jensen, T., Multhaupt, H. A., and Couchman, J. R. (2013). Mapping of matrix metalloproteinase cleavage sites on syndecan-1 and syndecan-4 ectodomains. *Febs J.* 280 (10), 2320–2331. doi:10.1111/febs.12174

Miyazaki, D., Nakamura, A., Fukushima, K., Yoshida, K., Takeda, S. I., and Ikeda, S. I. (2011). Matrix metalloproteinase-2 ablation in dystrophin-deficient mdx muscles reduces angiogenesis resulting in impaired growth of regenerated muscle fibers. *Hum. Mol. Genet.* 20 (9), 1787–1799. doi:10.1093/hmg/ddr062

Mohammadzadeh, N., Lunde, I. G., Andenæs, K., Strand, M. E., Aronsen, J. M., Skrbic, B., et al. (2019). The extracellular matrix proteoglycan lumican improves survival and counteracts cardiac dilatation and failure in mice subjected to pressure overload. *Sci. Rep.* 9 (1), 9206. doi:10.1038/s41598-019-45651-9

Mudalal, S., Lorenzi, M., Soglia, F., Cavani, C., and Petracci, M. (2015). Implications of white striping and wooden breast abnormalities on quality traits of raw and marinated chicken meat. *Animal* 9 (4), 728–734. doi:10.1017/S175173111400295X

Noguer, O., Villena, J., Lorita, J., Vilaró, S., and Reina, M. (2009). Syndecan-2 downregulation impairs angiogenesis in human microvascular endothelial cells. *Exp. Cell Res.* 315 (5), 795–808. doi:10.1016/j.yexcr.2008.11.016

Oliveira, R. F., Mello, J. L. M., Ferrari, F. B., Souza, R. A., Pereira, M. R., Cavalcanti, E. N. F., et al. (2021). Effect of aging on the quality of breast meat from broilers affected by wooden breast myopathy. *Anim. (Basel)* 11 (7), 1960. doi:10.3390/ani11071960

Ozkok, A., Ozkok, S., Takır, M., Yakar, H., and Kanbay, A. (2018). Serum heparanase levels are associated with endothelial dysfunction in patients with obstructive sleep apnea. *Clin. Respir. J.* 12 (4), 1693–1699. doi:10.1111/crj.12731

Pap, T., and Bertrand, J. (2013). Syndecans in cartilage breakdown and synovial inflammation. *Nat. Rev. Rheumatol.* 9 (1), 43–55. doi:10.1038/nrrheum.2012.178

Papah, M. B., Brannick, E. M., Schmidt, C. J., and Abasht, B. (2018). Gene expression profiling of the early pathogenesis of wooden breast disease in commercial broiler chickens using RNA-sequencing. *PLOS ONE* 13 (12), e0207346. doi:10.1371/journal.pone.0207346

Parimon, T., Yao, C., Habiel, D. M., Ge, L., Bora, S. A., Brauer, R., et al. (2019). Syndecan-1 promotes lung fibrosis by regulating epithelial reprogramming through extracellular vesicles. *JCI Insight* 4 (17), e129359. doi:10.1172/jci.insight.129359

Partovian, C., Ju, R., Zhuang, Z. W., Martin, K. A., and Simons, M. (2008). Syndecan-4 regulates subcellular localization of mTOR Complex2 and Akt activation in a PKCalpha-dependent manner in endothelial cells. *Mol. Cell* 32 (1), 140–149. doi:10.1016/j.molcel.2008.09.010

Patro, R., Duggal, G., Love, M. I., Irizarry, R. A., and Kingsford, C. (2017). Salmon provides fast and bias-aware quantification of transcript expression. *Nat. Methods* 14 (4), 417–419. doi:10.1038/nmeth.4197

Petracci, M., and Berri, C. (2017). *Poultry quality evaluation: quality attributes and consumer values*. Editor M. Petracci and C. Berri (Cambridge, UK: Woodhead Publishing).

Petracci, M., Mudalal, S., Soglia, F., and Cavani, C. (2015). Meat quality in fast-growing broiler chickens. *World's Poult. Sci. J.* 71 (2), 363–374. doi:10.1017/S0043933915000367

Pisconti, A., Banks, G. B., Babaeijandaghi, F., Betta, N. D., Rossi, F. M. V., Chamberlain, J. S., et al. (2016). Loss of niche-satellite cell interactions in syndecan-3 null mice alters muscle progenitor cell homeostasis improving muscle regeneration. *Skelet. Muscle* 6 (1), 34. doi:10.1186/s13395-016-0104-8

Pisconti, A., Bernet, J. D., and Olwin, B. B. (2012). Syndecans in skeletal muscle development, regeneration and homeostasis. *Muscles, ligaments tendons J.* 2 (1), 1–9.

Praud, C., Jimenez, J., Pampouille, E., Couroussé, N., Godet, E., Le Bihan-Duval, E., et al. (2020). Molecular phenotyping of white striping and wooden breast myopathies in chicken. *Front. Physiology* 11, 633. doi:10.3389/fphys.2020.00633

Reine, T. M., Vuong, T. T., Jenssen, T. G., and Kolset, S. O. (2014). Serglycin secretion is part of the inflammatory response in activated primary human endothelial cells *in vitro*. *Biochim. Biophys. Acta* 1840 (8), 2498–2505. doi:10.1016/j.bbagen.2014.02.002

Rønning, S. B., Carlson, C. R., Aronsen, J. M., Pisconti, A., Høst, V., Lunde, M., et al. (2020). Syndecan-4(-/-) mice have smaller muscle fibers, increased akt/mTOR/S6K1 and notch/HES-1 pathways, and alterations in extracellular matrix components. *Front. Cell Dev. Biol.* 8, 730. doi:10.3389/fcell.2020.00730

Rønning, S. B., Carlson, C. R., Stang, E., Kolset, S. O., Hollung, K., and Pedersen, M. E. (2015). Syndecan-4 regulates muscle differentiation and is internalized from the plasma membrane during myogenesis. *PloS one* 10 (6), e0129288. doi:10.1371/journal.pone.0129288

Sanden, K. W., Bocker, U., Ofstad, R., Pedersen, M. E., Host, V., Afseth, N. K., et al. (2021). Characterization of collagen structure in normal, wooden breast and spaghetti meat chicken fillets by FTIR microspectroscopy and histology. *Foods* 10 (3), 548. doi:10.3390/foods10030548

Schaefer, L., Babelova, A., Kiss, E., Hausser, H.-J., Baliova, M., Krzyzankova, M., et al. (2005). The matrix component biglycan is proinflammatory and signals through Toll-like receptors 4 and 2 in macrophages. *J. Clin. investigation* 115 (8), 2223–2233. doi:10.1172/JCI23755

Schellings, M. W. M., Vanhoutte, D., Almen, G. C. v., Swinnen, M., Leenders, J. J. G., Kubben, N., et al. (2010). Syndecan-1 amplifies angiotensin II–induced cardiac fibrosis. *Hypertension* 55 (2), 249–256. doi:10.1161/HYPERTENSIONAHA.109.137885

Schmittgen, T. D., and Livak, K. J. (2008). Analyzing real-time PCR data by the comparative CT method. *Nat. Protoc.* 3 (6), 1101–1108. doi:10.1038/nprot.2008.73

Sihvo, H. K., Immonen, K., and Puolanne, E. (2014). Myodegeneration with fibrosis and regeneration in the pectoralis major muscle of broilers. *Vet. Pathol.* 51 (3), 619–623. doi:10.1177/0300985813497488

Støle, T. P., Lunde, M., Shen, X., Martinsen, M., Lunde, P. K., Li, J., et al. (2022). The female syndecan-4$^{-/-}$ heart has smaller cardiomyocytes, augmented insulin/pSer473-Akt/pSer9-GSK-3β signaling, and lowered SCOP, pThr308-Akt/Akt and GLUT4 levels. *Front. Cell Dev. Biol.* 10, 908126. doi:10.3389/fcell.2022.908126

Strand, M. E., Herum, K. M., Rana, Z. A., Skrbic, B., Askevold, E. T., Dahl, C. P., et al. (2013a). Innate immune signaling induces expression and shedding of the heparan sulfate proteoglycan syndecan-4 in cardiac fibroblasts and myocytes, affecting inflammation in the pressure-overloaded heart. *FEBS J.* 280 (10), 2228–2247. doi:10.1111/febs.12161

Strand, M. E., Herum, K. M., Rana, Z. A., Skrbic, B., Askevold, E. T., Dahl, C. P., et al. (2013b). Innate immune signaling induces expression and shedding of the heparan sulfate proteoglycan syndecan-4 in cardiac fibroblasts and myocytes, affecting inflammation in the pressure-overloaded heart. *Febs J.* 280 (10), 2228–2247. doi:10.1111/febs.12161

Sztretye, M., Singlár, Z., Ganbat, N., Al-Gaadi, D., Szabó, K., Köhler, Z. M., et al. (2023). Unravelling the effects of syndecan-4 knockdown on skeletal muscle functions. *Int. J. Mol. Sci.* 24 (8), 6933. doi:10.3390/ijms24086933

Velleman, S. G. (2012). Meat Science and Muscle Biology Symposium: extracellular matrix regulation of skeletal muscle formation. *J. Anim. Sci.* 90 (3), 936–941. doi:10.2527/jas.2011-4497

Velleman, S. G. (2015). Relationship of skeletal muscle development and growth to breast muscle myopathies: a review. *Avian Dis.* 59 (4), 525–531. doi:10.1637/11223-063015-Review.1

Velleman, S. G. (2020). Pectoralis major (breast) muscle extracellular matrix fibrillar collagen modifications associated with the wooden breast fibrotic myopathy in broilers. *Front. Physiology* 11, 461. doi:10.3389/fphys.2020.00461

Velleman, S. G., and Clark, D. L. (2015). Histopathologic and myogenic gene expression changes associated with wooden breast in broiler breast muscles. *Avian Dis.* 59 (3), 410–418. doi:10.1637/11097-042015-Reg.1

Velleman, S. G., Clark, D. L., and Tonniges, J. R. (2017). Fibrillar collagen organization associated with broiler wooden breast fibrotic myopathy. *Avian Dis.* 61 (4), 481–490. doi:10.1637/11738-080217-Reg.1

Velleman, S. G., and Song, Y. (2017). Development and growth of the avian pectoralis major (breast) muscle: function of syndecan-4 and glypican-1 in adult myoblast proliferation and differentiation. *Front. physiology* 8, 577. doi:10.3389/fphys.2017.00577

Wold, J. P., Måge, I., Løvland, A., Sanden, K. W., and Ofstad, R. (2019). Near-infrared spectroscopy detects woody breast syndrome in chicken fillets by the markers protein content and degree of water binding. *Poult. Sci.* 98 (1), 480–490. doi:10.3382/ps/pey351

Wold, J. P., O'Farrell, M., Tschudi, J., Eskildsen, C. E., Andersen, P. V., and Ottestad, S. (2020). In-line and non-destructive monitoring of core temperature in sausages during industrial heat treatment by NIR interaction spectroscopy. *J. Food Eng.* 277, 109921. doi:10.1016/j.jfoodeng.2020.109921

Wold, J. P., Veiseth-Kent, E., Høst, V., and Løvland, A. (2017). Rapid on-line detection and grading of wooden breast myopathy in chicken fillets by near-infrared spectroscopy. *PLOS ONE* 12 (3), e0173384. doi:10.1371/journal.pone.0173384

Wu, F., Vij, N., Roberts, L., Lopez-Briones, S., Joyce, S., and Chakravarti, S. (2007). A novel role of the lumican core protein in bacterial lipopolysaccharide-induced innate immune response. *J. Biol. Chem.* 282 (36), 26409–26417. doi:10.1074/jbc.M702402200

Wu, T., Hu, E., Xu, S., Chen, M., Guo, P., Dai, Z., et al. (2021). clusterProfiler 4.0: a universal enrichment tool for interpreting omics data. *Innov. (Camb)* 2 (3), 100141. doi:10.1016/j.xinn.2021.100141

Xian, X., Gopal, S., and Couchman, J. R. (2009). Syndecans as receptors and organizers of the extracellular matrix. *Cell Tissue Res.* 339 (1), 31–46. doi:10.1007/s00441-009-0829-3

Xing, T., Luo, D., Zhao, X., Xu, X., Li, J., Zhang, L., et al. (2021a). Enhanced cytokine expression and upregulation of inflammatory signaling pathways in broiler chickens affected by wooden breast myopathy. *J. Sci. Food Agric.* 101 (1), 279–286. doi:10.1002/jsfa.10641

Xing, T., Zhao, X., Zhang, L., Li, J. L., Zhou, G. H., Xu, X. L., et al. (2020). Characteristics and incidence of broiler chicken wooden breast meat under commercial conditions in China. *Poult. Sci.* 99 (1), 620–628. doi:10.3382/ps/pez560

Xing, T., Zhao, Z. R., Zhao, X., Xu, X. L., Zhang, L., and Gao, F. (2021b). Enhanced transforming growth factor-beta signaling and fibrosis in the pectoralis major muscle of broiler chickens affected by wooden breast myopathy. *Poult. Sci.* 100 (3), 100804. doi:10.1016/j.psj.2020.10.058

Yu, G., Wang, L.-G., Han, Y., and He, Q.-Y. (2012). clusterProfiler: an R Package for comparing biological themes among gene clusters. *OMICS* 16 (5), 284–287. doi:10.1089/omi.2011.0118

Zanotti, S., Negri, T., Cappelletti, C., Bernasconi, P., Canioni, E., Di Blasi, C., et al. (2005). Decorin and biglycan expression is differentially altered in several muscular dystrophies. *Brain* 128 (Pt 11), 2546–2555. doi:10.1093/brain/awh635

Zhao, W., Wang, X., Sun, K.-H., and Zhou, L. (2018). α-smooth muscle actin is not a marker of fibrogenic cell activity in skeletal muscle fibrosis. *PLOS ONE* 13 (1), e0191031. doi:10.1371/journal.pone.0191031

frontiers | Frontiers in Physiology

TYPE Original Research
PUBLISHED 20 May 2024
DOI 10.3389/fphys.2024.1397442

OPEN ACCESS

EDITED BY
Sandra G Velleman,
The Ohio State University, United States

REVIEWED BY
Massimiliano Petracci,
University of Bologna, Italy
Servet Yalcin,
Ege University, Türkiye

*CORRESPONDENCE
Casey M. Owens,
cmowens@uark.edu

RECEIVED 07 March 2024
ACCEPTED 23 April 2024
PUBLISHED 20 May 2024

CITATION
Maynard CJ, Gonzalez JM, Haginouchi T, Ellis OG, Jackson AR and Owens CM (2024), Effects of nicotinamide riboside *in ovo* feeding on high-yield broiler performance, meat quality, and myopathy incidence.
Front. Physiol. 15:1397442.
doi: 10.3389/fphys.2024.1397442

Effects of nicotinamide riboside *in ovo* feeding on high-yield broiler performance, meat quality, and myopathy incidence

Clay J. Maynard[1], John M. Gonzalez[2], Taketo Haginouchi[3], Olivia G. Ellis[2], Ashunti R. Jackson[4] and Casey M. Owens[1]*

[1]Department of Poultry Science, University of Arkansas, Fayetteville, AR, United States, [2]Department of Animal and Dairy Science, University of Georgia, Athens, GA, United States, [3]Department of Agriculture, Kagoshima University, Kagoshima, Japan, [4]Cobb-Vantress Inc., Siloam Springs, AR, United States

Introduction: The objective of this study was to examine the effects of *in ovo* nicotinamide riboside (NR) feeding on high-yield broiler growth and meat quality.

Methods: Fertilized Cobb 700 by-product eggs (N = 3,240) were randomly assigned to one of four in ovo treatments and injected with 0 (**0NR**), 250 (**250NR**), 500 (**500NR**), or 1,000 (**1,000NR**) mM NR at incubation-day 10. Chicks were hatched, vent sexed, and randomly placed 18 per pen in one of 32 floor pens. On day 48, birds were processed and deboned.

Results: There were dose effects for all part weights ($p < 0.05$). Pectoralis major weight of 250, 500, and 1,000NR carcasses were heavier than 0NR ($p < 0.03$) but did not differ from remaining NR doses ($p > 0.26$). Pectoralis minor weight of 250NR carcasses was greater ($p < 0.01$) than 0NR and did not differ from other NR tenders ($p > 0.21$). Pectoralis minor weight of 500 and 1,000NR carcasses was greater than 0NR ($p < 0.09$), but did not differ ($P = 0.82$) from each other. There were no dose effects for all Pectoralis major and minor myopathy scores and incidence except incidence of tenders scoring "0" and "1" for woody-like tender. Percentage of NR1,000 tenders scoring 0 and 1 for woody-like tender were less than and greater than all other treatments, respectively ($p < 0.05$). There were no differences among remaining NR doses and NR0 tenders ($p > 0.10$). There were dose effects for muscle fiber number ($P = 0.03$). There tended to be more muscle fibers within 250 and 1,000NR muscles compared to 0NR ($p < 0.09$). Pectoralis major muscle from 500NR did not differ in muscle fiber number compared to 250 and 1,000NR ($p > 0.18$), but had more ($p < 0.01$) fibers than 0NR muscle. There tended to be more fibers in 250 and 1,000NR muscles compared to 0NR muscle ($p < 0.09$).

Discussion: Nicotinamide riboside in ovo feeding caused birds to produce heavier parts; however, myopathy scores and incidence were minimally affected which may have been due greater muscle fiber number.

KEYWORDS

breast myopathies, broiler, meat quality, muscle fiber, vitamin B3

1 Introduction

Over the past 75 years, broiler muscle growth and processing yields have increased substantially. Zuidhof et al. (2014) reported that the broiler industry produced a broiler that utilized half the feed of their ancestors while increasing the breast meat yield by 67%. Since this publication, the industry has advanced these improvements. This is not only economically important but is also very sustainable to continue to meet the ever-growing demand for poultry. Velleman (2019) suggested that genetic selection improvements came from selected birds expressing greater hypertrophic growth. Compared to the ancestral bird, the majority of this growth is due to the modern bird producing more muscle fibers, which are larger (Velleman, 2007). Additionally, although these advancements have improved efficiency and yield, the occurrence of muscle myopathies has become a major issue, which Kuttappan et al. (2016) estimated to cost the industry up to $1 billion per year. Many current myopathy mitigation strategies employed by the commercial industry revolve around managing the bird's post-hatch growth rate; however, embryonic muscle development and growth manipulation may reduce myopathy incidence and severity.

Embryonic avian muscle development and growth occur in a two-step fashion. Primary myogenesis occurs between embryonic development days 3 and 7 (Ordahl et al., 2001), and secondary myogenesis begins between embryonic development days 8 and 9 (Kahane and Kalcheim, 1998). Secondary fiber formation allows for denser fibers to be present at birth and a greater satellite cell pool (Halevy et al., 2003; Velleman, 2007). Moreover, embryonic satellite cell creation is crucial to supporting post-hatch skeletal muscle growth and repair (Halevy et al., 2000; Halevy et al., 2003). Because the sequence of events associated with myogenesis is routine, many researchers have investigated *in ovo* feeding of numerous compounds to affect muscle fiber and satellite cell formation (Kocamis et al., 1999; Ohta et al., 2001; Grodzik et al., 2013). There has been extensive use of *in ovo* injections to improve the health and performance of poultry. A wide range of substances have been studied, with some showing positive or negative effects, while neutral effects have also been observed (Oliveira, et al., 2023). Growth performance, especially the growth of the *pectoralis major* (breast muscle), has been of great interest. Dayan et al. (2023) used *in ovo* feeding of creatine monohydrate (**CM**) to affect energy reserves and breast muscle development. *In ovo* feeding of CM resulted in a higher breast muscle % at hatching and a higher number of myofibers with a smaller diameter by day 14, suggesting a positive impact on breast muscle development.

The use of nicotinamide riboside (**NR**), a vitamin B_3 analog, has shown progressive steps in defending against muscle degenerative factors (Mehmel et al., 2020). In the experiment by Zhang et al. (2016), the authors reported that NR-supplemented mice had greater nicotinamide adenine dinucleotide (**NAD^+**) concentration and satellite cell proliferation. In commercial and high-yield broilers, *in ovo* injection with NR concentrations ranging between 250 and 1,000 nM resulted in increased weight of the hatched-chick *pectoralis major* muscle and muscle fiber density (Gonzalez and Jackson, 2020; Xu et al., 2021; Xu et al., 2022). Xu et al. (2021) also reported that the satellite cell number increased with *in ovo* NR feeding. All the experiments demonstrated NR's ability to positively influence embryonic muscle development and growth, but its effectiveness on growth performance, meat quality/yield, and myopathy scores were not assessed. Therefore, the objective of the current experiment was to evaluate four concentrations of NR, injected on day 10 of incubation, on broiler performance, carcass characteristics, and muscle myopathy occurrence when grown to 48 days post-hatching.

2 Materials and methods

2.1 Animal use statement

All animal procedures were approved by the Institutional Animal Care and Use Committee of the University of Arkansas (protocol # 22055).

2.2 Egg procurement and incubation

Fertilized Cobb 700 by-product broiler eggs were obtained from a primary breeder (N = 3,240; Cobb-Vantress, Siloam Springs, AR; eggs sourced from Blairsville, GA) and transported to the University of Arkansas Poultry Research Farm. Upon arrival, the eggs were kept in a storage cooler at 16°C to be further processed. The eggs were examined, and those possessing cracks, chips, pips, heavy residue, misshapen, or double-yolk eggs were removed. After selection, egg trays with a tray capacity of 84 eggs (Model #PB3179B, Jamesway Incubator Co., Cambridge, Ontario, Canada) were loaded on a trolly and placed in a commercial single-stage incubator (N = 3,158; Model #PS500 Incubator; Jamesway Incubator Co., Cambridge, Ontario, Canada) that was set to 37.5°C and 85% relative humidity. On incubation day 10, the trays were removed from the incubator, candled to identify infertile eggs, and then assigned to one of four **NR** injection concentrations in the form of NIAGEN® (ChromaDex, Los Angeles, CA, United States).

2.3 Injection procedure

Injection procedures were performed according to the protocol of Gonzalez and Jackson (2020). In brief, four concentrations of NR were mixed: 0 (**0-NR**), 250 (**250-NR**), 500 (**500-NR**), and 1,000 (**1,000-NR**) mM NR in a 0.9% saline solution (n = 534 eggs per treatment). Eggs were removed from the incubation trays and candled to determine the yolk location. Once the yolk location was determined, 70% methanol was used to clean the exterior surface of the shell's concave curve, and a 2.54 cm, 20-gauge hypodermic needle was used to pip the shell for injection. The injection needle was inserted approximately 1 cm into the yolk sack, and 100 µL of the solution was slowly depressed to not force amniotic fluid out of the egg. A 1-cm^2 portion of medical tape (Nexcare, 3M, Maplewood, MN, United States) was then applied over the injection site, and the eggs were returned to the incubator. In an attempt to reduce the thermocycling effects on embryo development upon removal from the incubator, the eggs were held at ~27°C before injection.

2.4 Hatching, sexing, and husbandry

On incubation day 18, the eggs were candled to detect early dead embryos and transferred to hatching baskets (Model #PB600; Jamesway Incubator Co., Cambridge, Ontario, Canada) arranged by treatment and covered with basket tops (Model #PB3179B; Jamesway Incubator Co., Cambridge, Ontario, Canada). A stack of 10 trays was utilized in this design, with an empty basket on the bottom to provide proper airflow according to the manufacturer's recommendation. The baskets were transitioned to a commercial hatcher (Model #PS500 Hatcher; Jamesway Incubator Co., Cambridge, Ontario, Canada). The conditions were set to meet industry standards, with an average temperature of 36.7°C and a relative humidity of 88%. On day 21, the broiler chicks were removed from the hatcher by treatment and vent-sexed by trained personnel.

Five-hundred seventy-six hatch-day male Cobb 700 by-product broiler chicks were separated by treatment, group-weighed by pen (N = 18 birds/pen), and placed into 32-floor pens (1.2 × 1.82 m; ~0.12 m^2 per bird; n = 8 pens/treatment). The experimental pens consisted of a used litter top dressed with fresh pine shavings, a hanging feeder, and a section of nipple-drinker water line with five nipples. The birds were allowed *ad libitum* access to food and water throughout the trial. Internal research house conditions were held constant at a set point temperature of 32°C when placed. The environmental temperature was reduced by ~2°C weekly until an endpoint temperature of ~17.7°C was met. Lighting was maintained from hours of light (**L**) to hours of darkness (**D**) as follows: 24L:0D from day 0–1, 23L:1D from days 1–7, and 16L:8D from days 7–48 (Maynard et al., 2019). A crumbled starter diet was fed from day 0 to day 14, whereas pelleted grower, finisher, and withdrawal diets were fed from 15 to 28, 29 to 42, and 43 to 48 days of age, respectively (Table 1). Bi-weekly body weight (**BW**) and feed consumption (**FI**) were recorded on a pen basis and used to calculate individual body weight gain (**BWG**) and mortality corrected feed conversion ratio (**FCR**). Mortality and the number of culled birds were assessed twice daily.

2.5 Processing and myopathy scoring

All broilers were individually tagged to maintain their identity throughout processing. Following a 10-h feed withdrawal period, birds from each pen were transported to the University of Arkansas pilot processing plant and individually weighed upon arrival. The birds were hung on inline shackles, electrically stunned (11 V and 11 mA for 11 s), exsanguinated (2 min), scalded in hot water (54.4°C, 2 min), and de-feathered (Mehaffey et al., 2006). Prior to mechanical evisceration, the necks and hocks were removed from each carcass, and the carcasses were weighed to record the hot carcass weight. Carcasses were subjected to a 0.25-h prechill at 12°C before being placed in 0°C immersion chilling tanks for 2.5 hours with manual agitation. At 3-h *postmortem*, the chill tanks were drained, and the carcasses were removed and reweighed to determine the chilled carcass weight. Chilled carcasses were deboned to determine *pectoralis major* (breast) and *pectoralis minor* (tender), wing, whole leg, and rack weights. The part weights were divided by individual back dock live weights to determine the relative part yields. Post-deboning, boneless breast butterflies and tenders were collected for further analysis.

Breast fillets were placed dorsal side down, and muscle thickness, length, and width at one-third the length from the caudal end were measured. Measurements were recorded by a single trained person continuously throughout using a calibrated caliper (Model 500-764-10* IP67, Mitutoyo U.S.A., Aurora, IL) according to the procedures outlined by Maynard et al. (2023).

Boneless breast butterflies were visually scored for white striping (**WS**) and woody breast (**WB**) by a single individual utilizing the palpation method. The measurements ranged from 0 to 3 in increments of 0.5, with 0 being myopathy absence and 3 being the most severe following the scales presented by Kuttappan et al. (2012) and Tijare et al. (2016), respectively. To reduce person-to-person variability, one trained person scored all fillets.

Tenders were scored for woody-like tender (**WT**) and tender feather (**TF**) utilizing the same palpation technique as for breast butterflies. All tenders were evaluated according to Maynard et al. (2023) and classified on a scale of 0–2, with half-point increments. Tenders that expressed no palpable hardness were given a 0 or 0.5 (normal/slight) score, tenders with hardness localized in the cranial region with flexibility in the caudal region received a 1 or 1.5 score, and finally, tenders with complete atrophy from green muscle disease were given a 2 score for WT. A score of 0 was considered if no visible fiber fraying was present or a 0.5 if two splits in the muscle were observed for TF. A score of 1 or 1.5 was considered if moderate fiber fraying was present (>2 split fibers per muscle), and lastly, a score of 2 was considered if severe fiber fraying was present throughout, paired with a soft texture. Attempting to reduce variability, a single trained individual scored all tenders.

Myopathy scoring was collapsed to match a 3-point scale prior to statistical analysis to produce pen occurrences. Scoring ranges were assigned as 0 for scores originally given a 0 or 0.5, 1 for scores originally given a 1 or 1.5, and 2 for scores given a 2, 2.5, or 3 originally.

2.6 Meat quality measurements

Butterflies were inverted (dorsal side up) on white plastic storage trays, and the instrumental color was recorded on each left fillet at 24-h *postmortem*. The color was recorded according to American Meat Science Association (AMSA), (2012) guidelines using a Minolta colorimeter equipped with SpectraMagic NX software (Minolta CM-400, Konica Minolta Sensing Americas Inc., Ramsey, N.J., United States). Prior to analysis, the colorimeter was calibrated to CIE specifications using a white calibration tile. Color readings were recorded using the D_{65} illuminant set with a 2-degree observer to decrease sample surface reflectance, and the aperture size was 8 mm. Three separate L*, a*, and b* values were measured for each fillet in the cranial, medial, and caudal locations, which were subsequently averaged.

Following color measurements, pH was calculated in the left-fillet wing-joint portion at 24-h *postmortem* using a calibrated spear-tip pH probe (Model 205, Testo instruments, West Chester, Pennsylvania, United States) inserted into each fillet and allowed to equilibrate for 3 seconds before recording. The pH meter was

10.3389/fphys.2024.1397442

TABLE 1 Experimental starter (0–14 d), grower (15–28 d), finisher (29–42 d), and withdrawal diets (43–48 d) fed to male Cobb 700 by-product broilers from 0 to 48 days of age.

Item, % as-fed	Starter	Grower	Finisher	Withdrawal
Corn	51.64	57.70	60.40	63.71
Soybean meal	41.60	35.43	31.88	29.25
Poultry fat	2.97	3.45	4.56	4.05
DL-methionine	0.40	0.36	0.34	0.31
L-lysine-HCL	0.22	0.26	0.22	0.22
L-threonine	0.16	0.15	0.13	0.12
L-valine	0.04	0.07	0.05	0.04
Dicalcium phosphate	0.89	0.79	0.67	0.64
Limestone	1.25	0.95	0.91	0.87
Salt	0.45	0.45	0.45	0.45
Vitamin and mineral premix[a]	0.15	0.15	0.15	0.15
Choline chloride (60%)	0.09	0.10	0.09	0.10
OptiPhos Plus (1,000 FTU)	0.01	0.01	0.01	0.01
Coccidiostat[b]	0.05	0.05	0.05	0.00
Filler[c]	0.08	0.08	0.08	0.08
Calculated composition, % unless noted otherwise				
AME, kcal/kg	3,000	3,100	3,200	3,200
CP	23.35	21.00	19.50	18.50
Ca	1.00	0.84	0.78	0.75
Available P	0.45	0.42	0.39	0.38
Na	0.18	0.18	0.18	0.18
Digestible Lys	1.32	1.21	1.10	1.04
Digestible TSAA	1.00	0.91	0.86	0.81
Digestible Thr	0.90	0.81	0.74	0.70
Digestible Val	0.99	0.92	0.84	0.79
Digestible Ile	0.87	0.78	0.72	0.68
Digestible Arg	1.44	1.27	1.17	1.10
Digestible Trp	0.26	0.23	0.21	0.20

[a]The vitamin and mineral premix contained (per kg of complete feed) manganese, 100.0 mg; zinc, 100.0 mg; iron, 50.0 mg; copper, 11.3 mg; iodine, 1.5 mg; selenium, 0.2 mg; vitamin A, 7716 IU; vitamin D_3, 2756 ICU; vitamin E, 17 IU; vitamin B_{12}, 0.01 mg; menadione, 0.83 mg; riboflavin, 6.61 mg; d-pantothenic acid, 6.61 mg; thiamine, 1.10 mg; niacin, 27.56 mg; pyridoxine, 1.38 mg; folic acid, 0.69 mg; biotin, 0.03 mg; and choline, 385.81 mg.
[b]Supplied 60 g of salinomycin Na per 907.2 kg of complete feed to prevent coccidiosis.
[c]Sand was considered as filler.

calibrated to American Meat Science Association (AMSA), (2012) guidelines, utilizing two solutions of 4 and 7.

All breast butterflies were collected, arranged on white plastic storage trays, and wrapped in plastic overwrap film. After 24 h at 4°C, the butterflies were removed, patted dry with a paper towel, and reweighed to determine drip loss. Drip loss was calculated using the percent loss method in relation to deboned-part weight.

Fillets were excised down the center line, individually tagged, reweighed, and placed eight in a vacuum seal bag prior to storage at −20°C in a blast freezer for 21 days. Fillets were removed from the freezer and allowed to thaw for 48 h at 4°C before being patted dry and reweighed to determine relative thawing loss. While weighing, fillets of relative size (within 75 g) were then placed in aluminum foil-covered baking pans, eight to a pan (65 × 395 × 290 mm), on elevated baking racks, and then covered with aluminum foil tented in the center. Fillets were cooked in a commercial convection oven (Model E101-E, Duke Manufacturing Company, St. Louis, Missouri, United States), held at 167°C, and cooked to a final end-point

10.3389/fphys.2024.1397442

TABLE 2 Live performance of male Cobb 700 by-product broilers injected with one of four nicotinamide riboside (vitamin B_3 complex) concentrations on incubation day 10 and reared to 47 days of age.

	Nicotinamide riboside[a], mM					
	0	250	500	1,000	SEM	*p*-value
0 to 14						
Body weight, kg	0.39	0.41	0.40	0.40	0.006	0.11
Body weight gain, kg	0.35	0.37	0.35	0.36	0.006	0.12
Feed intake, kg	0.45	0.46	0.44	0.45	0.008	0.46
Feed conversion rate	1.33	1.32	1.33	1.34	0.029	0.95
0 to 28						
Body weight, kg	1.56[a]	1.61[b]	1.55[a]	1.58[a,b]	0.017	0.09
Body weight gain, kg	1.52[a]	1.57[b]	1.51[a]	1.54[a,b]	0.017	0.09
Feed intake, kg	1.99	2.04	1.99	2.04	0.040	0.64
Feed conversion rate	1.35	1.34	1.36	1.37	0.015	0.44
0 to 42						
Body weight, kg	3.21[a]	3.34[b]	3.22[a,b]	3.27[a,b]	0.036	0.05
Body weight gain, kg	3.17[a]	3.30[b]	3.18[a,b]	3.23[a,b]	0.036	0.05
Feed intake, kg	4.52	4.66	4.52	4.62	0.066	0.31
Feed conversion rate	1.47	1.45	1.47	1.47	0.011	0.36
0 to 47						
Body weight, kg	3.87[a]	4.05[b]	3.92[a,b]	4.02[a,b]	0.046	0.04
Body weight gain, kg	3.83[a]	4.01[b]	3.88[a,b]	3.98[a,b]	0.046	0.04
Feed intake, kg	5.63	5.81	5.69	5.77	0.067	0.26
Feed conversion rate	1.50	1.48	1.51	1.50	0.011	0.27

[a,b]Means without a common superscript within a row are significantly different ($p \leq 0.05$).
[a]Nicotinamide riboside mixed in 0.9% saline.

temperature of 74°C, which was verified using a handheld thermometer (Model HT1000 thermometer, Cooper Instruments, Concord, Canada). Fillets were removed from the baking sheet and placed on trays to cool to room temperature (~21°C) while covered with loose aluminum foil. Fillets were reweighed to determine cook loss as the percent weight from the initial thaw loss weight. After being weighed, fillets were individually wrapped in aluminum sheets (305 × 273 mm) and stored overnight in a 4°C cooler prior to instrumental texture analysis.

Instrumental tenderness was determined using the Meullenet–Owens Razor Shear method presented by Cavitt et al. (2004). Fillets were sheared perpendicular to the muscle fibers in four separate cranial locations using a texture analyzer (Model TA-XT2 Plus, Texture Technologies, Scarsdale, N.Y., United States). A 5-kg load cell using a razor blade with a height of 24 mm and a width of 8.9 mm was set to a 20 mm penetration depth. The machine crosshead speed was set at 5 mm/s and was triggered by a 5 g contact force. Data points were collected with an acquisition rate of 200 points per second, and the shear data included MORS force (MORSF, N) and MORS energy (MORSE, N.mm) values per sample.

2.7 Breast cross-sectional area and muscle fiber morphometrics

Breast fillet cross-sectional area (CSA) was collected for two broilers from each pen. Once deboned and scored, fillets were excised down the keel line and again excised down the center of the left fillet at the thickest point to provide the largest footprint of each fillet. Once excised, the largest area was blotted on a sheet of legal paper (22 × 36 cm), outlined with a fine-tip black marker, and a 2.54-cm line was drawn. Papers were scanned using a Xerox scanner (Model #: WorkCentre 5,845; Xerox Corporation, Norwalk, CT; 1,200 × 1,200 dpi), and images were converted to jpeg files for analysis using ImageJ (National Institutes of Health, Bethesda, MD, United States). Images were calibrated using the 2.54-cm line, and the area of the breast fillet (CSA) was measured as the area within the black marker boundary.

Immunohistochemistry analysis was conducted according to Gonzalez and Jackson (2020). In brief, two cryosections (10 µm) were collected on positively charged slides (Diamond White Glass; Globe Scientific Inc., Paramus, NJ., United States) and incubated in 5% horse serum and 0.2% Triton X-100 in phosphate-buffered saline (PBS) for 30 min. Cryosections were incubated at room temperature for 45 min with a blocking solution containing 1:1,000 wheat germ agglutinin-Alexa Fluor 594 (cat no. W11262; Thermo Fischer Scientific, Waltham, MA, United States), washed three times with PBS for 5 min, and 5 µL of 9:1 glycerol in PBS were placed on each cryosection and coverslip for imaging.

Cryosections were visualized at 100-fold magnification using an ECHO Revolve Microscope (ECHO, San Diego, CA, United States). Photomicrographs were collected, stored, and analyzed using ECHO Pro software (ECHO) operating on an iPad Pro (Apple, Cupertino, CA, United States). The cross-sectional area was determined for 1,000 fibers (minimum) as the area within the wheat germ agglutinin

TABLE 3 Back dock live weight, carcass, and part yields of male Cobb 700 by-product broilers injected with one of four nicotinamide riboside (vitamin B_3 complex) concentrations on day 10 of incubation and reared to 48 days of age.

	Nicotinamide riboside[a], mM					
	0	250	500	1,000	SEM	*p*-value
Carcass weights, g						
Live	3,839[a]	3,999[b]	3,944[b]	3,952[b]	39	0.02
Hot carcass	2,938[a,x]	3,080[b]	3,013[a,y]	3,031[b]	32	<0.01
Cold carcass	3,010[a]	3,161[b]	3,094[b]	3,112[b]	32	<0.01
Part weights, g						
Breast	956[a]	1,013[b]	995[b]	994[b]	13	<0.01
Tender	164[a,x]	171[b]	168[a,b,y]	168[a,b,y]	2	0.03
Wing	291[a,x]	307[b]	305[b]	302[a,b,y]	4	0.03
Whole leg	860[a]	894[b]	862[a]	876[a,b]	10	0.05
Rack	717[a]	749[b]	742[b]	745[b]	8	<0.01
Yield[b], %						
Hot carcass	76.5[a]	77.1[b,x]	76.4[a]	76.6[a,b,y]	0.18	0.03
Cold carcass	78.4[a]	79.1[b,x]	78.5[a]	78.7[a,b,y]	0.15	<0.01
Breast	24.8	25.3	25.2	25.1	0.17	0.14
Tender	4.3	4.3	4.3	4.3	0.03	0.94
Wing	7.6	7.7	7.7	7.7	0.01	0.70
Whole leg	22.3[a]	22.3[a]	21.9[b]	22.1[a,b]	0.13	0.01
Rack	18.7	18.8	18.8	18.9	0.08	0.22

[a,b,c]Means without a common superscript within a row are different ($p < 0.05$).
[x,y]Means without a common superscript by row tended to be different ($0.05 < p \leq 0.10$).
[a]Nicotinamide riboside mixed in 0.9% saline.
[b]Yields based on back dock live weights taken immediately prior to harvest.

border. Muscle fiber number was estimated by dividing the whole muscle CSA by the average muscle fiber CSA (Thayer et al., 2019).

2.8 Statistical analysis

Data were analyzed as a completely randomized design, with the pen as the experimental unit for live parameters and myopathy scores, while the bird served as the experimental unit for all other measures. The nicotinamide riboside dose served as the fixed effect, and the pen-analyzed data utilized the pen as the random effect. Data were analyzed with the mixed procedure of SAS 9.4 (SAS Inst. Inc., Cary, NC). Pairwise comparisons between the least squares means of the factor level comparisons were computed using the PDIFF option of the LSMEANS statement. Statistical significance was considered at $p \leq 0.05$. Tendencies were declared at $0.05 < p \leq 0.10$.

3 Results

All live performance results for the rearing period until day 47 can be found in Table 2. There were no dose effects for all 0-to-14-day performance characteristics and the remainder of the periods' FI and FCR ($p > 0.11$). There tended to be dose effects for 0- to 28-day BW and BWG ($p = 0.09$). Broilers from the 250-NR treatment group had greater BW and BWG compared to 0-NR and 500-NR broilers ($p < 0.04$) but did not differ ($p = 0.24$) from 1,000-NR broilers. Body weight and BWG did not differ among 0-NR, 500-NR, and 1,000-NR broilers ($p > 0.23$). There were dose effects for 0–42 and 0–47-day BW and BWG ($p < 0.05$). During both periods, 250-NR broilers had greater BW and BWG than 0-NR broilers ($p < 0.05$) but did not differ from other NR broilers ($p > 0.10$). Broilers from embryos injected with 0-NR did not differ in BW or BWG compared to broilers that received the other NR treatments ($p > 0.10$).

There were dose effects for all carcass weights, part weights, and yield percentages ($p < 0.03$), except breast, tender, wing, and rack yields ($p > 0.14$; Table 3). Birds from all NR treatments had greater live and cold carcass weights than 0-NR birds ($p < 0.05$) but did not differ from each other ($p > 0.16$). Carcasses from 250-NR to 1,000-NR had greater hot carcass weights than 0-NR carcasses ($p < 0.03$), while 500-NR carcasses tended ($p = 0.07$) to be heavier than 0-NR carcasses.

Breast and rack weights were greater for all NR treatments compared to 0-NR ($p < 0.03$), but they did not differ from each other ($p > 0.26$). Tender weights from 250-NR carcasses weighed more ($p < 0.01$) than 0-NR tenders but did not differ from 500- or 1,000-NR tenders ($p > 0.21$). Tender weights from 500- and 1,000-NR carcasses did not differ ($p = 0.82$) but tended to be greater than 0-NR tenders ($p < 0.09$). Wing weights from 250- and 500-NR carcasses did not differ ($p = 0.68$) but were greater than 0-NR wings ($p < 0.02$). Wing weights from 1,000-NR carcasses did not differ from 250- or 500-NR wings ($p > 0.40$) but tended to be greater ($p < 0.06$) than 0-NR wings. Whole-leg weights from 250-NR carcasses were greater than 0- and 250-NR weights ($p < 0.03$), but all other comparisons were not different from each other ($p > 0.21$).

Hot and cold carcass yields from 250-NR carcasses were greater than those of 0- and 500-NR carcasses ($p < 0.01$) and only tended to be greater than 1,000-NR carcasses ($p < 0.10$). Hot and cold carcass yields from 0-, 500-, and 1,000-NR did not differ ($p > 0.11$). Whole-leg yields from 500-NR carcasses did not differ ($p > 0.13$) from 1,000-NR yields but were greater than 0- and 250-NR yields ($p < 0.01$). Whole-leg yields from 0-, 250-, and 1,000-NR did not differ ($p > 0.15$).

There were no dose effects for all *pectoralis major* and *minor* myopathy scores ($p > 0.19$), except for tendencies for WT 0 and 1 scores ($p < 0.08$; Table 4). Percentages of 1,000-NR tenders scoring 0 and 1 for woody-like tender were less than and greater than all other treatments, respectively ($p < 0.05$). There were no differences among the remaining treatment groups ($p > 0.10$).

There were no dose effects for all raw and cooked meat measures ($p > 0.11$), except for b* value ($p = 0.02$, Table 5). Breast b* values of 500- and 1,000-NR breasts were greater than those of 0-NR breasts ($p < 0.05$) but did not differ ($p > 0.10$) from each other. The b* value of 250-NR breasts did not differ from that of all other treatments ($p > 0.10$).

There were no dose effects for whole breast width and thickness ($p > 0.41$), but there tended to be an effect ($p = 0.08$) for length (Table 6). Breasts from 0- and 250-NR birds did not differ from each other or 1,000-NR breasts ($p > 0.32$) but were longer than 500-NR breasts ($p < 0.04$). Breasts from 500- and 1,000-NR birds did not differ ($p = 0.14$) in length. There were no dose effects ($p = 0.22$) for breast muscle CSA, but there were effects for muscle fiber CSA and number ($p < 0.05$). Muscle fiber CSA from 500- and 1,000-NR

10.3389/fphys.2024.1397442

TABLE 4 *Pectoralis major* and *minor* myopathies of male Cobb 700 by-product broilers injected with one of four concentrations of nicotinamide riboside (vitamin B_3 complex) on day 10 of incubation and reared to 48 days of age.

Treatment[c] (*n* = 8)	Woody breast[a]				White striping[b]			
	Average	0, %	1, %	2, %	Average	0, %	1, %	2, %
0	1.02	42.19	39.12	17.93	1.27	6.93	61.30	31.77
250	1.17	29.53	49.78	20.69	1.42	1.74	54.69	43.57
500	1.14	30.85	47.56	21.59	1.34	3.88	59.54	36.58
1,000	1.16	29.65	42.94	27.41	1.36	7.39	53.95	38.66
SEM	0.064	4.625	0.501	4.450	0.051	1.920	4.082	4.436
p-value	0.22	0.14	0.45	0.51	0.19	0.15	0.52	0.32
	Woody-like tender[d]				Tender feathering[e]			
	Average	0, %	1, %	2, %	Average	0, %	1, %	2, %
0	0.37	91.97[a]	8.03[a]	0.00	0.82	48.99	38.38	12.63
250	0.44	89.21[a]	10.79[a]	0.00	0.81	48.10	40.51	11.39
500	0.41	90.60[a]	9.40[a]	0.00	0.74	51.39	41.71	6.90
1,000	0.41	73.32[b]	25.21[b]	1.47	0.82	45.00	42.64	12.36
SEM	0.030	5.294	5.141	0.735	0.065	3.969	3.598	2.475
p-value	0.42	0.06	0.08	0.40	0.77	0.72	0.85	0.34

[a,b]Means without a common superscript within a column are different ($p < 0.05$).
[a]Breast fillets were considered to have a score of 0, 1, or 2 for woody breasts if the fillet was flexible throughout, stiff in the cranial region, or stiff in the cranial and caudal regions, respectively.
[b]Breast fillets were considered to have a score of 0, 1, or 2 for white striping if the fillet displayed no visible stripes, stripes less than 1 mm, or stripes larger than 1 mm, respectively.
[c]Injection of 0.9% saline with 0, 250, 500, or 1,000 mmol of nicotinamide riboside.
[d]Tenders were considered to have a score of 0, 1, or 2 for woody-like tender if the fillet was flexible throughout, stiff in the cranial region, or stiff in the cranial and caudal regions, respectively.
[e]Tenders were considered to have a score of 0, 1, or 2 for tender feathering if the tender displayed no visible fiber fraying, moderate fiber fraying throughout, or severe fiber fraying throughout the length of the tender, respectively.

pectoralis major muscles did not differ from each other or 250-NR muscles ($p > 0.48$) but were larger than 0-NR fibers ($p < 0.03$). Muscle fiber CSA from 250-NR *pectoralis major* muscles tended to be larger ($p = 0.07$) than that of 0-NR fibers. There were more ($p < 0.01$) muscle fibers within 500-NR *pectoralis major* muscles when compared to 0-NR muscles, but the number did not differ from 250- and 1,000-NR muscles ($p > 0.18$). There tended to be more muscle fibers within 250 and 1,000-NR muscles compared to 0-NR muscles ($p < 0.09$).

4 Discussion

The responses in post-hatching BW and BWG observed in the current experiment are the first reported in the literature because previous studies harvested chicks from NR-injected embryos 24 h post-hatching. In all previous studies, BW among the control and birds from NR-injected embryos did not differ (Alcocer et al., 2021; Xu et al., 2021; Xu et al., 2022). The current data agree with this trend as there was no dose effect for day 0–14 BW and BWG; however, it should be noted that the effect was close to a tendency. The treatment effect on BW was apparent during the 0–28-day period, where 250- and 1,000-NR birds were heavier than 0-NR birds by 50 to 20 g, respectively. During the remaining two periods, 250-NR birds were heavier than 0-NR birds by 130 and 180 g, respectively, due to BWG improvements. Similar to foundational chick data (Alcocer et al., 2021; Xu et al., 2021; Xu et al., 2022), there was no BW or BWG advantage when NR was injected above the 250-mM dose. Although the exact biological mechanisms responsible for post-hatch growth remain unknown, current study data indicated that it may have taken more than 14 d of growth for enough protein to be synthesized for the increased muscle fiber formation of NR birds to result in weight differences.

Bekhit et al. (2019) suggested that vitamin B_3 (niacin) provided fresh meat color stability as a natural antioxidant. In a pilot study, Gonzalez et al. (2019) reported that dietary NR supplementation improved pork redness and color stability. In the current experiment, all broilers supplemented with NR *in ovo* had an increased yellowness but lacked any difference in redness or lightness compared to the control. Given the nature of vitamin B_3 as an antioxidant, there is reason to believe the vitamin itself provided some objective color variation, but due to the difference only being half a point, visual differences were probably not detectable by the human eye. In addition, the NR salt that was used in the current experiment to produce stock solutions was highly fluorescent in nature, giving it a severe yellow hue. Pigmentation attributed to this solution may have been a direct cause of increased yellowness in NR-injected broilers (Alcocer et al., 2021). In contrast, the relative lightness and redness of the fillets were unaffected, which could be a result of the antioxidant and color stability properties of the vitamin complex. No differences in pH were observed, and no research is currently available at this time to understand the effects of supplemented vitamins on pH progression in broilers.

Meat tenderness is important for consumer satisfaction. Nicotinamide riboside had no effect on the instrumental tenderness of broilers injected in comparison to the control. Dransfield and Sosnicki (1999) originally suggested stacking larger numbers of fibers in an area would produce an increase in toughness for broilers reared for meat production. Furthering

TABLE 5 Raw and cooked meat quality attributes of male Cobb 700 by-product broilers injected with one of four concentrations of nicotinamide riboside (vitamin B_3 complex) on day 10 of incubation and reared to 48 days of age.

Parameter (n = 101)	Nicotinamide riboside, mM				SEM	*p*-value
	0	250	500	1,000		
Raw measures						
pH[a]	5.91	5.95	5.91	5.90	0.020	0.33
Drip loss, %[b]	0.69	0.76	0.73	0.80	0.054	0.46
Thaw loss, %[b]	6.77	7.07	6.87	7.53	0.275	0.19
L*[c]	56.87	57.61	57.34	57.58	0.258	0.11
a*[c]	3.41	3.25	3.43	3.38	0.131	0.76
b*[c]	9.56[a]	10.06[a,b]	10.15[b]	10.16[a]	0.164	0.02
Cooked measures						
Cook loss[b], %	25.38	24.96	24.13	25.14	0.640	0.51
MORSF[d], N	14.07	13.25	13.63	13.84	0.269	0.13
MORSE[d], N.mm	196.97	186.41	188.89	192.72	3.902	0.19

[a,b]Means without a common superscript by row were determined to be different ($p \leq 0.05$).
[a]pH was collected 24 h *postmortem*.
[b]Drip loss was calculated as percent loss of fillets by weight from deboned weight. Thaw loss was calculated as percent loss of fillets by weight from drip loss weight. Cook loss was calculated as percent loss of fillets by weight from thaw loss weight.
[c]All color measurements were recorded on the dorsal side of breast fillets 24 h *postmortem*.
[d]Meullenet–Owens Razor Shear (MORS). F, force; E, energy.

TABLE 6 Effects of nicotinamide riboside (vitamin B_3 complex) dose on incubation day 10 on day-48 post-hatch Cobb 700 *pectoralis major* whole muscle and muscle fiber morphometrics.

Parameter (*n* = 24)	Nicotinamide riboside, mM				SEM	*p*-value
	0	250	500	1,000		
Whole breast morphometrics, cm						
Length	187.8[a]	186.9[a]	182.3[b]	185.6[a,b]	1.58	0.08
Width	106.0	108.3	104.8	106.8	1.46	0.41
Thickness	38.2	39.4	39.6	38.8	0.81	0.65
Muscle fiber morphometrics						
Breast CSA[a], cm	75.3	77.1	78.9	74.7	1.65	0.22
Fiber CSA[a], μm^2	6,187[a,x]	5,453[a,b,y]	5,160[b]	5,340[b]	297	0.05
Fiber number[3], # × 10^6	0.81[a,x]	0.98[a,b,y]	1.07[b]	0.95[a,b,y]	0.102	0.03

[a-b]Means without a common superscript by row were significantly different ($p \leq 0.05$).
[x,y]Means without a common superscript by row tended to be different ($0.05 < p \leq 0.10$).
[a]Cross-sectional area; CSA.

this notion, Ebarb et al. (2016) concluded that larger fibers (when fiber density decreased) produced tougher meat compared to smaller fibers (when fiber density increased). When considering the effects of the current experiment and past work by Xu et al. (2021), the number of muscle fibers increased linearly with NR injection concentration to 500 mmol NR. It is possible that the effect of sarcomere shortening due to early deboning (3-h *postmortem*) masked the effects of increased muscle fiber number.

In the first NR study, Gonzalez and Jackson (2020) reported that commercial-yield broilers injected with 250 mM NR as embryos had 38% heavier breasts than birds not injected with NR as embryos. Subsequently, Xu et al. (2021) found there was no increase in breast weight as the NR dose increased from 250 to 1,000 mM, and the weight increase averaged 35% when compared to controls. Using high-yield broilers, Xu et al. (2022) reported that supplementing 100× less NR during embryogenesis increased breast weight by 33%, and they hypothesized that high-yield broilers may require a smaller NR dose than commercial-yield broilers. When grown to market weight, breast weight increased for all birds from NR-injected embryos by 44.6 g (5%) compared to non-injected birds. Similar to chick studies, injecting NR at greater doses did produce an additional increase in breast weight.

The current study provides valuable insight into the *in ovo* feeding effects on the remaining carcass parts. On average, compared to 0-NR parts, injecting embryos with NR caused increases in tender, wing, and rack weights of 5, 14, and 28 g, respectively. Additionally, injecting embryos with 250 mM NR increased whole-leg weight by 34 g compared to 0-NR whole-leg weight. Increases in part weight would produce more salable product volume and return more profit to the

industry; however, part weight increases were not surprising because BW increased with NR administration.

The administration of 250 mM NR increased hot and cold carcass weights by 0.6% and 0.7%, respectively, compared to 0-NR carcasses, while the other two NR doses did differ. This difference in NR responses was mainly driven by the whole-leg increase. Except for whole-leg yield, the remaining part yields were unaffected by NR administration in the current experiment. Additionally, NR did not affect breast morphometric measures, but this could mainly be due to the small number measured, given that this was not the main objective of the study. In the work by Fatemi et al. (2021), *in ovo* injection of vitamin D_3 provided an increase in carcass yield and breast meat yield, with no effect on other carcass part yields. Although not the same vitamin, a breast yield response was not identified with NR injection. Kidd et al. (2004) reported that increasing amino acid density linearly improved breast meat yield. Typically, when a response is noted in leg yield, the opposite effect is noted in breast yield (Kidd et al., 2004). In the current experiment, amino acid concentration was elevated compared to breeder recommendations (Cobb-Vantress, 2019), which should have induced an increase in breast meat yield rather than leg yield. Even so, the response observed in leg yield is not fully understood.

According to Petracci et al. (2015), myopathies began to appear in the industry in the 1980s, and the two most prevalent myopathies, WS and WB, appeared in the 2010s. Condition severity can vary, and both have been associated with heavier, fast-growing birds, especially from high-yield broiler strains (2.72–4.54 kg BW; Kuttappan et al., 2013; Kuttappan et al., 2016; Mueller et al., 2023). Cruz et al. (2017) reported that 32% and 89% of commercial broilers exhibit WB when raised to 35 and 42 days of age, respectively. Therefore, raising broilers to heavier weights and greater ages to meet consumer demand is not attractive in terms of meat quality unless countermeasures to these conditions are developed. Despite increasing breast weight, almost 44 g in the current study, there were no dose effects on WB or WS scores or distributions. Average tender myopathy scores were unaffected by dose, and only 1,000-NR tenders had a 19% decline in "0" tenders with an 18% increase in "1" tenders compared to 0-NR. Using a four-point (0–3) system, Aguirre et al. (2020) demonstrated that the frequency of breasts scoring 2 or 3 increased dramatically when weights were greater than 1,000 g. Although histology was not conducted on tenders to understand the increased incidence of "1" scores, two interesting trends are seen within the data. First, it is encouraging that a dramatic shift in frequency was not seen with heavier breasts produced by NR birds. Second, the greatest increase in breast weight seen by 250-NR breasts did not result in greater WB or WS scores. Third, when NR was injected at smaller NR doses, tender myopathy "0" and "1" scores did not differ from 0-NR scores. Therefore, these results may indicate that NR injection provided a protective mechanism against rampant myopathy formation. Greene et al. (2020) reported that WB fillets had downregulated NAD^+ content compared to normal fillets, and Xu et al. (2021) found injecting NR at 1,000 mM increased hatched-chick NAD + content. While this could be a protective mechanism, an increased muscle fiber number could also have served as a protective mechanism.

In examining the studies documenting poultry muscle myopathies' biological origins, one theme becomes clear: enlarged muscle fiber diameter or CSA could be the mechanism initiating the muscle myopathy onset. Dransfield and Sosnicki (1999) were one of the first to report that fast-growing broilers had 42% larger muscle fibers than slow-growing birds. Daughtry et al. (2017) found that large 8-week-old Cobb 500 broilers had approximately 45% larger muscle fibers than small broilers. Additionally, the authors demonstrated that large broilers had a fiber distribution that shifted to the right compared to small broilers; further indicating that muscle fibers were larger in these birds. Clark and Velleman (2017) reported that muscle fibers were the largest in the antero-dorsal portion of the PM muscle, where WB was the most severe. Macrae et al. (2006) suggested that the muscle fibers of myopathy-affected poultry were reaching functional size constraints, which resulted in poor capillary development and reduced efficiency of oxygen delivery and waste removal. In the current study, breasts from NR-injected birds had 15% smaller muscle fibers, which resulted in them having approximately 233,000 (23%) more muscle fibers. While foundational NR studies could not estimate muscle fiber number, fiber density increases ranged between 34% and 75% based on the dose and broiler strain (Gonzalez and Jackson, 2020; Xu et al., 2021; 2022). Based on these results, it could be postulated that NR exhibits an effect on muscle growth and could potentially be utilized to promote muscle hyperplasia in growing broilers.

5 Conclusion

The *in ovo* NR feeding had minor performance effects but was able to produce heavier broilers. Producing heavier bird-produced part weights could add millions of pounds of meat available for sale, depending on market conditions. This could result in billions of dollars of extra revenue. There were no detrimental effects on traditional meat quality measurements, and only tender myopathy incidence was negatively affected. Adding 44 more grams of breast weight without greatly affecting myopathy incidence could be due to NR birds' increase in muscle fiber number, but other mechanisms also need to be explored.

Data availability statement

The raw data supporting the conclusion of this article will be made available by the authors, without undue reservation.

Ethics statement

The animal study was approved by the University of Arkansas Institutional Animal Care and Use Committee. The study was conducted in accordance with the local legislation and institutional requirements.

Author contributions

CM: writing–original draft, project administration, methodology, investigation, and data curation. JG: writing–review and editing, visualization, supervision, methodology, formal analysis, data curation, and conceptualization. TH: writing–review and editing and investigation. OE: writing–review

and editing and investigation. AJ: writing–review and editing and resources. CO: writing–review and editing, writing–original draft, visualization, supervision, resources, project administration, methodology, formal analysis, data curation, and conceptualization.

Funding

The author(s) declare that no financial support was received for the research, authorship, and/or publication of this article.

Acknowledgments

The authors would like to thank ChromaDex Inc. for their donation of the nicotinamide riboside utilized in the study. The authors would like to thank Cobb-Vantress, Inc. for egg donation.

Conflict of interest

Author AJ was employed by Cobb-Vantress Inc.

The remaining authors declare that the research was conducted in the absence of any commercial or financial relationships that could be construed as a potential conflict of interest.

Publisher's note

References

Aguirre, M. E., Leyva-Jimenez, H., Travis, R., Lee, J. T., Athrey, G., and Alvarado, C. Z. (2020). Evaluation of growth production factors as predictors of the incidence and severity of white striping and woody breast in broiler chickens. *Poul. Sci.* 99, 3723–3732. doi:10.1016/j.psj.2020.03.026

Alcocer, H. M., Xu, X., Gravely, M. E., and Gonzalez, J. M. (2021). In ovo feeding of commercial broiler eggs: an accurate and reproducible method to affect muscle development and growth. *J. Vis. Exp.* 2021, 1–10. doi:10.3791/63006

American Meat Science Association (AMSA) (2012). Meat color measurement guidelines. *Champaign (IL): AMSA*.

Bekhit, A. E. D. A., Morton, J. D., Bhat, Z. F., and Kong, L. (2019). in *Meat color: factors affecting color stability*. Editors L. Melton, F. Shahidi, and P. Varelis (United States: Academic Press/Elsevier).

Cavitt, L. C., Youm, G. W., Meullenet, J. F., Owens, C. M., and Xiong, R. (2004). Prediction of poultry meat tenderness using razor blade shear, allo-kramer shear, and sarcomere length. *J. Food Sci.* 69, 11–15. doi:10.1111/j.1365-2621.2004.tb17879.x

Clark, D. L., and Velleman, S. G. (2017). Spatial influence on breast muscle morphological structure, myofiber size, and gene expression associated with the wooden breast myopathy in broilers. *Poult. Sci.* 95, 2930–2945. doi:10.3382/ps/pew243

Cobb-Vantress (2019) *Cobb broiler management guide*.

Cruz, R. F. A., Vieira, S. L., Kindlein, L., Kipper, M., Cemin, H. S., and Rauber, S. M. (2017). Occurrence of white striping and wooden breast in broilers fed grower and finisher diets with increasing lysine levels. *Poult. Sci.* 96, 501–510. doi:10.3382/ps/pew310

Daughtry, M. R., Berio, E., Shen, Z., Suess, E. J. R., Shah, N., Geiger, A. E., et al. (2017). Satellite cell-mediated breast muscle regeneration decreases with broiler size. *Poult. Sci.* 96, 3457–3464. doi:10.3382/ps/pex068

Dayan, J., Melkman-Zehavi, T., Goldman, N., Soglia, F., Zampiga, M., Petracci, M., et al. (2023). In-ovo feeding with creatine monohydrate: implications for chicken energy reserves and breast muscle development during the pre-post hatching period. *Front. Physiol.* 14, 1296342. doi:10.3389/fphys.2023.1296342

Dransfield, E., and Sosnicki, A. A. (1999). Relationship between muscle growth and poultry meat quality. *Poult. Sci.* 78, 743–746. doi:10.1093/ps/78.5.743

Ebarb, S. M., Drouillard, J. S., Maddock-Carlin, K. R., Phelps, K. J., Vaughn, M. A., Burnett, D. D., et al. (2016). Effect of growth-promoting technologies on *Longissimus lumborum* muscle fiber morphometrics, collagen solubility, and cooked meat tenderness. *J. Anim. Sci.* 94, 869–881. doi:10.2527/jas.2015-9888

Fatemi, S. A., Alqhtani, A., Elliott, K. E. C., Bello, A., Zhang, H., and Peebles, E. D. (2021). Effects of the in ovo injection of vitamin D3 and 25-hydroxyvitamin D3 in Ross 708 broilers subsequently fed commercial or calcium and phosphorus-restricted diets. I. Performance, carcass characteristics, and incidence of woody breast myopathy. *Poult. Sci.* 100, 101220. doi:10.1016/j.psj.2021.101220

Gonzalez, J. M., and Jackson, A. R. (2020). In ovo feeding of nicotinamide riboside affects broiler pectoralis major muscle development. *Transl. Anim. Sci.* 4, txaa126–7. doi:10.1093/tas/txaa126

Gonzalez, J. M., Paulk, C. B., Dunmire, K., Houser, T. A., and O'Quinn, T. G. (2019). PSXIV-2 Late-Breaking: the effect of nicotinamide riboside on pork loin chop color stability – a pilot study. *J. Anim. Sci.* 97, 332. doi:10.1093/jas/skz258.664

Greene, E. S., Cauble, R., Dhamad, A. E., Kidd, M. T., Kong, B. W., Howard, S. M., et al. (2020). Muscle metabolome profiles in woody breast-(un)Affected broilers: effects of quantum blue phytase-enriched diet. *Front. Vet. Sci.* 7, 458–515. doi:10.3389/fvets.2020.00458

Grodzik, M. S., Sawosz, E., Sawosz, A., Hotowy, M., Wierbicki, M., Kutwin, S., et al. (2013). Nano-nutrition of chicken embyros. The effect of in ovo administration of diamond nanoparticles and L-glutamine on molecular responses in chicken embryo. *International J. Molecular Sciences* 14 (11), 23033–23044.

Halevy, O., Geyra, A., Barak, M., Uni, Z., and Sklan, D. (2000). Early posthatch starvation decreases satellite cell proliferation and skeletal muscle growth in chicks. *J. Nutr.* 130, 858–864. doi:10.1093/jn/130.4.858

Halevy, O., Nadel, Y., Barak, M., Rozenboim, I., and Sklan, D. (2003). Early posthatch feeding stimulates satellite cell proliferation and skeletal muscle growth in Turkey poults. *J. Nutr.* 133, 1376–1382. doi:10.1093/jn/133.5.1376

Kahane, N., and Kalcheim, C. (1998). Identification of early postmitotic cells in distinct embryonic sites and their possible roles in morphogenesis. *Cell Tissue Res.* 294, 297–307. doi:10.1007/s004410051180

Kidd, M. T., McDaniel, C. D., Branton, S. L., Miller, E. R., Boren, B. B., and Fancher, B. I. (2004). Increasing amino acid density improves live performance and carcass yields of commercial broilers. *J. Appl. Poult. Res.* 13, 593–604. doi:10.1093/japr/13.4.593

Kocamis, H., Yeni, Y. N., Kirkpatrick-Keller, D. C., and Killefer, J. (1999). Postnatal growth of broilers in response to in ovo administration of chicken growth hormone. *Poult. Sci.* 78 (8), 1219–1226.

Kuttappan, V. A., Brewer, V. B., Mauromoustakos, A., McKee, S. R., Emmert, J. L., Meullenet, J. F., et al. (2013). Estimation of factors associated with the occurrence of white striping in broiler breast fillets. *Poult. Sci.* 92, 811–819. doi:10.3382/ps.2012-02506

Kuttappan, V. A., Hargis, B. M., and Owens, C. M. (2016). White striping and woody breast myopathies in the modern poultry industry: a review. *Poult. Sci.* 95, 2724–2733. doi:10.3382/ps/pew216

Kuttappan, V. A., Lee, Y. S., Erf, G. F., Meullenet, J. F., Mckee, S. R., and Owens, C. M. (2012). Consumer acceptance of visual appearance of broiler breast meat with varying degrees of white striping. *Poult. Sci.* 91, 1240–1247. doi:10.3382/ps.2011-01947

Macrae, V. E., Mahon, M., Gilpin, S., Sandercock, D. A., and Mitchell, M. A. (2006). Skeletal muscle fibre growth and growth associated myopathy in the domestic chicken (*Gallus domesticus*). *Brit. Poult. Sci.* 47, 264–272. doi:10.1080/00071660600753615

Maynard, C. J., Jackson, A. R., Caldas-Cueva, J. P., Mauromoustakos, A., Kidd, M. T., Rochell, S. J., et al. (2023). Meat quality attributes of male and female broilers from 4 commercial strains processed for 2 market programs. *Poult. Sci.* 102, 102570. doi:10.1016/j.psj.2023.102570

Maynard, C. W., Latham, R. E., Brister, R., Owens, C. M., and Rochell, S. J. (2019). Effects of dietary energy and amino acid density during finisher and withdrawal phases on live performance and carcass characteristics of Cobb MV × 700 broilers. *J. Appl. Poult. Res.* 28, 729–742. doi:10.3382/japr/pfz025

Mehaffey, J. M., Pradhan, S. P., Meullenet, J. F., Emmert, J. L., McKee, S. R., and Owens, C. M. (2006). Meat quality evaluation of minimally aged broiler breast fillets from five commercial genetic strains. *Poult. Sci.* 85, 902–908. doi:10.1093/ps/85.5.902

Mehmel, M., Jovanović, N., and Spitz, U. (2020). Nicotinamide riboside—the current state of research and therapeutic uses. *Nutrients* 12, 1616–1622. doi:10.3390/nu12061616

Mueller, A. J., Maynard, C. J., Jackson, A. R., Mauromoustakos, A., Kidd, M. T., Rochell, S. J., et al. (2023). Assessment of meat quality attributes of four commercial broiler strains processed at various market weights. *Poult. Sci.* 102 (5), 102571. doi:10.1016/j.psj.2023.102571

Oliveira, G. d.S., McManus, C., Salgado, C. B., and dos Santos, V. M. (2023). Bibliographical mapping of research into the relationship between in ovo injection practice and hatchability in poultry. *Vet. Sci.* 10, 296. doi:10.3390/vetsci10040296

Ohta, A., and Sitkovksy, M. (2001). Role of G-protein-coupled adenosine receptors in downregulation of inflammation and protection from tissue damage. *Nature* 414 (6866), 916–920.

Ordahl, C. P., Berdougo, E., Venters, S. J., and Denetclaw, W. F., Jr. (2001). The dermomyotome dorsomedial lip drives growth and morphogenesis of both the primary myotome and dermomyotome epithelium. *Development* 128, 1731–1744. doi:10.1242/dev.128.10.1731

Petracci, M., Mudalal, S., Soglia, F., and Cavani, C. (2015). Meat quality in fast-growing broiler chickens. *World. poul. Sci. J.* 71, 363–374. doi:10.1017/S0043933915000367

Tijare, V. V., Yang, F. L., Kuttappan, V. A., Alvarado, C. Z., Coon, C. N., and Owens, C. M. (2016). Meat quality of broiler breast fillets with white striping and woody breast muscle myopathies. *Poult. Sci.* 95, 2167–2173. doi:10.3382/ps/pew129

Thayer, M. T., Nelssen, J. L., Langemeier, A. J., Morton, J. M., Gonzalez, J. M., Kruger, S. R., et al. (2019). The effects of maternal dietary supplementation of cholecalciferol (vitamin D_3) and 25(OH)D_3 on sow and progeny performance. *Transl. Anim. Sci.* 3, 692–708. doi:10.1093/tas/txz029

Velleman, S. G. (2007). Muscle development in the embryo and hatchling. *Poult. Sci.* 86, 1050–1054. doi:10.1093/ps/86.5.1050

Velleman, S. G. (2019). Recent developments in breast muscle myopathies associated with growth in poultry. *Annu. Rev. Anim. Biosci.* 7, 289–308. doi:10.1146/annurev-animal-020518-115311

Xu, X., Alcocer, H. M., Gravely, M. E., Jackson, A. R., and Gonzalez, J. M. (2022). Effects of in ovo injection of nicotinamide riboside on high-yield broiler myogenesis. *J. Anim. Sci.* 100, skac203–10. doi:10.1093/jas/skac203

Xu, X., Jackson, A. R., and Gonzalez, J. M. (2021). The effects of in ovo nicotinamide riboside dose on broiler myogenesis. *Poult. Sci.* 100, 100926. doi:10.1016/j.psj.2020.12.024

Zhang, H., Ryu, D., Wu, Y., Gariani, K., Wang, X., Luan, P., et al. (2016). NAD^+ repletion improves mitochondrial and stem cell function and enhances life span in mice. *Sci. (80-.).* 352, 1436–1443. doi:10.1126/science.aaf2693

Zuidhof, M. J., Schneider, B. L., Carney, V. L., Korver, D. R., and Robinson, F. E. (2014). Growth, efficiency, and yield of commercial broilers from 1957, 1978, and 2005. *Poult. Sci.* 93, 2970–2982. doi:10.3382/ps.2014-04291

frontiers | Frontiers in Physiology

TYPE Mini Review
PUBLISHED 13 August 2024
DOI 10.3389/fphys.2024.1458151

OPEN ACCESS

EDITED BY
Wei Guo,
University of Wisconsin-Madison, United States

REVIEWED BY
Xing Fu,
Louisiana State University Agricultural Center, United States
Liubin Yang,
Huazhong Agricultural University, China

*CORRESPONDENCE
Brynn H. Voy,
bhvoy@utk.edu

RECEIVED 02 July 2024
ACCEPTED 25 July 2024
PUBLISHED 13 August 2024

CITATION
Jung U, Kim M and Voy BH (2024), Fibroadipogenic progenitors: a potential target for preventing breast muscle myopathies in broilers.
Front. Physiol. 15:1458151.
doi: 10.3389/fphys.2024.1458151

Fibroadipogenic progenitors: a potential target for preventing breast muscle myopathies in broilers

Usuk Jung, Minjeong Kim and Brynn H. Voy*

Department of Animal Science, University of Tennessee, Knoxville, TN, United States

Genetic selection for high growth rate, breast muscle yield, and feed efficiency in modern broilers has been a double-edged sword. While it has resulted in marked benefits in production, it has also introduced widespread incidence of breast muscle myopathies. Broiler myopathies are phenotypically characterized by myodegeneration and fibrofatty infiltration, which compromise meat quality. These lesions resemble those of various myopathies found in humans, such as Duchenne muscular dystrophy, Limb-girdle muscular dystrophy, and sarcopenia. Fibroadipogenic progenitors (FAPs) are interstitial muscle-resident mesenchymal stem cells that are named because of their ability to differentiate into both fibroblasts and adipocytes. This cell population has clearly been established to play a role in the development and progression of myopathies in mice and humans. Gene expression studies of wooden breast and other related disorders have implicated FAPs in broilers, but to our knowledge this cell population have not been characterized in chickens. In this review, we summarize the evidence that FAPs may be a novel, new target for interventions that reduce the incidence and development of chicken breast muscle myopathies.

KEYWORDS

broiler, fibroadipogenic progenitors, myopathy, pectoralis major, white stripping, wooden breast

Introduction

Lesions in broiler breast muscle myopathies, such as wooden breast and white striping, are characterized by infiltration of fibrous and fatty tissue in place of healthy muscle fibers. These are thought to arise from localized fiber damage that results from physiological consequences of extremely rapid muscle growth, and disruption of the normal, highly synchronized process of muscle repair. For very different reasons, fibroadipogenic lesions develop in a range of diseases and disorders in humans, where they compromise muscle strength and mobility. A novel cell type, fibroadipogenic progenitors (FAPs) has been shown to be the source of such lesions in humans, opening up new therapeutic targets to prevent this pathology. Here we review evidence that this same cell type plays a comparable role in development of broiler breast muscle myopathies.

Myopathies are prevalent in the breast muscle of broiler chickens

Modern broilers require less feed and a shorter amount of time to reach heavier market weight than their 1970s counterparts (National Chicken Council, 2022). However, improvements have resulted in prevalence of myopathies, primarily in the pectoralis major muscle. Different types of myopathies have been described and named based on various features of lesions, including wooden breast, white striping, deep pectoral myopathy, and spaghetti meat (Petracci et al., 2019). Each alters the biochemical and morphological properties of skeletal muscle and compromises meat quality in ways that impose significant losses to the broiler industry. Lesions negatively affect the appearance and texture of broiler meat and discourage consumer acceptance, and lesioned filets are downgraded or discarded (Kuttappan et al., 2016). The incidence of lesions in broilers is widespread, with estimates of incidence in commercial flocks are as high as 90% (Tijare et al., 2016). Lesions are not restricted to a specific broiler line and occur across the globe. The US broiler industry alone has been estimated to lose ~ $1B due to these myopathies (Barbut, 2019).

Wooden breast and white striping are the two most prevalent forms of myopathies in common commercial lines of broilers (Figure 1). Wooden breast lesions result when areas of the breast muscle (pectoralis major) become hardened and thickened, with hemorrhagic areas on the surface of the muscle. White striping describes white fibrotic, lipid-rich striations on the surface of the pectoralis major. These two types of lesions are interrelated and are often found together in the broiler pectoralis major muscle (Sihvo et al., 2014; Aguirre et al., 2020), and share many histological features (Velleman and Clark, 2015). Histopathologically, both types of lesions in birds at slaughter age (~42 days) are characterized by signs of muscle fiber damage, inflammation, and fibrosis. Lesions include ectopic deposition of adipose tissue, immune cell infiltration, myofiber necrosis, degenerative fibers, accumulation of interstitial connective tissue and collagen, and severe fibrosis (Papah et al., 2017; Velleman, 2019). Numerous transcriptomic studies have described widespread differences in gene expression between muscles of affected and non-affected broilers (Zambonelli et al., 2016; Pampouille et al., 2019; Bordini et al., 2022). As would be expected from the visible features of lesions, these studies have consistently shown upregulation of genes related to adipogenesis, lipid accumulation, inflammation, and fibrosis in muscle from affected birds (Papah et al., 2017; Lake et al., 2019).

Consequences of rapid growth that may damage muscle

Myopathies in broilers are a consequence of intense selection for extremely rapid growth of the *p. major* muscle. The incidence and

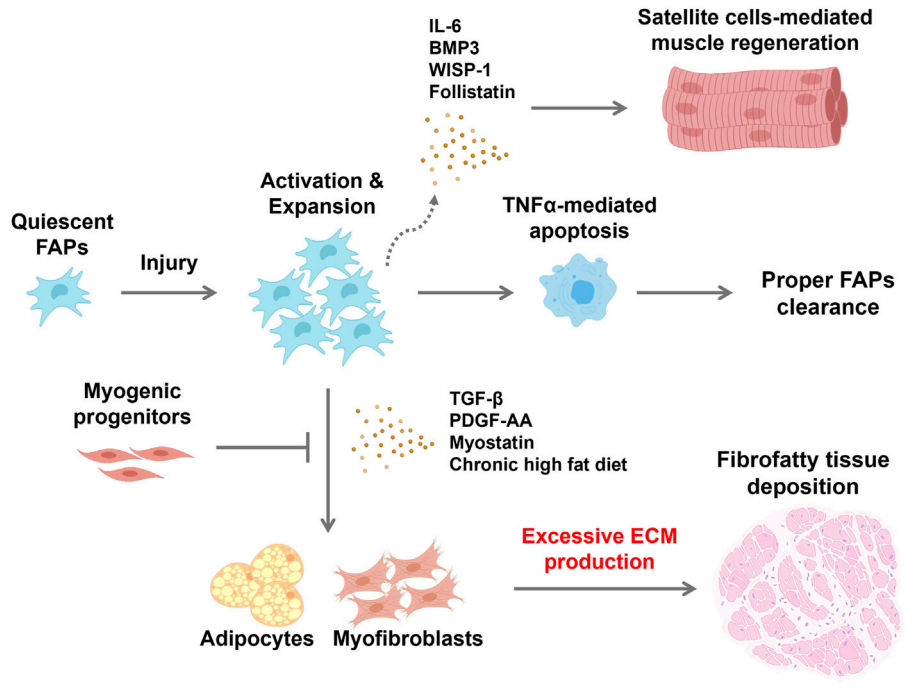

FIGURE 1
Schematic showing fibrofatty tissue infiltration in response to changes in FAP behavior within the environment of an injured skeletal muscle FAPs are normally quiescent but are activated in response to muscle injury. Proliferating FAPs release both extracellular matrix components and promyogenic cytokines to support satellite cell-mediated skeletal muscle regeneration. Satellite cells produce mediators that maintain FAPs in their undifferentiated state while repair proceeds. Immune cells that infiltrate the site of injury produce TNFα that induces apoptotic clearance of FAPs, restoring their numbers to the baseline state. However, cues within the microenvironment of dystrophic muscle can lead to persistence of FAPs and subsequent differentiation to fibroblasts and adipocytes, and fibrofatty tissue accumulation within muscle tissue. Consequently, satellite cell-mediated muscle regeneration is hampered and disrupted. Created with BioRender.com.

severity of lesions is diminished by slowing growth through management practices, or by introducing slow-growing genetics into commercial broiler lines. Rapid growth of skeletal muscle is a desired trait in meat animals, and in and of itself does not result in myopathies or increased adipose deposition in muscle. For example, myostatin mutations that cause double muscling in cattle are associated with reduced intramuscular fat (Hanset et al., 1982). In broilers, however, rapid growth specifically of the *p. major* muscle is thought to damage myofibers and compromises muscle repair, resulting in fibrofatty infiltration that characterizes wooden breast and other myopathies (Mann et al., 2011). Several causes of myofiber damage and development of myopathies have been proposed, such as deficiency of antioxidants, alterations in lipid and glucose metabolism, and tissue hypoxia (Bordini et al., 2022; Malila et al., 2022; Velleman, 2022). A prevailing hypothesis is that fiber damage results from a very rapid rate of muscle growth that outstrips the ability of the vascular system to deliver oxygen and nutrients and remove metabolic wastes (Kuttappan et al., 2013). This inadequate perfusion is thought to result in localized damage to myofibers, initiating a cascade of failed regeneration. A relative deficit in capillary density relative to myofiber area in pectoralis major has been described as an early feature of wooden breast, suggesting that reduced blood supply to myofibers precedes the development of focal lesions at 2 weeks of age (Sihvo et al., 2018). Reduced vascularization compared to the needs of the muscle compromises the ability of the circulatory system to effectively deliver oxygen and nutrients and remove metabolic wastes such as lactic acid that can damage myofibers (Velleman, 2015). These structural changes are thought to further cause localized hypoxia within myofibers that induces inflammation and oxidative stress production, which eventually affect skeletal muscle homeostasis (Mutryn et al., 2015; Jung et al., 2024)

Early changes during development of myopathies in broiler breast muscle

One of the major challenges in identifying the factors that cause wooden breast and other myopathies is that incidence is not detected until slaughter and processing. Papah et al. (2017) conducted a novel prospective study in which they used a needle biopsy technique to sample breast muscle tissue over time in a large number of birds from 1 week of age to market age. They identified which birds went on to develop lesions at slaughter and then compared changes in histology and gene expression over time between affected and unaffected birds. They found that localized lipogranulomas and lipid infiltration between myofibers were detectable as early as 1 week of age in birds that eventually developed wooden breast lesions. By 2–3 weeks of age affected birds showed signs of single myofiber degeneration and inflammation, and increased expression of genes involved in lipid metabolism and adipogenesis (Papah et al., 2017). Similar initial changes have been reported for development of white striping (Griffin et al., 2018). Collectively, these findings implicate lipid infiltration in the early etiology of breast muscle myopathies in broilers.

Similarities between myopathies in human and broiler

In the context of poultry production, skeletal muscle myopathies are primarily restricted to the pectoralis major muscle of broilers due to its uniquely disproportionate rate of growth. In contrast, fibrous and fatty lesions within muscle are shared by a wide range of diseases and disorders that compromise muscle function in humans (Theret et al., 2021). Infiltration of adipose and fibrotic tissue in place of healthy muscle occurs in heritable muscular dystrophies such as Duchenne Muscular Dystrophy (DMD). In this disease, the most common muscular dystrophy, loss of the protein dystrophin compromises cytoskeletal integrity and results in progressive muscle wasting (Mendell and Lloyd-Puryear, 2013). Adipose and fibrous deposition with muscle also occurs secondarily to a range of physiological conditions, including aging, obesity, and Type 2 diabetes (Brack and Rando, 2007; Lukjanenko et al., 2019; Uezumi et al., 2021). Repeated injury and repair to the muscle itself can also result in lesions that histologically resemble those of broiler breast. For example, rotator cuff tears often occur incrementally and result in fibrofatty deposits that influence the functional outcome of surgical repair (Meyer et al., 2004). Clinically, these pathological changes to the composition of skeletal muscle are a major concern because they compromise muscle strength and mobility.

Fibroadipogenic progenitors

Satellite cells are committed to a myogenic fate, but as a mesenchymal cell they have been shown to have some capacity for differentiation to adipocytes and other lineages (Yin et al., 2013). Accordingly, this population was initially thought to be responsible for the fibrofatty infiltration of myopathic lesions as a result of inappropriate differentiation into adipocytes and myofibroblasts. However, this role is now attributed to FAPs, a non-myogenic cell population that was identified by two independent research groups in 2010. FAPs were originally isolated from single cell isolates of healthy skeletal muscle based on expression of mesenchymal surface markers and their capacity to spontaneously differentiate into adipocytes and fibroblasts *in vitro* (Joe et al., 2010; Uezumi et al., 2010). Each group demonstrated that FAPs transiently proliferate but remain undifferentiated in muscle undergoing healthy regeneration, but they undergo adipogenic differentiation in a degenerative muscle environment. FAPs arises from a lineage that is distinct from that of satellite cells, does not express Pax7, and is not capable of myogenic differentiation. FAPs are characterized by surface expression of platelet-derived growth factor receptor alpha (PDGFRα), a membrane-bound tyrosine kinase receptor (Contreras et al., 2021) that regulates their proliferation. They reside in the interstitial space and are relatively abundant in skeletal muscle, as PDGFRα^{+} cells account for 5%–15% of the total nuclei and 20%–30% of the interstitial mononuclear cells in adult muscles (Contreras et al., 2021). Lineage tracing studies *in vivo* have confirmed that FAPs are the primary, if not the only source of adipocytes that develop in damaged muscle and yield fat infiltrates that characterize myopathic lesions (Kopinke et al., 2017).

FAPs are required for healthy muscle repair

FAPs were initially discovered based on their role in muscle pathology. However, they are now understood to also play a critical role in muscle repair through their interactions with muscle stem cells and immune cells. Repair of muscle damage requires a series of coordinated steps and interactions between multiple cell types. Upon damage, both satellite cells and FAPs are promptly activated and enter the cell cycle, with expansion of FAPs preceding that of satellite cells. Rapid proliferation of FAPs is mediated in part through paracrine effects of PDGF that is released by invading macrophages (Contreras et al., 2019). Proliferating FAPs secrete a cocktail of cytokines and promyogenic factors, including IL-6, IL-10, IL-33, BMP3, WISP-1, and follistatin, that promote satellite cell differentiation and myofiber maturation (Joe et al., 2010; Fiore et al., 2016; Biferali et al., 2019; Wosczyna et al., 2019). In addition, FAPs are the primary source of extracellular matrix components, including collagen, metalloproteinases, fibronectin, laminin, and proteoglycans that are necessary for new muscle fiber formation (Arnold et al., 2007; Wynn, 2008). In turn, myofibers provide paracrine signals that inhibit adipogenesis and maintain FAPs in their undifferentiated state (Murphy et al., 2011; Fiore et al., 2016). The rapidly expanded population of FAPs is transient. As muscle regeneration proceeds, FAPs are induced to undergo apoptosis through the actions of TNF-α secreted from pro-inflammatory M1 macrophages recruited to the site of injury, restoring the population back to its original level (Natarajan et al., 2010; Lemos et al., 2015). The critical role of FAPs in this process, and ultimately in maintenance of healthy muscle tissue, has been demonstrated by their genetic deletion. Loss of FAPs over time leads to muscle atrophy, with decreased muscle mass, reduced fiber size, and diminished satellite cell pool (Petrilli et al., 2020). Therefore, the supportive role of FAPs in muscle homeostasis is key for maintaining the satellite cell pool and the long-term capacity for growth and repair.

Aberrant differentiation of FAPs in dystrophic muscle

Aberrant differentiation of FAPs to fibroblasts or adipocytes results from cues that arise within the muscle environment and disrupt the tightly orchestrated balance of signals that govern regeneration, yielding the fibrofatty infiltrations that are characteristic of myopathies (Uezumi et al., 2010; Uezumi et al., 2011; Mozzetta et al., 2013; Lemos et al., 2015; Kopinke et al., 2017; Buras et al., 2019; Hogarth et al., 2022). This was initially demonstrated by Uezumi et al. (2010) upon the identification of FAPs. Activated FAPs were shown to undergo adipogenic differentiation when residing in a dystrophic muscle environment, but to remain undifferentiated when transplanted into muscle undergoing healthy repair. The specific signals that drive fibrogenesis and adipogenesis in muscle *in vivo* are still poorly understood but are of key therapeutic interest. Several secreted factors, including TGF-β, PDGF-AA, myostatin, and wnt3A, have been shown to induce fibroblastic differentiation of FAPs. TGF-β is known as a hallmark of fibrosis and is a secreted protein of macrophages, FAPs, and regenerating myofibers in skeletal muscle. TGF-β promotes fibrogenic differentiation of FAPs (Klingberg et al., 2014; Contreras et al., 2019; Lodyga and Hinz, 2020) by activating the canonical Wnt/β-catenin signaling pathway, which can also suppress adipogenesis upon nuclear translocation of β-catenin (Akhmetshina et al., 2012; Reggio et al., 2020). Signaling through the Notch, retinoic acid receptor, and Hedgehog pathways also mediates FAPs fate decisions. Notch signaling is thought to play a pivotal role in preventing adipogenesis of FAPs. Marinkovic et al. (2019) reported that Delta1 secreted from satellite cells and myofibers activates the Notch pathway, inhibiting FAPs adipogenic differentiation. Interestingly, FAPs isolated from chronically dystrophic muscle are unresponsive to Notch-mediated adipogenic inhibition, suggesting that the local environment influences this checkpoint on FAPs fate. Signaling through the retinoic acid receptor has also been shown to enhance proliferation of FAPs and suppress adipogenesis and fibrogenesis (Zhao et al., 2020). Blocking this signaling pathway was shown to promote adipogenesis and to suppress apoptotic clearance of FAPs in regenerating muscle. FAPs express a single central cilium that is also implicated in control of differentiation through its connection to the Hedgehog signaling pathway. Ablation of ciliary signaling in FAPs was shown to inhibit adipogenesis by repressing Hedgehog signaling in a glycerol-induced muscle injury model, resulting in enhanced muscle regeneration (Kopinke et al., 2017).

Fibroadipogenic progenitors – a contributor to myopathies in broilers?

FAPs have clearly been established to play a role in the formation of myopathies in humans. Whether they play a similar role in broiler breast myopathies has not yet been determined, however evidence supporting this relationship is emerging from the literature. Yablonka-Reuveni et al. (1988) first demonstrated the presence of a non-myogenic cell population that exhibits a fibroblast-like morphology and receptor-mediated binding of PDGF in embryonic chicken breast muscle More recently, transcriptomic studies have reported that PDGFRα is expressed at higher levels in breast muscle of broilers affected with myopathies (Papah et al., 2018; Pampouille et al., 2019; Praud et al., 2020). Expression was significantly increased in birds of a fast-growing commercial line that were affected with white striping or wooden breast in comparison to both unaffected fat-growing counterparts and to a slow-growing line (Pampouille et al., 2019). Malila et al. (2022) also demonstrated that expression of PDGFRα increases with age in breast muscle of fast-growing, but not medium-growing chickens. These findings uncouple the contribution of fast growth *per se* from the association with myopathy incidence and from age-dependent changes in market birds. A genome-wide association study also identified PDGFRα as a candidate gene for contribution to the incidence of white striping in broilers (Pampouille et al., 2019). Based on these findings, and on the established role of FAPs in human myopathies, our lab has begun to characterize this cell population in broilers. We have successfully isolated a PDGFRα+ cell population from pectoralis major that is adipogenic but non-myogenic, and that exhibits morphological features consistent with

FAPs from humans and mice (unpublished data). Taken together, these findings suggest that, as in human myopathies, FAPs may contribute to the pathology of breast muscle lesions in broilers.

Potential implications for alleviating the incidence of breast myopathies in broilers

Because of the clinical relevance, a growing list of pharmacological compounds has been shown to influence the fibrogenic and adipogenic behavior of FAPs in humans (Contreras et al., 2021). Although these types of interventions are not feasible in broilers, they do provide direct evidence that manipulating the cell fate of FAPs reduces or prevents fibrous and fatty infiltration that characterize myopathic lesions. Accordingly, this population may hold new approaches to reduce the development of myopathies in broilers. Dietary means to manipulate FAPs and alleviate myopathies may be feasible based on previous studies in humans and mice. In dystrophies such as DMD, FAPs undergo mitochondrial alterations that compromise oxidative metabolism and a shift from reliance on fatty acid oxidation towards use of glycolysis and the pentose phosphate pathway to derive cellular energy (Vila et al., 2017). Interestingly, this Warburg-like resembles the metabolic consequences of hypoxia that have been linked to broiler breast muscle myopathies. This detrimental metabolic rewiring of FAPs promotes FAPs proliferation and adipogenesis. Restoring fatty acid oxidation by treatment with metformin, which induces fatty acid oxidation by activating AMPK, or by a short-term high fat diet corrects the metabolic and phenotypic defect (Pala et al., 2018; Reggio et al., 2020). Suppression of AMPK signaling through genetic means has also been shown to induce fibrogenic differentiation of FAPs (Liu et al., 2023). Dietary or production strategies that promote fatty acid oxidation or AMPK activation may therefore be a means to influence the behavior of FAPs in broilers. Numerous plant-based sources of polyphenols have been shown to activate AMPK (Ferreira et al., 2024), including in broilers (Huang et al., 2017; Wan et al., 2021; Ding et al., 2023), although their specific effects on fatty and fibrotic infiltrates of breast muscle are unknown. Nitric oxide has also been shown to inhibit FAPs adipogenesis and intramuscular fat accumulation in rodent models (Cordani et al., 2014). *In vivo* treatment with molsidomine, a NO donor, reduced fibrosis and adipogenesis, and lesions in mdx mice, a model of DMD (Cordani et al., 2014). Conversely, blocking NO synthesis with a nitric oxide synthase inhibitor, L-NAME, increased fibrotic tissue deposition and reduced satellite cell activation during muscle regeneration (Filippin et al., 2011). Interestingly, increased activity of the arginine-citrulline-NO synthesis pathway has been associated with reduced severity of wooden breast in broilers, although this was not specifically associated with effects on FAPs (Greene et al., 2019). In addition, including a stabilized form of arginine (inositol-stabilized arginine silicate) that preferentially increases NO production in broiler diets was recently shown to reduce the incidence of wooden breast (Meyer and Bobeck, 2023).

Summary

FAPs have now been established as the cellular source of fibrofatty infiltrates in human muscular dystrophies. Moreover, multiple studies have demonstrated that the fate of FAPs is a promising therapeutic target for reducing the incidence and progression of these disorders. The extensive histological similarities between myopathic lesions in humans and those found in broiler breast muscle myopathies strongly suggests that this cell type plays a similar role in development of wooden breast, white striping, and other challenges to broiler production. Accumulating evidence from gene expression studies supports this causative role, which suggests new means to potentially alleviate the incidence of myopathies in broilers. Collectively, these findings warrant characterization of this novel cell type as a potential new target of production and dietary approaches to reduce the incidence of breast muscle lesions.

Author contributions

UJ: Writing–review and editing, Writing–original draft. MK: Writing–review and editing. BV: Writing–review and editing, Supervision, Project administration, Funding acquisition.

Funding

The author(s) declare that financial support was received for the research, authorship, and/or publication of this article. MJ is supported as a graduate student by funding to BV from USDA-NIFA (1018835).

Acknowledgments

The authors would like to acknowledge UT AgResearch and the Department of Animal Science for their support.

Conflict of interest

The authors declare that the research was conducted in the absence of any commercial or financial relationships that could be construed as a potential conflict of interest.

Publisher's note

References

Aguirre, M. E., Leyva-Jimenez, H., Travis, R., Lee, J. T., Athrey, G., and Alvarado, C. Z. (2020). Evaluation of growth production factors as predictors of the incidence and severity of white striping and woody breast in broiler chickens. *Poult. Sci.* 99 (7), 3723–3732. doi:10.1016/j.psj.2020.03.026

Akhmetshina, A., Palumbo, K., Dees, C., Bergmann, C., Venalis, P., Zerr, P., et al. (2012). Activation of canonical Wnt signalling is required for TGF-β-mediated fibrosis. *Nat. Commun.* 3, 735. doi:10.1038/ncomms1734

Arnold, D. M., Foster, C., Huryn, D. M., Lazo, J. S., Johnston, P. A., and Wipf, P. (2007). Synthesis and biological activity of a focused library of mitogen-activated protein kinase phosphatase inhibitors. *Chem. Biol. Drug Des.* 69 (1), 23–30. doi:10.1111/j.1747-0285.2007.00474.x

Barbut, S. (2019). Recent myopathies in broiler's breast meat fillets. *World's Poult. Sci. J.* 75 (4), 559–582. doi:10.1017/S0043933919000436

Biferali, B., Proietti, D., Mozzetta, C., and Madaro, L. (2019). Fibro-adipogenic progenitors cross-talk in skeletal muscle: the social network. *Front. Physiol.* 10, 1074. doi:10.3389/fphys.2019.01074

Bordini, M., Soglia, F., Davoli, R., Zappaterra, M., Petracci, M., and Meluzzi, A. (2022). Molecular pathways and key genes associated with breast width and protein content in white striping and wooden breast chicken pectoral muscle. *Front. Physiol.* 13, 936768. doi:10.3389/fphys.2022.936768

Brack, A. S., and Rando, T. A. (2007). Intrinsic changes and extrinsic influences of myogenic stem cell function during aging. *Stem Cell Rev.* 3 (3), 226–237. doi:10.1007/s12015-007-9000-2

Buras, E. D., Converso-Baran, K., Davis, C. S., Akama, T., Hikage, F., Michele, D. E., et al. (2019). Fibro-adipogenic remodeling of the diaphragm in obesity-associated respiratory dysfunction. *Diabetes* 68 (1), 45–56. doi:10.2337/db18-0209

Contreras, O., Cruz-Soca, M., Theret, M., Soliman, H., Tung, L. W., Groppa, E., et al. (2019). Cross-talk between TGF-β and PDGFRα signaling pathways regulates the fate of stromal fibro-adipogenic progenitors. *J. Cell Sci.* 132 (19), jcs232157. doi:10.1242/jcs.232157

Contreras, O., Rossi, F. M. V., and Theret, M. (2021). Origins, potency, and heterogeneity of skeletal muscle fibro-adipogenic progenitors-time for new definitions. *Skelet. Muscle* 11 (1), 16. doi:10.1186/s13395-021-00265-6

Cordani, N., Pisa, V., Pozzi, L., Sciorati, C., and Clementi, E. (2014). Nitric oxide controls fat deposition in dystrophic skeletal muscle by regulating fibro-adipogenic precursor differentiation. *Stem Cells* 32 (4), 874–885. doi:10.1002/stem.1587

Ding, X., Giannenas, I., Skoufos, I., Wang, J., and Zhu, W. (2023). The effects of plant extracts on lipid metabolism of chickens - a review. *Anim. Biosci.* 36 (5), 679–691. doi:10.5713/ab.22.0272

Ferreira, C., Vieira, P., Sa, H., Malva, J., Castelo-Branco, M., Reis, F., et al. (2024). Polyphenols: immunonutrients tipping the balance of immunometabolism in chronic diseases. *Front. Immunol.* 15, 1360065. doi:10.3389/fimmu.2024.1360065

Filippin, L. I., Cuevas, M. J., Lima, E., Marroni, N. P., Gonzalez-Gallego, J., and Xavier, R. M. (2011). Nitric oxide regulates the repair of injured skeletal muscle. *Nitric Oxide* 24 (1), 43–49. doi:10.1016/j.niox.2010.11.003

Fiore, D., Judson, R. N., Low, M., Lee, S., Zhang, E., Hopkins, C., et al. (2016). Pharmacological blockage of fibro/adipogenic progenitor expansion and suppression of regenerative fibrogenesis is associated with impaired skeletal muscle regeneration. *Stem Cell Res.* 17 (1), 161–169. doi:10.1016/j.scr.2016.06.007

Greene, E., Flees, J., Dadgar, S., Mallmann, B., Orlowski, S., Dhamad, A., et al. (2019). Quantum blue reduces the severity of woody breast myopathy via modulation of oxygen homeostasis-related genes in broiler chickens. *Front. Physiol.* 10, 1251. doi:10.3389/fphys.2019.01251

Griffin, J. R., Moraes, L., Wick, M., and Lilburn, M. S. (2018). Onset of white striping and progression into wooden breast as defined by myopathic changes underlying Pectoralis major growth. Estimation of growth parameters as predictors for stage of myopathy progression. *Avian Pathol.* 47 (1), 2–13. doi:10.1080/03079457.2017.1356908

Hanset, R., Michaux, C., Dessy-Doize, C., and Burtonboy, G. (1982). *Muscle Hypertrophy of Genetic Origin and Its Use to Improve Beef Production*Editor J. W. B. King and F. Ménissier (The Hague, Netherlands: Nijhoff), 341–349.

Hogarth, M. W., Uapinyoying, P., Mazala, D. A. G., and Jaiswal, J. K. (2022). Pathogenic role and therapeutic potential of fibro-adipogenic progenitors in muscle disease. *Trends Mol. Med.* 28 (1), 8–11. doi:10.1016/j.molmed.2021.10.003

Huang, J., Zhou, Y., Wan, B., Wang, Q., and Wan, X. (2017). Green tea polyphenols alter lipid metabolism in the livers of broiler chickens through increased phosphorylation of AMP-activated protein kinase. *PLoS One* 12 (10), e0187061. doi:10.1371/journal.pone.0187061

Joe, A. W., Yi, L., Natarajan, A., Le Grand, F., So, L., Wang, J., et al. (2010). Muscle injury activates resident fibro/adipogenic progenitors that facilitate myogenesis. *Nat. Cell Biol.* 12 (2), 153–163. doi:10.1038/ncb2015

Jung, U., Kim, M., Dowker-Key, P., Noe, S., Bettaieb, A., Shepherd, E., et al. (2024). Hypoxia promotes proliferation and inhibits myogenesis in broiler satellite cells. *Poult. Sci.* 103 (1), 103203. doi:10.1016/j.psj.2023.103203

Klingberg, F., Chow, M. L., Koehler, A., Boo, S., Buscemi, L., Quinn, T. M., et al. (2014). Prestress in the extracellular matrix sensitizes latent TGF-β1 for activation. *J. Cell Biol.* 207 (2), 283–297. doi:10.1083/jcb.201402006

Kopinke, D., Roberson, E. C., and Reiter, J. F. (2017). Ciliary Hedgehog signaling restricts injury-induced adipogenesis. *Cell* 170 (2), 340–351.e12. doi:10.1016/j.cell.2017.06.035

Kuttappan, V. A., Hargis, B. M., and Owens, C. M. (2016). White striping and woody breast myopathies in the modern poultry industry: a review. *Poult. Sci.* 95 (11), 2724–2733. doi:10.3382/ps/pew216

Kuttappan, V. A., Shivaprasad, H. L., Shaw, D. P., Valentine, B. A., Hargis, B. M., Clark, F. D., et al. (2013). Pathological changes associated with white striping in broiler breast muscles. *Poult. Sci.* 92 (2), 331–338. doi:10.3382/ps.2012-02646

Lake, J. A., Papah, M. B., and Abasht, B. (2019). Increased expression of lipid metabolism genes in early stages of wooden breast links myopathy of broilers to metabolic syndrome in humans. *Genes (Basel)* 10 (10), 746. doi:10.3390/genes10100746

Lemos, D. R., Babaeijandaghi, F., Low, M., Chang, C. K., Lee, S. T., Fiore, D., et al. (2015). Nilotinib reduces muscle fibrosis in chronic muscle injury by promoting TNF-mediated apoptosis of fibro/adipogenic progenitors. *Nat. Med.* 21 (7), 786–794. doi:10.1038/nm.3869

Liu, X., Zhao, L., Gao, Y., Chen, Y., Tian, Q., Son, J. S., et al. (2023). AMP-activated protein kinase inhibition in fibro-adipogenic progenitors impairs muscle regeneration and increases fibrosis. *J. Cachexia Sarcopenia Muscle* 14 (1), 479–492. doi:10.1002/jcsm.13150

Lodyga, M., and Hinz, B. (2020). TGF-β1 - a truly transforming growth factor in fibrosis and immunity. *Semin. Cell Dev. Biol.* 101, 123–139. doi:10.1016/j.semcdb.2019.12.010

Lukjanenko, L., Karaz, S., Stuelsatz, P., Gurriaran-Rodriguez, U., Michaud, J., Dammone, G., et al. (2019). Aging disrupts muscle stem cell function by impairing matricellular WISP1 secretion from fibro-adipogenic progenitors. *Cell Stem Cell* 24 (3), 433–446.e7. doi:10.1016/j.stem.2018.12.014

Malila, Y., Sanpinit, P., Thongda, W., Jandamook, A., Srimarut, Y., Phasuk, Y., et al. (2022). Influences of thermal stress during three weeks before market age on histology and expression of genes associated with adipose infiltration and inflammation in commercial broilers, native chickens, and crossbreeds. *Front. Physiol.* 13, 858735. doi:10.3389/fphys.2022.858735

Mann, C. J., Perdiguero, E., Kharraz, Y., Aguilar, S., Pessina, P., Serrano, A. L., et al. (2011). Aberrant repair and fibrosis development in skeletal muscle. *Skelet. Muscle* 1 (1), 21. doi:10.1186/2044-5040-1-21

Marinkovic, M., Fuoco, C., Sacco, F., Cerquone Perpetuini, A., Giuliani, G., Micarelli, E., et al. (2019). Fibro-adipogenic progenitors of dystrophic mice are insensitive to NOTCH regulation of adipogenesis. *Life Sci. Alliance* 2 (3), e201900437. doi:10.26508/lsa.201900437

Mendell, J. R., and Lloyd-Puryear, M. (2013). Report of MDA muscle disease symposium on newborn screening for Duchenne muscular dystrophy. *Muscle Nerve* 48 (1), 21–26. doi:10.1002/mus.23810

Meyer, D. C., Jacob, H. A., Nyffeler, R. W., and Gerber, C. (2004). *In vivo* tendon force measurement of 2-week duration in sheep. *J. Biomech.* 37 (1), 135–140. doi:10.1016/s0021-9290(03)00260-4

Meyer, M. M., and Bobeck, E. A. (2023). Dietary vasodilator and vitamin C/L-arginine/choline blend improve broiler feed efficiency during finishing and reduce woody breast severity at 6 and 7 wks. *Poult. Sci.* 102 (2), 102421. doi:10.1016/j.psj.2022.102421

Mozzetta, C., Consalvi, S., Saccone, V., Tierney, M., Diamantini, A., Mitchell, K. J., et al. (2013). Fibroadipogenic progenitors mediate the ability of HDAC inhibitors to promote regeneration in dystrophic muscles of young, but not old Mdx mice. *EMBO Mol. Med.* 5 (4), 626–639. doi:10.1002/emmm.201202096

Murphy, M. M., Lawson, J. A., Mathew, S. J., Hutcheson, D. A., and Kardon, G. (2011). Satellite cells, connective tissue fibroblasts and their interactions are crucial for muscle regeneration. *Development* 138 (17), 3625–3637. doi:10.1242/dev.064162

Mutryn, M. F., Brannick, E. M., Fu, W., Lee, W. R., and Abasht, B. (2015). Characterization of a novel chicken muscle disorder through differential gene expression and pathway analysis using RNA-sequencing. *BMC Genomics* 16 (1), 399. doi:10.1186/s12864-015-1623-0

Natarajan, A., Lemos, D. R., and Rossi, F. M. (2010). Fibro/adipogenic progenitors: a double-edged sword in skeletal muscle regeneration. *Cell Cycle* 9 (11), 2045–2046. doi:10.4161/cc.9.11.11854

National Chicken Council (2022). U.S. Broiler performance. Available at: https://www.nationalchickencouncil.org/about-the-industry/statistics/u-s-broiler-performance/.

Pala, F., Di Girolamo, D., Mella, S., Yennek, S., Chatre, L., Ricchetti, M., et al. (2018). Distinct metabolic states govern skeletal muscle stem cell fates during prenatal and postnatal myogenesis. *J. Cell Sci.* 131 (14), jcs212977. doi:10.1242/jcs.212977

Pampouille, E., Hennequet-Antier, C., Praud, C., Juanchich, A., Brionne, A., Godet, E., et al. (2019). Differential expression and co-expression gene network analyses reveal molecular mechanisms and candidate biomarkers involved in breast muscle myopathies in chicken. *Sci. Rep.* 9 (1), 14905. doi:10.1038/s41598-019-51521-1

Papah, M. B., Brannick, E. M., Schmidt, C. J., and Abasht, B. (2017). Evidence and role of phlebitis and lipid infiltration in the onset and pathogenesis of Wooden Breast Disease in modern broiler chickens. *Avian Pathol.* 46 (6), 623–643. doi:10.1080/03079457.2017.1339346

Papah, M. B., Brannick, E. M., Schmidt, C. J., and Abasht, B. (2018). Gene expression profiling of the early pathogenesis of wooden breast disease in commercial broiler chickens using RNA-sequencing. *PLoS One* 13 (12), e0207346. doi:10.1371/journal.pone.0207346

Petracci, M., Soglia, F., Madruga, M., Carvalho, L., Ida, E., and Estevez, M. (2019). Wooden-breast, white striping, and spaghetti meat: causes, consequences and consumer perception of emerging broiler meat abnormalities. *Compr. Rev. Food Sci. Food Saf.* 18 (2), 565–583. doi:10.1111/1541-4337.12431

Petrilli, L. L., Spada, F., Palma, A., Reggio, A., Rosina, M., Gargioli, C., et al. (2020). High-dimensional single-cell quantitative profiling of skeletal muscle cell population dynamics during regeneration. *Cells* 9 (7), 1723. doi:10.3390/cells9071723

Praud, C., Jimenez, J., Pampouille, E., Courousse, N., Godet, E., Le Bihan-Duval, E., et al. (2020). Molecular phenotyping of white striping and wooden breast myopathies in chicken. *Front. Physiol.* 11, 633. doi:10.3389/fphys.2020.00633

Reggio, A., Rosina, M., Palma, A., Cerquone Perpetuini, A., Petrilli, L. L., Gargioli, C., et al. (2020). Adipogenesis of skeletal muscle fibro/adipogenic progenitors is affected by the WNT5a/GSK3/β-catenin axis. *Cell Death Differ.* 27 (10), 2921–2941. doi:10.1038/s41418-020-0551-y

Sihvo, H. K., Airas, N., Linden, J., and Puolanne, E. (2018). Pectoral vessel density and early ultrastructural changes in broiler chicken wooden breast myopathy. *J. Comp. Pathol.* 161, 1–10. doi:10.1016/j.jcpa.2018.04.002

Sihvo, H. K., Immonen, K., and Puolanne, E. (2014). Myodegeneration with fibrosis and regeneration in the pectoralis major muscle of broilers. *Vet. Pathol.* 51 (3), 619–623. doi:10.1177/0300985813497488

Theret, M., Rossi, F. M. V., and Contreras, O. (2021). Evolving roles of muscle-resident fibro-adipogenic progenitors in health, regeneration, neuromuscular disorders, and aging. *Front. Physiol.* 12, 673404. doi:10.3389/fphys.2021.673404

Tijare, V. V., Yang, F. L., Kuttappan, V. A., Alvarado, C. Z., Coon, C. N., and Owens, C. M. (2016). Meat quality of broiler breast fillets with white striping and woody breast muscle myopathies. *Poult. Sci.* 95 (9), 2167–2173. doi:10.3382/ps/pew129

Uezumi, A., Fukada, S., Yamamoto, N., Takeda, S., and Tsuchida, K. (2010). Mesenchymal progenitors distinct from satellite cells contribute to ectopic fat cell formation in skeletal muscle. *Nat. Cell Biol.* 12 (2), 143–152. doi:10.1038/ncb2014

Uezumi, A., Ikemoto-Uezumi, M., Zhou, H., Kurosawa, T., Yoshimoto, Y., Nakatani, M., et al. (2021). Mesenchymal Bmp3b expression maintains skeletal muscle integrity and decreases in age-related sarcopenia. *J. Clin. Invest.* 131 (1), e139617. doi:10.1172/JCI139617

Uezumi, A., Ito, T., Morikawa, D., Shimizu, N., Yoneda, T., Segawa, M., et al. (2011). Fibrosis and adipogenesis originate from a common mesenchymal progenitor in skeletal muscle. *J. Cell Sci.* 124 (Pt 21), 3654–3664. doi:10.1242/jcs.086629

Velleman, S. G. (2015). Relationship of skeletal muscle development and growth to breast muscle myopathies: a review. *Avian Dis.* 59 (4), 525–531. doi:10.1637/11223-063015-Review.1

Velleman, S. G. (2019). Recent developments in breast muscle myopathies associated with growth in poultry. *Annu. Rev. Anim. Biosci.* 7, 289–308. doi:10.1146/annurev-animal-020518-115311

Velleman, S. G. (2022). Why breast muscle satellite cell heterogeneity is an issue of importance for the poultry industry: an opinion paper. *Front. Physiol.* 13, 987883. doi:10.3389/fphys.2022.987883

Velleman, S. G., and Clark, D. L. (2015). Histopathologic and myogenic gene expression changes associated with wooden breast in broiler breast muscles. *Avian Dis.* 59 (3), 410–418. doi:10.1637/11097-042015-Reg.1

Vila, M. C., Rayavarapu, S., Hogarth, M. W., Van der Meulen, J. H., Horn, A., Defour, A., et al. (2017). Mitochondria mediate cell membrane repair and contribute to Duchenne muscular dystrophy. *Cell Death Differ.* 24 (2), 330–342. doi:10.1038/cdd.2016.127

Wan, X., Yang, Z., Ji, H., Li, N., Yang, Z., Xu, L., et al. (2021). Effects of lycopene on abdominal fat deposition, serum lipids levels and hepatic lipid metabolism-related enzymes in broiler chickens. *Anim. Biosci.* 34 (3), 385–392. doi:10.5713/ajas.20.0432

Wosczyna, M. N., Konishi, C. T., Perez Carbajal, E. E., Wang, T. T., Walsh, R. A., Gan, Q., et al. (2019). Mesenchymal stromal cells are required for regeneration and homeostatic maintenance of skeletal muscle. *Cell Rep.* 27 (7), 2029–2035.e5. doi:10.1016/j.celrep.2019.04.074

Wynn, T. A. (2008). Cellular and molecular mechanisms of fibrosis. *J. Pathol.* 214 (2), 199–210. doi:10.1002/path.2277

Yablonka-Reuveni, Z., Anderson, S. K., Bowen-Pope, D. F., and Nameroff, M. (1988). Biochemical and morphological differences between fibroblasts and myoblasts from embryonic chicken skeletal muscle. *Cell Tissue Res.* 252 (2), 339–348. doi:10.1007/BF00214376

Yin, H., Price, F., and Rudnicki, M. A. (2013). Satellite cells and the muscle stem cell niche. *Physiol. Rev.* 93 (1), 23–67. doi:10.1152/physrev.00043.2011

Zambonelli, P., Zappaterra, M., Soglia, F., Petracci, M., Sirri, F., Cavani, C., et al. (2016). Detection of differentially expressed genes in broiler pectoralis major muscle affected by White Striping - wooden Breast myopathies. *Poult. Sci.* 95 (12), 2771–2785. doi:10.3382/ps/pew268

Zhao, L., Son, J. S., Wang, B., Tian, Q., Chen, Y., Liu, X., et al. (2020). Retinoic acid signalling in fibro/adipogenic progenitors robustly enhances muscle regeneration. *EBioMedicine* 60, 103020. doi:10.1016/j.ebiom.2020.103020

frontiers | Frontiers in Physiology

TYPE Opinion
PUBLISHED 26 August 2024
DOI 10.3389/fphys.2024.1453322

OPEN ACCESS

EDITED BY
Sandra G. Velleman,
The Ohio State University, United States

REVIEWED BY
Colin Guy Scanes,
University of Wisconsin–Milwaukee,
United States

*CORRESPONDENCE
Sunoh Che,
sche@umd.edu

RECEIVED 22 June 2024
ACCEPTED 13 August 2024
PUBLISHED 26 August 2024

CITATION
Che S and Hall P (2024) Spaghetti meat and woody breast myopathies in broiler chickens: similarities and differences.
Front. Physiol. 15:1453322.
doi: 10.3389/fphys.2024.1453322

Spaghetti meat and woody breast myopathies in broiler chickens: similarities and differences

Sunoh Che[1]* and Parker Hall[2]

[1]Department of Animal and Avian Sciences, University of Maryland, College Park, MD, United States, [2]Perdue Foods LLC, Salisbury, MD, United States

KEYWORDS

broiler, transcriptomics, processing, peroxy acetic acid, heritability

Introduction

Spaghetti meat (SM) and woody breast (WB) are two economically significant myopathies affecting the quality of broiler chicken breast meat (Barbut, 2019). Another type of breast myopathy, white striping (WS), was not included in this paper as it has become a common occurrence, observed in nearly all breast fillets from commercial broiler production systems (Che et al., 2022b). These conditions lead to reduced consumer acceptance and product depreciation, causing substantial losses in the poultry industry (Barbut, 2019). SM is characterized by the separation of muscle fiber bundles in the *Pectoralis major* muscle, resulting in a mushy and stringy texture (Baldi et al., 2018). In contrast, WB is characterized by an abnormal hardening or firmness of the breast muscle, often accompanied by pale color and occasional petechial hemorrhages (Sihvo et al., 2017). This paper aims to compare and contrast SM and WB, highlighting their similarities and differences in various aspects.

Prevalence and economic impact

The prevalence of both myopathies is substantial, with SM ranging from 35% to 36% and severe WB ranging from 7.3% to 12%, respectively (Sihvo et al., 2017; Zampiga et al., 2018; Xing et al., 2020; Che et al., 2022b; Kang et al., 2022). However, these figures likely underestimate the true incidence, particularly for WB, due to challenges in assessment methods. While SM can be visually detected (Che et al., 2022a), the palpation-based scoring of WB lacks objectivity. The phenotypic incidence of WB in broiler chickens does not align with the microscopic assessment for necrosis and fibrosis, with the incidence can be higher when evaluated microscopically (Velleman, 2020). Moreover, the dorsal recumbent syndrome (DRS), potentially associated with WB, further highlights the underreported symptoms in live birds. DRS-affected broilers inexplicably fall onto their backs, unable to right themselves, leading to the descriptive term "turtle chicken." Ultimately, these recumbent broilers succumb to pulmonary failure, congestion, and edema, possibly due to the pressure exerted on the cardiopulmonary system (Che et al., 2023). Developing effective strategies to mitigate these myopathies and safeguard the economic viability of the poultry industry is essential.

Risk factors

Common risk factors, such as higher live weight at slaughter and elevated temperatures during the grow-out period, contribute to the development of both SM and WB (Che et al., 2022b). In fast-growing broiler chickens affected by WB, muscle fibers have larger diameters,

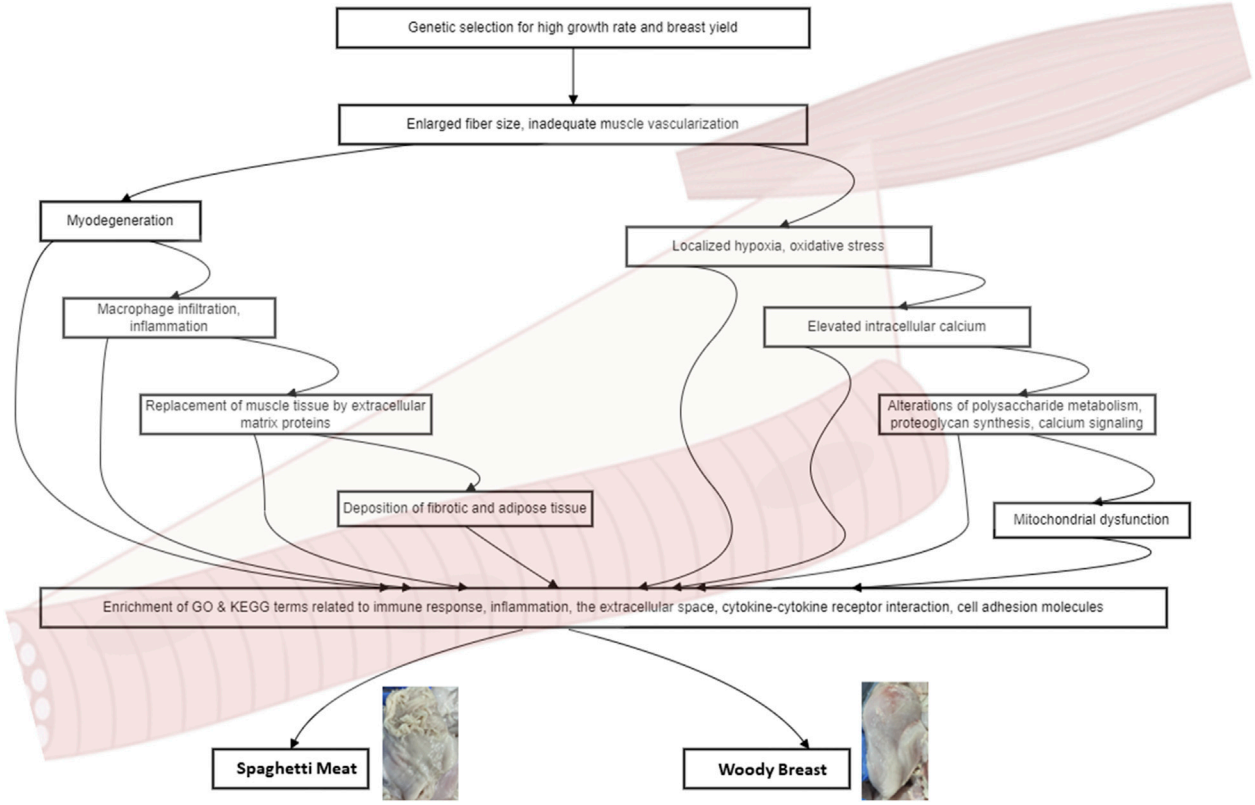

FIGURE 1
Cellular and molecular mechanisms of Woody Breast and Spaghetti Meat. The diagram shows the progression from initial genetic selection to various physiological alterations and their consequences. Genetic selection leads to enlarged fiber size and inadequate muscle vascularization, which in turn triggers two main pathways: myodegeneration and localized hypoxia/oxidative stress. The myodegeneration pathway involves macrophage infiltration, replacement of muscle tissue by extracellular matrix proteins, and deposition of fibrotic and adipose tissue. The hypoxia/oxidative stress pathway leads to elevated intracellular calcium, alterations in polysaccharide metabolism, proteoglycan synthesis, and calcium signaling, ultimately resulting in mitochondrial dysfunction. These processes converge to enrich GO and KEGG terms related to immune response, inflammation, extracellular space, cytokine-cytokine receptor interaction, and cell adhesion molecules. These molecular and cellular changes contribute to the development of two meat quality issues in poultry: Woody Breast and Spaghetti Meat.

and the connective tissue spacing is reduced compared to unaffected muscle (Velleman and Clark, 2015; Sihvo et al., 2018). This alteration in muscle structure leads to myodegeneration, characterized by disorganization of the sarcomeric structure (Velleman et al., 2018). In response to myodegeneration, macrophages infiltrate the affected area and secrete cytokines, promoting the replacement of muscle tissue by extracellular matrix proteins, such as collagen and proteoglycans, and the deposition of fat (Mann et al., 2011). Consequently, fibrosis occurs, characterized by an overproduction of fibrillar collagens, primarily types I and III. The organization and crosslinking of these collagens lead to the formation of collagen fibers, further contributing to the abnormal texture of the affected muscle (Velleman, 2020) (Figure 1).

Fast-growing broilers with high breast meat yields have a decreased ability to regulate their body temperature, which makes them more prone to the negative effects of thermal stress (Petracci et al., 2015). While exposure to cold temperatures can negatively impact satellite cell growth and differentiation, resulting in reduced muscle fiber size and overall muscle mass (Clark et al., 2016; Harding et al., 2016), exposure to high temperatures has been specifically associated with an increased incidence of WB and SM (Che et al., 2022b). Thermal stress, especially hot temperatures, can cause satellite cells to develop into adipose cells instead of muscle cells (Xu et al., 2022), which is associated with changes in breast meat quality, such as increased fat content (Velleman, 2023).

These findings suggest that managing growth rates and environmental conditions could be crucial in reducing the incidence of these quality defects. Interestingly, several risk factors have different effects on SM and WB. For example, coccidiosis vaccination is associated with an increased risk of SM but a decreased risk of WB. The source of chicks and hold time on lairage at the processing plant also have different effects on the two myopathies (Che et al., 2022b). These differential risk factors highlight the complexity of the underlying mechanisms and the need for targeted approaches in managing SM and WB.

Transcriptomic profiles and molecular mechanisms

Multiple studies have revealed key molecular features and pathways associated with WB. These include localized hypoxia, oxidative stress, elevated intracellular calcium, and potential muscle fiber-type switching, which were supported by observed microscopic lesions (Mutryn et al., 2015). Alterations in pathways related to muscle development,

polysaccharide metabolism, proteoglycan synthesis, inflammation, and calcium signaling have been observed (Zambonelli et al., 2016). Age-dependent transcriptional differences in WB development involve changes in glucose and lipid metabolism, cell junction dynamics, and various signaling pathways (Malila et al., 2021). Mitochondrial dysfunction in WB muscle is characterized by elevated monoacylglycerol levels, downregulation of lipid production genes, impaired fatty acid β-oxidation, and oxidative phosphorylation (Wang et al., 2023). It was suggested that selection for fast growth and breast meat yield has induced metabolic shifts towards alternative catabolic pathways for energy production, leading to oxidative stress and the initiation of inflammatory, regenerative, and fibrotic processes. (Pampouille et al., 2019). A transcriptomic meta-analysis revealed critical pathological processes in WB, including fibrosis, apoptosis, and alterations in Ca^{2+}-related signaling, as well as suppression of the tricarboxylic acid cycle and mitochondrial electron transport chain (Zhang et al., 2024).

While fewer studies have focused specifically on SM, recent research has revealed important insights. Both SM and WB samples exhibit significantly elevated mRNA levels of vimentin (VIM) and desmin (DES) genes, which encode essential components of the extra-sarcomeric cytoskeleton in muscle cells, compared to normal tissue. Their analysis revealed significantly elevated mRNA levels of both *VIM* and *DES* in WB and SM samples compared to normal tissue (Soglia et al., 2020).

Comparative analysis of SM and WB transcriptomes has revealed a high degree of similarity in their transcriptomic profiles (Che et al., 2024). Compared to normal breast muscle, both SM and WB samples exhibit a substantial number of differentially expressed genes, indicating extensive transcriptomic changes associated with the development of these myopathies. Gene Ontology (GO) enrichment analysis reveals an enrichment of terms related to immune response, inflammation, and the extracellular space. Kyoto Encyclopedia of Genes and Genomes (KEGG) pathway analysis further supports the involvement of immune and inflammatory processes, with the cytokine-cytokine receptor interaction and cell adhesion molecules pathways being enriched in both myopathies (Figure 1). The lack of significant differences in gene expression between SM and WB samples suggests that these myopathies may share a common pathogenesis at the molecular level. This finding has important implications for understanding the underlying mechanisms and developing targeted interventions.

Divergent phenotypic manifestations

Despite sharing similar molecular mechanisms and histological features, WB and SM exhibit distinct phenotypic characteristics due to differences in the extent and timing of the pathological processes involved. WB can be observed as early as week 2 after hatch (Chen et al., 2019), while SM is not typically assessed in live birds (Cahaner, 2024).

The WB phenotype is primarily attributed to the excessive deposition of fibrous tissue within the muscle, resulting from prolonged and severe fibrosis. The fibrotic process in WB is thought to be driven by sustained hypoxia and oxidative stress, leading to the activation of pro-fibrotic signaling pathways and the excessive production of extracellular matrix components, such as collagen (Soglia et al., 2017; Petracci et al., 2019).

In contrast, the SM phenotype is believed to arise from the weakening of the connective tissue structures within the muscle, potentially due to the degradation of extracellular matrix components or alterations in the organization of muscle fibers (Baldi et al., 2018). The weakened connective tissue may render the muscle more susceptible to mechanical stress during processing steps, leading to the separation of muscle fibers (Baldi et al., 2021). This vulnerability could explain why SM prevalence is significantly higher in processing plants using water chilling compared to those using air chilling (Che et al., 2022b). The increased mechanical stress from water movement during chilling may exacerbate the condition in already weakened muscle tissue.

Heritability and genetic factors

Recent research into the genetic basis of these myopathies has revealed important insights about their heritability, highlighting the complex nature of these conditions and the potential for genetic selection as a mitigation strategy. Heritability estimates vary significantly between WB and SM, and between purebred lines and commercial crossbreds. In purebred lines, WB shows a low heritability of 0.07, while SM demonstrates a very low heritability of 0.04 (Bailey et al., 2020). However, in commercial crossbred broilers, WB exhibits a notably higher heritability of 0.49 (Lake et al., 2022). The substantial difference in heritability estimates between purebred and crossbred populations underscores the importance of studying commercially relevant populations. Multiple quantitative trait loci associated with WB have been identified, primarily clustered on chromosome 5, providing specific genetic targets for future breeding efforts (Lake et al., 2022). The higher heritability of WB in crossbreds suggests that genetics plays a more significant role in its development than previously thought, opening up greater potential for genetic selection against this myopathy.

Processing factors and mitigation strategies

Understanding the impact of processing factors on the incidence and severity of WB and SM is crucial for developing effective mitigation strategies. Slow cooling has been reported to increase the relative incidence of SM significantly (Anton et al., 2019). Moreover, the defeathering process, including the number and configuration of defeathering machines, can also impact SM incidence and severity (Cahaner, 2024).

Peroxyacetic acid (PAA) is an oxidizing antimicrobial agent widely used in poultry processing plants in the USA to reduce levels of foodborne pathogens like *Salmonella* on raw chicken carcasses. PAA solutions up to 2000 ppm are permitted for online reprocessing of poultry in the USA (Cano et al., 2021). While PAA is effective at inactivating bacteria, there are concerns that it may negatively impact meat quality at certain concentrations and exposure times. The effects of PAA on meat quality parameters such as texture, water-holding capacity, and drip loss are not well understood. More research is needed to investigate how PAA treatment conditions influence these important quality attributes. Interestingly, SM has been reported from Italy and Canada, where PAA was not used in processing plants. To fully understand the implications of PAA use in poultry processing, additional research is necessary. Studies should focus on how PAA affects meat quality characteristics and whether it plays a role in the occurrence of SM.

Such investigations will help optimize the use of PAA while maintaining product quality and safety.

Conclusion

In conclusion, while SM and WB share common ground in their molecular underpinnings, their distinct phenotypic characteristics, heritability patterns, and sensitivity to processing factors necessitate a multifaceted approach to mitigation. Future efforts should integrate genetic selection (particularly for WB), refined management practices, and optimized processing techniques. Additionally, further research into the potential role of antimicrobial agents like PAA in meat quality and myopathy development is warranted.

Author contributions

SC: Writing–original draft, Writing–review and editing. PH: Writing–review and editing.

Funding

The author(s) declare that no financial support was received for the research, authorship, and/or publication of this article.

Conflict of interest

Author PH was employed by Perdue Foods LLC.

The remaining author declares that the research was conducted in the absence of any commercial or financial relationships that could be construed as a potential conflict of interest.

Publisher's note

References

Anton, P., Avendano, S., Bailey, R. A., Bilgili, S., Canela, L., Corzo, A., et al. (2019). Breast muscle myopathies (BMM). Available at: https://aviagen-na.aviagen.com/assets/Tech_Center/Broiler_Breeder_Tech_Articles/English/Breast-Muscle-Myopathies-2019-EN.pdf (Accessed August 1, 2024).

Bailey, R. A., Souza, E., and Avendano, S. (2020). Characterising the influence of genetics on breast muscle myopathies in broiler chickens. *Front. Physiol.* 11, 1041. doi:10.3389/fphys.2020.01041

Baldi, G., Soglia, F., Mazzoni, M., Sirri, F., Canonico, L., Babini, E., et al. (2018). Implications of white striping and spaghetti meat abnormalities on meat quality and histological features in broilers. *Animal* 12, 164–173. doi:10.1017/S1751731117001069

Baldi, G., Soglia, F., and Petracci, M. (2021). Spaghetti meat abnormality in broilers: current understanding and future research directions. *Front. Physiol.* 12, 684497. doi:10.3389/fphys.2021.684497

Barbut, S. (2019). Recent myopathies in broiler's breast meat fillets. *World's Poult. Sci. J.* 75, 559–582. doi:10.1017/S0043933919000436

Cahaner, A. (2024). *Defeathering and its implications on the spaghetti meat syndrome 113th poultry science association annual meeting*. Champaign, IL: Louisville, KY, 283–284.

Cano, C., Meneses, Y., and Chaves, B. D. (2021). Application of peroxyacetic acid for decontamination of raw poultry products and comparison to other commonly used chemical antimicrobial interventions: a Review. *J. Food Prot.* 84, 1772–1783. doi:10.4315/JFP-21-107

Che, S., Pham, P. H., Barbut, S., Bienzle, D., and Susta, L. (2024). Transcriptomic profiles of Pectoralis major muscles affected by spaghetti meat and woody breast in broiler chickens. *Animals* 14 (2), 176. doi:10.3390/ani14020176

Che, S., Wang, C., Iverson, M., Varga, C., Barbut, S., Bienzle, D., et al. (2022a). Characteristics of broiler chicken breast myopathies (spaghetti meat, woody breast, white striping) in Ontario, Canada. *Poult. Sci.* 101, 101747. doi:10.1016/j.psj.2022.101747

Che, S., Wang, C., Varga, C., Barbut, S., and Susta, L. (2022b). Prevalence of breast muscle myopathies (spaghetti meat, woody breast, white striping) and associated risk factors in broiler chickens from Ontario Canada. *PLoS ONE* 17, e0267019. doi:10.1371/journal.pone.0267019

Che, S., Weber, L., Novy, A., Barbut, S., and Susta, L. (2023). Characterization of dorsal recumbency syndrome associated with woody breast in broiler flocks from Ontario, Canada. *Poult. Sci.* 102, 102307. doi:10.1016/j.psj.2022.102307

Chen, L. R., Suyemoto, M. M., Sarsour, A. H., Cordova, H. A., Oviedo-Rondón, E. O., Wineland, M., et al. (2019). Temporal characterization of wooden breast myopathy ("woody breast") severity and correlation with growth rate and lymphocytic phlebitis in three commercial broiler strains and a random-bred broiler strain. *Avian Pathol.* 48, 319–328. doi:10.1080/03079457.2019.1598541

Clark, D. L., Coy, C. S., Strasburg, G. M., Reed, K. M., and Velleman, S. G. (2016). Temperature effect on proliferation and differentiation of satellite cells from turkeys with different growth rates. *Poult. Sci.* 95, 934–947. doi:10.3382/ps/pev437

Harding, R. L., Halevy, O., Yahav, S., and Velleman, S. G. (2016). The effect of temperature on proliferation and differentiation of chicken skeletal muscle satellite cells isolated from different muscle types. *Physiol. Rep.* 4, e12770. doi:10.14814/phy2.12770

Kang, K., Zhou, N., Peng, W., Peng, F., Ma, M., Li, L., et al. (2022). Multi-omics analysis of the microbiome and metabolome reveals the relationship between the gut microbiota and wooden breast myopathy in broilers. *Front. Vet. Sci.* 9, 922516. doi:10.3389/fvets.2022.922516

Lake, J. A., Yan, Y., Dekkers, J. C. M., Qiu, J., Brannick, E. M., and Abasht, B. (2022). Identification of circulating metabolites associated with wooden breast and white striping. *PLoS ONE* 17, e0274208. doi:10.1371/journal.pone.0274208

Malila, Y., Uengwetwanit, T., Thanatsang, K. V., Arayamethakorn, S., Srimarut, Y., Petracci, M., et al. (2021). Insights into transcriptome profiles associated with wooden breast myopathy in broilers slaughtered at the age of 6 or 7 weeks. *Front. Physiol.* 12, 691194. doi:10.3389/fphys.2021.691194

Mann, C. J., Perdiguero, E., Kharraz, Y., Aguilar, S., Pessina, P., Serrano, A. L., et al. (2011). Aberrant repair and fibrosis development in skeletal muscle. *Skelet. Muscle* 1, 21. doi:10.1186/2044-5040-1-21

Mutryn, M. F., Brannick, E. M., Fu, W., Lee, W. R., and Abasht, B. (2015). Characterization of a novel chicken muscle disorder through differential gene expression and pathway analysis using RNA-sequencing. *BMC Genomics* 16, 399. doi:10.1186/s12864-015-1623-0

Pampouille, E., Hennequet-Antier, C., Praud, C., Juanchich, A., Brionne, A., Godet, E., et al. (2019). Differential expression and co-expression gene network analyses reveal molecular mechanisms and candidate biomarkers involved in breast muscle myopathies in chicken. *Sci. Rep.* 9, 14905. doi:10.1038/s41598-019-51521-1

Petracci, M., Mudalal, S., Soglia, F., and Cavani, C. (2015). Meat quality in fast-growing broiler chickens. *World's Poult. Sci. J.* 71, 363–374. doi:10.1017/S0043933915000367

Petracci, M., Soglia, F., Madruga, M., Carvalho, L., Ida, E., and Estévez, M. (2019). Wooden-breast, white striping, and spaghetti meat: causes, consequences and consumer perception of emerging broiler meat abnormalities. *Comp. Rev. Food Sci. Food Safe* 18, 565–583. doi:10.1111/1541-4337.12431

Sihvo, H.-K., Airas, N., Lindén, J., and Puolanne, E. (2018). Pectoral vessel density and early ultrastructural changes in broiler chicken wooden breast myopathy. *J. Comp. Pathol.* 61, 1–10. doi:10.1016/j.jcpa.2018.04.002

Sihvo, H.-K., Lindén, J., Airas, N., Immonen, K., Valaja, J., and Puolanne, E. (2017). Wooden breast myodegeneration of *pectoralis major* muscle over the growth period in broilers. *Vet. Pathol.* 54, 119–128. doi:10.1177/0300985816658099

Soglia, F., Gao, J., Mazzoni, M., Puolanne, E., Cavani, C., Petracci, M., et al. (2017). Superficial and deep changes of histology, texture and particle size distribution in broiler wooden breast muscle during refrigerated storage. *Poult. Sci.* 96, 3465–3472. doi:10.3382/ps/pex115

Soglia, F., Mazzoni, M., Zappaterra, M., Di Nunzio, M., Babini, E., Bordini, M., et al. (2020). Distribution and expression of vimentin and desmin in broiler *pectoralis major*

affected by the growth-related muscular abnormalities. *Front. Physiol.* 10, 1581. doi:10.3389/fphys.2019.01581

Velleman, S. G. (2020). *Pectoralis major* (breast) muscle extracellular matrix fibrillar collagen modifications associated with the wooden breast fibrotic myopathy in broilers. *Front. Physiol.* 11, 461. doi:10.3389/fphys.2020.00461

Velleman, S. G. (2023). Satellite cell-mediated breast muscle growth and repair: the impact of thermal stress. *Front. Physiol.* 14, 1173988. doi:10.3389/fphys.2023.1173988

Velleman, S. G., and Clark, D. L. (2015). Histopathologic and myogenic gene expression changes associated with wooden breast in broiler breast muscles. *Avian Dis.* 59, 410–418. doi:10.1637/11097-042015-Reg.1

Velleman, S. G., Clark, D. L., and Tonniges, J. R. (2018). The effect of the wooden breast myopathy on sarcomere structure and organization. *Avian Dis.* 62, 28–35. doi:10.1637/11766-110217-Reg.1

Wang, Z., Brannick, E., and Abasht, B. (2023). Integrative transcriptomic and metabolomic analysis reveals alterations in energy metabolism and mitochondrial functionality in broiler chickens with wooden breast. *Sci. Rep.* 13, 4747. doi:10.1038/s41598-023-31429-7

Xing, T., Zhao, X., Zhang, L., Li, J. L., Zhou, G. H., Xu, X. L., et al. (2020). Characteristics and incidence of broiler chicken wooden breast meat under commercial conditions in China. *Poult. Sci.* 99, 620–628. doi:10.3382/ps/pez560

Xu, J., Strasburg, G. M., Reed, K. M., and Velleman, S. G. (2022). Temperature and growth selection effects on proliferation, differentiation, and adipogenic potential of Turkey myogenic satellite cells through frizzled-7-mediated wnt planar cell polarity pathway. *Front. Physiol.* 13, 892887. doi:10.3389/fphys.2022.892887

Zambonelli, P., Zappaterra, M., Soglia, F., Petracci, M., Sirri, F., Cavani, C., et al. (2016). Detection of differentially expressed genes in broiler pectoralis major muscle affected by white striping – wooden breast myopathies. *Poult. Sci.* 95, 2771–2785. doi:10.3382/ps/pew268

Zampiga, M., Laghi, L., Petracci, M., Zhu, C., Meluzzi, A., Dridi, S., et al. (2018). Effect of dietary arginine to lysine ratios on productive performance, meat quality, plasma and muscle metabolomics profile in fast-growing broiler chickens. *J. Anim. Sci. Biotechnol.* 9, 79. doi:10.1186/s40104-018-0294-5

Zhang, X., Xing, T., Zhao, L., Zhang, L., and Gao, F. (2024). Transcriptomic meta-analysis and exploration of differentially expressed gene functions in wooden breast myopathy of broilers. *Poult. Sci.* 103, 104047. doi:10.1016/j.psj.2024.104047

frontiers | Frontiers in Physiology

TYPE Review
PUBLISHED 29 August 2024
DOI 10.3389/fphys.2024.1452318

OPEN ACCESS

EDITED BY
Gale Strasburg,
Michigan State University, United States

REVIEWED BY
Peter Groves,
The University of Sydney, Australia
Colin Guy Scanes,
University of Wisconsin–Milwaukee,
United States

*CORRESPONDENCE
Adnan A. K. Alrubaye,
aakhalaf@uark.edu

†These authors have contributed equally to this work and share first authorship

RECEIVED 20 June 2024
ACCEPTED 06 August 2024
PUBLISHED 29 August 2024

CITATION
Anthney A, Do ADT and Alrubaye AAK (2024) Bacterial chondronecrosis with osteomyelitis lameness in broiler chickens and its implications for welfare, meat safety, and quality: a review. *Front. Physiol.* 15:1452318.
doi: 10.3389/fphys.2024.1452318

Bacterial chondronecrosis with osteomyelitis lameness in broiler chickens and its implications for welfare, meat safety, and quality: a review

Amanda Anthney[1†], Anh Dang Trieu Do[1,2†] and Adnan A. K. Alrubaye[1,2*]

[1]Center of Excellence for Poultry Science, University of Arkansas, Fayetteville, AR, United States, [2]Cell and Molecular Biology Program, University of Arkansas, Fayetteville, AR, United States

The exponential increase in global population continues to present an ongoing challenge for livestock producers worldwide to consistently provide a safe, high-quality, and affordable source of protein for consumers. In the last 50 years, the poultry industry has spearheaded this effort thanks to focused genetic and genomic selection for feed-efficient, high-yielding broilers. However, such intense selection for productive traits, along with conventional industry farming practices, has also presented the industry with a myriad of serious issues that negatively impacted animal health, welfare, and productivity–such as woody breast and virulent diseases commonly associated with poultry farming. Bacterial chondronecrosis with osteomyelitis (BCO) lameness is one such issue, having rapidly become a key issue affecting the poultry industry with serious impacts on broiler welfare, meat quality, production, food safety, and economic losses since its discovery in 1972. This review focuses on hallmark clinical symptoms, diagnosis, etiology, and impact of BCO lameness on key issues facing the poultry industry.

KEYWORDS

poultry, bacterial chondronecrosis with osteomyelitis, lameness, animal welfare, food safety, meat quality

1 Introduction

Since the 1940s, the poultry industry has consistently led the field of livestock production in terms of volume of meat produced and affordability for consumers annually, the demand of which is projected to continuously grow in upcoming years (USDA, 2023). At a glance, approximately more than nine billion broilers were grown in 2018, to a total of 25.6 billion kilograms in live weight produced with the United States, Brazil, and China leading global production volumes (National Chicken Council, 2021a). Per capita consumption of chicken meat in the United States was estimated at 42.4 kg in the same year and has consistently increased per annum, with 2024 estimation at 45.5 kg (National Chicken Council, 2021b). This popularity has resulted in the making of the modern broiler, which would grow significantly larger in a shorter time frame while improving feed efficiency over the years, thanks to intense genetic selection for productive parameters and advancements in broiler nutrition (Tallentire et al., 2016; Castro et al.,

2023). Such a drastic change in broiler strain physiology in the 5 decades from 1957 to 2005 was highlighted by Zuidhof et al. (2014), who reported a 400% increase in broiler growth rate while the FCR is reduced by half. The high production volumes and low consumer prices enjoyed by the poultry industry compared to other major livestock species like beef and pork (USDA, 2024) is largely possible thanks to this outstanding growth rate and extremely efficient feed conversion of the modern broiler–along with a vertically integrated business model employed by the industry (Vukina, 2001) – even with feed ingredient procurement and production often constituting a significant production cost in livestock farming. Unfortunately, this rapid increase in growth rate to meet production and consumption demands, coupled with conventional industrial poultry farming practices, has resulted in significant physiological pressure on the animals, leading to negative impacts on broiler welfare, health, and productivity. For example, the increased prevalence of woody breast syndrome–signified by the drastic hardening of breast muscle tissue–has been linked to multiple causes stemming from physiological, genetic, and production factors (Hoving-Bolink et al., 2000; Sihvo et al., 2018; Tixier-Boichard, 2020; Welter et al., 2022). Similarly, modern poultry farming has also been the subject of some scrutiny, with high stocking densities and poor housing conditions more likely to give rise to rapid pathogenic spread of diseases between flocks and other welfare issues, such as pododermatitis and hock burns (Berg, 2004; Buijs et al., 2009; Jacob et al., 2016).

In the same vein, lameness is one of the most prevalent issues currently affecting modern broiler health and welfare (Julian, 1998; EFSA, 2012; Granquist et al., 2019). More specifically, in addition to common hock burn or pododermatitis-associated lameness that may result in painful gait for the animal, bacterial chondronecrosis with osteomyelitis (BCO) lameness has rapidly become a condition of great concern to the poultry industry due to its increasingly apparent impact on welfare and economic losses since its first reported case in 1972 (Nairn and Watson, 1972), which has been reported in both current literature (McNamee et al., 1998; Cook, 2000; Bradshaw et al., 2002; Dinev, 2009) as well as industrial communications over time. Initiated by leg bone microfractures that worsen as the broiler ages and eventually become bacterial infection sites, BCO lameness results in severely reduced animal mobility, morbidity, and mortality–often with no recourse. Annually, BCO lameness was estimated to result in losses of roughly $100 million to broiler culls in the United States (Cook, 2000; McNamee et al., 2000) and is reported as a common cause of lameness with increasing prevalence in various regions globally (Pattison, 1992; Dinev, 2009; Herdt et al., 2009; Stalker et al., 2010a; Braga et al., 2016; Ekesi et al., 2021). This review will thus focus on several aspects regarding BCO-associated lameness's potential pathogenesis, clinical symptoms, diagnosis, and implications in relation to economic impacts, food safety, and meat quality concerns.

2 Pathogenesis and pathophysiology

2.1 Rapid body weight gain and mechanical stress

Current proposed mechanisms of BCO lameness pathophysiology often involve a combination of the rapid weight gain in the modern broiler in a short period of time and the comparatively disproportionate growth rate of the broiler's skeletal integrity to support it (Wideman and Prisby, 2013; Wideman, 2016). While the average modern broiler will have gained roughly a hundred-fold in body weight by the eighth week of age (Bellairs and Osmond, 2005; Zuidhof et al., 2014; Aviagen Inc, 2022; Cobb-Vantress Inc, 2022), both the femora and tibiae will have only increased by approximately four times in length and about three to five times in mid-shaft diameter in the first 6 weeks by comparison (Applegate and Lilburn, 2002; Damaziak et al., 2019). While exhaustive academic and industrial improvements in genetic selection (Kapell et al., 2012; Siegel et al., 2019) as well as research of broiler nutrition and environmental enrichment (Nakhon et al., 2019; Pedersen et al., 2020; Biesek et al., 2022) have provided valuable insights into healthier broiler leg development, the negative relationship between fast-growing genetics and healthy broiler skeletal and leg bone development remains to this day, where rapid muscling and weight gain are at odds with the latter–particularly during the earlier stage of rapid weight gain (Rath et al., 2000; González-Cerón et al., 2015; Kierończyk et al., 2017; Santos et al., 2022). In the short productive lifetime of the commercial broiler, the long bones of the leg are exposed to excessive mechanical stress from its drastically disproportionate body weight as the broiler locomotes, causing shear stress and torque on the immature skeletal system (Wideman, 2016). Long chondrocyte columns in the proximal growth plates commonly seen in the avian femur and tibia are also especially susceptible to such mechanical stress, causing microfractures between layers of cartilage that often transect blood vessels, causing reduced blood flow and eventual necrosis (McNamee et al., 1998; Wideman and Prisby, 2013; Wideman, 2016; Haynes, 2023). Due to the significantly longer columns of chondrocytes and thicker growth plates in the proximal ends of the femur and tibia, they are far more susceptible to lesions compared to the distal ends. Resultant infection of these osteochondrotic clefts in femoral and tibial proximal growth plates usually follow, whether through bacterial translocation of the broiler's gastrointestinal and/or respiratory systems, or acquired through the surrounding environment, giving rise to further necrosis–and eventually, the associated lameness (Wideman, 2016). While BCO infections most commonly manifest in the proximal ends of the femur and tibia, they can also be found affecting the fourth thoracic vertebra (T4), causing the condition known as spondylitis, which may be clinically misclassified as "kinky back" – or non-bacterial spondylolisthesis (Carnaghan, 1966; Wideman, 2016; Choppa and Kim, 2023).

2.2 Bacterial hematogenous translocation

The introduction of bacteria to damaged femoral and tibial growth plates, which leads to subsequent worsening infection and necrosis, is linked to the hematogenous translocation of opportunistic bacteria from the intestinal microbiota or aerosolized bacteria from the respiratory system (Wideman, 2016). Figure 1, summarizes the hypothesized hematogenous translocation model.

Overwhelmingly, *Staphylococcus* spp. make up the majority of represented species within BCO lesions, although others like

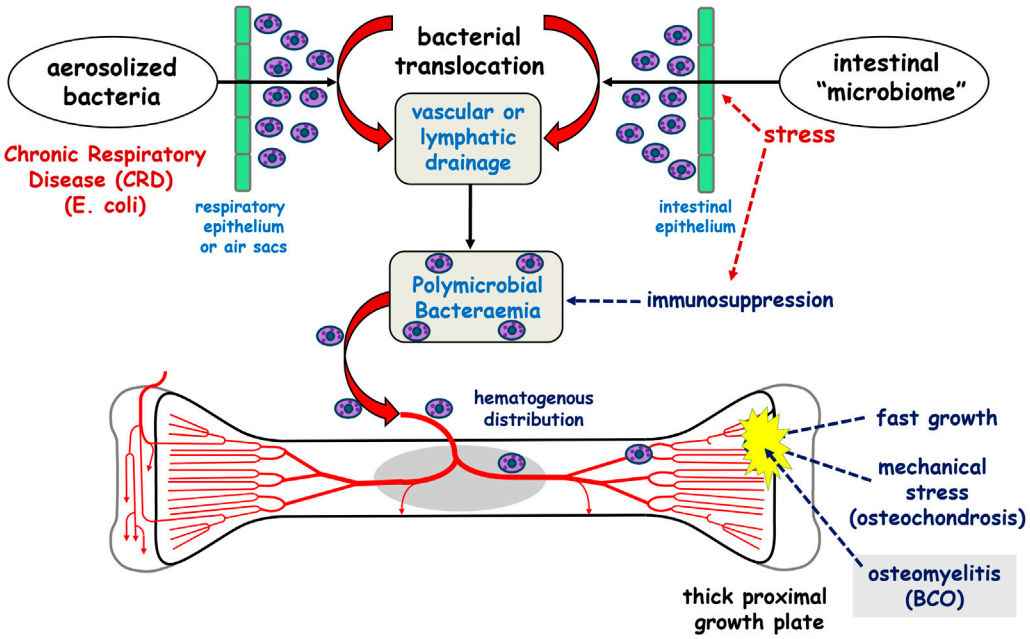

FIGURE 1
The current postulated hypothesis of bacterial chondronecrosis with osteomyelitis (BCO) pathogenesis. Bacteria translocate from acquired aerosolized bacteria in the respiratory system or from the intestinal microbiome and colonize osteochondrotic clefts in the proximal growth plates on the weight bearing bones of the leg. Reproduced from Wideman (2016) with permission from Elsevier.

Enterococcus spp. and *Escherichia coli* have also been identified (Jiang et al., 2015; Wideman, 2016; Szafraniec et al., 2022). Within the *Staphylococcus* genus, while *S. aureus* has been widely associated with lesions and associated lameness, *S. agnetis* has also been identified as another potential key species of interest due to its unique virulence factor, which is composed of homologs for both pathogenic and non-pathogenic Staphylococci such as ORF531, ORF1179-1182, and ORF2344, which are also responsible for *Staphylococcus aureus* virulence factors (Al-Rubaye et al., 2015). A similar study at the University of Arkansas successfully demonstrated BCO lameness induction capability of the hypervirulent *Staphylococcus agnetis* strain 908 in drinking water challenges, where tested probiotic preventive measures proved less effective in clinical BCO lameness reduction compared to other *Staphylococcus* species (Al-Rubaye et al., 2017). It has been hypothesized that such evolved virulence may have been the result of intense selection from past focused lameness research efforts using the unique and effective wire-flooring model at the facility (Wideman Jr et al., 2012; Wideman Jr et al., 2013; Al-Rubaye et al., 2015; Al-Rubaye et al., 2017; Shwani et al., 2020).

2.3 Gastrointestinal bacterial translocation ("leaky gut") and respiratory bacterial translocation

One of the prevailing proposed mechanisms behind BCO pathogenesis is the translocation of bacteria from the gastrointestinal tract due to poor integrity of the intestinal barrier, also commonly known as "leaky gut" (Wideman and Prisby, 2013; Wideman, 2016; Ducatelle et al., 2023). The lining of the small intestine comprises a layer of epithelial cells maintained by "tight junctions" (TJ) – or multi-complexes of proteins (such as occludin and claudin) responsible for integrity and permeability of this layer (Tomita et al., 2004). These junctions, along with the associated epithelial layer, are generally considered the first barrier between the small intestine and the bloodstream and is thus subject to disruption from enteric pathogens and other initiating factors (Tomita et al., 2004; Ducatelle et al., 2023). When a broiler is subjected to environmental stress, compromised immunity, or a poor diet, these tight junctions may have reduced functionality, leading to increased permeability between epithelial layers and hematogenous translocation of pathogenic bacteria (Wideman and Prisby, 2013; Wideman, 2016; Alharbi et al., 2024b). This passage from the gut microbiota into the bloodstream can induce inflammation of the gut and surrounding tissues, as well as resultant BCO infection and lameness when bacteria colonize osteochondrotic clefts in the growth plates of weight-bearing bones (Wideman, 2016; De Meyer et al., 2019). It has been reported that supplementation of high-quality essential trace minerals such as copper, manganese, and magnesium in the broiler diet may have a positive effect in the strengthening and increased expression of TJ proteins, leading to decreased chances of translocation events and subsequent clinical BCO lameness incidence (Alrubaye et al., 2020).

Broilers are also often exposed to airborne environmental pathogens in a multitude of environments, including the hatchery or the housing itself, which may potentially result in persistent complications throughout the broiler's productive life and decreased food safety for the consumers (Quarles and Caveny, 1979; Cox et al., 2002; Heyndrickx et al., 2002). In stressed and immunocompromised birds, aspirated bacteria may

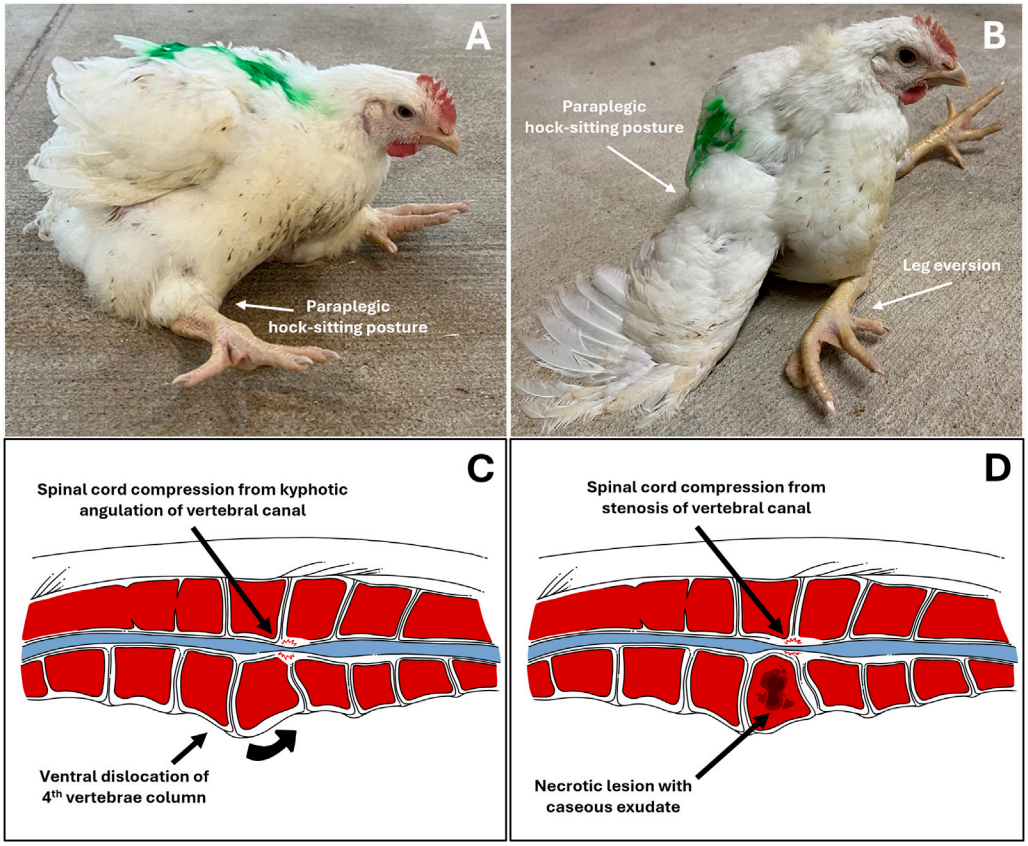

FIGURE 2
Left to Right, Top Down; **(A,B)** Depictions of broilers exhibiting clinical symptoms of vertebral lameness (spondylitis/spondylolisthesis, "kinky back") in a paraplegic, hock-sitting posture; **(C,D)** Illustrated anatomical comparison of spondylolisthesis and spondylitis. **(A)**. Typical sitting posture of broilers afflicted with vertebral lameness; **(B)**. Severe vertebral lameness sitting posture, with eversion of the legs; **(C)**. Illustrated transversal cross-section of vertebral column afflicted with spondylolisthesis of the fourth vertebra and compression of the spinal cord in the area due to physical kyphotic angulation of the vertebral canal. Note the relatively intact bone tissue; **(D)**. Illustrated transversal cross-section of vertebral column afflicted with bacterial spondylitis of the fourth vertebral and compression of the spinal cord in the area due to stenosis of the vertebral canal. Note the damaged necrotic bone tissue with caseous exudate within the vertebral body compared to **(C)**.

colonize the upper respiratory tract's mucosal surfaces or avian air sacs, and subsequently proliferate. This colonization of opportunistic bacteria allows for translocation into the bloodstream in a similar fashion as the gastrointestinal route, which can lead to BCO infections (Jiang et al., 2015). While current literature regarding BCO-associated lameness remains somewhat scarce in this topic, examination of the avian and poultry respiratory environment in various conditions had been previously conducted using bronchoalveolar lavage fluid (Bottje et al., 1998; Zhou et al., 2023), which may open up future opportunities in this research aspect.

3 Symptoms and diagnosis

Clinical diagnosis of abnormal behavior, morbidity, and lameness is essential as the first step to address BCO-associated lameness as pathogenesis and pathophysiology of the disease take place almost entirely internally within the animal. Clinical symptoms of BCO-associated lameness often include awkward gait, limping, wing dropping to support the body, hesitancy to move, or even complete inability to walk when gently prompted (Wideman, 2016; Al-Rubaye et al., 2017; Alrubaye et al., 2020; Alharbi et al., 2024a; Asnayanti et al., 2024b; Asnayanti et al., 2024c; Do et al., 2024). In rarer cases of severe spondylitis (also known as "kinky back") the bird will typically be sitting with its legs extended from paralysis, unable to walk and correct to an upright posture (Figure 2). Birds experiencing symptoms of lameness often have great difficulty reaching feed and water sources, which leads to dehydration, impaired growth, and eventual death. Clinical diagnosis of lameness must be addressed as early as possible to maintain the highest standard of animal health and welfare, as well as accuracy of BCO assessment. Typically, BCO diagnosis is conducted via *postmortem* necropsy to assess femoral and tibial lesions, as outlined in Figure 3.

3.1 Femoral lesions

Disease progression of femoral head lesions commonly associated with BCO lameness is shown in Figure 4.

A combination of compromised blood flow, bacterial infection, and mechanical stress leads to lesions in the femoral head, which is diagnosed by *postmortem* disarticulation of the proximal head from the acetabulum for assessment (Wideman, 2016). Lesion categories for the proximal femur head, from least severe to most severe

include normal (N), femoral head separation (FHS), femoral head transitional degeneration (FHT), and femoral head necrosis (FHN) (Dinev, 2009; Wideman, 2016; Do et al., 2024). As shown in Figure 4, worsening disease progression states are indicated by several hallmark characteristics as the healthy proximal femoral head transitions from a healthy state, complete with intact articular epiphyseal cartilage and smooth joint articulation, to the FHN stage. Starting with FHS, mechanical stress exacerbated by the bird's heavy weight leads to the erosion or disarticulation of the epiphyseal cartilage, which usually remains in the acetabulum, exposing the epiphysis to further damage as the bird locomotes. In the transitional stage of FHT, the effects become even more evident, with the epiphysis exhibiting a significant amount of damage. Finally, once disease progression reaches the terminal FHN stage, its necrosis and complete fracturing of the femoral head upon disarticulation renders the bird almost completely unable to move. While transitional states (FHS and FHT) are arguably less extensive in damage to the femoral epiphysis compared to FHN, afflicted birds all exhibit great difficulty in mobility that can be clinically diagnosed with an awkward gait, reluctance to walk, or even tonic immobility (Wideman, 2016; Alrubaye et al., 2020; Alharbi et al., 2024a; Asnayanti et al., 2024b; Do et al., 2024). Most importantly, damage to the exposed epiphysis in all disease progression stages allows for translocated bacterial infection to take place as discussed, leading to increased chances of worsening BCO-associated pathological lameness (McNamee et al., 2000; Wideman, 2016; Alrubaye et al., 2020; Choppa and Kim, 2023).

3.2 Tibial lesions

Much like femoral lesions, tibial lesions result from the combination of mechanical stress and bacterial infection. However, most of the damage is observed by dissecting the proximal tibial head to expose a cross-section of the growth plate. Tibial lesion progression commonly associated with BCO lameness is depicted in Figure 5.

As characterized by Wideman Jr et al. (2012) and similarly by Do et al. (2024), tibial lesions are also categorized based on severity, ranging from normal (N), tibial head necrosis (THN) to tibial head necrosis severe (THNS). In rare cases, lesions presenting with caseous exudate are also categorized as tibial head necrosis caseous (THNC) (similar to tibial head necrosis sever with a large necrotic void and growth plate damage, but additional caseous bacterial infection appearing as a bright yellow section within the tibial head). As shown in Figure 6, normal healthy tibial cross-sections are presented with an intact and clearly defined metaphyseal growth plate along with firm cancellous (spongy) bone. With disease progression taking place, necrotic degeneration of the cancellous bone leads to soft lesions and necrotic voids (THN) that may increase in size and encroach upon the growth plate, often with visible clefts (THNS) at its most severe stage. In the case of THNC, a cheese-like caseous exudate can often be observed in close vicinity of necrotic lesions, which may mark possible sites of bacterial deposit and infection. Occasionally, tibial cross-sections may also present overgrowths of cartilaginous tissue replacing cancellous bone growth in birds afflicted with tibial dyschondroplasia (TD), caused by chondrocyte death due to insufficient blood supply to the region (Huang et al., 2019). While not directly linked to BCO pathophysiology, TD is also a significant cause for concern in the poultry industry as it can also lead to severe broiler lameness and reduced welfare (Sanotra et al., 2001; Bradshaw et al., 2002).

3.3 Vertebral lesions (spondylitis)

In addition to lesions typically found in the proximal femoral and tibial heads, broilers suffering from BCO can also develop vertebral lesions in the same manner as that seen in leg bones–via hematogenous distribution of translocated pathogenic bacteria into osteochondrotic clefts in the damaged thoracic vertebrae from mechanical stress, causing swelling and abscessation of the fourth vertebral body (T4) (Wideman, 2016). Broilers affected by BCO vertebral lesions (or spondylitis) can be clinically diagnosed by the hallmark hock recumbency posture and paralysis, causing a complete inability to maintain an upright posture in these animals. While the presenting clinical symptoms of BCO-associated vertebral lesions are almost identical to that of spondylolisthesis, which is often referred to as "kinky back", the latter is usually noninfectious in nature compared to infectious spondylitis, and care must be taken in diagnostic evaluation of this specific clinical symptom with regards to vertebral BCO/spondylitis (Duff, 1990; Dinev, 2012; Robbins et al., 2012; Dinev, 2014; Borst et al., 2017). Similar to leg bone lesions caused by the disease, spondylitis causes severely reduced animal welfare standards from the inability to access feed and water, and results in culling of afflicted birds. In addition to species commonly associated with femoral and tibial lesions such as *Staphylococcus* spp., there is a wide breadth of reports in current literature attributed to Enterococci in poultry spondylitis, with pathogenic *Enterococcus cecorum* as a major etiological agent throughout the years (Stalker et al., 2010b; Robbins et al., 2012; Dunnam et al., 2023). Origination, lineage, and pathogenicity of pathogenic strains of interest–which differ significantly to their commensal counterpart (Borst et al., 2015) – remain under investigation, with a previous work from Laurentie et al. (2023) suggesting a common lineage among poultry pathogenic isolates. Findings from Borst et al. (2017) also highlighted a significant impact of early *E. cecorum* infection, coupled with a natural susceptibility to osteochondrosis dissecans lesions in the free thoracic vertebrae of the broiler, in spondylitis development. More recently, Rhoads et al. (2024) identified a possible polyphyletic origin to pathogenic isolates associated with BCO lameness and reported outbreaks in recent years using publicly available *E. cecorum* genomes, with pathogenicity suggested to have been caused by mutations rather than gene acquisition, though–as the authors have noted–much more evidence collection and analyses remain to determine pathogen genomic diversity in reported outbreaks within the same facility, as well as a pressing need for expansion of genome databases, which are currently poorly documented.

4 Findings and recent advancements

To this day, Wideman (2016) and Wideman and Prisby (2013) still constitute some of the most exhaustive and documented sources in BCO pathophysiology and clinical

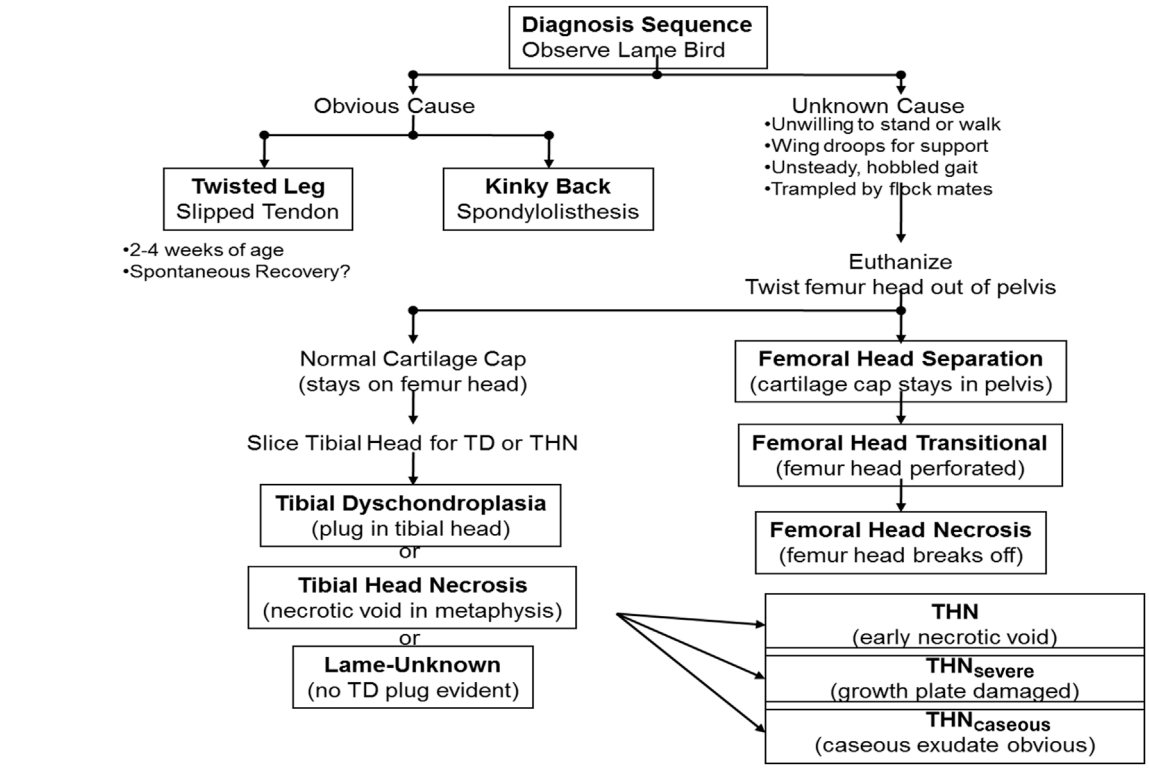

FIGURE 3
Current process used for BCO diagnosis. Once a lame bird is observed, clinical symptoms are addressed. From this information, it is determined whether the bird has spondylitis/spondylolisthesis, a twisted leg, or must be euthanized and necropsied to gather further information.

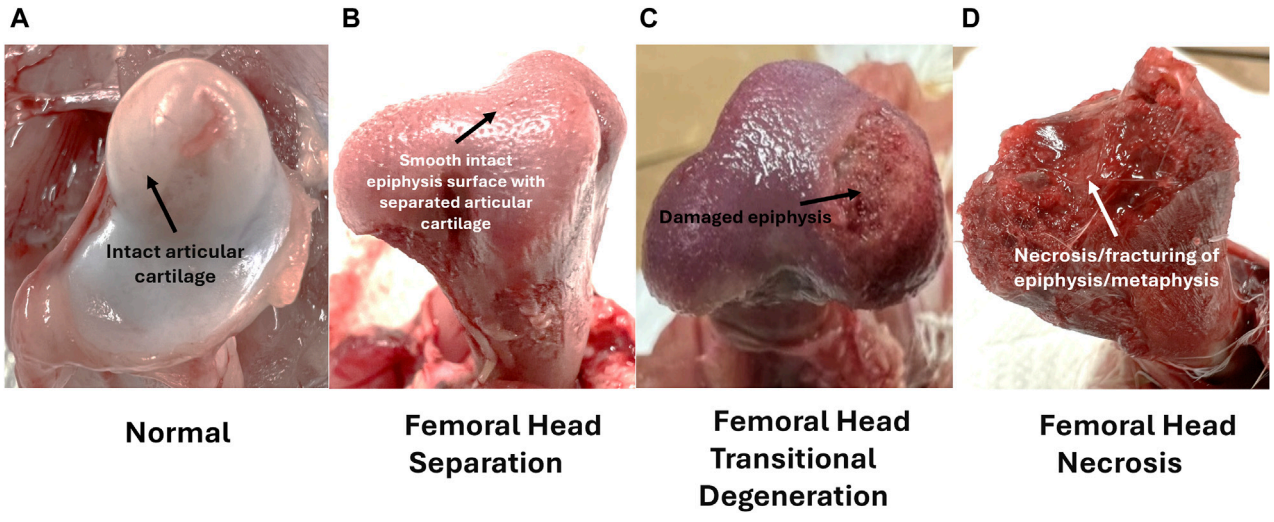

FIGURE 4
Left to Right; **(A–D)** Femoral ratings for birds diagnosed as lame. Femoral lesion categories are ordered with increasing severity, with arrows marking diagnostic characteristics–**(A)** Normal femoral head with intact cartilage; **(B)** Femoral Head Separation with disarticulated cartilage and smooth intact epiphyseal surface; **(C)** Femoral Head Transitional Degeneration with disarticulated cartilage and somewhat damaged epiphyseal surface; **(D)** Femoral Head Necrosis with extensive damage to the epiphysis and fracturing of the physis. Adapted from Do et al. (2024).

diagnosis of the disease, both from past literature and the authors' own bodies of work. Additionally, Wideman et al. (2012) also introduced the first highly effective wire-flooring model to induce BCO lameness in experimental broilers, which had traditionally been accomplished–albeit to varying degrees of success–via injection of *Staphylococcus* spp. to induce bacteremia

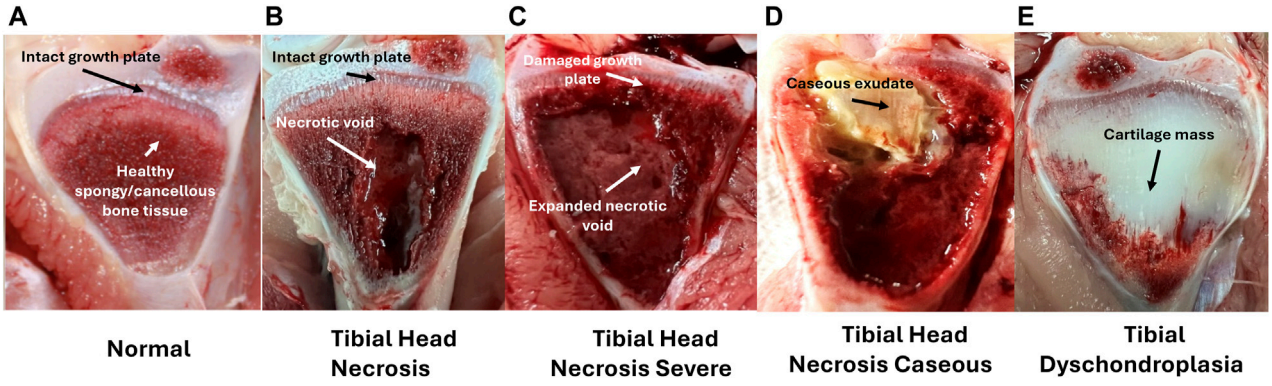

FIGURE 5
Left to Right; **(A–E)** Tibial ratings for birds diagnosed as lame. Tibial lesion categories are ordered with increasing severity (excluding E) with arrows marking diagnostic characteristics–**(A)** Normal tibial head with intact growth plate and firm, healthy cancellous bone tissue (2); **(B)** Tibial Head Necrosis with intact growth plate and developing necrotic void in cancellous bone tissue; **(C)** Tibial Head Necrosis Severe with damaged growth plate and large necrotic void in cancellous bone tissue; **(D)** Tibial Head Necrosis Caseous with caseous exudate, possibly marking bacterial infiltration site; **(E)** Tibial Dyschondroplasia with accumulated non-vascularized, non-mineralized cartilaginous mass replacing cancellous bone tissue. Adapted from Do et al. (2024).

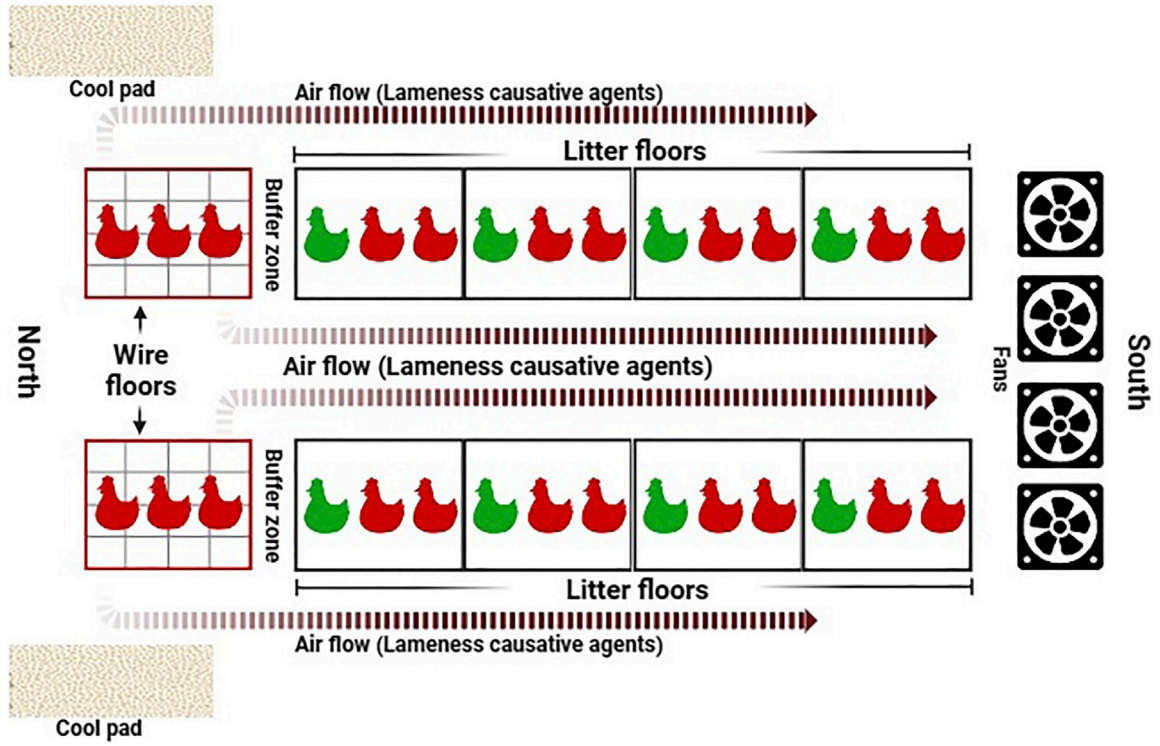

FIGURE 6
Schematic of the aerosol transmission model. Airflow facilitated by automated mechanical ventilation carries upwind aerosolized BCO etiological agents, released by stressed birds reared on wire flooring, and spreads them to remaining litter-floored birds in the same housing environment. Reproduced from Asnayanti et al. (2024a) with permission from Elsevier.

and subsequent osteomyelitis (Emslie and Nade, 1983; Daum et al., 1990). This model leverages the postulated BCO pathophysiology, which involves the stress imposed on immature leg bones by the animal's weight and exacerbated by the uneven wire flooring the animals traverse on without direct handling by research personnel, thus eliminating the stress from this factor (Wideman Jr et al., 2012). Whether in its original iteration (Ramser et al., 2021; Weimer et al., 2021) or as an incorporation into other approaches (Asnayanti et al., 2024b; Greene et al., 2024), the wire flooring remains a gold standard in

reliable induction of experimental BCO-associated lameness. These foundational findings have equipped researchers with valuable insights, upon which constant findings and advancements pertaining to various aspects of BCO-associated lameness have been made, and will continue to be explored in this relatively young field of research.

4.1 A novel BCO induction model

In the years following findings from Wideman et al. (2012), investigation of novel approaches to BCO induction model and other mitigatory measures–mainly in the form of feed additives and supplements–have taken place. Expanding upon the effective wire-flooring model, Asnayanti et al. (2024b) developed the aerosol transmission model, the schematic of which is shown in Figure 6:

While the wire-flooring model is highly effective, being able to induce over 70% of cumulative lameness incidence in the respective animals (Wideman et al., 2012; Wideman, 2016; Al-Rubaye et al., 2017) it is also aggressive and unrepresentative of normal rearing conditions, thus potentially reducing research translatability into a practical industrial setting. Moreover, fabrication and breakdown of wire-flooring pens is a highly laborious and time-consuming process, which makes accessible experimental replication a challenging task. The novel approach of the aerosol transmission model seeks to improve these aspects. Relying on aerobic horizontal transmission of aerosolized etiological agents from stress-imposed, wire flooring-reared seeder birds to others within the same housing environment, this induction model resembles infectious transmission and outbreaks commonly seen within poultry houses with active ventilation (Adell et al., 2015; Elliott et al., 2019). As validated through a series of trials, the aerosol transmission model has been shown to be capable of inducing experimental lameness incidence rates comparable to the wire-flooring model, which range from 60% to 73% of experimental animals (Asnayanti et al., 2024b), thus providing a reliable alternative induction method that further expands the repertoire of BCO research methods alongside the wire-flooring model and experimental inoculation.

4.2 Mitigatory strategies

As briefly discussed, the productive life cycle of conventional meat broilers is incredibly short compared to other livestock species, averaging 6 weeks of age at processing. An inability to effectively treat individual animals in the field due to flock turnaround on such a short time frame has led to immediate culling of lame birds–BCO-associated or otherwise–as the only appropriate response to negative animal welfare and production efficiency (Mitchell, 2014; Granquist et al., 2019). From an integrator's perspective, early preventive and mitigatory strategies, such as feed additives and supplements, along with good management practices have become increasingly important to protect flocks from significant economic losses due to BCO lameness. It has been reported that supplementation of high-quality essential trace minerals such as copper, manganese, and magnesium in the broiler diet may have a positive effect in the strengthening and increased expression of TJ proteins, leading to decreased chances of translocation events and subsequent clinical BCO lameness incidence (Alrubaye et al., 2020). Other prophylactic dietary supplements, such as 1, 25-dihydroxyvitamin D_3-glycosides and Fe-CNP (iron-loaded chitooligosaccharide nanoparticles) have also demonstrated positive outcomes in clinical BCO lameness incidence reduction (Yousefi and Saki, 2019; Asnayanti et al., 2024a). Similarly, a recent study using isolated environmental chambers by Do et al. (2024), which evaluated prophylactic spraying of day-of-hatch chicks with probiotic *Enterococcus faecium* on the same lameness reduction parameters has revealed positive results, which also suggests a dose-dependent effect of the examined probiotic. Interestingly, supplement inclusion timing has consistently revealed a trend across different types in the overall outcome regarding lameness reduction rate, with early supplementation–usually the first 4 to 6 weeks of the experiment–often conferring the same performance as that throughout the entire experimental period, compared to inclusion within the latter half (Alharbi et al., 2024a; Asnayanti et al., 2024a). While the modes of action in these supplements are continuously under investigation, these findings are consistent with the well-established developmental timeline of physiological systems across species, including gastrointestinal and skeletal, where early influence of various nature on the respective immature environments often has lasting impacts as the organism grows–positively or negatively (Montgomery et al., 1999; Karsenty and Wagner, 2002; Di Mauro et al., 2013; Van Oudenhove et al., 2016).

4.3 Molecular investigation

In terms of molecular underpinnings, evidence of various cellular functional dysregulation has been implicated in the pathogenicity of BCO lameness. For example, signs of mitochondrial dysfunction, including increased mitochondrial biogenesis responses (maintained by PGC-1α and PGC-1β), increased trend of mitochondrial fission/fragmentation state (OMA1) rather than fusion state (OPA1), and decreased mitochondrial respiratory activity (regulated by FOXO3, FOXO4, and av-UCP) as well as functional genes (ANT, COXIV, and COX5A), have been documented in BCO-affected tissue (Ferver et al., 2021). Results from Ramser et al. (2022) also suggest dysregulation in autophagic mechanisms and downregulation of genes associated with autophagy (ATG13, SQSTM1, ATG9B, ATG16L, ATG12, LC3C and RAB7A) – which are crucial in maintaining cellular homeostasis, elimination of foreign entities, and have been previously linked to various skeletal diseases and disorders (Liu et al., 2014; Ichimiya et al., 2020) – leading to decreased cell viability after *in vitro* inoculation of the known BCO isolate *S. agnetis* 908, in a similar fashion to direct autophagy inhibition via exposure to 3-Methyladenine and chloroquine. These results also offer an insight into possible mechanisms through which bacterial infection influences and exacerbates colonization sites that eventually lead to increasing severity and lameness, an aspect that has not yet been clearly defined in literature. Finally, high-throughput metabolomics has recently been employed in examination of dysregulated metabolic cascades and their outcomes in BCO-affected tissue (Ramser et al.,

2023) with metabolite profile from affected bones showing distinctive differences compared to that seen in healthy bone tissue, including activation of CD40 and AQP7 – the former of which has been associated with decreased bone mineral density and *S. aureus* bacterial infection, both major contributors to BCO etiology (Pineda et al., 2011; Schlievert et al., 2019). While much further research is needed for a complete picture regarding BCO pathogenesis and pathophysiological changes on the molecular level, these early encouraging results will nonetheless be invaluable in future research direction.

5 Industrial concerns of BCO lameness

As mentioned, due to its increasingly overwhelming and widespread impact, the issue of bacterial chondronecrosis with osteomyelitis is accompanied by a wide range of concerns within the poultry industry. Alongside major animal welfare issues and tremendous economic losses from impacted birds due to mortality and carcass condemnations, BCO and its associated lameness may also be implicated in other aspects of poultry meat production–such as meat quality and food safety.

5.1 Economical concerns

Lameness is often regarded as the main source of economic loss in meat birds as it not only results in bird loss, but can negatively impact the growth and performance of meat birds, leading to reduced productivity and economic losses (Pearce et al., 2023). In 2022, the USDA reported 9.17 billion broilers produced in the United States, and BCO can be linked to a loss of between $80 million and $120 million in sales (Granquist et al., 2019; Adnan Yousaf et al., 2021). Modern industrial broiler production often relies on an "all in, all out" model, in which a broiler flock of a similar age/background goes through production stages at the same time with housekeeping downtime between flocks (Biosecurity Nova Scotia, 2020; Brothers, 2022). This model allows greater control from the integrator in maintaining biosecurity and reducing transmission of diseases among animals due to a lack of mid-flock movement and the possibility of thorough cleanout between flocks, which is extremely important in cases of disease outbreaks that may require thorough containment and disinfection–or depopulation of the entire flock as mandated by regulatory bodies (UC Davis Veterinary Medicine, 2019; APHIS, 2022). Despite the advantages offered, however, an inherent downside to this model lies in the turnaround speed at which a flock enters and leaves a complex that does not allow for isolation of affected individuals and prolonged disease treatment plans like other major livestock species while maintaining productive efficiency (LeBlanc et al., 2006; Seaman and Fangman, 2023). Considering the intractably internal nature of BCO pathogenesis and pathophysiological changes, as well as this lack of individual treatment plans for birds with an already incredibly short productive life cycle, there has yet been an effective therapeutic treatment for BCO as of current, placing the onus on preventive measures and strategies instead–or prompt culling of birds exhibiting clinical signs, resulting in animal losses. While several preventive approaches using dietary supplements (Alrubaye et al., 2020; Alharbi et al., 2024a; Asnayanti et al., 2024c) and early spraying of a probiotic strain (Do et al., 2024) have shown promising results in reduction of observable clinical BCO-associated lameness diagnosis, much more work remains to be done to find a potential cure. In addition to the loss in meat production, manually assessing individual poultry in a commercial setting is infeasibly time-consuming and labor-intensive, as a standard grow out barn is commonly responsible for approximately 36,000 to 52,000 broiler heads produced every 42 days on average, a complex of which may consist of multiple houses on the same productive timeline (Brothers, 2022). Moreover, extensive worker handling could cause undue distress to birds (Pearce et al., 2023), leading to further productivity and time loss, as well as potentially increased broiler injuries and lameness.

5.2 Animal welfare concerns

Discussions of poultry welfare would not be complete without extensive consideration of leg issues and lameness as an overarching topic. In addition to several common leg or foot conditions caused by inadequate housing and nutritional management such as foot pad dermatitis and hock burns (Berg, 2004; Shepherd and Fairchild, 2010), weight-induced lameness–whether through developmental issues, mechanical injuries, or bacterial infection as a cause–contributes to a significant part of this conversation. Broilers afflicted with increasing degrees of lameness have been observed to spend much less time walking, standing upright, with fewer feeding visits compared to healthy birds (Weeks et al., 2000; Nääs et al., 2009) which are all associated with reduced productivity and welfare standards. Similarly, not only is BCO-associated lameness considered painful to the animal and predisposes them to the same lameness-related issues, but the condition also leads to loss of marketable products from culls and condemnations (Granquist et al., 2019). Furthermore, as a species with an established hierarchy, broilers outwardly exhibiting clinical lameness will frequently experience aggression from more dominant littermates, pushing them further down the social "pecking order" within the flock and exacerbating negative welfare impacts (Favati et al., 2014a; Favati et al., 2014b; Marino, 2017). As another unfortunate consequence of this innate behavior, some broilers may modify their behavior to "mask" any apparent indication of pain and avoid flock hostility, which greatly contributes to the difficulty in accurate diagnosis of BCO-associated lameness–or other lameness evaluations in general–outside of clinical diagnosis as suggested by several studies indicating BCO lesion development even in apparently healthy birds (Alharbi et al., 2024a; Asnayanti et al., 2024b). Today, lameness is one of the most important welfare concerns for the poultry industry, particularly with regards to broilers (Granquist et al., 2019). Alongside the obvious negative impacts to animal health, consumers are increasingly becoming aware of industrial practices and animal welfare impacts in agricultural production (Estes and Edgar, 2013). As such, addressing lameness remains a top priority for the poultry industry to improve consumer perception and confidence, an aspect it has constantly striven to achieve (McCulloch, 2017; Sinclair et al., 2019; Sonntag et al., 2019). Kapell et al. (2012) and Siegel et al. (2019) highlighted genetic improvements to skeletal strength and integrity made within the past 2 decades, which have resulted in encouraging findings regarding decreased heritability and prevalence of common leg disorders such as long bone deformation

(valgus/varus, bowed legs), and tibial dyschondroplasia while maintaining a similar level of performance increase. Despite this, current literature remains quite lacking in studies examining whether such genetic improvements have resulted in any appreciable effects on bone parameters associated with BCO pathogenesis and pathophysiology. Interestingly, a study by Chen et al. (2018) has found that osteochondrotic severity remains similar between a random-bred line representative of 1950s broilers and several modern broiler lines–with the former weighing significantly less during development–suggesting such a condition may not be weight-dependent. It is clear that much more research in this aspect is warranted for a thorough understanding of BCO pathology and effective breeding selection strategies, as well as management practices to decrease its prevalence.

5.3 Possible links to meat safety and quality concerns

The quality and safety of poultry products remain a major concern for both consumers and producers (Rouger et al., 2017). In terms of microbial contamination and food safety, risks of salmonellosis have become an assumed facet of poultry meat and eggs (Morris and Wells, 1970; Whiley and Ross, 2015; Antunes et al., 2016) that necessitates thorough rules and regulations regarding poultry meat and egg handling because of the massive and highly complex scale of poultry production and processing in the United States. Just as frequently, contamination of enterococci and staphylococci from the animal's gut has also been reported due to lower processing standards compared to other livestock species (Bortolaia et al., 2016). Considering the etiology, pathogenesis, and pathophysiology of BCO, there are grounds for heightened attention regarding poultry meat contamination from potential internal lesions that have gone undetected during carcass processing, especially in birds that do not show the associated clinical symptoms essential to pre-mortem BCO-associated lameness diagnosis (Alharbi et al., 2024a; Asnayanti et al., 2024b).

Product quality from injured or affected animals is often influenced by excess inflammation in the tissue around wound sites (Gifford et al., 2012). Due to the damage of connective tissue surrounding affected joints, the integrity of the meat structure may also be compromised, which is not only a loss of product, but is often unappealing to consumers (Lee and Mienaltowski, 2023). While it is unclear whether BCO and its associated lameness may have a significant direct impact on issues pertaining to meat quality aside from these points of consideration, such a dialogue may still benefit from a broader point of view with regard to the physiology of the modern broiler. Having become a "hot button" topic of discussion since their rising prevalence in the past decade, pectoralis major muscle myopathy (woody breast–WB, Figure 7) and deep pectoral myopathy (green muscle disease–DPM, Figure 8) are some of the most recognizable examples of degenerative myopathies miring product quality within the industry that have been linked to the heavy weight and rapid muscling of commercial broilers (Bilgili and Hess, 2008; Sihvo et al., 2018).

Breast muscle affected by WB syndrome is characterized by an abnormally tough and rubbery texture, usually with high calcium content (Welter et al., 2022), resulting in poor palatability for the consumer. Several postulated pathogenesis and pathophysiological changes have been proposed in current literature of WB syndrome. Hoving-Bolink et al. (2000) entertained the possibility of switching toward glycolytic pathways in muscle development of the animal to fit selection pressure for higher breast yield and efficiency, which could potentially lead to higher development rates of muscular abnormalities as suggested by Petracci and Berri (2017). At the same time, decreased blood and oxygen supplies to muscle tissue due to poor vasculature may also contribute to the issue, as evident by a decrease in myopathy severity as muscle tissue is examined moving inward relative to the pectoralis major's surface (Hoving-Bolink et al., 2000; Sihvo et al., 2018). Finally, several studies have also explored and suggested the possibility of metabolic waste product displacement playing a significant role, which introduces highly oxidative and stressful internal conditions for cellular functions, resulting in inflammation, mitochondrial damage and dysfunction, and prompting regenerative processes that ultimately lead to characteristics distinctive to growth abnormalities associated with woody breast (Boerboom et al., 2018; Papah et al., 2018; Sihvo et al., 2018). While no singular definitive cause has been determined, it is accepted that WB is a multi-faceted issue with wide reaches to fast-growth genetics, nutrition, and growth management of heavier birds (Caldas-Cueva and Owens, 2020). On the other hand, DPM is characterized by a hidden unappealing "greening" (necrosis) of the deep pectoralis minor muscle (tender) that would escape detection in unfabricated broiler carcasses. The disease is caused by excessive wing-flapping in heavier birds, leading to blood supply cutoffs and injuries to the pectoralis minor muscle as the superficial pectoralis major grows in size and resulting in necrosis of the former (Bilgili and Hess, 2008). Despite these inherent differences in pathogenesis between discussed myopathies and BCO and their impact on broiler meat quality, the heavy body weight and rapid muscling of the modern broiler seem to be the singular converging factor that leads to physiological strain on both breast muscle and leg bones, resulting in their respective associated pathologies. Indeed, reports of all three conditions are much scarcer in layers, which are much smaller and slower in growth rates compared to their meat broiler counterparts. In this sense, a movement toward reduced broiler sizes, achievable through limitations on the maximum potential genetic growth such as those implemented in European markets (Bos et al., 2018; Tixier-Boichard, 2020) could be the answer to improving meat quality and reducing BCO incidence at the same time. Of course, careful considerations must be taken with this approach to maintain production efficiency, profits, and product affordability for the consumers, as well as the potential environmental impacts of such changes (Leinonen et al., 2012). Evidently, it would be remiss to acknowledge such a connection between these conditions at face value due to a severe gap in current literature regarding this topic, where incidence of BCO-associated lameness and common breast myopathies are concurrently examined. Inherent factors contributing to such a dearth of knowledge include the different models employed in the respective line of research, as well as the expertise necessary for rapid accurate diagnosis and evaluation of the associated pathologies (Pang et al., 2020; Hisasaga Jr, 2021). However, science is a collective of collaborative efforts, and therein lies a significant opportunity for researchers in both fields to contribute to the overall understanding of these respective pathologies and possible interactive effects between them.

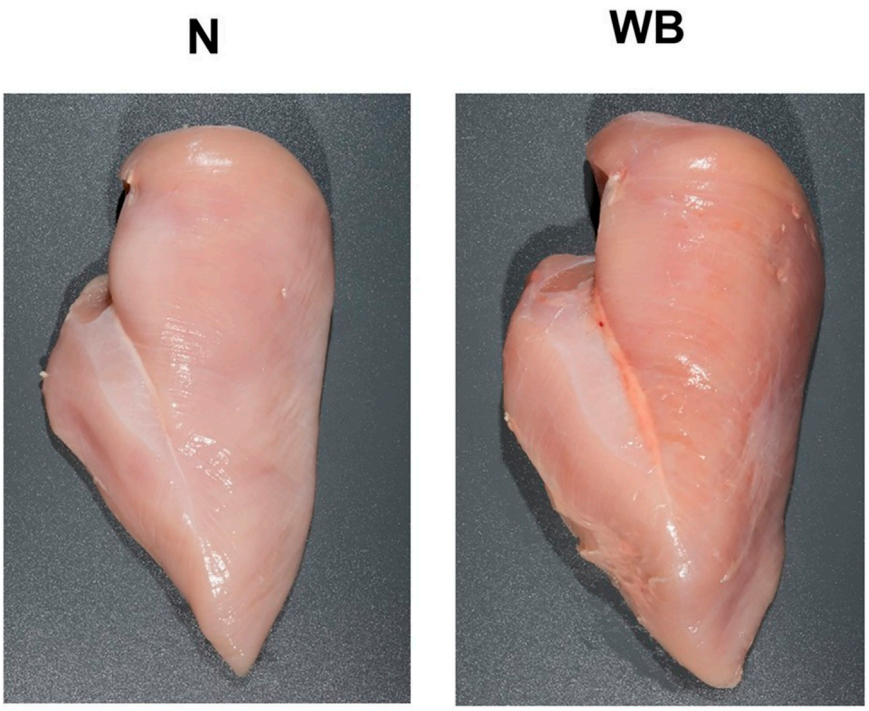

FIGURE 7
Exhibition of a normal (N) broiler pectoralis major muscle compared to one afflicted with woody breast syndrome (WB). Note the visually enlarged, darker, and firmer texture of the cranial region and caudal pronounced caudal ridge region of WB in comparison to N. Reproduced from Welter et al. (2022).

FIGURE 8
Exhibition of the pectoralis minor afflicted with severe deep pectoral myopathy (DPM). **(A)** Breast complex including both the pectoralis major and pectoralis minor muscles. **(B)** Separation of the complex. Reproduced from Giampietro-Ganeco et al. (2022) with permission from Elsevier.

6 Conclusion

Bacterial chondronecrosis with osteomyelitis poses a formidable challenge to avian health and welfare, with potentially dire implications for poultry meat safety and quality, necessitating comprehensive strategies for prevention, diagnosis, and management. Collaboration between all aspects of the industry, including primary breeders, commercial producers, veterinarians, and research bodies is essential to addressing the ever-present issue of lameness. By understanding the complexity of this condition, its pathology, and learning to assess affected birds, producers can better manage flock health and condition as well as optimize production through pre-emptive preventive measures. Most importantly, in prioritizing the animal's health and welfare by keeping an open-minded point of view, poultry producers will be better equipped for dialogues regarding the future direction of the modern broiler, greatly aiding the sustainability and resilience of the industry in its continuous goal of providing the growing populace with an affordable, safe, and high-quality source of animal protein.

Author contributions

AAn: Conceptualization, Data curation, Investigation, Visualization, Writing–original draft, Writing–review and editing. AD: Conceptualization, Data curation, Investigation, Visualization, Writing–original draft, Writing–review and editing. AAl: Conceptualization, Data curation, Project administration, Resources, Supervision, Writing–original draft, Writing–review and editing.

Funding

The author(s) declare that no financial support was received for the research, authorship, and/or publication of this article.

Acknowledgments

We would like to extend our deepest gratitude to all partners supporting the Alrubaye research program, including Federal, State, industry partners, as well as the University of Arkansas and the Division of Agriculture.

Conflict of interest

The authors declare that the research was conducted in the absence of any commercial or financial relationships that could be construed as a potential conflict of interest.

Publisher's note

References

Adell, E., Calvet, S., Pérez-Bonilla, A., Jiménez-Belenguer, A., García, J., Herrera, J., et al. (2015). Air disinfection in laying hen houses: effect on airborne microorganisms with focus on Mycoplasma gallisepticum. *Biosyst. Eng.* 129, 315–323. doi:10.1016/j.biosystemseng.2014.10.010

Adnan Yousaf, S. T., Kumar, LOOKESH, Rahman, SAIF.-U. R., Channo, ABDULLAH, Panhwar, MUHAMMAD IBRAHIM, Soomro, A. L. I. G. U. L., et al. (2021). A review study on legs lameness and weaknesses assessment methods in commercial broiler farming in Pakistan. *Biomed. J. Sci. and Tech. Res.* 40. doi:10.26717/bjstr.2021.40.006433

Alharbi, K., Asnayanti, A., Do, A. D. T., Perera, R., AL-Mitib, L., Shwani, A., et al. (2024a). Identifying dietary timing of organic trace minerals to reduce the incidence of osteomyelitis lameness in broiler chickens using the aerosol transmission model. *Animals* 14, 1526. doi:10.3390/ani14111526

Alharbi, K., Ekesi, N., Hasan, A., Asnayanti, A., Liu, J., Murugesan, R., et al. (2024b). Deoxynivalenol and fumonisin predispose broilers to bacterial chondronecrosis with osteomyelitis lameness. *Poult. Sci.* 103, 103598. doi:10.1016/j.psj.2024.103598

AL-Rubaye, A. A. K., Couger, M. B., Ojha, S., Pummill, J. F., Koon, J. A., Wideman, R. F., et al. (2015). Genome analysis of Staphylococcus agnetis, an agent of lameness in broiler chickens. *PLOS ONE* 10, e0143336. doi:10.1371/journal.pone.0143336

Alrubaye, A. A. K., Ekesi, N. S., Hasan, A., Elkins, E., Ojha, S., Zaki, S., et al. (2020). Chondronecrosis with osteomyelitis in broilers: further defining lameness-inducing models with wire or litter flooring to evaluate protection with organic trace minerals. *Poult. Sci.* 99, 5422–5429. doi:10.1016/j.psj.2020.08.027

AL-Rubaye, A. A. K., Ekesi, N. S., Zaki, S., Emami, N. K., Wideman, R. F., and Rhoads, D. D. (2017). Chondronecrosis with osteomyelitis in broilers: further defining a bacterial challenge model using the wire flooring model. *Poult. Sci.* 96, 332–340. doi:10.3382/ps/pew299

Antunes, P., Mourão, J., Campos, J., and Peixe, L. (2016). Salmonellosis: the role of poultry meat. *Clin. Microbiol. Infect.* 22, 110–121. doi:10.1016/j.cmi.2015.12.004

APHIS (2022). in *HPAI response - response goals and depopulation policy*. Editor U. S. D. O. AGRICULTURE (United States: USDA).

Applegate, T. J., and Lilburn, M. S. (2002). Growth of the femur and tibia of a commercial broiler line. *Poult. Sci.* 81, 1289–1294. doi:10.1093/ps/81.9.1289

Asnayanti, A., Alharbi, K., Do, A. D. T., AL-Mitib, L., Bühler, K., VAN Der Klis, J. D., et al. (2024a). Early 1,25-dihydroxyvitamin D3-glycosides supplementation: an efficient feeding strategy against bacterial chondronecrosis with osteomyelitis lameness in broilers assessed by using an aerosol transmission model. *J. Appl. Poult. Res.* 33, 100440. doi:10.1016/j.japr.2024.100440

Asnayanti, A., Do, A. D. T., Alharbi, K., and Alrubaye, A. (2024b). Inducing experimental bacterial chondronecrosis with osteomyelitis lameness in broiler chickens using aerosol transmission model. *Poult. Sci.* 103, 103460. doi:10.1016/j.psj.2024.103460

Asnayanti, A., Hasan, A., Alharbi, K., Hassan, I., Bottje, W., Rochell, S. J., et al. (2024c). Assessing the impact of Spirulina platensis and organic trace minerals on the incidence of bacterial chondronecrosis with osteomyelitis lameness in broilers using an aerosol transmission model. *J. Appl. Poult. Res.* 33, 100426. doi:10.1016/j.japr.2024.100426

AVIAGEN INC (2022). *Ross 708 broiler performance objectives - 2022*. Management Handbook. United States.

Bellairs, R., and Osmond, M. (2005). *Atlas of chick development*. Elsevier Science and Technology Books.

Berg, C. (2004). *Pododermatitis and hock burn in broiler chickens*. Measuring and auditing broiler welfare. Wallingford UK: CABI publishing.

Biesek, J., Banaszak, M., Kądziołka, K., Wlaźlak, S., and Adamski, M. (2022). Growth of broiler chickens, and physical features of the digestive system, and leg bones after aluminosilicates used. *Sci. Rep.* 12, 20425. doi:10.1038/s41598-022-25003-w

Bilgili, S., and Hess, J. (2008). Green muscle disease. *Reducing incidence broiler flock. Ross Tech* 8, 3.

BIOSECURITY NOVA SCOTIA (2020). *Tips for "all in/all out" production*. Canada.

Boerboom, G., VAN Kempen, T., Navarro-Villa, A., and Pérez-Bonilla, A. (2018). Unraveling the cause of white striping in broilers using metabolomics. *Poult. Sci.* 97, 3977–3986. doi:10.3382/ps/pey266

Borst, L. B., Suyemoto, M. M., Sarsour, A. H., Harris, M. C., Martin, M. P., Strickland, J. D., et al. (2017). Pathogenesis of enterococcal spondylitis caused by Enterococcus cecorum in broiler chickens. *Veterinary Pathol.* 54, 61–73. doi:10.1177/0300985816658098

Borst, L. B., Suyemoto, M. M., Scholl, E. H., Fuller, F. J., and Barnes, H. J. (2015). Comparative genomic analysis identifies divergent genomic features of pathogenic

Enterococcus cecorum including a type IC CRISPR-cas system, a capsule locus, an epa-like locus, and putative host tissue binding proteins. *PLOS ONE* 10, e0121294. doi:10.1371/journal.pone.0121294

Bortolaia, V., Espinosa-Gongora, C., and Guardabassi, L. (2016). Human health risks associated with antimicrobial-resistant enterococci and *Staphylococcus aureus* on poultry meat. *Clin. Microbiol. Infect.* 22, 130–140. doi:10.1016/j.cmi.2015.12.003

Bos, J. M., VAN Den Belt, H., and Feindt, P. H. (2018). Animal welfare, consumer welfare, and competition law: the Dutch debate on the Chicken of Tomorrow. *Anim. Front.* 8, 20–26. doi:10.1093/af/vfx001

Bottje, W. G., Wang, S., Kelly, F. J., Dunster, C., Williams, A., and Mudway, I. (1998). Antioxidant defenses in lung lining fluid of broilers: impact of poor ventilation conditions. *Poult. Sci.* 77, 516–522. doi:10.1093/ps/77.4.516

Bradshaw, R., Kirkden, R., and Broom, D. (2002). A review of the aetiology and pathology of leg weakness in broilers in relation to welfare. *Avian Poult. Biol. Rev.* 13, 45–103. doi:10.3184/147020602783698421

Braga, J. F. V., Silva, C. C., Teixeira, M. D. P. F., Martins, N. R. D. S., and Ecco, R. (2016). Vertebral osteomyelitis associated with single and mixed bacterial infection in broilers. *Avian Pathol.* 45, 640–648. doi:10.1080/03079457.2016.1193843

Brothers, D. (2022). New farmer's Guide to the commercial broiler industry: poultry husbandry and biosecurity basics. *Ala. Coop. Ext. Syst*. Available at: https://www.aces.edu/blog/topics/farm-management/new-farmers-guide-to-the-commercial-broiler-industry-poultry-husbandry-biosecurity-basics/(Accessed June 10, 2024).

Buijs, S., Keeling, L., Rettenbacher, S., VAN Poucke, E., and Tuyttens, F. A. M. (2009). Stocking density effects on broiler welfare: identifying sensitive ranges for different indicators. *Poult. Sci.* 88, 1536–1543. doi:10.3382/ps.2009-00007

Caldas-Cueva, J. P., and Owens, C. M. (2020). A review on the woody breast condition, detection methods, and product utilization in the contemporary poultry industry. *J. Animal Sci.* 98, skaa207. doi:10.1093/jas/skaa207

Carnaghan, R. (1966). Spinal cord compression in fowls due to spondylitis caused by Staphylococcus Pyogenes. *J. Comp. Pathol.* 76, 9–14. doi:10.1016/0021-9975(66)90042-9

Castro, F. L. S., Chai, L., Arango, J., Owens, C. M., Smith, P. A., Reichelt, S., et al. (2023). Poultry industry paradigms: connecting the dots. *J. Appl. Poult. Res.* 32, 100310. doi:10.1016/j.japr.2022.100310

Chen, L. R., Suyemoto, M. M., Sarsour, A. H., Cordova, H. A., Oviedo-Rondón, E. O., Barnes, H. J., et al. (2018). Prevalence and severity of osteochondrosis of the free thoracic vertebra in three modern broiler strains and the Athens Canadian Random Bred control broiler. *Avian Pathol.* 47, 152–160. doi:10.1080/03079457.2017.1388499

Choppa, V. S. R., and Kim, W. K. (2023). A review on pathophysiology, and molecular mechanisms of bacterial chondronecrosis and osteomyelitis in commercial broilers. *Biomolecules* 13, 1032. doi:10.3390/biom13071032

COBB-VANTRESS INC (2022). *Cobb500 broiler* Performance and Nutrition Supplement. United States.

Cook, M. E. (2000). Skeletal deformities and their causes: introduction. *Poult. Sci.* 79, 982–984. doi:10.1093/ps/79.7.982

Cox, N. A., Stern, N. J., Hiett, K. L., and Berrang, M. E. (2002). Identification of a new source of Campylobacter contamination in poultry: transmission from breeder hens to broiler chickens. *Avian Dis.* 46, 535–541. doi:10.1637/0005-2086(2002)046[0535:IOANSO]2.0.CO;2

Damaziak, K., Charuta, A., Niemiec, J., Tatara, M. R., Krupski, W., Gozdowski, D., et al. (2019). Femur and tibia development in meat-type chickens with different growth potential for 56 days of rearing period. *Poult. Sci.* 98, 7063–7075. doi:10.3382/ps/pez445

Daum, R. S., Davis, W. H., Farris, K. B., Campeau, R. J., Mulvihill, D. M., and Shane, S. M. (1990). A model of *Staphylococcus aureus* bacteremia, septic arthritis, and osteomyelitis in chickens. *J. Orthop. Res.* 8, 804–813. doi:10.1002/jor.1100080605

De Meyer, F., Eeckhaut, V., Ducatelle, R., Dhaenens, M., Daled, S., Dedeurwaerder, A., et al. (2019). Host intestinal biomarker identification in a gut leakage model in broilers. *Veterinary Res.* 50, 46. doi:10.1186/s13567-019-0663-x

Di Mauro, A., Neu, J., Riezzo, G., Raimondi, F., Martinelli, D., Francavilla, R., et al. (2013). Gastrointestinal function development and microbiota. *Italian J. Pediatr.* 39, 15. doi:10.1186/1824-7288-39-15

Dinev, I. (2009). Clinical and morphological investigations on the prevalence of lameness associated with femoral head necrosis in broilers. *Br. Poult. Sci.* 50, 284–290. doi:10.1080/00071660902942783

Dinev, I. (2012). Pathomorphological investigations on the incidence of clinical spondylolisthesis (kinky back) in different commercial broiler strains. *Rev. médecine vétérinaire* 163, 511–515. doi:10.2141/jpsa.0120144

Dinev, I. (2014). Axial skeleton pathology in broiler chickens. *World's Poult. Sci. J.* 70, 303–308. doi:10.1017/s0043933914000312

Do, A. D. T., Anthney, A., Alharbi, K., Asnayanti, A., Meuter, A., and Alrubaye, A. A. K. (2024). Assessing the impact of spraying an Enterococcus faecium-based probiotic on day-old broiler chicks at hatch on the incidence of bacterial chondronecrosis with osteomyelitis lameness using a Staphylococcus challenge model. *Animals* 14, 1369. doi:10.3390/ani14091369

Ducatelle, R., Goossens, E., Eeckhaut, V., and VAN Immerseel, F. (2023). Poultry gut health and beyond. *Anim. Nutr.* 13, 240–248. doi:10.1016/j.aninu.2023.03.005

Duff, S. R. I. (1990). Do different forms of spondylolisthesis occur in broiler fowls? *Avian Pathol.* 19, 279–294. doi:10.1080/03079459008418680

Dunnam, G., Thornton, J. K., and Pulido-Landinez, M. (2023). Characterization of an emerging Enterococcus cecorum outbreak causing severe systemic disease with concurrent leg problems in a broiler integrator in the southern United States. *Avian Dis.* 67, 137–144. doi:10.1637/aviandiseases-D-22-00085

EFSA (2012). European Food Safety Authority Panel on Animal Health and Welfare (AHAW): scientific opinion on the use of animal-based measures to assess welfare of broilers. *EFSA J.* 10, 2774. doi:10.2903/j.efsa.2012.2774

Ekesi, N. S., Dolka, B., Alrubaye, A. A. K., and Rhoads, D. D. (2021). Analysis of genomes of bacterial isolates from lameness outbreaks in broilers. *Poult. Sci.* 100, 101148. doi:10.1016/j.psj.2021.101148

Elliott, K. E. C., Branton, S. L., Evans, J. D., and Peebles, E. D. (2019). Occurrence of horizontal transmission in layer chickens after administration of an in ovo strain F Mycoplasma gallisepticum vaccine1,2,3. *Poult. Sci.* 98, 4492–4497. doi:10.3382/ps/pez306

Emslie, K. R., and Nade, S. (1983). Acute hematogenous staphylococcal osteomyelitis. A description of the natural history in an avian model. *Am. J. Pathol.* 110, 333–345.

Estes, S., and Edgar, L. D. (2013). Consumer perceptions of poultry production in Arkansas: perceptions analysis. *Discov. Student J. Dale Bump. Coll. ofs Agric. Food Life Sci.* 14.

Favati, A., Leimar, O., and Løvlie, H. (2014a). Personality predicts social dominance in male domestic fowl. *PLoS One* 9, e103535. doi:10.1371/journal.pone.0103535

Favati, A., Leimar, O., Radesäter, T., and Løvlie, H. (2014b). Social status and personality: stability in social state can promote consistency of behavioural responses. *Proc. Biol. Sci.* 281, 20132531. doi:10.1098/rspb.2013.2531

Ferver, A., Greene, E., Wideman, R., and Dridi, S. (2021). Evidence of mitochondrial dysfunction in bacterial chondronecrosis with osteomyelitis–affected broilers. *Front. Veterinary Sci.* 8, 640901. doi:10.3389/fvets.2021.640901

Giampietro-Ganeco, A., Fidelis, H. D. A., Cavalcanti, E. N., Mello, J. L. M., Borba, H., De Souza, R. A., et al. (2022). Research Note: quality parameters of Turkey hens breast fillets detected in processing plant with deep pectoral myopathy and white striping anomaly. *Poult. Sci.* 101, 101709. doi:10.1016/j.psj.2022.101709

Gifford, C. A., Holland, B. P., Mills, R. L., Maxwell, C. L., Farney, J. K., Terrill, S. J., et al. (2012). Growth and Development Symposium: impacts of inflammation on cattle growth and carcass merit. *J. Animal Sci.* 90, 1438–1451. doi:10.2527/jas.2011-4846

González-Cerón, F., Rekaya, R., and Aggrey, S. E. (2015). Genetic analysis of bone quality traits and growth in a random mating broiler population. *Poult. Sci.* 94, 883–889. doi:10.3382/ps/pev056

Granquist, E. G., Vasdal, G., De Jong, I. C., and Moe, R. O. (2019). Lameness and its relationship with health and production measures in broiler chickens. *Animal* 13, 2365–2372. doi:10.1017/S1751731119000466

Greene, E. S., Ramser, A., Wideman, R., Bedford, M., and Dridi, S. (2024). Dietary inclusion of phytase and stimbiotic decreases mortality and lameness in a wire ramp challenge model in broilers. *Avian Pathol.* 53, 1–18. doi:10.1080/03079457.2024.2359592

Haynes, J. S. (2023). Pathology of the bones and joints. *Atlas Veterinary Surg. Pathology*, 59–89. doi:10.1002/9781119261254.ch2

Herdt, P., Defoort, P., Steelant, J., Swam, H., Tanghe, L., Goethem, S., et al. (2009). Enterococcus cecorum osteomyelitis and arthritis in broiler chickens. *Vlaams Diergeneeskd. Tijdschr.* 78, 44–48. doi:10.21825/vdt.87495

Heyndrickx, M., Vandekerchove, D., Herman, L., Rollier, I., Grijspeerdt, K., and De Zutter, L. (2002). Routes for salmonella contamination of poultry meat: epidemiological study from hatchery to slaughterhouse. *Epidemiol. Infect.* 129, 253–265. doi:10.1017/s0950268802007380

Hisasaga, C. (2021). *Assessing the accuracy of a woody breast identification technique and evaluating the association between mitochondria values to woody breast severity*. Fresno: California State University.

Hoving-Bolink, A. H., Kranen, R. W., Klont, R. E., Gerritsen, C. L. M., and De Greef, K. H. (2000). Fibre area and capillary supply in broiler breast muscle in relation to productivity and ascites. *Meat Sci.* 56, 397–402. doi:10.1016/s0309-1740(00)00071-1

Huang, S., Kong, A., Cao, Q., Tong, Z., and Wang, X. (2019). The role of blood vessels in broiler chickens with tibial dyschondroplasia. *Poult. Sci.* 98, 6527–6532. doi:10.3382/ps/pez497

Ichimiya, T., Yamakawa, T., Hirano, T., Yokoyama, Y., Hayashi, Y., Hirayama, D., et al. (2020). Autophagy and autophagy-related diseases: a review. *Int. J. Mol. Sci.* 21, 8974. doi:10.3390/ijms21238974

Jacob, F. G., Baracho, M. S., Nääs, I. A., Lima, N. S. D., Salgado, D. D., and Souza, R. (2016). Risk of incidence of hock burn and pododermatitis in broilers reared under commercial conditions. *Braz. J. Poult. Sci.* 18, 357–362. doi:10.1590/1806-9061-2015-0183

Jiang, T., Mandal, R. K., Wideman, R. F., JR., Khatiwara, A., Pevzner, I., and Min Kwon, Y. (2015). Molecular survey of bacterial communities associated with bacterial chondronecrosis with osteomyelitis (BCO) in broilers. *PLOS ONE* 10, e0124403. doi:10.1371/journal.pone.0124403

Julian, R. (1998). Rapid growth problems: ascites and skeletal deformities in broilers. *Poult. Sci.* 77, 1773–1780. doi:10.1093/ps/77.12.1773

Kapell, D. N. R. G., Hill, W. G., Neeteson, A. M., Mcadam, J., Koerhuis, A. N. M., and Avendaño, S. (2012). Twenty-five years of selection for improved leg health in purebred broiler lines and underlying genetic parameters. *Poult. Sci.* 91, 3032–3043. doi:10.3382/ps.2012-02578

Karsenty, G., and Wagner, E. F. (2002). Reaching a genetic and molecular understanding of skeletal development. *Dev. cell* 2, 389–406. doi:10.1016/s1534-5807(02)00157-0

Kierończyk, B., Rawski, M., Józefiak, D., and Świątkiewicz, S. (2017). Infectious and non-infectious factors associated with leg disorders in poultry–a review. *Ann. animal Sci.* 17, 645–669. doi:10.1515/aoas-2016-0098

Laurentie, J., Loux, V., Hennequet-Antier, C., Chambellon, E., Deschamps, J., Trotereau, A., et al. (2023). Comparative genome analysis of Enterococcus cecorum reveals intercontinental spread of a lineage of clinical poultry isolates. *mSphere* 8, e0049522–22. doi:10.1128/msphere.00495-22

Leblanc, S. J., Lissemore, K. D., Kelton, D. F., Duffield, T. F., and Leslie, K. E. (2006). Major advances in disease prevention in dairy cattle. *J. Dairy Sci.* 89, 1267–1279. doi:10.3168/jds.S0022-0302(06)72195-6

Lee, J., and Mienaltowski, M. J. (2023). Broiler white striping: a review of its etiology, effects on production, and mitigation efforts. *Poultry* 2, 292–304. doi:10.3390/poultry2020022

Leinonen, I., Williams, A. G., Wiseman, J., Guy, J., and Kyriazakis, I. (2012). Predicting the environmental impacts of chicken systems in the United Kingdom through a life cycle assessment: broiler production systems. *Poult. Sci.* 91, 8–25. doi:10.3382/ps.2011-01634

Liu, Y.-J., Zhang, L., Papasian, C. J., and Deng, H.-W. (2014). Genome-wide association studies for osteoporosis: a 2013 update. *jbm* 21, 99–116. doi:10.11005/jbm.2014.21.2.99

Marino, L. (2017). Thinking chickens: a review of cognition, emotion, and behavior in the domestic chicken. *Anim. Cogn.* 20, 127–147. doi:10.1007/s10071-016-1064-4

Mcculloch, V. (2017). Public Perception and Poultry Production: comparing public awareness and opinion of the UK poultry industry with published data. *Anim. Welf. Found.*

Mcnamee, P. T., Mccullagh, J. J., Thorp, B. H., Ball, H. J., Graham, D., Mccullough, S. J., et al. (1998). Study of leg weakness in two commercial broiler flocks. *Veterinary Rec.* 143, 131–135. doi:10.1136/vr.143.5.131

Mcnamee, P. T., Smyth, J. A., and Smyth, J. A. (2000). Bacterial chondronecrosis with osteomyelitis ('femoral head necrosis') of broiler chickens: a review. *Avian Pathol.* 29, 253–270. doi:10.1080/03079450050118386

Mitchell, R. (2014). Broiler lameness in the United States: an industry perspective. 25 th ANNUAL AUSTRALIAN. *Poult. Sci. SYMPOSIUM*, 175.

Montgomery, R. K., Mulberg, A. E., and Grand, R. J. (1999). Development of the human gastrointestinal tract: twenty years of progress. *Gastroenterology* 116, 702–731. doi:10.1016/s0016-5085(99)70193-9

Morris, G. K., and Wells, J. G. (1970). Salmonella contamination in a poultry-processing plant. *Appl. Microbiol.* 19, 795–799. doi:10.1128/am.19.5.795-799.1970

Nääs, I. A., Paz, I. C. L. A., Baracho, M. S., Menezes, A. G., Bueno, L. G. F., Almeida, I. C. L., et al. (2009). Impact of lameness on broiler well-being. *J. Appl. Poult. Res.* 18, 432–439. doi:10.3382/japr.2008-00061

Nairn, M., and Watson, A. (1972). *Leg weakness of poultry-a clinical and pathological characterisation.*

Nakhon, S., Numthuam, S., Charoensook, R., Tartrakoon, W., Incharoen, P., and Incharoen, T. 2019. Growth performance, meat quality, and bone-breaking strength in broilers fed dietary rice hull silicon. *Anim. Nutr,* 5, 152–155. doi:10.1016/j.aninu.2018.11.003

NATIONAL CHICKEN COUNCIL (2021a). Broiler chicken industry key facts 2021. Available at: https://www.nationalchickencouncil.org/about-the-industry/statistics/broiler-chicken-industry-key-facts/ (Accessed June 2, 2024).

NATIONAL CHICKEN COUNCIL (2021b). "*Per capita* consumption of poultry and livestock, 1965 to forecast 2022," in *Pounds*. Available at: https://www.nationalchickencouncil.org/about-the-industry/statistics/per-capita-consumption-of-poultry-and-livestock-1965-to-estimated-2012-in-pounds/ (Accessed June 2, 2024).

Pang, B., Bowker, B., Yang, Y., Zhang, J., and Zhuang, H. (2020). Relationships between instrumental texture measurements and subjective woody breast condition scores in raw broiler breast fillets. *Poult. Sci.* 99, 3292–3298. doi:10.1016/j.psj.2019.12.072

Papah, M. B., Brannick, E. M., Schmidt, C. J., and Abasht, B. (2018). Gene expression profiling of the early pathogenesis of wooden breast disease in commercial broiler chickens using RNA-sequencing. *PLOS ONE* 13, e0207346. doi:10.1371/journal.pone.0207346

Pattison, M. (1992). Impacts of bone problems on the poultry meat industry. *Poult. Sci. Symposium*.

Pearce, J., Chang, Y. M., and Abeyesinghe, S. (2023). Individual monitoring of activity and lameness in conventional and slower-growing breeds of broiler chickens using accelerometers. *Anim. (Basel)* 13, 1432. doi:10.3390/ani13091432

Pedersen, I. J., Tahamtani, F. M., Forkman, B., Young, J. F., Poulsen, H. D., and Riber, A. B. (2020). Effects of environmental enrichment on health and bone characteristics of fast growing broiler chickens. *Poult. Sci.* 99, 1946–1955. doi:10.1016/j.psj.2019.11.061

Petracci, M., and Berri, C. (2017). *Poultry quality evaluation: quality attributes and consumer values*. Sawston, Cambridge, United Kingdom: Woodhead Publishing.

Pineda, B., Tarín, J., Hermenegildo, C., Laporta, P., Cano, A., and García-Pérez, M. (2011). Gene–gene interaction between CD40 and CD40L reduces bone mineral density and increases osteoporosis risk in women. *Osteoporos. Int.* 22, 1451–1458. doi:10.1007/s00198-010-1324-0

Quarles, C. L., and Caveny, D. D. (1979). Effect of air contaminants on performance and quality of broilers. *Poult. Sci.* 58, 543–548. doi:10.3382/ps.0580543

Ramser, A., Greene, E., Alrubaye, A. A. K., Wideman, R., and Dridi, S. (2022). Role of autophagy machinery dysregulation in bacterial chondronecrosis with osteomyelitis. *Poult. Sci.* 101, 101750. doi:10.1016/j.psj.2022.101750

Ramser, A., Greene, E., Wideman, R., and Dridi, S. (2021). Local and systemic cytokine, chemokine, and FGF profile in bacterial chondronecrosis with osteomyelitis (BCO)-Affected broilers. *Cells* 10, 3174. doi:10.3390/cells10113174

Ramser, A., Hawken, R., Greene, E., Okimoto, R., Flack, B., Christopher, C. J., et al. (2023). Bone metabolite profile differs between normal and femur head necrosis (FHN/BCO)-Affected broilers: implications for dysregulated metabolic cascades in FHN pathophysiology. *Metabolites* 13, 662. doi:10.3390/metabo13050662

Rath, N. C., Huff, G. R., Huff, W. E., and Balog, J. M. (2000). Factors regulating bone maturity and strength in poultry. *Poult. Sci.* 79, 1024–1032. doi:10.1093/ps/79.7.1024

Rhoads, D. D., Pummill, J., and Alrubaye, A. A. K. (2024). Molecular genomic analyses of Enterococcus cecorum from sepsis outbreaks in broilers. *Microorganisms* 12, 250. doi:10.3390/microorganisms12020250

Robbins, K. M., Suyemoto, M. M., Lyman, R. L., Martin, M. P., Barnes, H. J., and Borst, L. B. (2012). An outbreak and source investigation of enterococcal spondylitis in broilers caused by Enterococcus cecorum. *Avian Dis.* 56, 768–773. doi:10.1637/10253-052412-Case.1

Rouger, A., Tresse, O., and Zagorec, M. (2017). Bacterial contaminants of poultry meat: sources, species, and dynamics. *Microorganisms* 5, 50. doi:10.3390/microorganisms5030050

Sanotra, G. S., Lawson, L. G., Vestergaard, K. S., and Thomsen, M. G. (2001). Influence of stocking density on tonic immobility, lameness, and tibial dyschondroplasia in broilers. *J. Appl. Animal Welf. Sci.* 4, 71–87. doi:10.1207/s15327604jaws0401_4

Santos, M. N., Widowski, T. M., Kiarie, E. G., Guerin, M. T., Edwards, A. M., and Torrey, S. (2022). In pursuit of a better broiler: tibial morphology, breaking strength, and ash content in conventional and slower-growing strains of broiler chickens. *Poult. Sci.* 101, 101755. doi:10.1016/j.psj.2022.101755

Schlievert, P. M., Cahill, M. P., Hostager, B. S., Brosnahan, A. J., Klingelhutz, A. J., Gourronc, F. A., et al. (2019). Staphylococcal superantigens stimulate epithelial cells through CD40 to produce chemokines. *MBio* 10, e00214. doi:10.1128/mbio.00214-19

Seaman, J., and Fangman, T. (2023). *Biosecurity for today's swine operation*. United States: University of Missouri Extension. Available at: https://extension.missouri.edu/publications/g2340 (Accessed July 17, 2024).

Shepherd, E., and Fairchild, B. (2010). Footpad dermatitis in poultry. *Poult. Sci.* 89, 2043–2051. doi:10.3382/ps.2010-00770

Shwani, A., Adkins, P. R., Ekesi, N. S., Alrubaye, A., Calcutt, M. J., Middleton, J. R., et al. (2020). Whole-genome comparisons of Staphylococcus agnetis isolates from cattle and chickens. *Appl. Environ. Microbiol.* 86, 004844–e520. doi:10.1128/AEM.00484-20

Siegel, P. B., Barger, K., and Siewerdt, F. (2019). Limb health in broiler breeding: history using genetics to improve welfare. *J. Appl. Poult. Res.* 28, 785–790. doi:10.3382/japr/pfz052

Sihvo, H. K., Airas, N., Lindén, J., and Puolanne, E. (2018). Pectoral vessel density and early ultrastructural changes in broiler chicken wooden breast myopathy. *J. Comp. Pathology* 161, 1–10. doi:10.1016/j.jcpa.2018.04.002

Sinclair, M., Yan, W., and Phillips, C. J. C. (2019). Attitudes of pig and poultry industry stakeholders in guandong province, China, to animal welfare and farming systems. *Animals* 9, 860. doi:10.3390/ani9110860

Sonntag, W. I., Spiller, A., and Von Meyer-Höfer, M. (2019). Discussing modern poultry farming systems—insights into citizen's lay theories. *Poult. Sci.* 98, 209–216. doi:10.3382/ps/pey292

Stalker, M. J., Brash, M. L., Weisz, A., Ouckama, R. M., and Slavic, D. (2010a). Arthritis and osteomyelitis associated with Enterococcus cecorum infection in broiler and broiler breeder chickens in Ontario, Canada. *J. Vet. Diagn Invest* 22, 643–645. doi:10.1177/104063871002200426

Stalker, M. J., Brash, M. L., Weisz, A., Ouckama, R. M., and Slavic, D. (2010b). Arthritis and osteomyelitis associated with Enterococcus cecorum infection in broiler and broiler breeder chickens in ontario, Canada. *J. Veterinary Diagnostic Investigation* 22, 643–645. doi:10.1177/104063871002200426

Szafraniec, G. M., Szeleszczuk, P., and Dolka, B. (2022). Review on skeletal disorders caused by Staphylococcus spp. in poultry. *Veterinary Q.* 42, 21–40. doi:10.1080/01652176.2022.2033880

Tallentire, C. W., Leinonen, I., and Kyriazakis, I. (2016). Breeding for efficiency in the broiler chicken: a review. *Agron. Sustain. Dev.* 36, 66. doi:10.1007/s13593-016-0398-2

Tixier-Boichard, M. (2020). From the jungle fowl to highly performing chickens: are we reaching limits? *World's Poult. Sci. J.* 76, 2–17. doi:10.1080/00439339.2020.1729676

Tomita, M., Ohkubo, R., and Hayashi, M. (2004). Lipopolysaccharide transport system across colonic epithelial cells in normal and infective rat. *Drug metabolism Pharmacokinet.* 19, 33–40. doi:10.2133/dmpk.19.33

UC DAVIS VETERINARY MEDICINE (2019). *All out - all in" poultry management approach to disease control - a guide for poultry owners*. Davis, CA, United States: A Guide for Poultry Owners.

USDA (2023). Poultry sector at a glance United States department of agriculture. Available at: https://www.ers.usda.gov/topics/animal-products/poultry-eggs/sector-at-a-glance/ (Accessed June 2, 2024).

USDA (2024). *Livestock, poultry and grain*. Washington, DC, United States: United States Department of Agriculture. Available at: https://www.ams.usda.gov/market-news/livestock-poultry-grain (Accessed June 2, 2024).

VAN Oudenhove, L., Levy, R. L., Crowell, M. D., Drossman, D. A., Halpert, A. D., Keefer, L., et al. (2016). Biopsychosocial aspects of functional gastrointestinal disorders: how central and environmental processes contribute to the development and expression of functional gastrointestinal disorders. *Gastroenterology* 150, 1355–1367.e2. doi:10.1053/j.gastro.2016.02.027

Vukina, T. (2001). Vertical integration and contracting in the US poultry sector. *J. Food Distribution Res.* 32, 29–38. doi:10.22004/ag.econ.27819

Weeks, C., Danbury, T., Davies, H., Hunt, P., and Kestin, S. (2000). The behaviour of broiler chickens and its modification by lameness. *Appl. animal Behav. Sci.* 67, 111–125. doi:10.1016/s0168-1591(99)00102-1

Weimer, S. L., Wideman, R. F., Scanes, C. G., Mauromoustakos, A., Christensen, K. D., and Vizzier-Thaxton, Y. (2021). Impact of experimentally induced bacterial chondronecrosis with osteomyelitis (BCO) lameness on health, stress, and leg health parameters in broilers. *Poult. Sci.* 100, 101457. doi:10.1016/j.psj.2021.101457

Welter, A. A., Wu, W. J., Maurer, R., O'Quinn, T. G., Chao, M. D., Boyle, D. L., et al. (2022). An investigation of the altered textural property in woody breast myopathy using an integrative omics approach. *Front. Physiol.* 13, 860868. doi:10.3389/fphys.2022.860868

Whiley, H., and Ross, K. (2015). Salmonella and eggs: from production to plate. *Int. J. Environ. Res. public health* 12, 2543–2556. doi:10.3390/ijerph120302543

Wideman, R. F. (2016). Bacterial chondronecrosis with osteomyelitis and lameness in broilers: a review. *Poult. Sci.* 95, 325–344. doi:10.3382/ps/pev320

Wideman, R. F., and Prisby, R. D. (2013). Bone circulatory disturbances in the development of spontaneous bacterial chondronecrosis with osteomyelitis: a translational model for the pathogenesis of femoral head necrosis. *Front. Endocrinol.* 3, 183. doi:10.3389/fendo.2012.00183

Wideman, R., AL-Rubaye, A., Gilley, A., Reynolds, D., Lester, H., Yoho, D., et al. (2013). Susceptibility of 4 commercial broiler crosses to lameness attributable to bacterial chondronecrosis with osteomyelitis. *Poult. Sci.* 92, 2311–2325. doi:10.3382/ps.2013-03150

Wideman, R., Hamal, K., Stark, J., Blankenship, J., Lester, H., Mitchell, K., et al. (2012). A wire-flooring model for inducing lameness in broilers: evaluation of probiotics as a prophylactic treatment. *Poult. Sci.* 91, 870–883. doi:10.3382/ps.2011-01907

Yousefi, A., and Saki, A. (2019). Iron loaded chitooligosaccharide nanoparticles reduces incidence of bacterial chondronecrosis with osteomyelitis in broiler chickens. *Iran. J. Appl. Animal Sci.* 9, 329–336.

Zhou, Z., Shen, D., Wang, K., Liu, J., Li, M., Win-Shwe, T.-T., et al. (2023). Pulmonary microbiota intervention alleviates fine particulate matter-induced lung inflammation in broilers. *J. Animal Sci.* 101, skad207. doi:10.1093/jas/skad207

Zuidhof, M. J., Schneider, B. L., Carney, V. L., Korver, D. R., and Robinson, F. E. (2014). Growth, efficiency, and yield of commercial broilers from 1957, 1978, and 2005. *Poult. Sci.* 93, 2970–2982. Available at:. doi:10.3382/ps.2014-04291

frontiers | Frontiers in Physiology

TYPE Original Research
PUBLISHED 09 October 2024
DOI 10.3389/fphys.2024.1456664

OPEN ACCESS

EDITED BY
Gale M. Strasburg,
Michigan State University, United States

REVIEWED BY
Elisabeth Duval,
Institut National de recherche pour l'agriculture, l'alimentation et l'environment (INRAE), France
Wei Guo,
University of Wisconsin-Madison, United States

*CORRESPONDENCE
Hong Zhuang,
hong.zhuang@usda.gov

RECEIVED 28 June 2024
ACCEPTED 18 September 2024
PUBLISHED 09 October 2024

CITATION
Choi J, Shakeri M, Kim WK, Kong B, Bowker B and Zhuang H (2024) Comparative metabolomic analysis of spaghetti meat and wooden breast in broiler chickens: unveiling similarities and dissimilarities.
Front. Physiol. 15:1456664.
doi: 10.3389/fphys.2024.1456664

Comparative metabolomic analysis of spaghetti meat and wooden breast in broiler chickens: unveiling similarities and dissimilarities

Janghan Choi[1], Majid Shakeri[1], Woo Kyun Kim[2], Byungwhi Kong[1], Brian Bowker[1] and Hong Zhuang[1]*

[1]USDA-ARS, US National Poultry Research Center, Athens, GA, United States, [2]Department of Poultry Science, University of Georgia, Athens, GA, United States

Introduction: Spaghetti meat (SM) and wooden breast (WB) are emerging myopathies in the breast meat of fast-growing broiler chickens. The purpose of the study was to investigate the metabolomic differences between normal (N), SM, and WB fillets 24 h postmortem.

Materials and methods: Eight chicken breasts for each experimental group were collected from a commercial processing plant. Supernatant from tissue homogenates were subjected to ultra-performance liquid chromatographytandem mass spectrometry (UPLC-MS) analysis.

Results and methods: A total of 3,090 metabolites were identified in the chicken breast meat. The comparison of WB and N showed 850 differential metabolites ($P < 0.05$), and the comparison of SM and N displayed 617 differential metabolites. The comparison of WB and SM showed 568 differential metabolites. The principal component analysis (PCA) plots showed a distinct separation between SM and N and between WB and N except for one sample, but SM and WB were not distinctly separated. Compared to N, 15-Hydroxyeicosatetraenoic acid (15-HETE) increased, and D-inositol-4-phosphate decreased in both SM and WB, indicating that cellular homeostasis and lipid metabolism can be affected in SM and WB. The abundance of nicotinamide adenine dinucleotide (NAD) + hydrogen (H) (NADH) was exclusively decreased between SM and N ($P < 0.05$). Purine metabolism was upregulated in SM and WB compared to N with a greater degree of upregulation in WB than SM. Folic acid levels decreased in SM and WB compared to N ($P < 0.05$). Steroid hormone biosynthesis was downregulated in SM compared to N ($P < 0.05$). Carbon metabolism was downregulated in SM and WB compared to N with greater degree of downregulation in WB than SM ($P < 0.05$). These data suggest both shared and unique metabolic alterations in SM and WB, indicating commonalities and differences in their underlying etiologies and meat quality traits. Dietary supplementation of deficient nutrients, such as NADH, folic acids, etc. and modulation of altered pathways in SM and WB would be strategies to reduce the incidence and severity of SM and WB.

KEYWORDS

spaghetti meat, wooden breast, meat quality, metabolomics, NADH, steroid hormones

1 Introduction

In 2022, broiler meat was the most consumed meat in the US at approximately 45 kg *per capita* (Shahbandeh, 2023). The fast growth and high feed efficiency traits of broiler chickens, achieved through advancements in genetic selection and nutritional programs, have significantly contributed to making broiler meat an affordable and nutritious protein source for human consumption (Choi et al., 2023). However, it is critical to acknowledge that muscle myopathies including spaghetti meat (SM), wooden breast (WB), and white stripping (WS) are frequently observed in the breast meat of fast-growing broiler chickens (Che et al., 2022). The incidence of WB is estimated to be 5%–10% in the commercial condition (Baltic et al., 2024) and could be greater than 50% in certain cases (Xing et al., 2020). The incidence of SM could be up to 20% in certain cases (Baldi et al., 2021).

A number of studies investigated the potential etiologies and meat quality traits of WB, characterized by tough texture and high-water content, and of WS, characterized by the development of white striations parallel to the orientation of the myofibers (Kuttappan et al., 2012; Velleman and Clark, 2015; Abasht et al., 2016; Choi et al., 2024; Bailey et al., 2015) suggested that WB and WS may have similarities in their etiologies because of their macroscopic and microscopic similarities. Although diverse omics analyses including transcriptomic, proteomics, metabolomics, and lipidomics were performed in WB and WS (Kong et al., 2021; Kang et al., 2022; Liu et al., 2022; Wang et al., 2023; Kong et al., 2024), there are still no clear explanations for exact etiologies to date for WB. SM, described by soft texture and loss of muscle integrity due to the detachment of muscle fibers, is another emerging muscle myopathy in broilers (Baldi et al., 2021). Not many studies have been conducted on SM due to its recentness (Baldi et al., 2021; Che et al., 2024) demonstrated that SM exhibited inflammation and fibrosis similar to those observed in WB, both of which are common traits of muscle myopathies. However, etiologies and quality characteristics of SM are also not fully understood. Understanding the similarities and dissimilarities between SM and WB would be instrumental in finding the etiologies of these myopathies and potential solutions to reduce their incidence and severity in broiler chickens. A recent study by Che et al. (2024) investigated the transcriptomic differences between SM, WB, and N and demonstrated that SM may have similar etiologies with WB at the transcriptomic level. However, to our best knowledge, there are no published studies that compared SM and WB at the metabolomic level. Therefore, the purpose of the study was to investigate the metabolomic differences between SM, WB, and N at 24 h *postmortem*.

2 Materials and methods

2.1 Sample collection

Eight fillets (pectoralis major) for each experimental groups, N without any muscle myopathies, severe WB [score 3 according to Bowker et al. (2019)], and severe SM [score 2 according to Baldi et al. (2021)] were selected from a batch of broiler breast meat collected from a commercial slaughterhouse. Samples (size 1 cm × 1 cm × 1 cm) were excised from the cranial-ventral portion of the muscle at 24 h *postmortem* and stored at −80°C until further analysis. For metabolomics analysis, 100 mg of the frozen samples were placed in 2 mL tubes with liquid nitrogen and shipped with dry ice to a commercial company (Metware Biotechnology, Woburn, MA).

2.2 Untargeted metabolomic analysis

Samples were homogenized in a ball-mill grinder at 30 Hz (Hz) for 20 s. 400 μL solution (Methanol:Water = 7:3, V/V) containing internal standard was mixed with 20 mg of ground sample and mixed in a shaker at 2,500 rpm for 5 min. The mixture was placed on ice for 15 min and centrifuged at 12,000 rpm for 10 min at 4°C (5430R; Eppendorf, Hamburg, Germany). The 300 μL of the supernatant was collected and placed in −20°C for 30 min. The sample was then centrifuged at 12,000 rpm for 3 min at 4°C, and the supernatant was collected for the untargeted metabolomic analysis. Ultra-performance liquid chromatography (ExionLC; SCIEX, CA)-tandem mass spectrometry (TripleTOF 6,600+; SCIEX, CA) (UPLC-MS) equipped with Acquity UPLC HSS T3 (1.8 μm, 2.1 mm × 100 mm) column (Waters, Milford, MA) was used for untargeted metabolomics. The column temperature was 40°C, and ultrapure water and acetonitrile were mobile phase A and B, respectively. Both mobile phases contained 0.1% formic acid. The flow rate was 0.4 mL/min, and the injection volume was 2 μL.

2.3 Quality control

A quality control (QC) sample was prepared from a mixture of all sample extracts to examine the reproducibility of the entire metabolomics process. During data collection, one quality control sample was inserted for every 10 test samples.

2.4 Data processing, multivariate, and enrichment analyses

The original data file acquired by UPLC-MS was converted to mzXML format by ProteoWizard. Peak extraction, peak alignment and retention time correction were performed by XCMS program. The peaks with missing rate >50% in each group of samples were filtered. The blank values were filled with k-nearest neighbors (KNN), and the peak area was corrected by the support vector regression (SVR) method. The metabolites were annotated by searching the MetwareBio's in-house database, integrated public database, prediction database and metDNA. Finally, substances with a comprehensive identification score above 0.7 and a coefficient of variation (CV) value of QC samples less than 0.3 were extracted, and then positive and negative mode were combined (substances with the greatest qualitative grade and the lowest CV value were retained) to obtain the ALL_sample_data file.

Principal component analysis (PCA) was calculated by using the base package of R software (version 4.1.2) with parameter scale = True indicating unit variance Scaling (UV) for normalizing the data. Discriminant analysis by orthogonal partial least squares (OPLS-DA) was analyzed by using MetaboAnalystR of R software (version

TABLE 1 Number of differential metabolites with statistical significance ($P < 0.05$) in the comparisons of spaghetti meat (SM) and normal (N) fillets, spaghetti meat (SM) and wooden breast (WB), and spaghetti meat (SM) and wooden breast (WB).

Comparisons	Total	Downregulated	Upregulated
SM and N	617	342	275
SM and WB	568	314	254
WB and N	850	362	488

4.1.2). R^2Y (goodness of fit) was higher than 0.99 in the comparison between SM and N, SM and WB, and WB and N. Cumulative Q^2 (goodness of prediction) was 0.844, 0.667, and 0.690 in the comparison between SM and N, SM and WB, and WB and N, respectively. $Q^2 > 0.5$ can be considered as an effective model, and $Q^2 > 0.9$ can be considered as an excellent model. OPLS-DA S-plots were generated by setting variable importance in projection (VIP) value >1 as significant. The horizontal axis is the covariance between the principal components and metabolites, the vertical axis represents the correlation coefficient between the principal components and the metabolites. The closer the points are to the top right corner or bottom left corner, the more significant the difference in metabolite abundance. Red dots indicate metabolites with VIP value >1 and green dots indicate metabolites with VIP value ≤1. Volcano plots were generated with VIP, $\log_2$ fold changes, and $-\log_{10}P$-value by using R software. Hierarchical clustering trees were generated according to the relative intensity of the differential metabolites by using R software. Differential metabolites were screened by using the following condition: VIP >1 and $P < 0.05$. The top 20 differentially expressed metabolites regardless of up- and downregulation were selected by using the values of $\log_2$ fold change between N, SM, and WB. The top 10 up- and downregulated differentially expressed metabolites were also screened by using the values of $\log_2$ fold change between N, SM, and WB. To identify metabolites with significant alterations unique to SM and WB, as well as those shared between them compared to N, the product of the log2 fold changes between SM and N and between WB and N was calculated. Uniquely differential metabolites in SM or WB with high fold changes (the top 10 up- and downregulated) were selected by identifying the screened metabolites ($P < 0.05$) in one group but not screened ($P > 0.05$) in the other group. For enrichment analysis, differential metabolites ($P < 0.05$) were annotated using the KEGG database (Kanehisa and Goto, 2000).

3 Results

3.1 Number of the differential metabolites

A total of 3,090 metabolites were identified in the chicken breast meat. Table 1 showed the number of differential metabolites between the experimental groups. The comparison of SM and N, SM and WB, and WB and N showed 617-, 568-, and 850 differential metabolites, respectively. The Venn diagram shows the number of shared and unique differential metabolites in the different comparisons (Figure 1).

3.2 PCA and OPLS-DA plots

As shown in Figure 2, the QC samples were tightly clustered in a specific area, which indicates the variations among the samples are

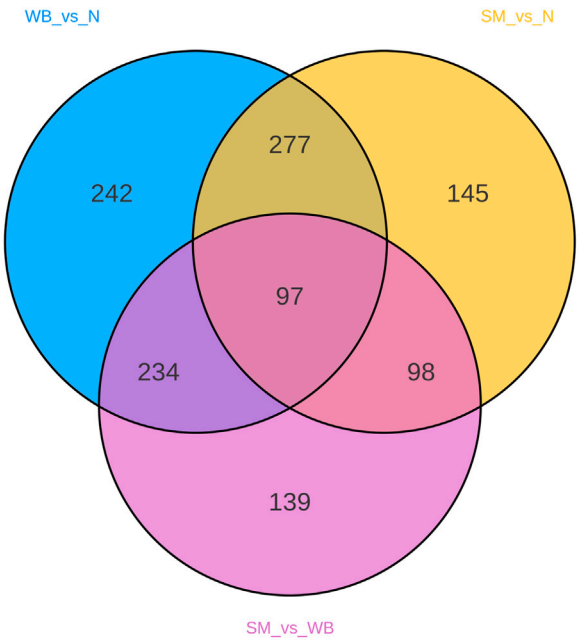

FIGURE 1
Venn diagram of differential metabolites between spaghetti meat (SM), wooden breast (WB), and normal (N) fillets.

10.3389/fphys.2024.1456664

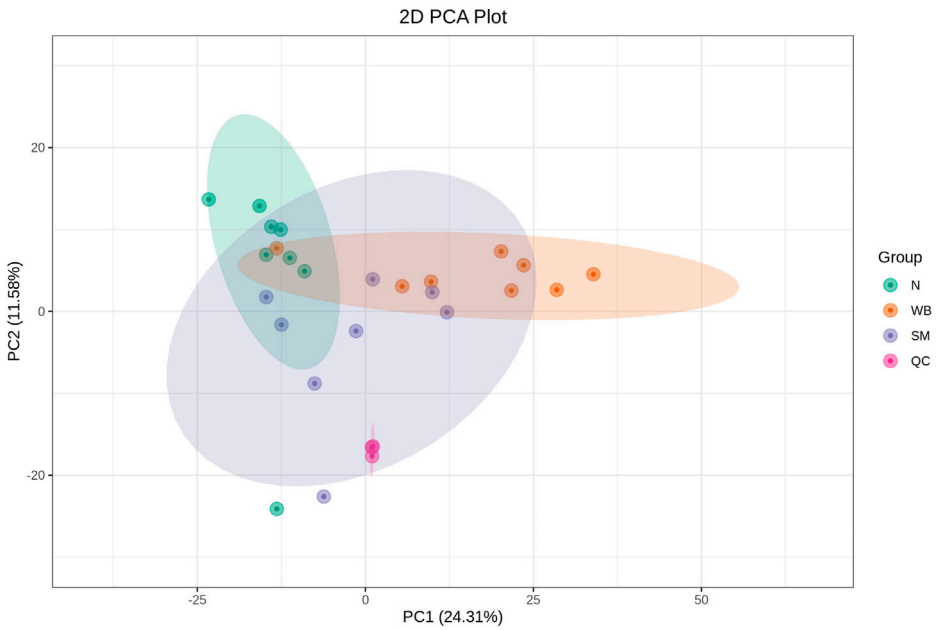

FIGURE 2
Principal component analysis (PCA) score diagrams of different experimental groups including spaghetti meat (SM), wooden breast (WB), and normal (N) with quality control (QC) samples.

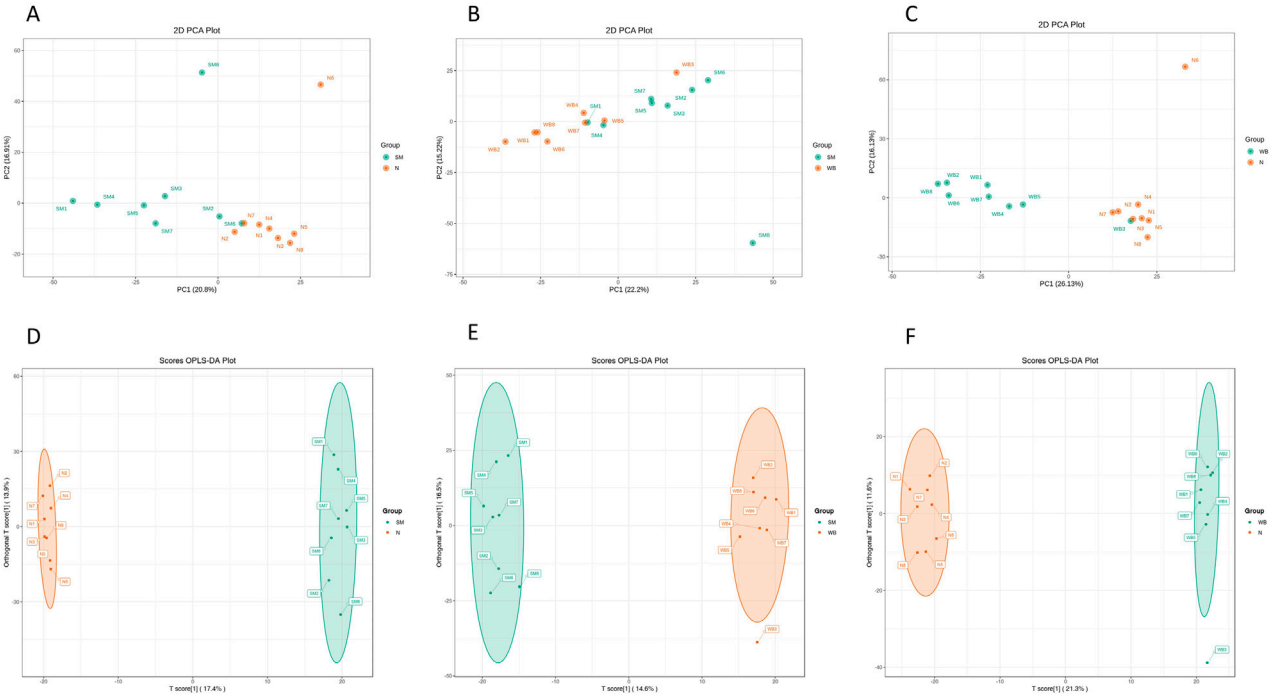

FIGURE 3
Principal component analysis PCA; **(A–C)** and discriminant analysis by orthogonal partial least squares [(OPLS-DA; **(D, E, and F)**] of spaghetti meat (SM), wooden breast (WB), and normal (N) groups based on differential metabolites when wooden breast (WB) or spaghetti meat (SM) compared to normal (N) fillets and each other. A and D: SM and N, B and E: SM and WB, C and F: WB and N.

attributed to biological differences. The PCA plots showed distinct separation between SM and N and between WB and N except for one sample and have PC1 greater than 20% and PC2 greater than 15% in the comparisons (Figures 3A, C). However, SM and WB were not distinctly separated in the PCA plot (Figure 3B). The OPLS-DA plots displayed distinct separation between SM and N, SM and WB,

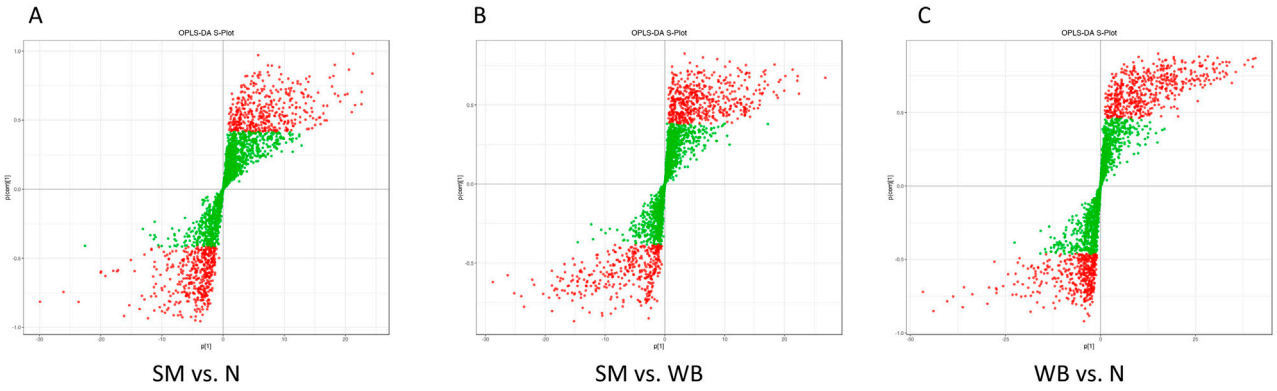

FIGURE 4
Discriminant analysis by orthogonal partial least squares (OPLS-DA) S-plot of spaghetti meat (SM), wooden breast (WB), and normal (N) groups. **(A)** SM and N; **(B)** SM and WB; and **(C)** WB and N. The *X*-axis represents the covariance between the principal components and metabolites, the *Y*-axis represents the correlation coefficient between the principal components and the metabolites. The closer the points are to the top right corner or bottom left corner, the more significant the difference in metabolite abundance. Red dots indicate metabolites with variable importance in projection (VIP) value >1 and green dots indicate metabolites with VIP value ≤1.

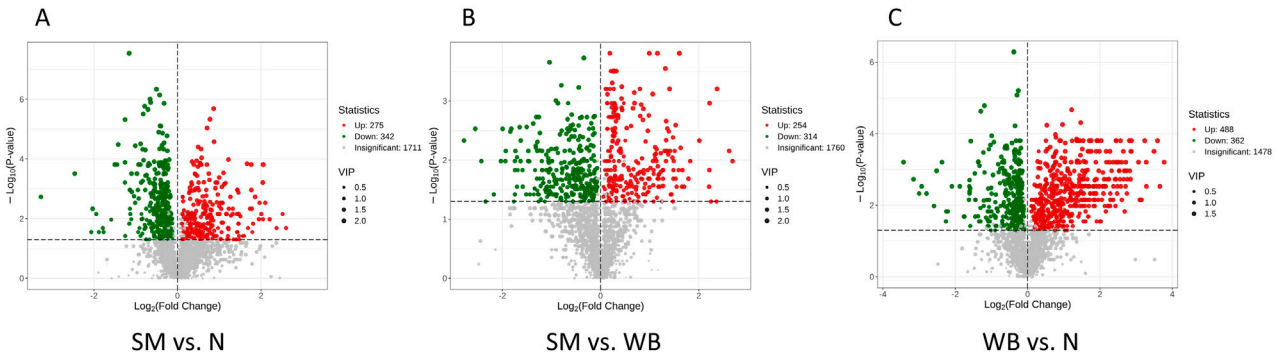

FIGURE 5
Volcano plots of differential metabolites when spaghetti meat (SM) or wooden breast (WB) compared to normal (N) fillets and each other. A: SM and N; B: SM and WB; and C: WB and N. Each point in the volcano plot represents a metabolite with green points representing downregulated differential metabolite, red points upregulated differential metabolite, and gray points the detected metabolites but show no significant differences. The *X*-axis represents the $\log_2$ fold change value of metabolites between two groups, and the Y-axis represent the level of significant differences (-log10 *P*-value). The size of each dot represents the variable importance in projection (VIP) value.

and WB and N (Figures 3D–F). The OPLS-DA S-plots (Figure 4) indicated that numerous metabolites contributed to separating the comparison groups. The comparison of SM and WB seemed more clustered near the *Y*-axis, which indicated that there were less significant metabolites for the separation.

3.3 Volcano plots of differential metabolites and hierarchical clustering trees

The volcano plots of the comparisons between N, SM, and WB are shown in Figure 5. The comparisons of WB and N and of SM and WB showed the greatest- and the lowest number of differential metabolites, respectively. The hierarchical clustering trees of the comparisons of SM and N, SM and WB, and WB and N were shown in Figure 6. The comparisons of SM and N and of WB and N showed that either SM or WB were distinctly separated compared to the N, but the comparison of SM and WB did not show distinct separation.

3.4 Differential metabolites

Differential metabolites between N, SM, and WB are presented in Supplementary Table 1. Table 2 displays the top 10 up- and downregulated metabolites between N, SM, and WB. Folic acid was observed in the top 10 downregulated differential metabolites in comparisons between SM and N and between WB and N. Neoxanthin was observed in the top 10 downregulated differential metabolites in comparisons between WB and N. Taurine, glutathione, and reduced glutathione were upregulated in SM compared to N and WB compared to N ($P < 0.05$). In the comparisons between SM and WB and between WB and N, 13 and 10 differential metabolites, respectively, were amino acid related

10.3389/fphys.2024.1456664

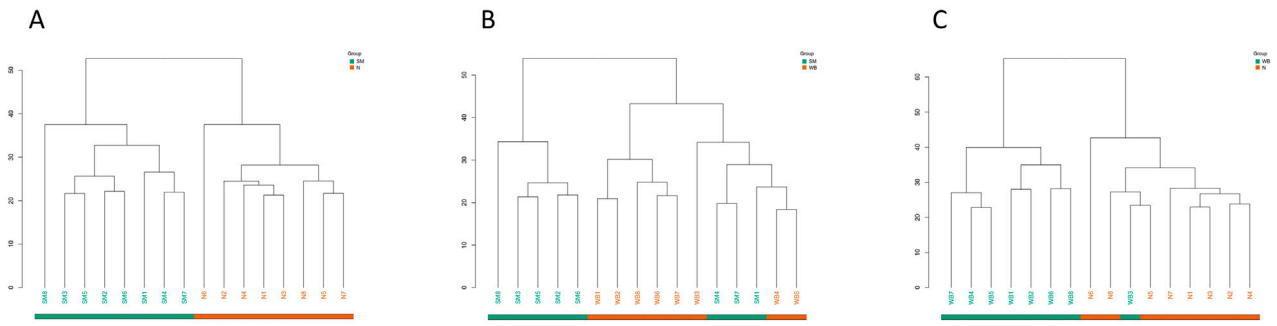

FIGURE 6
Hierarchical clustering trees of differential metabolites when spaghetti meat (SM) or wooden breast (WB) compared to normal (N) fillets and each other. **(A)** SM and N; **(B)** SM and WB; and **(C)** WB and N.

metabolites among the top 10 upregulated or downregulated metabolites. There were only 6 amino acid related metabolites (amino acids, polypeptides, small peptides, and amino acid derivatives) among the top 10 upregulated or downregulated metabolites between SM and N. Several differential metabolites associated with amino acid related metabolites were observed in SM (185) and WB (312) when compared to N. Between SM and N, 103 amino acid related metabolites were downregulated, but 82 amino acid related metabolites were upregulated. Between WB and N, 111 amino acid related metabolites were downregulated, but 201 amino acid related metabolites were upregulated. Between SM and WB, there were 211 amino acid related differential metabolites (up: 86 and down: 125) were associated with amino acid related metabolites.

3.5 Co-expressed and uniquely expressed metabolites in SM and WB

Co-expressed and uniquely expressed metabolites in SM and WB compared to N are presented in Supplementary Table 2. Between SM and N, 140 out of 617 differential metabolites were co-expressed with those from the comparison of WB and N, and 477 metabolites were uniquely expressed in both WB and SM. Between WB and N, 373 out of 850 differential metabolites were co-expressed with the screened metabolites from the comparison of SM and N. The top 10 co-expressed metabolites between SM and WB are shown in Table 3. 15-hydroxyeicosatetraenoic acid (15-HETE) increased and D-inositol-4-phosphate decreased with high fold changes in both SM and WB compared to N ($P < 0.05$). Several lipid related metabolites including alpha-dimorphecolic acid, 15(S)-HETE, and (±) 18-HEPE were upregulated in SM and WB compared to N. Stigmastane-3,6-dione was the most decreased differential metabolites in SM and WB compared to N. In addition, Ala-Lys and beta-Alanyl-L-lysine were one of the most decreased differential metabolites in SM and WB compared to N. There were no metabolites showing opposite direction of fold change (e.g., minus values after multiplication of fold changes) between the SM and WB compared to N. The top 10 uniquely expressed in SM or WB compared to N are shown in Table 4. The abundance of nicotinamide adenine dinucleotide (NAD) + hydrogen (H) (NADH) was exclusively decreased in SM compared with N ($P < 0.05$). However, no significant differences were observed between WB and N ($P > 0.05$).

3.6 Kyoto encyclopedia of genes and genomes (KEGG)-enriched analysis of differentiated metabolites

The top 10 differentiated Kyoto Encyclopedia of Genes and Genomes (KEGG) pathways between N, SM, and WB are presented in Table 5. The top 20 upregulated or downregulated KEGG pathways between N, SM, and WB are shown in Figure 7. Metabolic pathways and biosynthesis of cofactors were the two most annotated KEGG pathways between N, SM, and WB. There were 10 and 5 differential metabolites that were related to steroid hormone biosynthesis between SM and N and between WB and N, respectively. The 7 and 3 differential metabolites related to steroid hormone biosynthesis were downregulated and upregulated, respectively, between SM and N. 21-deoxycortisol, aldosterone hemiacetal, tetrahydrodeoxycorticosterone, androsterone, cortisone, 11 beta-hydroxyandrostenedione, and (8S,9S,10S,13S,14S)-17-(2-hydroxyacetyl)-10,13-dimethyl-2,4,5,6,7,8,9,12,14,15,16,17-dodecahydro-1H-cyclopenta [a] phenanthrene-3,11-dione, were downregulated, testosterone, 16 alpha-hydroxyestrone, and 2-methoxyestradiol were upregulated in SM compared to N. There were 21, 10, and 16 differential metabolites related to ATP-binding cassette (ABC) transporters; 20, 10, and 19 related to biosynthesis of amino acids; 13, 3, and 13 related to aminoacyl-tRNA biosynthesis; 14, 5, and 14 related to carbon metabolism; and 16, 12, and 11 related to purine metabolism between WB and N, SM and N, and SM and WB, respectively. Between SM and WB, 8 differential metabolites related to purine metabolism biosynthesis were downregulated and 3 upregulated.

4 Discussion

The purpose of the study was to investigate the metabolomic differences between N (non-myopathic), SM, and WB meat at 24 h *postmortem*. The research interests were: 1) to identify similar

TABLE 2 The top 10 upregulated or downregulated differential metabolites when spaghetti meat (SM) or wooden breast (WB) compared to normal (N) fillets and each other.

Comparison	Up- or downregulated	Order	Compounds	VIP	*p*-value	Log_2FC
SM vs. N	Up	1	(±)15-HETE	1.476	0.021	2.601
		2	Phe-Tyr-Phe-Lys-Ile	1.315	0.007	2.517
		3	alpha-Dimorphecolic acid	1.457	0.021	2.371
		4	NCGC00386087-01_C43H60N2O12_(2S)-N-[(2E,4E,6S,7R)-7-{(3S,4R)-3,4-Dihydroxy-5-[(1E,3E,5E)-7-(4-hydroxy-2-oxo-1,2-dihydro-3-pyridinyl)-6-methyl-7-oxo-1,3,5-heptatrien-1-yl]tetrahydro-2-furanyl}-6-methoxy-5-methyl-2,4-octadien-1-yl]-2-{(2R,3R,4R,6S)-2,3,4-trihydroxy-5,5-dimethyl-6-[(1E,3E)-1,3-pentadien-1-yl]tetrahydro-2H-pyran-2-yl}butanamide	1.685	0.010	2.207
		5	N-Acetyl-L-aspartic acid	1.654	0.003	2.102
		6	Indoleacetaldehyde	2.351	<0.001	2.051
		7	15(S)-Hydroxyeicosatrienoic acid	1.519	0.010	2.046
		8	1-Palmitoyl-2-oleoyl-sn-glycero-3-phosphocholine	2.076	0.001	2.043
		9	Asn-Gly-Glu-Val-Lys	1.619	0.007	2.007
		10	Lys-Met-Val-Ser-Arg	1.652	0.003	1.966
	Down	1	Stigmastane-3,6-dione	1.779	0.002	−3.271
		2	NADH	1.953	<0.001	−2.461
		3	methyl 4-(6-(4-(methoxycarbonylamino)phenyl)-4-morpholino-1H-pyrazolo [3,4-d]pyrimidin-1-yl)piperidine-1-carboxylate	1.425	0.028	−2.065
		4	PE-NMe(22:6 (4Z,7Z,10Z,13Z,16Z,19Z)/18:1 (9Z))	1.948	0.005	−2.032
		5	D-inositol-4-phosphate	1.422	0.007	−1.946
		6	Ala-Lys	1.413	0.028	−1.883
		7	6-o-Phosphonohexopyranose	1.444	0.021	−1.789
		8	beta-Alanyl-L-lysine	1.400	0.028	−1.769
		9	Folic acid	1.226	0.011	−1.587
		10	Furathiocarb	2.196	<0.001	−1.499
SM vs. WB	Up	1	Leucylvaline	1.805	0.010	2.687
		2	Leu-Val	1.856	0.007	2.618
		3	Valylcysteine	2.027	0.001	2.372
		4	Cycluron	1.433	0.050	2.362
		5	His-Phe-Tyr-Asp	1.509	0.050	2.248
		6	Carnitine C10:0	2.099	0.001	2.220
		7	2-[(2-Amino-3-phenylpropanoyl)amino]-3-methylbutanoic acid	1.816	0.015	2.215
		8	Val-val	1.666	0.028	2.208
		9	L-Octanoylcarnitine	1.885	0.005	2.010
		10	Phe-Glu	1.676	0.010	1.825
	Down	1	Lys-Thr-His	1.757	0.005	−2.781
		2	Val-Leu-Ser-Pro-Ala	1.894	0.003	−2.552
		3	N-tridecanoyl-L-Homserine lactone	1.708	0.010	−2.428
		4	PA (18:0/18:3 (9Z,12Z,15Z))	1.493	0.049	−2.341

(Continued on following page)

10.3389/fphys.2024.1456664

TABLE 2 (*Continued*) The top 10 upregulated or downregulated differential metabolites when spaghetti meat (SM) or wooden breast (WB) compared to normal (N) fillets and each other.

Comparison	Up- or downregulated	Order	Compounds	VIP	*p*-value	Log_2FC
		5	Maytansine	1.545	0.038	−2.174
		6	Tyr-Leu-Ala-Lys	1.785	0.010	−2.029
		7	NADH	1.880	0.003	−1.995
		8	Tyr-Pro-His	1.724	0.010	−1.939
		9	N-Acetylserotonin	1.784	0.007	−1.931
		10	Tyr-Phe-Lys	1.689	0.003	−1.838
WB vs. N	Up	1	Lys-Thr-Glu	1.758	0.001	3.775
		2	Lys-Thr-His	1.682	0.003	3.657
		3	(±)15-HETE	1.886	<0.001	3.590
		4	alpha-Dimorphecolic acid	1.874	<0.001	3.493
		5	Pro-Gln-Lys	1.643	0.003	3.283
		6	Tyr-Pro-His	1.787	0.001	3.279
		7	15-Hydroxy-5,8,11,13-eicosatetraenoic acid	1.857	<0.001	3.237
		8	Leu-Thr-Pro-Asp-Ala	1.610	0.007	3.149
		9	D-myo-Inositol-1,3,4,5,6-pentaphosphate	1.692	0.007	3.102
		10	Ala-Pro-Asp-Ala-Lys	1.825	0.001	3.066
	Down	1	D-inositol-4-phosphate	1.785	0.001	−3.429
		2	Ala-Lys	1.698	0.002	−3.154
		3	Stigmastane-3,6-dione	1.473	0.005	−2.999
		4	beta-Alanyl-L-lysine	1.628	0.003	−2.928
		5	Folic acid	1.596	0.005	−2.793
		6	(2RS)-Lotaustralin	1.559	0.010	−2.587
		7	His-Phe-Tyr-Asp	1.842	0.001	−2.514
		8	Valylcysteine	1.736	0.001	−2.366
		9	Neoxanthin	1.292	0.028	−2.256
		10	Clopidogrel	1.490	0.015	−2.245

VIP, variable importance in the projection; FC, fold change; (±) 15-HETE, 15-Hydroxyeicosatetraenoic acid; NADH, Nicotinamide adenine dinucleotide.

metabolites expressed in SM and WB and 2) to identify unique metabolites expressed exclusively in SM or WB. These findings are instrumental in understanding the similarities and differences in the etiologies and meat quality traits of SM and WB in broiler fillets. In the current study, the 24 h *postmortem* time point was selected because we aimed to compare metabolomic differences between the groups after the completion of rigor mortis and other changes that take place in the tissue during the early *postmortem* conversion of muscle to meat. PCA and OPLS-DA plots showed that SM or WB was distinctly separated compared to N, which indicates that SM or WB retains different metabolic state compared to N. However, SM and WB samples were not distinctly separated when compared each other according to the PCA plot. Furthermore, hierarchical clustering tree analysis also showed consistent trends. These results may indicate that there are common etiologies or traits in meat quality in SM and WB. A recent transcriptomics study by Che et al. (2024), which had a similar experimental design to the current study, reported that some traits of SM and WB were similar but the other dissimilar at the transcriptomic level of SM and WB. Our current results also indicate similarity and also dissimilarity in SM and WB traits at the metabolic level.

In the current study, 15-HETE increased in both SM and WB compared to N. 15-HETE is an eicosanoid, a metabolite of arachidonic acid, and it is involved in inhibiting inflammation response (Zhu and Ran, 2012). Consistently, a previous study by Wu et al. (2024) reported that 14,15-dihydroxyeicosatrienoic acid was increased in SM compared to N, potentially due to inflammatory response in SM. A previous study by Wang et al. (2010) reported that 15-HETE had important roles in inhibiting cell apoptosis and improving cell survival in pulmonary arterial smooth

10.3389/fphys.2024.1456664

TABLE 3 The top 10 co-expressed differential metabolites and their fold changes (FC) and multiplied values in spaghetti meat (SM) and wooden breast (WB) compared to normal (N) fillets.

	Metabolites	SM and N Log_2FC	WB and N Log_2FC	Multiplied value
1	Stigmastane-3,6-dione	−3.271	−2.999	9.810
2	(±)15-Hydroxyeicosatetraenoic acid (HETE)	2.601	3.590	9.337
3	alpha-Dimorphecolic acid	2.371	3.493	8.282
4	D-inositol-4-phosphate	−1.946	−3.429	6.672
5	Phe-Tyr-Phe-Lys-Ile	2.517	2.534	6.379
6	Ala-Lys	−1.883	−3.154	5.937
7	N-Acetyl-L-aspartic acid	2.102	2.814	5.915
8	Leu-Thr-Pro-Asp-Ala	1.810	3.149	5.699
9	15(S)-Hydroxyeicosatrienoic acid	2.046	2.714	5.553
10	beta-Alanyl-L-lysine	−1.769	−2.928	5.179

TABLE 4 The top 10 uniquely expressed metabolites between spaghetti meat (SM) or wooden breast (WB) compared to normal (N) fillets.

Unique differential metabolites between SM and N			
Metabolites	VIP	*p*-value	Log_2FC
NADH	1.953	<0.001	−2.461
NCGC00386087-01_C43H60N2O12_(2S)-N-[(2E,4E,6S,7R)-7-[(3S,4R)-3,4-Dihydroxy-5-[(1E,3E,5E)-7-(4-hydroxy-2-oxo-1,2-dihydro-3-pyridinyl)-6-methyl-7-oxo-1,3,5-heptatrien-1-yl]tetrahydro-2-furanyl]-6-methoxy-5-methyl-2,4-octadien-1-yl]-2-[(2R,3R,4R,6S)-2,3,4-trihydroxy-5,5-dimethyl-6-[(1E,3E)-1,3-pentadien-1-yl]tetrahydro-2H-pyran-2-yl]butanamide	1.685	0.010	2.207
PE-NMe(22:6 (4Z,7Z,10Z,13Z,16Z,19Z)/18:1 (9Z))	1.948	0.005	−2.032
Asn-Gly-Glu-Val-Lys	1.619	0.007	2.007
Etoposide	2.006	0.002	1.859
Lyso-PAF C-16-d4	1.782	0.005	1.779
Ile-Ile	1.937	0.001	1.768
CDP-ethanolamine	1.487	0.015	1.462
(2S,4S)-1-Acetoxy-16-heptadecene-2,4-diol	1.637	0.001	−1.258
Aspartylthreonine	1.235	0.050	1.221
Unique differential metabolites between WB and N			
Lys-Thr-Glu	1.758	0.001	3.775
Lys-Thr-His	1.682	0.003	3.657
15-Hydroxy-5,8,11,13-eicosatetraenoic acid	1.857	<0.001	3.237
D-myo-Inositol-1,3,4,5,6-pentaphosphate	1.692	0.007	3.102
13-HOTE	1.776	<0.001	2.873
N-Acetylserotonin	1.831	<0.001	2.865
Phe-Lys-Tyr	1.826	<0.001	2.855
Pro-Ile-Thr	1.668	0.001	2.825
Phe-Val-Ser	1.646	0.002	2.755
3,5-Pyridinedicarboxylic acid, 1,4-dihydro-2,4,6-trimethyl-, diethyl ester	1.520	0.005	2.743

VIP, variable importance in the projection; FC, fold change; NADH, nicotinamide adenine dinucleotide.

TABLE 5 Top 10 differentiated Kyoto Encyclopedia of Genes and Genomes (KEGG) pathways based on number of significant differential metabolites between spaghetti meat (SM), wooden breast (WB), and normal (N) fillets.

SM and N		SM and WB		WB and N	
KEGG pathway	Number of differential metabolites	KEGG pathway	Number of differential metabolites	KEGG pathway	Number of differential metabolites
Metabolic pathways	87	Metabolic pathways	98	Metabolic pathways	147
Biosynthesis of cofactors	17	Biosynthesis of cofactors	25	Biosynthesis of cofactors	32
Purine metabolism	12	Biosynthesis of amino acids	19	ATP-binding cassette (ABC) transporters	21
Nucleotide metabolism	11	ATP-binding cassette (ABC) transporters	16	Biosynthesis of amino acids	20
ABC transporters	10	Carbon metabolism	14	Nucleotide metabolism	17
Steroid hormone biosynthesis	10	Glycine, serine and threonine metabolism	14	Purine metabolism	16
Glycerophospholipid metabolism	8	Aminoacyl-tRNA biosynthesis	13	Carbon metabolism	14
Alanine, aspartate and glutamate metabolism	7	Nucleotide metabolism	11	Aminoacyl-tRNA biosynthesis	13
Pyrimidine metabolism	5	Purine metabolism	11	Cysteine and methionine metabolism	12
Neuroactive ligand-receptor interaction	5	2-Oxocarboxylic acid metabolism	10	Glycerophospholipid metabolism	11

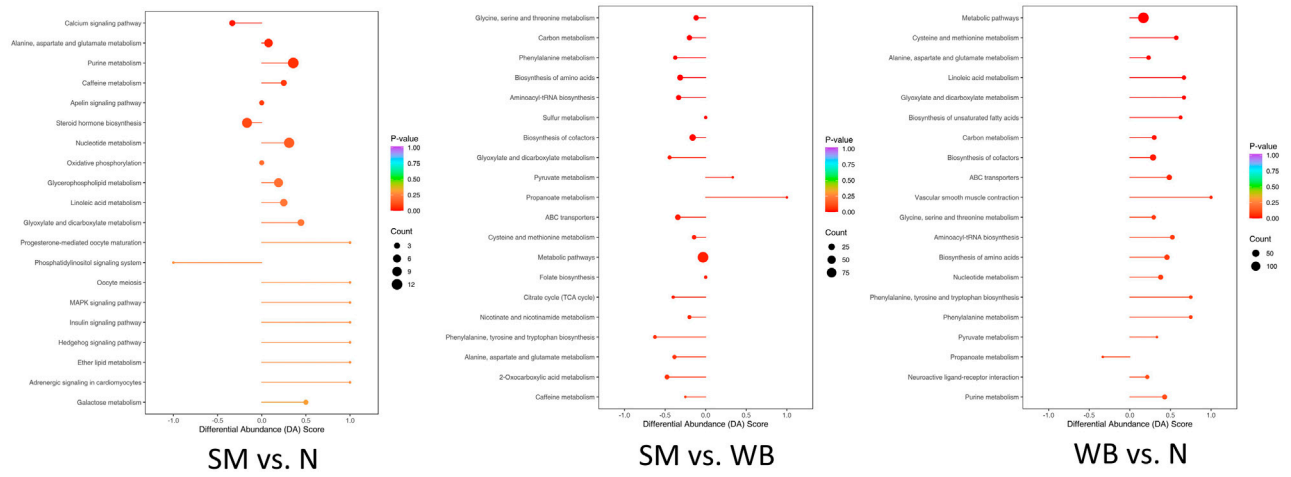

FIGURE 7
Top 20 Kyoto Encyclopedia of Genes and Genomes (KEGG) enriched pathways with *P*-value and differential abundance (DA) score. DA score was calculated as follows: number of upregulated differential metabolites annotated to a pathway−number of downregulated differential metabolites annotated to the pathway)/total number of metabolites annotated to the pathway.

muscle cells of rats. Moreover, Abasht et al. (2016) demonstrated that elevated 15-HETE in WB would be a defensive mechanism to inhibit inflammation due to muscle myopathies. These results indicate that inflammation was induced in both SM and WB. A previous study by Lake et al. (2019) demonstrated that ectopic lipid accumulation is one of the primary metabolic characteristics of WB in broiler chickens. Accordingly, in the current study, several lipid related metabolites including alpha-dimorphecolic acid, 15(S)-HETE, and (±) 18-HEPE were upregulated in SM and WB compared to N. The SM and WB are known to have the greater fat content level compared to normal breast meat (Tasoniero et al., 2020; Liu et al., 2022). The increased 15-HETE could be due to upregulated lipid metabolism and increased fat accumulation in WB and SM compared to N.

Inositol phosphates play important roles in regulating various signal transduction pathways responsible for cell growth and differentiation, cell signaling, apoptosis, DNA repair, RNA export, regeneration of ATP, etc. (Kuksis, 2003). In the current study, D-inositol-4-phosphate decreased in SM and WB compared to N. Reduced D-inositol-4-phosphate in SM and WB indicates problems in cell homeostasis, which could induce muscle myopathies in the breast meat. The WB and SM had 19 and 10 upregulated metabolites related to ABC transporters, respectively, in the current study. ABC transporters have important roles in transporting various substrates and importing nutrients and exporting toxic metabolites in an energy dependent manner (Linton, 2007). The analysis of KEGG classification revealed that differential metabolites related to metabolic pathways and biosynthesis were the greatest among the KEGG pathways in both SM and WB when compared to N. These results suggest that altered cellular metabolism could play a role in the development of SM and WB, but there would be more dramatic changes in cellular metabolism of WB compared to SM.

In the current study, purine metabolism was found to be upregulated in both SM and WB compared to N, with WB showing greater number of differential metabolites related to purine metabolism compared to SM. Consistently, Lake et al. (2022) also demonstrated that purine metabolism was upregulated in the blood of broilers with WB. Purine metabolism, which includes the *de novo* purine biosynthetic pathway, purine salvage pathway, and degradation, is essential not only for DNA and RNA synthesis but also for supplying vital energy and cofactors to promote cell survival and proliferation (Pedley and Benkovic, 2017; Yin et al., 2018). Boerboom et al. (2022) suggested that increased purine metabolism in WB would be associated with increased carbon metabolism and/or decreased utilization of nucleotides. Moreover, in the current study, the differential metabolites associated with nucleotide metabolism were overall upregulated in SM and WB. Potentially, the repair and regeneration process would be induced in SM and WB. Upregulated metabolites related to purine metabolism, particularly uric acid, could be associated with muscle myopathies since uric acid inhibits xanthine oxidase, which plays crucial roles in alleviating diverse health issues including endothelial dysfunction, insulin resistant, hepatic steatosis, and muscle atrophy (Derbre et al., 2012; Miller et al., 2024). However, in the current study, folic acid levels decreased in SM and WB compared to N. Folic acid, which can only be obtained from the diet, is an essential water-soluble vitamin B9 and crucial for cell division and growth by regulating the biosynthesis of nucleic acids and proteins (Ratajczak et al., 2021). In addition, folic acid may regulate the functions and integrity of skeletal muscle cells (Hwang et al., 2019). Liang et al. (2022) demonstrated that supplementation with a high dose of folic acid exhibited beneficial effects on broiler meat production by activating the mammalian target of rapamycin (mTOR) pathway, leading to increased protein deposition in the breast muscle. To our knowledge, there were no studies demonstrating the interaction between folic acid and muscle myopathies in broiler chickens. It would be of interest to investigate the association between the different folic acid levels and muscle myopathies in broiler chickens.

Neoxanthin, which is a kind of carotenoid and xanthophyll that can be found in corns (major feed ingredient in broiler feed), has health promoting effects in animals (Moreno et al., 2016). In the current study, neoxanthin decreased in WB compared to N. Carotenoids as vitamins, can also play important roles as antioxidants in animals (Nogareda et al., 2016). Oxidative stress can be readily induced in broiler chickens due to diverse factors including fast-growth, bacterial and parasitic infection, stimulated immune system, and consumption of mycotoxin (Choi et al., 2020). In the current study, taurine, glutathione, and the reduced form of glutathione were increased in SM and WB compared to N, which indicates that oxidative stress was induced in SM and WB. A previous study by Abasht et al. (2016) demonstrated that the increase in taurine and glutathione could be due to the tissues' exposure to high levels of oxidants in WB. Based on our current results, induced oxidative stress could be one of the etiologies for SM and WB. Potentially, decreasing the oxidative stress and increasing antioxidants in the feeds could be strategies to reduce the incidence and severity of SM and WB.

In the current study, differential amino acid related metabolites (amino acids, polypeptides, small peptides, and amino acid derivatives) were observed in SM (185) and WB (312) compared to N. Moreover, between SM and WB, there were 211 differential amino acid related metabolites. The analysis of KEGG classification revealed that 20- and 4 differential metabolites associated with biosynthesis of amino acids were observed in the comparisons between WB and N and between SM and N. This result indicates that the WB condition had more impacts on amino acid metabolism compared to the SM. Between WB and N, 111 amino acid related metabolites were downregulated, but 201 amino acids related metabolites were upregulated. Between SM and N, 103 amino acid related metabolites were downregulated, but 82 amino acids related metabolites were upregulated. Overall, these results suggest that amino acid related metabolites in WB were upregulated (201 up and 111 down), but amino acid related metabolites in SM were generally downregulated (82 up and 103 down). Soglia et al. (2019) reported that free amino acids were increased in WB potentially due to myogenesis within the abnormal muscle. Potentially, myogenesis in WB could induce the overproduction of amino acids. However, a previous study by Dalle Zotte et al. (2020) reported that WB had reduced amino acid content and modulated profile of amino acids compared to the N. Our previous study also displayed that the WB had lower crude protein content compared to N, which suggest reduced free amino acids in WB (Choi et al., 2024). This difference could originate from the analytic method. This would be because the untargeted metabolomics analysis does not incorporate the actual concentrations of metabolites. The overall reduction in amino acid related metabolites in SM relative to N is consistent with our previous study showing that there were alterations and reductions in myofibrillar proteins in SM (Tasoniero et al., 2022). Thus, the lack or the modulation of certain amino acids in the breast muscle would be associated with the detachment of muscle myofibers in SM. In addition, aminoacyl-tRNA biosynthesis is an important process for protein synthesis, pairing tRNAs with their corresponding amino acids for decoding mRNA (Gomez and Ibba, 2020). When WB were compared to SM or N, the 13 differential metabolites related to aminoacyl-tRNA biosynthesis were upregulated. This would be consistent with upregulated amino acids related metabolites in WB. The alterations in aminoacyl-tRNA biosynthesis could explain the modulation of amino acids and it could be one of the etiologies in WB.

TABLE 6 Overall description of differential metabolites and pathways between spaghetti meat (SM), wooden breast (WB), and normal (N) fillets.

Distinct in SM		Shared in SM and WB		Distinct in WB	
NADH	↓	Metabolic pathways	↑↓	Amino acids	↑
Amino acids	↓	Biosynthesis of cofactors	↑↓	Aminoacyl-tRNA biosynthesis	↑
Steroid hormone biosynthesis	↓	Stigmastane-3,6-dione	↓	ATP-binding cassette (ABC) transporters	↑
		(±)15-Hydroxyeicosatetraenoic acid (HETE)	↑	Carbon metabolism	↓
		D-inositol-4-phosphate	↓	Neoxanthin	↓
		Amino acids	↑↓		
		Folic acid	↓		
		Oxidative stress	↑		
		Purine metabolism	↑		

Nicotinamide adenine dinucleotide (NAD) + hydrogen (H) (NADH) plays a vital role as a cofactor in cellular respiration, participating in both glycolysis and the citric acid cycle by serving as an electron carrier. In the present study, the abundance of NADH was exclusively decreased in SM compared with N. However, significant differences in NADH were not observed between WB and N. This implies that reduced levels of NADH may be the main distinguishing factor in SM compared to WB. This is consistent with the observation by Mazzoni et al. (2020) that the stained area for reduced NADH- tetrazolium reductase (NADH-TR) was significantly smaller in meat with the SM condition, whereas no differences were observed in WS and WB compared with N. These results indicate that there could be severe defects in the energetic metabolism and mitochondrial disorders in SM. High energy demands are implicated in the development of skeletal muscle in fast-growing broilers (Mohammadabadi et al., 2021). These results suggest that malfunctions in energy metabolism can result in detachment of fiber bundles (e.g., SM). A previous study by Wang et al. (2023) showed that the etiologies of WB would be associated with reduced glycogenesis, glycolysis, and energy metabolism. Consistently, in the current study, the compromised carbon metabolism was one of the top 10 differential metabolomic pathways according to KEGG analysis between WB compared to N. However, only 3 differential metabolites were associated with carbon metabolism between SM to N. Whereas SM had lower abundance of NADH compared to N, reduced NADH in SM did not result in a modulation of carbon metabolism, which is a potential etiology to induce WB. More studies are needed 1) to elucidate the association between the deficiency of NADH and the SM condition and 2) to investigate the effects of dietary supplementation of NADH or NADH precursors on the incidence and severity of SM.

It is well known that steroid hormones have important roles in promoting muscle protein synthesis and hypertrophy in skeletal muscles (Dalle Zotte et al., 2020). In the current study, stigmastane-3,6-dione, a natural sterol, was the most decreased differential metabolites in SM and WB compared to N. This result indicates that alterations in steroid hormones could be one of etiologies for both SM and WB. In the present study, there were 10 differential metabolites related to steroid hormone biosynthesis between SM and N; however, there were only 5 between WB and N. Although 21-deoxycortisol, aldosterone hemiacetal, tetrahydrodeoxycorticosterone, androsterone, cortisone, 11 beta-hydroxyandrostenedione, (8S,9S,10S,13S,14S)-17-(2-hydroxyacetyl)-10,13-dimethyl-2,4,5,6,7,8,9,12,14,15,16,17-dodecahydro-1H-cyclopenta[a]phenanthrene-3,11-dione were downregulated, testosterone, 16 alpha-hydroxyestrone, and 2-methoxyestradiol were upregulated in SM. Reduction of steroid hormones potentially induced detachment of fiber bundles (e.g., symptoms of SM) (Carson and Manolagas, 2015). The lack of the movement of broiler chickens in the finisher stage could decrease the biosynthesis of steroid hormones because movement is an important factor to induce synthesis of steroid hormones in skeletal muscles (Sato and Iemitsu, 2015). A previous study by Iresjö et al. (2019) demonstrated that supplementation of amino acids, especially branched chain amino acids (BCAA), induced biosynthesis of estrogen in cultured skeletal muscle cells. In broiler chickens, BCAA play a significant role in muscle development, and the results from our current study may suggest that supplementation of BCAA may reduce the incidence and severity of SM by stimulating biosynthesis of steroid hormones. Further studies are required to verify whether BCAA could regulate biosynthesis of steroid hormones and affect SM in broiler chickens.

In summary, there were similarly and distinctly differential metabolites in SM and WB when compared to N as well as each other as shown in Table 6. Although SM did not induce as substantial alterations in metabolites as WB, there were still significant metabolic changes observed in SM compared with N. These data suggest both shared and unique metabolic alterations in SM and WB, indicating commonalities and differences in their underlying etiologies and meat quality traits. These findings suggest that dietary supplementation of deficient nutrients (e.g., NADH, folic acid, etc.) and modulation of altered pathways in SM and WB could be strategies to decrease the incidence and severity of SM and WB. More focused studies are required to suggest dietary and genetic interventions to decrease incidence and severity of SM and WB in broiler chickens.

Data availability statement

The raw data supporting the conclusions of this article will be made available by the authors, without undue reservation.

Ethics statement

Ethical approval was not required for the study involving animals in accordance with the local legislation and institutional requirements because Poultry meat tissues came from a commercial plant.

Author contributions

JC: Conceptualization, Data curation, Formal Analysis, Investigation, Methodology, Writing–original draft. MS: Conceptualization, Investigation, Writing–review and editing. WK: Writing–review and editing. BK: Conceptualization, Investigation, Writing–review and editing. BB: Conceptualization, Investigation, Writing–review and editing. HZ: Conceptualization, Methodology, Writing–review and editing, Supervision.

Funding

The author(s) declare that no financial support was received for the research, authorship, and/or publication of this article.

Acknowledgments

We extend our gratitude to Sophia Zaninovich, our HAKU intern, for her valuable assistance with sampling and sample processing.

Conflict of interest

The authors declare that the research was conducted in the absence of any commercial or financial relationships that could be construed as a potential conflict of interest.

Publisher's note

Supplementary material

The Supplementary Material for this article can be found online at: https://www.frontiersin.org/articles/10.3389/fphys.2024.1456664/full#supplementary-material

SUPPLEMENTARY TABLE S1
Differential metabolites between normal (N), spaghetti meat (SM), and wooden breast (WB).

SUPPLEMENTARY TABLE S2
Co-expressed and uniquely expressed metabolites in spaghetti meat (SM) and wooden breast (WB) compared to normal (N).

References

Abasht, B., Mutryn, M. F., Michalek, R. D., and Lee, W. R. (2016). Oxidative stress and metabolic perturbations in wooden breast disorder in chickens. *PloS one* 11, e0153750. doi:10.1371/journal.pone.0153750

Bailey, R. A., Watson, K. A., Bilgili, S., and Avendano, S. (2015). The genetic basis of pectoralis major myopathies in modern broiler chicken lines. *Poult. Sci.* 94, 2870–2879. doi:10.3382/ps/pev304

Baldi, G., Soglia, F., and Petracci, M. (2021). Spaghetti meat abnormality in broilers: current understanding and future research directions. *Front. Physiol.* 12, 684497. doi:10.3389/fphys.2021.684497

Baltic, M., Rajcic, A., Laudanovic, M., Nesic, S., Baltic, T., Ciric, J., et al. (2024). "Wooden breast–a novel myopathy recognized in broiler chickens," in *IOP conference series: earth and environmental science* (USA: IOP Publishing).

Boerboom, G. M., Navarro-Villa, A., and Van Kempen, T. A. (2022). Metabolomic analysis of wooden breast myopathy shows a disturbed lipid metabolism. *Metabolites* 13, 20. doi:10.3390/metabo13010020

Bowker, B., Zhuang, H., Yoon, S., Tasoniero, G., and Lawrence, K. (2019). Relationships between attributes of woody breast and white striping myopathies in commercially processed broiler breast meat. *J. Appl. Poult. Res.* 28, 490–496. doi:10.3382/japr/pfz007

Carson, J. A., and Manolagas, S. C. (2015). Effects of sex steroids on bones and muscles: similarities, parallels, and putative interactions in health and disease. *Bone* 80, 67–78. doi:10.1016/j.bone.2015.04.015

Che, S., Pham, P. H., Barbut, S., Bienzle, D., and Susta, L. (2024). Transcriptomic profiles of Pectoralis major muscles affected by spaghetti meat and woody breast in broiler chickens. *Animals* 14, 176. doi:10.3390/ani14020176

Che, S., Wang, C., Iverson, M., Varga, C., Barbut, S., Bienzle, D., et al. (2022). Characteristics of broiler chicken breast myopathies (spaghetti meat, woody breast, white striping) in Ontario, Canada. *Poult. Sci.* 101, 101747. doi:10.1016/j.psj.2022.101747

Choi, J., Kong, B., Bowker, B. C., Zhuang, H., and Kim, W. K. (2023). Nutritional strategies to improve meat quality and composition in the challenging conditions of broiler production: a review. *Animals* 13, 1386. doi:10.3390/ani13081386

Choi, J., Li, W., Schindell, B., Ni, L., Liu, S., Zhao, X., et al. (2020). Molecular cloning, tissue distribution and the expression of cystine/glutamate exchanger (xCT, SLC7A11) in different tissues during development in broiler chickens. *Anim. Nutr.* 6, 107–114. doi:10.1016/j.aninu.2019.10.001

Choi, J., Shakeri, M., Kim, W. K., Kong, B., Bowker, B., and Zhuang, H. (2024). Water properties in intact wooden breast fillets during refrigerated storage. *Poult. Sci.* 103, 103464. doi:10.1016/j.psj.2024.103464

Dalle Zotte, A., Ricci, R., Cullere, M., Serva, L., Tenti, S., and Marchesini, G. (2020). Research Note: effect of chicken genotype and white striping–wooden breast condition on breast meat proximate composition and amino acid profile. *Poult. Sci.* 99, 1797–1803. doi:10.1016/j.psj.2019.10.066

Derbre, F., Ferrando, B., Gomez-Cabrera, M. C., Sanchis-Gomar, F., Martinez-Bello, V. E., Olaso-Gonzalez, G., et al. (2012). Inhibition of xanthine oxidase by allopurinol prevents skeletal muscle atrophy: role of p38 MAPKinase and E3 ubiquitin ligases. *PloS one* 7, e46668. doi:10.1371/journal.pone.0046668

Gomez, M. a.R., and Ibba, M. (2020). Aminoacyl-tRNA synthetases. *Rna* 26, 910–936. doi:10.1261/rna.071720.119

Hwang, S. Y., Sung, B., and Kim, N. D. (2019). Roles of folate in skeletal muscle cell development and functions. *Arch. Pharmacal Res.* 42, 319–325. doi:10.1007/s12272-018-1100-9

Iresjö, B.-M., Landin, A., Ohlsson, C., and Lundholm, K. (2019). Estrogen biosynthesis in cultured skeletal muscle cells (L6) induced by amino acids. *Genes. Nutr.* 14, 29–36. doi:10.1186/s12263-019-0652-8

Kanehisa, M., and Goto, S. (2000). KEGG: kyoto encyclopedia of genes and genomes. *Nucleic acids Res.* 28, 27–30. doi:10.1093/nar/28.1.27

Kang, K., Zhou, N., Peng, W., Peng, F., Ma, M., Li, L., et al. (2022). Multi-omics analysis of the microbiome and metabolome reveals the relationship between the gut Microbiota and wooden breast myopathy in broilers. *Front. Vet. Sci.* 9, 922516. doi:10.3389/fvets.2022.922516

Kong, B., Khatri, B., Kang, S., Shouse, S., Kadhim, H., Kidd Jr, M., et al. (2021). Blood plasma biomarkers for woody breast disease in commercial broilers. *Front. Physiol.* 12, 712694. doi:10.3389/fphys.2021.712694

Kong, B., Owens, C., Bottje, W., Shakeri, M., Choi, J., Zhuang, H., et al. (2024). Proteomic analyses on chicken breast meat with white striping myopathy. *Poult. Sci.* 103, 103682. doi:10.1016/j.psj.2024.103682

Kuksis, A. (2003). *Inositol phospholipid metabolism and phosphatidyl inositol kinases*. Germany: Elsevier.

Kuttappan, V., Brewer, V., Apple, J., Waldroup, P., and Owens, C. (2012). Influence of growth rate on the occurrence of white striping in broiler breast fillets. *Poult. Sci.* 91, 2677–2685. doi:10.3382/ps.2012-02259

Lake, J. A., Papah, M. B., and Abasht, B. (2019). Ectopic lipid accumulation is key feature in early 2 stages of wooden breast 3. *Agri. Food Sci.* doi:10.20944/PREPRINTS201906.0194.V1

Lake, J. A., Yan, Y., Dekkers, J. C., Qiu, J., Brannick, E. M., and Abasht, B. (2022). Identification of circulating metabolites associated with wooden breast and white striping. *PloS one* 17, e0274208. doi:10.1371/journal.pone.0274208

Liang, S., Liu, X., Zhao, J., Liu, R., Huang, X., Liu, Y., et al. (2022). Effects of high-dose folic acid on protein metabolism in breast muscle and performance of broilers. *Poult. Sci.* 101, 101935. doi:10.1016/j.psj.2022.101935

Linton, K. J. (2007). Structure and function of ABC transporters. *Physiology* 22, 122–130. doi:10.1152/physiol.00046.2006

Liu, R., Kong, F., Xing, S., He, Z., Bai, L., Sun, J., et al. (2022). Dominant changes in the breast muscle lipid profiles of broiler chickens with wooden breast syndrome revealed by lipidomics analyses. *J. Anim. Sci. Biotechnol.* 13, 93. doi:10.1186/s40104-022-00743-x

Mazzoni, M., Soglia, F., Petracci, M., Sirri, F., Lattanzio, G., and Clavenzani, P. (2020). Fiber metabolism, procollagen and collagen type III immunoreactivity in broiler pectoralis major affected by muscle abnormalities. *Animals* 10, 1081. doi:10.3390/ani10061081

Miller, S. G., Matias, C., Hafen, P. S., Law, A. S., Witczak, C. A., and Brault, J. J. (2024). Uric acid formation is driven by crosstalk between skeletal muscle and other cell types. *JCI insight* 9, e171815. doi:10.1172/jci.insight.171815

Mohammadabadi, M., Bordbar, F., Jensen, J., Du, M., and Guo, W. (2021). Key genes regulating skeletal muscle development and growth in farm animals. *Animals* 11, 835. doi:10.3390/ani11030835

Moreno, J. A., Díaz-Gómez, J., Nogareda, C., Angulo, E., Sandmann, G., Portero-Otin, M., et al. (2016). The distribution of carotenoids in hens fed on biofortified maize is influenced by feed composition, absorption, resource allocation and storage. *Sci. Rep.* 6, 35346. doi:10.1038/srep35346

Nogareda, C., Moreno, J. A., Angulo, E., Sandmann, G., Portero, M., Capell, T., et al. (2016). Carotenoid-enriched transgenic corn delivers bioavailable carotenoids to poultry and protects them against coccidiosis. *Plant Biotechnol. J.* 14, 160–168. doi:10.1111/pbi.12369

Pedley, A. M., and Benkovic, S. J. (2017). A new view into the regulation of purine metabolism: the purinosome. *Trends biochem. Sci.* 42, 141–154. doi:10.1016/j.tibs.2016.09.009

Ratajczak, A. E., Szymczak-Tomczak, A., Rychter, A. M., Zawada, A., Dobrowolska, A., and Krela-Kaźmierczak, I. (2021). Does folic acid protect patients with inflammatory bowel disease from complications? *Nutrients* 13, 4036. doi:10.3390/nu13114036

Sato, K., and Iemitsu, M. (2015). Exercise and sex steroid hormones in skeletal muscle. *J. Steroid Biochem. Mol. Biol.* 145, 200–205. doi:10.1016/j.jsbmb.2014.03.009

Shahbandeh, M. (2023). Poultry industry in the United States - statistics and facts. Available at: https://www.statista.com/topics/6263/poultry-industry-in-the-united-states/#topicOverview (Accessed December 18, 2023).

Soglia, F., Silva, A., Lião, L., Laghi, L., and Petracci, M. (2019). Effect of broiler breast abnormality and freezing on meat quality and metabolites assessed by 1 H-NMR spectroscopy. *Poult. Sci.* 98, 7139–7150. doi:10.3382/ps/pez514

Tasoniero, G., Zhuang, H., and Bowker, B. (2022). Biochemical and physicochemical changes in spaghetti meat during refrigerated storage of chicken breast. *Front. Physiol.* 13, 894544. doi:10.3389/fphys.2022.894544

Tasoniero, G., Zhuang, H., Gamble, G. R., and Bowker, B. C. (2020). Effect of spaghetti meat abnormality on broiler chicken breast meat composition and technological quality. *Poult. Sci.* 99, 1724–1733. doi:10.1016/j.psj.2019.10.069

Velleman, S. G., and Clark, D. L. (2015). Histopathologic and myogenic gene expression changes associated with wooden breast in broiler breast muscles. *Avian Dis.* 59, 410–418. doi:10.1637/11097-042015-Reg.1

Wang, S., Wang, Y., Jiang, J., Wang, R., Li, L., Qiu, Z., et al. (2010). 15-HETE protects rat pulmonary arterial smooth muscle cells from apoptosis via the PI3K/Akt pathway. *Prostagl. Other Lipid Mediat* 91, 51–60. doi:10.1016/j.prostaglandins.2009.12.007

Wang, Z., Brannick, E., and Abasht, B. (2023). Integrative transcriptomic and metabolomic analysis reveals alterations in energy metabolism and mitochondrial functionality in broiler chickens with wooden breast. *Sci. Rep.* 13, 4747. doi:10.1038/s41598-023-31429-7

Wu, T., Liu, P., Wu, J., Jiang, Y., Zhou, N., Zhang, Y., et al. (2024). Broiler spaghetti meat abnormalities: muscle characteristics and metabolomic profiles. *Animals* 14, 1236. doi:10.3390/ani14081236

Xing, T., Zhao, X., Zhang, L., Li, J., Zhou, G., Xu, X., et al. (2020). Characteristics and incidence of broiler chicken wooden breast meat under commercial conditions in China. *Poult. Sci.* 99, 620–628. doi:10.3382/ps/pez560

Yin, J., Ren, W., Huang, X., Deng, J., Li, T., and Yin, Y. (2018). Potential mechanisms connecting purine metabolism and cancer therapy. *Front. Immunol.* 9, 1697. doi:10.3389/fimmu.2018.01697

Zhu, D., and Ran, Y. (2012). Role of 15-lipoxygenase/15-hydroxyeicosatetraenoic acid in hypoxia-induced pulmonary hypertension. *J. Physiol. Sci.* 62, 163–172. doi:10.1007/s12576-012-0196-9

frontiers | Frontiers in Physiology

TYPE Review
PUBLISHED 30 October 2024
DOI 10.3389/fphys.2024.1501362

OPEN ACCESS

EDITED BY
Wei Guo,
University of Wisconsin-Madison,
United States

REVIEWED BY
Susumu Muroya,
Kagoshima University, Japan
Liubin Yang,
Huazhong Agricultural University, China

*CORRESPONDENCE
Morgan D. Zumbaugh,
mdzumbaugh@ksu.edu

RECEIVED 24 September 2024
ACCEPTED 21 October 2024
PUBLISHED 30 October 2024

CITATION
Rimmer LA and Zumbaugh MD (2024) Skeletal muscle metabolic characteristics and fresh meat quality defects associated with wooden breast.
Front. Physiol. 15:1501362.
doi: 10.3389/fphys.2024.1501362

Skeletal muscle metabolic characteristics and fresh meat quality defects associated with wooden breast

Linnea A. Rimmer and Morgan D. Zumbaugh*

Department of Animal Sciences and Industry, Kansas State University, Manhattan, KS, United States

Wooden breast (WB) is a myopathy that occurs in pectoralis major (PM) muscles, predominately affecting large, fast-growing broilers. Severe myodegeneration, increased hypoxia, reduced blood flow, and increased collagen deposition are hallmark characteristics of WB that culminate in unsatisfactory fresh meat quality attributes, such as poor water-holding capacity, tenderness, and processing characteristics. Therefore, WB meat is often downgraded resulting in economic losses for the United States poultry industry. Although WB has been well characterized, its etiology remains undefined. As the scientific community continues to resolve mechanisms responsible for WB onset, understanding biochemical changes associated with WB may facilitate solutions to negate its poor meat quality attributes. Given changes in metabolism of living muscle can alter biochemical processes during the conversion of muscle to meat, this review aims to summarize and discuss the current knowledge of WB muscle and meat biochemistry. For example, it appears metabolic pathways that support combating stress are upregulated in WB muscle at the expense of glycolytic flux, which presumably contributes to the high ultimate pH of WB meat. Further, perturbed function of WB mitochondria, such as altered calcium handling, impacts aspects of postmortem metabolism and proteolysis. Collectively, metabolic dysfunction of WB muscle alters the biochemical processes that occur during the conversion of muscle to meat, and thus contributes to the poor WB meat quality.

KEYWORDS

wooden breast, myopathy, poultry, skeletal muscle metabolism, fresh meat quality

1 Introduction

Poultry is the fastest growing sector of the meat industry in the United States (Interagency Agricultural Projections Committee, 2020), largely because of its affordable price and positive nutritional benefits. Rising global demand for high-quality poultry products has driven the U.S. poultry industry to nearly double production from 2001 to 2021 (Miller et al., 2022). To accomplish this feat, the industry has implemented genetic selection and nutritional advancements to achieve superior broiler growth rates

(Baker et al., 1999; Kidd et al., 2001; National Chicken Council, 2022). For example, broilers in 1970 were an average of 3.62 lbs at market after approximately 56 days, whereas broilers in 2023 took approximately 47 days to reach an average of 6.54 lbs at market (National Chicken Council, 2022). While the industry improved production efficiency and yields, an unexpected increase in the prevalence of myopathies accompanied these advancements. In fact, fast growth rate is associated with an increase in WB prevalence, and affected broilers can begin presenting symptoms of the pathology as early as 2 weeks of age (Sihvo et al., 2014; Sihvo et al., 2017). Affected filets are characterized as being palpably hard to the touch, pale in color, and having occasional white striping that results in low acceptance by consumers due to poor texture and usability of the meat (Kuttappan et al., 2012; Mudalal et al., 2015; Xing et al., 2020). Although the etiology of WB largely remains undefined, many factors have been identified that contribute to the onset and progression of the myopathy. This review aims to summarize the current knowledge of the underlying muscle physiology and fresh meat quality defects associated with the WB myopathy.

2 Skeletal muscle metabolic characteristics associated with WB

Skeletal muscle is composed of a heterogeneous population of muscle fibers that can be classified by metabolism (oxidative or glycolytic) and contractile speed (slow or fast). While slow fibers (type I) rely heavily on oxidative metabolism, presumably to fuel long or continuous bouts of work, fast fibers (type IIA, IIX, and IIB) vary in their metabolic capability and can range from having a high oxidative capacity to a high glycolytic capacity. Composition of muscle fibers varies within muscles and determines overall muscle phenotype as well as susceptibility to disease (Talbot and Maves, 2016). Pectoralis major muscles of broilers are nearly 100% type IIB fibers, which are characterized as highly glycolytic with a fast contraction speed (Smith and Fletcher, 1988; Roy et al., 2006; Verdiglione and Cassandro, 2013a; Hosotani et al., 2021). Indeed, PM muscles of healthy broilers exhibit low mitochondrial content, high glycolytic capacity, and thus can function under anaerobic conditions (Dransfield and Sosnicki, 1999; Verdiglione and Cassandro, 2013b; Du et al., 2017; Huo et al., 2022). In WB muscle, insufficient angiogenesis during periods of rapid growth results in diminished vascularization and hypoxic conditions (Mutryn et al., 2015; Thanatsang et al., 2020). In fact, an increase in gene expression and protein abundance of hypoxia-inducible factor 1 (HIF-1α; transcription factor that mediates cellular responds to low oxygen levels) as well as an increase in associated proteins involved in the hypoxic response supports the notion of a limited oxygen environment in WB muscle (Greene et al., 2019; Greene et al., 2020). Although highly glycolytic muscle fibers of PM muscles should be able to accommodate a reduced oxygen environment (Minchenko et al., 2002; Kierans and Taylor, 2021), WB muscle exhibits metabolic dysfunction (Abasht et al., 2016; Kuttappan et al., 2017a; Hosotani et al., 2020; Hasegawa et al., 2022; Carvalho et al., 2023; Wang et al., 2023). Indeed, an increase in reactive oxygen species (ROS) and markers of cellular stress are often reported in WB muscle (Figure 1) (Hasegawa et al., 2022; Carvalho et al., 2023; Wang et al., 2023). While WB muscle also upregulates scavenging pathways to combat stress (Hasegawa et al., 2022; Carvalho et al., 2023; Wang et al., 2023), WB muscle is not able to counteract the onset of disease.

2.1 Overview of glycolysis and its ancillary pathways

After glucose enters myofibers, hexokinase phosphorylates glucose to generate glucose-6-phoshate (G-6-P), which can be used for energy storage, energy production, supporting anabolic pathways, or as a precursor for metabolic signaling depending on cellular needs. For example, G-6-P is used to synthesize glycogen during times of energy surplus or to fuel glycolysis during times of energy scarcity (Rao et al., 2015; Matarneh et al., 2018b). Alternatively, G-6-P can be shunted into the pentose phosphate pathway (PPP) to generate NADPH for lipid synthesis and scavenging ROS or to produce five-carbon precursors for nucleotide synthesis (Stincone et al., 2015). In addition, G-6-P can be converted to fructose-6-phosphate (F-6-P) and shunted into the hexosamine biosynthetic pathway (HBP) to synthesize UDP-GlcNAc, which is used by the enzyme O-GlcNAc transferase (OGT) to catalyze the O-linked addition of β-N-acetyl glucosamine to target proteins (Hart and Akimoto, 2009). One of the most abundant post-translational modifications, O-GlcNAcylation regulates over 4,000 target proteins in response to cellular nutrient availability (Ma and Hart, 2014). While the HBP only consumes 2%–5% of cellular glucose utilization, O-GlcNAcylation has widespread implications on skeletal muscle metabolism (Marshall et al., 1991; Bond and Hanover, 2015). The multiple fates of glycolytic intermediates contribute to the plastic nature and metabolic flexibility of healthy skeletal muscle.

2.1.1 Glycolytic flux

Given the highly glycolytic nature of broiler PM muscles, it is reasonable to assume WB muscles would adapt to hypoxic conditions associated with the myopathy. However, WB muscles exhibit reduced levels of glycogen, G-6-P, and F-6-P suggesting WB decreases glycolytic flux (Abasht et al., 2016; Baldi et al., 2020). This notion is supported by diminished levels of the glycolytic end products pyruvate and lactate in WB muscle (Abasht et al., 2016). Further, protein abundance of several enzymes in the latter half of glycolysis are also decreased in WB muscle including phosphoglycerate kinase, phosphoglycerate mutase, and pyruvate kinase (Abasht et al., 2016; Soglia et al., 2016; Kuttappan et al., 2017a; Carvalho et al., 2023). The final glycolytic intermediate, pyruvate, can either be converted to lactate through lactate dehydrogenase alpha (LDHα) or enter the tricarboxylic acid (TCA) cycle through pyruvate dehydrogenase (PDH) or pyruvate carboxylase (PC). Glycolytic type IIB fibers predominately divert pyruvate through LDHα to produce lactate, which is then shuttled out of muscle through monocarboxylate transporter 4 (MCT4) into the bloodstream to be carried to the liver for gluconeogenesis (Dimmer et al., 2000). Glucose is then stored in the liver as glycogen or circulated as glucose, which can be consumed by skeletal muscle in a process termed the Cori Cycle. Most reports agree

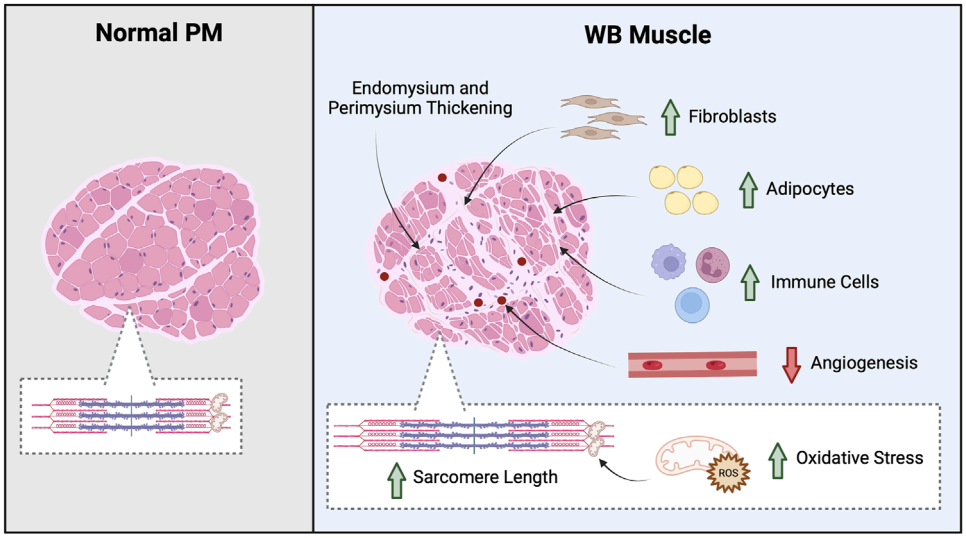

FIGURE 1
Overview of WB tissue morphology. Greater myodegeneration and an increase in fibroblast, adipocyte, and immune cells suggests WB muscle coordinates a response to repair the damaged tissue; however, non-muscle cells infiltrate the tissue. For example, an increase in macrophages and neutrophils as well as thicker endomysium and perimysium connective tissue layers are found in WB muscle. In addition, WB muscles often exhibit an increase in oxidative stress and decrease angiogenesis. Created in BioRender.

gene expression and protein abundance of LDHα decreases in WB muscle (Kuttappan et al., 2017a; Malila et al., 2019; Thanatsang et al., 2020; Zhao et al., 2020; Wang et al., 2023), which corresponds to the decrease in lactate. Contradicting reports indicate no difference (Zhao et al., 2020) or an increase in protein abundance in WB muscles (Soglia et al., 2016); however, the latter report did not indicate the LDH subunit evaluated. Lactate dehydrogenase beta (LDHβ) converts lactate to pyruvate (Cahn et al., 1962; Dawson et al., 1964; Pesce et al., 1964), and LDHβ gene expression as well as protein abundance increased 8.4- and 13.6- fold in WB muscles compared to unaffected PM muscles, respectively (Zhao et al., 2020; Wang et al., 2023). Interestingly, Zhao et al., 2020 reported no differences in protein abundance of monocarboxylate transporter 1 (MCT1; facilitates lactate uptake into cells), while protein abundance of MCT4 (facilitates lactate export) increased 3.4-fold in WB muscles compared to unaffected PM muscles. In osteosarcoma cells, MCT4 is upregulated during hypoxic conditions, which is partially attributed to a HIF-1α mediated mechanism and may be employed by cells to compensate for an increase in lactate production (Sheng et al., 2023). Although an increase in MCT4 would normally suggest an increase in lactate production and efflux from myofibers feeding into the Cori Cycle, this does not appear to be the case in WB muscle. Collectively, these reports suggest WB muscles still employ mechanisms to accommodate anaerobic conditions; however, glycolytic flux and lactate production are obstructed (Figure 2).

2.1.2 Pentose phosphate pathway

Interestingly, there is little evidence that indicates impaired glucose uptake is responsible for the diminished glycolytic flux, which questions if all metabolic pathways associated with glycolysis are also impaired in WB muscle. For example, G-6-P may be diverted into the PPP to support $NADP^+$ reduction to replenish NADPH pools, which is necessary for fatty acid synthesis and reduction of glutathione to scavenge ROS (Stincone et al., 2015). In addition to hypoxia, oxidative stress is also a hallmark of WB. The notion that WB muscles divert glucose into the PPP to replenish NADPH pools is supported by an increase in hexokinase-1 protein abundance in WB muscles (Kuttappan et al., 2017a), which indicates an increase in glucose phosphorylation to G-6-P. Although G-6-P levels are lower in WB muscles, it is possible G-6-P is being diverted into the PPP to restore a diminishing NADPH pool. Indeed, levels of the PPP intermediates 6-phosphogluconate and sedoheptulose 7-phosphate are 2.84 - and 3.73- fold higher in WB muscles compared to unaffected PM muscles, respectively (Abasht et al., 2016). Further, cytidine, thymidine, adenine, and guanosine levels increase in WB (Abasht et al., 2016), which are synthesized using ribose-5-phosphate from the PPP. There is also evidence of increased nucleotide catabolism in WB (Abasht et al., 2016), which is associated with a mitochondrial response to oxidative stress (Kristal et al., 1999). Therefore, it is possible the WB pathology forces muscle to shunt glucose into the PPP to combat oxidative stress at the expense of glycolytic capacity (Figure 2).

2.1.3 Serine biosynthesis pathway

In addition to an increase in PPP diverting glucose from ATP production, the serine biosynthesis pathway (SBP) may also shunt glycolytic intermediates to support additional glutathione synthesis to combat oxidative stress. Glutamate, cysteine, and glycine are amino acid precursors for glutathione synthesis. Glycine as well as cysteine are synthesized from serine, which is produced from the glycolytic intermediate 3-phopshoglycerate. In fact, gene expression of the enzyme that catalyzes the first step of serine biosynthesis, phosphoglycerate dehydrogenase (PHGDH), is upregulated 11.6-fold in WB muscle compared to unaffected

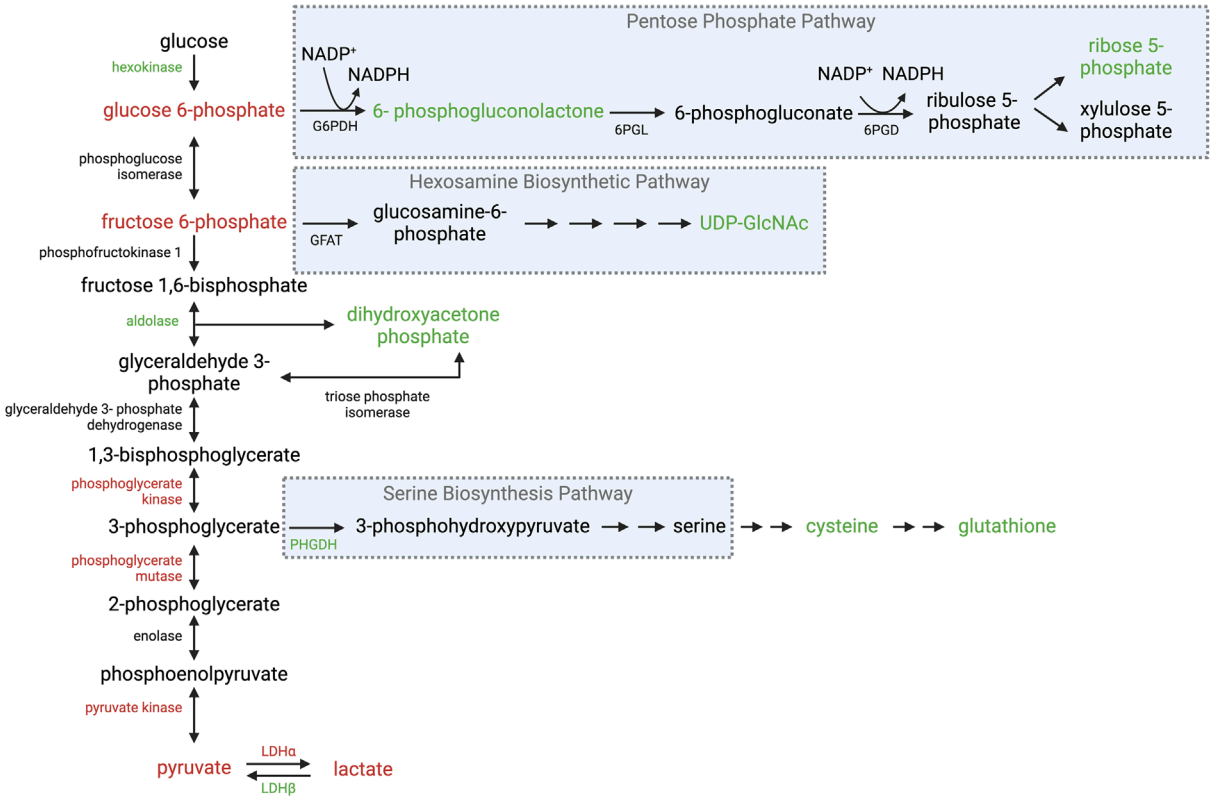

FIGURE 2
Overview of glycolysis and its ancillary pathways in WB muscle. Schematic of enzymatic and intermediate changes in glycolysis, the pentose phosphate pathway, hexosamine biosynthetic pathway, and serine biosynthesis pathway observed in WB muscle. Red text indicates a decrease in gene expression and/or protein abundance of the enzyme or intermediate. Green text indicates an increase in gene expression and/or protein abundance of the enzyme or intermediate. Black text was not evaluated or no changes were reported. Abbreviations: G6PDH, glucose-6-phosphate dehydrogenase; 6PGL, 6-phosphogluconolactonase; 6PGD, 6-phosphogluconate dehydrogenase; GFAT, glutamine fructose-6-phosphate aminotransferase; PHGDH, phosphoglycerate dehydrogenase; LDHα, lactate dehydrogenase alpha; LDHβ lactate dehydrogenase beta. Created in BioRender.

PM muscles (Mutryn et al., 2015). Further, gene expression of the enzyme that catalyzes the first step of glutathione synthesis is also upregulated in WB muscle (Zhang et al., 2023). This notion is supported by an increase in cysteine, glutathione, and oxidized glutathione levels in WB muscles (Abasht et al., 2016; Thanatsang et al., 2020) as well as an increase in gene expression and protein abundance of several enzymes involved in glutathione-mediated scavenging in WB muscles (Figure 2) (Carvalho et al., 2023; Zhang et al., 2023). These findings support the notion that glycolytic intermediates are being diverted into metabolic pathways to combat stress.

2.1.4 Hexosamine biosynthetic pathway

While it is apparent WB muscle employs metabolic pathways to counteract oxidative stress, it appears this occurs at the expense of ATP production to meet cellular energy demands. Indeed, ATP levels are decreased in WB muscle compared to unaffected PM muscles (Baldi et al., 2020). Given PM muscles are inherently glycolytic and commercial broilers are fed high energy diets, a potent underlying mechanism must be obstructing glycolytic capacity in WB. Interestingly, feeding low energy or low protein diets decreases the prevalence of myopathies in growing broilers (Trocino et al., 2015; Meloche et al., 2018b; Meloche et al., 2018a; Simoes et al., 2020; Vieira et al., 2021). While this may be attributed to a diet-induced slower growth rate, high energy diets may force muscle into a state of metabolic disease. In fact, UPD-GlcNAc levels are higher in WB muscles compared to unaffected PM muscles (Abasht et al., 2016), which is the precursor for the nutrient sensitive post-translational modification O-GlcNAcylation, and confirms WB muscle still responds to the high energy diet. This is a possible mechanism employed by WB muscle to divert glycolytic metabolites into the PPP or other pathways branching from glycolysis (Figure 2). This notion is supported by reports of O-GlcNAcylation increasing hexokinase-1 activity as well as glucose-6-phosphate dehydrogenase (Rao et al., 2015; Baldini et al., 2016; Liu et al., 2022), which catalyzes the first step of the PPP. Therefore, it is possible the high nutritional plane combined with an expedited growth rate culminate in metabolic conditions that signal a state of excess nutrients to "override" stress responses during the onset and progression of disease. However, such a mechanism has yet to be identified but further investigation into the regulation of glycolysis and its ancillary pathways will shed light on the unique metabolic fingerprint of WB muscle.

2.2 Mitochondrial metabolism in WB muscle

Alternative to its use in the Cori Cycle, pyruvate can be shuttled into mitochondria to enter the TCA cycle through PDH or PC. In addition, the TCA cycle can metabolize amino acids as well as acetyl-CoA from fatty acid beta-oxidation as alternative metabolite sources to carbohydrates. In highly glycolytic type IIB fibers, ATP production largely occurs through glycolysis, and thus mitochondrial metabolism is a minor contributor to cellular ATP production (Kunz, 2001). Indeed, mitochondrial content is low in type IIB fibers of PM muscles compared to more oxidative fiber types of broiler gastrocnemius muscles (Hosotani et al., 2021). Mitochondria in type IIB fibers of PM muscles are small, dispersed, and ellipsoid-shaped compared to elongated and interconnected mitochondrial networks found in oxidative fibers of gastrocnemius muscles (Hosotani et al., 2021). Although mitochondrial content in healthy PM muscles is low compared to more oxidative fiber types, PM mitochondria undergo fusion and fission events to preserve mitochondrial function, albeit in a more tempered manner than oxidative fibers (Hosotani et al., 2021). Mitochondrial dynamics are perturbed in WB muscle contributing to swollen mitochondria morphology, an increase in ROS production, and overall metabolic dysregulation (Hosotani et al., 2020; Hasegawa et al., 2022; Carvalho et al., 2023; Wang et al., 2023).

2.2.1 Metabolite utilization in the TCA cycle

Although the TCA cycle is often illustrated as a continuous cycle of enzymatic reactions, there are several entry and exit points within the cycle that enable mitochondria to accommodate cellular energy demands. The TCA cycle is not a carbon sink, and therefore an equilibrium exists between metabolites feeding into the TCA cycle and its intermediates exiting the cycle. These processes are termed anaplerosis and cataplerosis, where the former are a series of enzymatic reactions replenishing the pool of TCA intermediates and the latter remove TCA intermediates from the cycle. While anaplerosis (metabolites entering the TCA cycle) is often the center of discussion, cataplerosis (intermediates exiting the cycle) is often overlooked. Cataplerotic reactions are essential for regulating glucose, amino acid, and fatty acid metabolism. For example, in the glycolytic type IIB fibers of PM muscles, carbohydrate-derived metabolites are the predominate fuel source used in glycolysis, but pyruvate can also feed into the TCA cycle and then exit at several points to support amino acid synthesis. These cataplerotic reactions are necessary to support rapid protein accretion to enable the fast rate of muscle hypertrophy observed in commercial broilers. However, mitochondrial dysfunction in WB is presumably a rate limiting factor in successfully accommodating the high demands of amino acid metabolism in these fast-growing broilers.

A decrease in gene expression and protein abundance of most TCA cycle enzymes is observed in WB muscle (Kuttappan et al., 2017a; Papah et al., 2018; Carvalho et al., 2023; Wang et al., 2023). Interestingly, levels of α-ketoglutarate, fumarate, and malate increase in WB muscle but there is little evidence of changes in other TCA intermediates (Figure 3) (Abasht et al., 2016; Greene et al., 2020). These three intermediates are all involved in amino acid metabolism and may be an attempt for WB muscle to accommodate protein synthesis rate. For example, glutamate dehydrogenase catalyzes the reversible conversion of α-ketoglutarate to glutamate, which facilitates use of glutamate as a fuel source during times of energy scarcity or synthesis of glutamate during times of energy surplus (Plaitakis et al., 2017). As levels of glutamate are elevated in WB muscle (Greene et al., 2020; Wang et al., 2023) and it is a precursor for glutathione synthesis, this may be another point of diversion for metabolites to combat oxidative stress in WB muscle. However, a decrease in gene expression and protein abundance of isocitrate dehydrogenase 3 (Kuttappan et al., 2017a; Wang et al., 2023), the enzyme that catalyzes the oxidative decarboxylation of isocitrate to α-ketoglutarate, as well as a decrease in citrate synthase activity (Figure 3) (Li et al., 2022; Li et al., 2024) suggests the increase in glutamate is not attributed to carbohydrate metabolism but rather another metabolite source. An increase in histamine and arginine levels increase in WB muscle may be supporting glutamate synthesis but it remains ambiguous (Figure 3) (Abasht et al., 2016). These reports indicate mitochondria also divert metabolites to combat oxidative stress, although the intricacies of skeletal muscle metabolism make it difficult to elucidate the mechanisms of nutrient utilization in WB.

In addition, fumarate and malate levels are elevated in WB muscle (Abasht et al., 2016; Greene et al., 2020), although the biological implications of an increase in these intermediates is also unclear. For example, a decrease in abundance of fumarate hydratase (catalyzes the reversible conversion of malate to oxaloacetate) and malate dehydrogenase 2 (catalyzes the reversible conversion of malate to oxaloacetate) (Kuttappan et al., 2017a; Carvalho et al., 2023; Wang et al., 2023) but increase in fumarate and malate is counterintuitive (Figure 3). Further, cataplerotic enzymes that divert fumarate and malate out of the TCA cycle are also decreased in WB muscle. In healthy muscle, malate can be converted to oxaloacetate and used by glutamic-oxaloacetic transaminase 1 or 2 (GOT1 or GOT2) to generate aspartate or glutamate. However, a decrease protein abundance of GOT1 and GOT2 but an increase in aspartate levels in WB muscle is perplexing (Figure 3) (Abasht et al., 2016; Kuttappan et al., 2017a; Greene et al., 2020; Wang et al., 2023). Therefore, it is unclear if these intermediates are playing an important role in an unidentified metabolic process or if TCA intermediates "bottleneck" as fumarate and malate. Regardless, it is clear mitochondrial metabolic pathways are dysregulated in WB muscle.

2.2.2 Mitochondrial calcium handling

The obscurity of metabolite utilization makes it difficult to define the underlying cause of metabolic dysregulation in WB muscle. The metabolic fingerprint of WB muscle appears to be a unique combination of combating oxidative stress and responding to a state of excess nutrients as well as hypertrophic stimuli. Although the exact mechanism is undefined, an increase in cytoplasmic calcium (Ca^{2+}) and mitochondrial Ca^{2+} uptake provokes muscle hypertrophy (Klont et al., 1994; Scheffler et al., 2014; Mammucari et al., 2015; Gherardi et al., 2019); however, Ca^{2+} overload induces apoptosis and disease (Gommans et al., 2002). Cytoplasmic Ca^{2+} levels are 2- fold higher and sarcoplasmic reticulum (SR) Ca^{2+} levels are 4- fold lower in WB muscle compared to unaffected PM muscles suggesting either a leaky SR or impaired SR Ca^{2+} uptake (Zhang et al., 2023). Abundance of the sarcoendoplasmic reticulum calcium ATPase (SERCA) pump

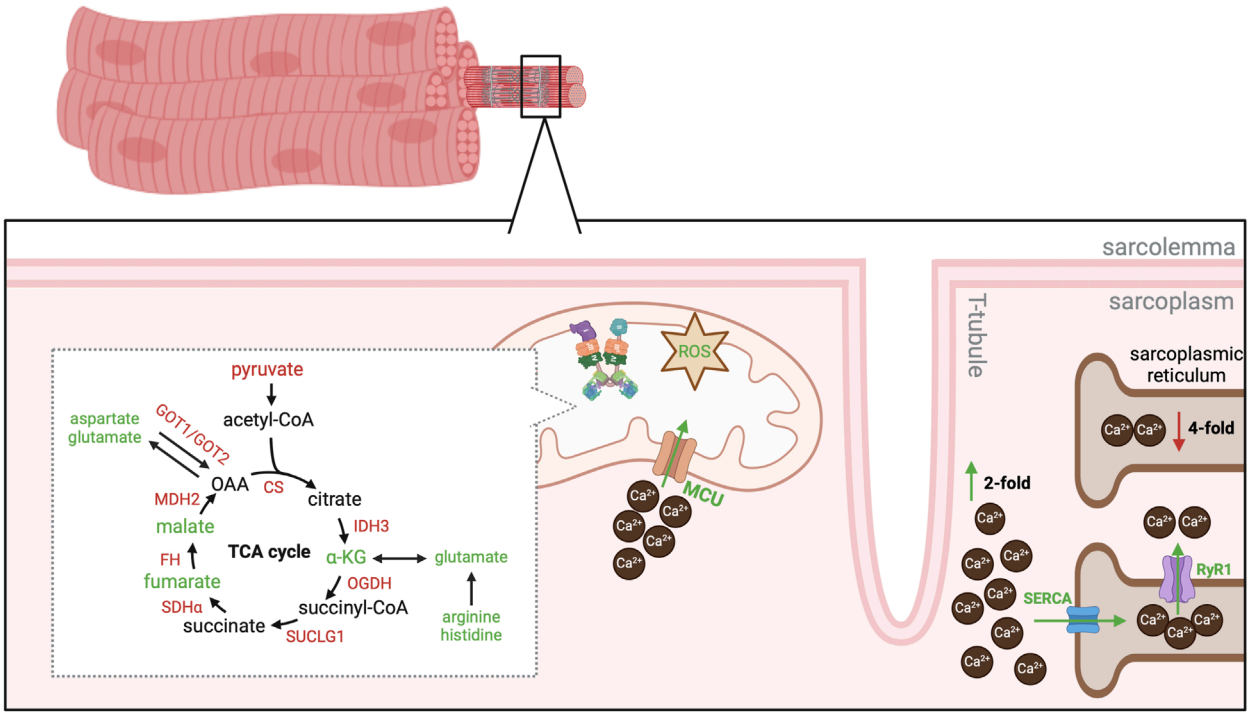

FIGURE 3
Overview of mitochondrial metabolism in WB muscle. Schematic of enzymatic and intermediate changes in the TCA cycle and associated cataplerotic / anaplerotic reactions. In addition, changes in calcium handling are also depicted. Red text or arrows indicates a decrease in either gene expression or protein abundance of the enzyme orintermediate. Green text or arrows indicates an increase in either gene expression or protein abundance of the enzyme or intermediate. Black text was either not evaluated or no changes were reported. Abbreviations: CS, citrate synthase; IDH3, isocitrate dehydrogenase 3; α-KG, alpha-ketoglutarate; OGDH, oxoglutarate dehydrogenase; SUCLG1, succinyl-CoA ligase; SDHα, succinate dehydrogenase alpha; FH, fumarate hydratase; MDH2, malate dehydrogenase 2; GOT1, glutamic-oxaloacetic transaminase 1; GOT2, glutamic-oxaloacetic transaminase 2; ROS, reactive oxygen species; MCU, mitochondrial calcium uniporter; SERCA, sarcoendoplasmic reticulum calcium ATPase; RyR1, ryanodine receptor 1.

is markedly higher in WB muscle compared to unaffected PM muscles (Soglia et al., 2016; Zhang et al., 2023), which points to a defect in Ca^{2+} release. Indeed, gene expression of the Ca^{2+} release channel ryanodine receptor 1 (RyR1) is higher in WB muscle (Zhang et al., 2023) as well as protein abundance of the chloride intracellular channel protein (Carvalho et al., 2023), which is a negative regulator of RyR1-mediated Ca^{2+} release. These reports suggest leaky Ca^{2+} release from the SR and an attempt to curb RyR1-mediated Ca^{2+} release (Figure 3). In aging human models, excessive and prolonged exposure to ROS results in irreversible damage of RyR1 (Fulle et al., 2004). As mitochondrial ROS generation is higher in WB muscle compared to unaffected PM muscles (Zhang et al., 2023), these reports question if impaired Ca^{2+} handling observed in WB muscle is attributed to selection for exacerbated muscle hypertrophy or ROS inducing SR damage. Regardless, it is clear the increase in cytoplasmic Ca^{2+} results in greater mitochondrial Ca^{2+} uptake (Zhang et al., 2023).

An increase in mitochondrial calcium uniporter gene expression and protein abundance confirms WB mitochondria attempt to buffer high cytoplasmic Ca^{2+} levels (Zhang et al., 2023). Mitochondrial metabolism is stimulated by Ca^{2+} uptake, which is thought to be a mechanism to match energy supply and energy demand in a process termed parallel activation (McCormack and Denton, 1981). Of note, Ca^{2+} stimulates ATP synthase to increase oxidative phosphorylation and ATP production (Jouaville et al., 1999). An increase in myoglobin gene expression and protein abundance supports the notion of WB muscle attempting to increase oxidative capacity (Mutryn et al., 2015; Carvalho et al., 2023). However, recent evidence also suggests Ca^{2+} binds to F-ATP synthase β subunit (ATP5β), which provokes conformational changes to induce opening of the mitochondrial permeability transition pore (mPTP) and eventually apoptosis (Giorgio et al., 2017). An increase in ATP5β abundance (Carvalho et al., 2023; Zhang et al., 2023) but decrease in mitochondrial respiratory capacity in WB muscle (Zhang et al., 2023) suggests a Ca^{2+} mediated mechanism is partially responsible for mitochondrial dysfunction in WB.

3 Postmortem metabolism and fresh meat quality attributes in WB meat

The poor quality of WB meat continues to cost the U.S. poultry industry millions of dollars annually (Kuttappan et al., 2016; Huang and Ahn, 2018). For example, WB meat has a poor visual appearance, high drip loss, low marinade uptake, high cook loss, and inferior tenderness when compared to non-affected filets (Mudalal et al., 2015; Soglia et al., 2016; Soglia et al., 2017). In fact, over 50% of consumers indicated

they would not buy moderately or severely affected WB filets (Kuttappan et al., 2012), which forces processors to downgrade WB products (Kuttappan et al., 2012; Petracci et al., 2013). While the development of fresh meat quality is a multifactorial process, several defects incurred from the myopathy contribute to the poor eating experience associated with WB meat.

Severe myodegeneration with partial myofibrillar regeneration in WB muscle culminates in abnormal tissue structure and composition (Sihvo et al., 2014). In fact, an increase in protein degradation as well as diminished sarcomere organization and longer sarcomeres are routinely observed in WB muscle (Soglia et al., 2016; Kuttappan et al., 2017b; Papah et al., 2017; Baldi et al., 2020; Greene et al., 2020; Puolanne et al., 2021; Carvalho et al., 2023; Wang et al., 2023), which are features associated with diminished tenderness and water-holding capacity. Further, regions of damaged muscle that are not repaired fully exhibit an increase in immune cells, fibroblasts, and adipocytes indicating WB muscle coordinate an attempt to repair the tissue, but non-muscle cells infiltrate the damaged tissue (Figure 1) (Sihvo et al., 2014; Sihvo et al., 2017; Ferreira et al., 2020; Andretta et al., 2021; Ziemkiewicz et al., 2021). Indeed, thickening of the endo- and perimysium connective tissue layers as well as an increase in total collagen content, heat-insoluble collagen, and adiposity occurs in WB muscle (Soglia et al., 2016; Geronimo et al., 2022; Li et al., 2023). These structural and compositional changes contribute to an increase in tensile strength and the hard palpable areas found in WB filets (Sihvo et al., 2014; Sihvo et al., 2017; Ferreira et al., 2020; Andretta et al., 2021; Ziemkiewicz et al., 2021). While these physiochemical characteristics contribute to an inferior meat product, the underlying biochemical changes also play a role in altered water holding capacity, textural characteristics, and processing abilities (Petracci et al., 2013; Kuttappan et al., 2017b; Sihvo et al., 2017; Bowker et al., 2018; Dalgaard et al., 2018).

3.1 Postmortem metabolism

The metabolic dysregulation observed in living WB muscle translates to altered postmortem metabolism during the conversion of muscle to meat. For example, high ultimate pH is one of the hallmark characteristics of WB meat (Sihvo et al., 2014; Mutryn et al., 2015; Soglia et al., 2016; Kuttappan et al., 2017b; Sihvo et al., 2017; Soglia et al., 2017; Baldi et al., 2019; Tasoniero et al., 2019; Baldi et al., 2020; Li et al., 2023; Li et al., 2024). Under normal conditions, high ultimate pH is typically associated with an increase in water-holding capacity; however, water-holding capacity is diminished in WB meat. This may be attributed to the structural changes observed in WB muscle, such as an increase in sarcomere length (Baldi et al., 2020; Puolanne et al., 2021), disorganized sarcomere structure (Papah et al., 2017), and an increase in protein degradation. Further, greater adiposity and collagen content in WB also contributes to poor water-holding capacity because muscle plays a major role in binding water during storage and processing. Therefore, defects in postmortem metabolism are not the sole contributor to poor meat quality in WB; however, biochemical changes in muscle play a role in fresh meat quality and understanding these changes may contribute to the development of intervention strategies to salvage WB meat.

In WB muscle, glycogen stores and enzymes involved in glycogen metabolism are reduced compared to unaffected PM muscles (Abasht et al., 2016; Kuttappan et al., 2017a; Baldi et al., 2020; Carvalho et al., 2023). As glycogen availability is a major factor dictating pH decline (Henckel et al., 2000; Immonen et al., 2000a; Immonen and Puolanne, 2000; Immonen et al., 2000b; Chauhan and England, 2018; Chauhan et al., 2019; Spires et al., 2023), this seemed to be the culprit for an abbreviated pH decline. However, Baldi et al., 2020 reported residual glycogen was present at 24 h, which suggests depleted glycogen stores are not responsible for arresting glycolysis prematurely in WB meat. In the presence of residual glycogen, activity of phosphofructokinase (PFK) is a key player in determining ultimate pH (Matarneh et al., 2018b), but PFK activity early postmortem is not different in WB suggesting PFK is not responsible for the high ultimate pH (Baldi et al., 2020). However, glycolytic capacity of WB meat is diminished (Baldi et al., 2020; Li et al., 2024), which questions if the biochemical changes observed in WB muscle impact postmortem metabolism. For example, WB muscle appears to divert glycolytic intermediates through ancillary pathways to combat oxidative stress through downregulation of many glycolytic enzymes, which may culminate in reduced glycolytic capacity and high ultimate pH in WB meat. This notion is supported by reduced levels of glucose and nearly undetectable levels of G-6-P at 24 h postmortem in WB meat (Baldi et al., 2020). Further, WB muscle downregulates LDHα and WB meat exhibits a decrease in lactate accumulation (Abasht et al., 2016; Kuttappan et al., 2017a; Malila et al., 2019; Baldi et al., 2020; Thanatsang et al., 2020; Zhao et al., 2020; Wang et al., 2023; Li et al., 2024). Although these metabolic changes have not been entirely defined, it is clear that changes in WB muscle impact postmortem metabolism in WB meat.

After exsanguination, and thus removal of oxygen supply, mitochondria retain functionality using oxygen stores provided by myoglobin postmortem (England et al., 2018). Although glycolysis unarguably drives postmortem metabolism, mitochondria are not obsolete during this process and contribute to pH decline (Scheffler et al., 2015; England et al., 2018; Matarneh et al., 2018a; Matarneh et al., 2018b). In fact, addition of mitochondria to an *in vitro* system that mimics postmortem metabolism alters the utilization of the glycolytic end product pyruvate (Matarneh et al., 2021). Further, addition of mitochondria increases ATP hydrolysis and thus glycolytic flux in this *in vitro* system; however, inhibition of ATP5β negates the mitochondrial enhancement of glycolytic flux (Matarneh et al., 2018a). In WB muscle, protein abundance of ATP5β is greater than unaffected PM muscle (Carvalho et al., 2023; Zhang et al., 2023), which would suggest an increase in ATP hydrolysis and glycolytic flux. However, mitochondrial metabolic dysregulation and decreased respiratory capacity (Kuttappan et al., 2017a; Papah et al., 2018; Carvalho et al., 2023; Wang et al., 2023; Zhang et al., 2023) may negate the contribution of WB mitochondria to postmortem metabolism.

3.2 Postmortem proteolysis

Tenderness is determined by many factors including connective tissue characteristics, myofibrillar structure, sarcomere length, protein degradation, and intramuscular fat. An increase in

shear force and tensile strength is often observed in WB meat (Chatterjee et al., 2016; Soglia et al., 2017; Hasegawa et al., 2020; Jarvis et al., 2020), which supports the notion that tenderness deteriorates in WB meat. In normal tissue, high free Ca^{2+} is associated with an increase in postmortem proteolysis and tenderness through calpain activation (Wheeler et al., 1992; Boleman et al., 1995; Dang et al., 2020). Although free Ca^{2+} is elevated in WB (Soglia et al., 2016; Tasoniero et al., 2019; Welter et al., 2022; Wang et al., 2023), calpain activation as well as proteolytic degradation of desmin and troponin T has been reported as either not different or increased in WB meat compared to unaffected filets (Soglia et al., 2017; Soglia et al., 2018; Hasegawa et al., 2020; Welter et al., 2022). Although there is not a consensus on whether calpain activation is unchanged or increased in WB meat, these reports agree that defects in postmortem proteolysis are not at fault in WB meat. However, changes in sarcomere length and structure (Papah et al., 2017; Baldi et al., 2020; Puolanne et al., 2021), altered protein composition (Baker et al., 1999; Soglia et al., 2016; Kuttappan et al., 2017a; Greene et al., 2020; Carvalho et al., 2023; Wang et al., 2023), and higher total collagen content as well as increased heat-insoluble collagen (Soglia et al., 2016; Geronimo et al., 2022; Li et al., 2023) in WB myofibers are presumably large drivers of poor tenderness in WB meat. In fact, Hasegawa et al., 2020 reported tensile strength remained high with minimal changes to connective tissue in WB meat between harvest and 5 days postmortem. While the exact mechanism responsible for diminishing tenderness of WB meat remains vague, these reports suggest defects in postmortem proteolytic process are not driving tenderness deterioration in WB meat.

4 Conclusion

Wooden breast is a complex myopathy that not only affects the structural and metabolic characteristics of muscle, but also culminates in poor fresh meat quality attributes. For example, WB muscle appears to shunt glycolytic intermediates into ancillary pathways of glycolysis to combat oxidative stress through downregulation of many glycolytic enzymes, which presumably contributes to diminished glycolytic capacity and high ultimate pH of WB meat. Further, mitochondrial dysfunction may contribute to altered postmortem metabolism, but its exact impact on metabolism remains vague. Interestingly, postmortem proteolytic processes do not appear to be obstructed in WB meat, but high amounts of connective tissue, altered protein composition, and changes in sarcomere structure presumably drive tenderness deterioration in WB meat. In summary, metabolic dysregulation plays a role in the WB myopathy, but it remains unclear if changes in metabolism contribute to the onset of the disease or are simply a secondary symptom.

Author contributions

LR: Writing–original draft, Writing–review and editing. MZ: Supervision, Writing–original draft, Writing–review and editing.

Funding

The author(s) declare that no financial support was received for the research, authorship, and/or publication of this article.

Conflict of interest

The authors declare that the research was conducted in the absence of any commercial or financial relationships that could be construed as a potential conflict of interest.

Publisher's note

References

Abasht, B., Mutryn, M. F., Michalek, R. D., and Lee, W. R. (2016). Oxidative stress and metabolic perturbations in wooden breast disorder in chickens. *PLoS One* 11 (4), e0153750. doi:10.1371/journal.pone.0153750

Andretta, I., Hickmann, F. M. W., Remus, A., Franceschi, C. H., Mariani, A. B., Orso, C., et al. (2021). Environmental impacts of pig and poultry production: insights from a systematic review. *Front. Vet. Sci.* 8, 750733. doi:10.3389/fvets.2021.750733

Baker, D. H., Edwards, H. M., Strunk, C. S., Emmert, J. L., Peter, C. M., Mavromichalis, I., et al. (1999). Single versus multiple deficiencies of methionine, zinc, riboflavin, vitamin B-6 and choline elicit surprising growth responses in young chicks. *J. Nutr.* 129 (12), 2239–2245. doi:10.1093/jn/129.12.2239

Baldi, G., Soglia, F., Laghi, L., Tappi, S., Rocculi, P., Tavaniello, S., et al. (2019). Comparison of quality traits among breast meat affected by current muscle abnormalities. *Food Res. Int.* 115, 369–376. doi:10.1016/j.foodres.2018.11.020

Baldi, G., Yen, C. N., Daughtry, M. R., Bodmer, J., Bowker, B. C., Zhuang, H., et al. (2020). Exploring the factors contributing to the high ultimate pH of broiler pectoralis major muscles affected by wooden breast condition. *Front. Physiol.* 11, 343. doi:10.3389/fphys.2020.00343

Baldini, S. F., Steenackers, A., Olivier-Van Stichelen, S., Mir, A. M., Mortuaire, M., Lefebvre, T., et al. (2016). Glucokinase expression is regulated by glucose through O-GlcNAc glycosylation. *Biochem. Biophys. Res. Commun.* 478 (2), 942–948. doi:10.1016/j.bbrc.2016.08.056

Boleman, S. J., Boleman, S. L., Bidner, T. D., McMillin, K. W., and Monlezun, C. J. (1995). Effects of Postmortem time of calcium chloride injection on beef tenderness and drip, cooking, and total loss. *Meat Sci.* 39 (1), 35–41. doi:10.1016/0309-1740(95)80005-0

Bond, M. R., and Hanover, J. A. (2015). A little sugar goes a long way: the cell biology of O-GlcNAc. *J. Cell Biol.* 208 (7), 869–880. doi:10.1083/jcb.201501101

Bowker, B. C., Maxwell, A. D., Zhuang, H., and Adhikari, K. (2018). Marination and cooking performance of portioned broiler breast fillets with the wooden breast condition. *Poult. Sci.* 97 (8), 2966–2970. doi:10.3382/ps/pey144

Cahn, R. D., Zwilling, E., Kaplan, N. O., and Levine, L. (1962). Nature and Development of Lactic Dehydrogenases: the two major types of this enzyme form molecular hybrids which change in makeup during development. *Science* 136 (3520), 962–969. doi:10.1126/science.136.3520.962

Carvalho, L. M., Rocha, T. C., Delgado, J., Diaz-Velasco, S., Madruga, M. S., and Estevez, M. (2023). Deciphering the underlying mechanisms of the oxidative perturbations and impaired meat quality in Wooden breast myopathy by label-free quantitative MS-based proteomics. *Food Chem.* 423, 136314. doi:10.1016/j.foodchem.2023.136314

Chatterjee, D., Zhuang, H., Bowker, B. C., Rincon, A. M., and Sanchez-Brambila, G. (2016). Instrumental texture characteristics of broiler pectoralis major with the wooden breast condition. *Poult. Sci.* 95 (10), 2449–2454. doi:10.3382/ps/pew204

Chauhan, S. S., and England, E. M. (2018). Postmortem glycolysis and glycogenolysis: insights from species comparisons. *Meat Sci.* 144, 118–126. doi:10.1016/j.meatsci.2018.06.021

Chauhan, S. S., LeMaster, M. N., Clark, D. L., Foster, M. K., Miller, C. E., and England, E. M. (2019). Glycolysis and pH decline terminate prematurely in oxidative muscles despite the presence of excess glycogen. *Meat Muscle Biol. 3doi* 3. doi:10.22175/mmb2019.02.0006

Dalgaard, L. B., Rasmussen, M. K., Bertram, H. C., Jensen, J. A., Møller, H. S., Aaslyng, M. D., et al. (2018). Classification of wooden breast myopathy in chicken pectoralis major by a standardised method and association with conventional quality assessments. *Int. J. Food Sci. and Technol.* 53 (7), 1744–1752. doi:10.1111/ijfs.13759

Dang, D. S., Buhler, J. F., Davis, H. T., Thornton, K. J., Scheffler, T. L., and Matarneh, S. K. (2020). Inhibition of mitochondrial calcium uniporter enhances postmortem proteolysis and tenderness in beef cattle. *Meat Sci.* 162, 108039. doi:10.1016/j.meatsci.2019.108039

Dawson, D. M., Goodfriend, T. L., and Kaplan, N. O. (1964). Lactic dehydrogenases: functions of the two types rates of synthesis of the two major forms can Be correlated with metabolic differentiation. *Science* 143 (3609), 929–933. doi:10.1126/science.143.3609.929

Dimmer, K. S., Friedrich, B., Lang, F., Deitmer, J. W., and Broer, S. (2000). The low-affinity monocarboxylate transporter MCT4 is adapted to the export of lactate in highly glycolytic cells. *Biochem. J.* 350 (Pt 1), 219–227. doi:10.1042/bj3500219

Dransfield, E., and Sosnicki, A. (1999). Relationship between muscle growth and poultry meat quality. *Poult. Sci.* 78 (5), 743–746. doi:10.1093/ps/78.5.743

Du, Y., Ding, Q., Li, Y., and Fang, W. (2017). Identification of differentially expressed genes and pathways for myofiber characteristics in soleus muscles between chicken breeds differing in meat quality. *Anim. Biotechnol.* 28 (2), 83–93. doi:10.1080/10495398.2016.1206555

England, E. M., Matarneh, S. K., Mitacek, R. M., Abraham, A., Ramanathan, R., Wicks, J. C., et al. (2018). Presence of oxygen and mitochondria in skeletal muscle early postmortem. *Meat Sci.* 139, 97–106. doi:10.1016/j.meatsci.2017.12.008

Ferreira, T. Z., Kindlein, L., Flees, J. J., Shortnacy, L. K., Vieira, S. L., Nascimento, V. P., et al. (2020). Characterization of pectoralis major muscle satellite cell population heterogeneity, macrophage density, and collagen infiltration in broiler chickens affected by wooden breast. *Front. Physiol.* 11, 529. doi:10.3389/fphys.2020.00529

Fulle, S., Protasi, F., Di Tano, G., Pietrangelo, T., Beltramin, A., Boncompagni, S., et al. (2004). The contribution of reactive oxygen species to sarcopenia and muscle ageing. *Exp. Gerontol.* 39 (1), 17–24. doi:10.1016/j.exger.2003.09.012

Geronimo, B. C., Prudencio, S. H., and Soares, A. L. (2022). Biochemical and technological characteristics of wooden breast chicken fillets and their consumer acceptance. *J. Food Sci. Technol.* 59 (3), 1185–1192. doi:10.1007/s13197-021-05123-3

Gherardi, G., Nogara, L., Ciciliot, S., Fadini, G. P., Blaauw, B., Braghetta, P., et al. (2019). Loss of mitochondrial calcium uniporter rewires skeletal muscle metabolism and substrate preference. *Cell Death Differ.* 26 (2), 362–381. doi:10.1038/s41418-018-0191-7

Giorgio, V., Burchell, V., Schiavone, M., Bassot, C., Minervini, G., Petronilli, V., et al. (2017). Ca2+ binding to F-ATP synthase β subunit triggers the mitochondrial permeability transition. *EMBO Rep.* 18 (7), 1065–1076. doi:10.15252/embr.201643354

Gommans, I. M., Vlak, M. H., de Haan, A., and van Engelen, B. G. (2002). Calcium regulation and muscle disease. *J. Muscle Res. Cell Motil.* 23 (1), 59–63. doi:10.1023/a:1019984714528

Greene, E., Flees, J., Dadgar, S., Mallmann, B., Orlowski, S., Dhamad, A., et al. (2019). Quantum blue reduces the severity of woody breast myopathy via modulation of oxygen homeostasis-related genes in broiler chickens. *Front. Physiol.* 10, 1251. doi:10.3389/fphys.2019.01251

Greene, E., Cauble, R., Dhamad, A. E., Kidd, M. T., Kong, B., Howard, S. M., et al. (2020). Muscle metabolome profiles in woody breast-(un)Affected broilers: effects of quantum blue phytase-enriched diet. *Front. Veterinary Sci.* 7 (Original Research), 458. doi:10.3389/fvets.2020.00458

Hart, G. W., and Akimoto, Y. (2009). "The O-GlcNAc modification," in *Essentials of glycobiology*. Editors A. Varki, R. D. Cummings, J. D. Esko, H. H. Freeze, P. Stanley, C. R. Bertozzi, et al. (Cold Spring Harbor (NY)).

Hasegawa, Y., Hara, T., Kawasaki, T., Yamada, M., Watanabe, T., and Iwasaki, T. (2020). Effect of wooden breast on postmortem changes in chicken meat. *Food Chem.* 315, 126285. doi:10.1016/j.foodchem.2020.126285

Hasegawa, Y., Hosotani, M., Saito, M., Nagasawa, T., Mori, Y., Kawasaki, T., et al. (2022). Mitochondrial characteristics of chicken breast muscle affected by wooden breast. *Comp. Biochem. Physiol. A Mol. Integr. Physiol.* 273, 111296. doi:10.1016/j.cbpa.2022.111296

Henckel, P., Karlsson, A., Oksbjerg, N., and Soholm Petersen, J. (2000). Control of post mortem pH decrease in pig muscles: experimental design and testing of animal models. *Meat Sci.* 55 (1), 131–138. doi:10.1016/s0309-1740(99)00135-7

Hosotani, M., Kawasaki, T., Hasegawa, Y., Wakasa, Y., Hoshino, M., Takahashi, N., et al. (2020). Physiological and pathological mitochondrial clearance is related to pectoralis major muscle pathogenesis in broilers with wooden breast syndrome. *Front. Physiol.* 11, 579. doi:10.3389/fphys.2020.00579

Hosotani, M., Kametani, K., Ohno, N., Hiramatsu, K., Kawasaki, T., Hasegawa, Y., et al. (2021). The unique physiological features of the broiler pectoralis major muscle as suggested by the three-dimensional ultrastructural study of mitochondria in type IIb muscle fibers. *J. Vet. Med. Sci.* 83 (11), 1764–1771. doi:10.1292/jvms.21-0408

Huang, X., and Ahn, D. U. (2018). The incidence of muscle abnormalities in broiler breast meat - a review. *Korean J. Food Sci. Anim. Resour.* 38 (5), 835–850. doi:10.5851/kosfa.2018.e2

Huo, W., Weng, K., Li, Y., Zhang, Y., Zhang, Y., Xu, Q., et al. (2022). Comparison of muscle fiber characteristics and glycolytic potential between slow- and fast-growing broilers. *Poult. Sci.* 101 (3), 101649. doi:10.1016/j.psj.2021.101649

Immonen, K., and Puolanne, E. (2000). Variation of residual glycogen-glucose concentration at ultimate pH values below 5.75. *Meat Sci.* 55 (3), 279–283. doi:10.1016/s0309-1740(99)00152-7

Immonen, K., Kauffman, R. G., Schaefer, D. M., and Puolanne, E. (2000a). Glycogen concentrations in bovine longissimus dorsi muscle. *Meat Sci.* 54 (2), 163–167. doi:10.1016/s0309-1740(99)00090-x

Immonen, K., Ruusunen, M., Hissa, K., and Puolanne, E. (2000b). Bovine muscle glycogen concentration in relation to finishing diet, slaughter and ultimate pH. *Meat Sci.* 55 (1), 25–31. doi:10.1016/s0309-1740(99)00121-7

Interagency Agricultural Projections Committee (2022). *USDA agricultural projections to 2031*. OCE-2022-1. Washington, DC: USDA.

Jarvis, T., Byron, M., Von Staden, M., Crist, C., Zhang, X., Rowe, C., et al. (2020). Quality differences in wooden and normal broiler breast meat marinated with traditional and clean label marinades. *Meat Muscle Biol.* 4 (1). doi:10.22175/mmb.9458

Jouaville, L. S., Pinton, P., Bastianutto, C., Rutter, G. A., and Rizzuto, R. (1999). Regulation of mitochondrial ATP synthesis by calcium: evidence for a long-term metabolic priming. *Proc. Natl. Acad. Sci. U. S. A.* 96 (24), 13807–13812. doi:10.1073/pnas.96.24.13807

Kidd, M. T., Morgan, G. W., Price, C. J., Welch, P. A., and Fontana, E. A. (2001). Enzyme supplementation to corn and soybean meal diets for broilers. *Appl. Poult. Res.* 10 (1), 65–70. doi:10.1093/japr/10.1.65

Kierans, S. J., and Taylor, C. T. (2021). Regulation of glycolysis by the hypoxia-inducible factor (HIF): implications for cellular physiology. *J. Physiol.* 599 (1), 23–37. doi:10.1113/JP280572

Klont, R., Lambooy, E., and Van Logtestijn, J. (1994). Effect of dantrolene treatment on muscle metabolism and meat quality of anesthetized pigs of different halothane genotypes. *J. animal Sci.* 72 (8), 2008–2016. doi:10.2527/1994.7282008x

Kristal, B. S., Vigneau-Callahan, K. E., Moskowitz, A. J., and Matson, W. R. (1999). Purine catabolism: links to mitochondrial respiration and antioxidant defenses? *Arch. Biochem. Biophys.* 370 (1), 22–33. doi:10.1006/abbi.1999.1387

Kunz, W. S. (2001). Control of oxidative phosphorylation in skeletal muscle. *Biochim. Biophys. Acta* 1504 (1), 12–19. doi:10.1016/s0005-2728(00)00235-8

Kuttappan, V. A., Lee, Y. S., Erf, G. F., Meullenet, J. F., McKee, S. R., and Owens, C. M. (2012). Consumer acceptance of visual appearance of broiler breast meat with varying degrees of white striping. *Poult. Sci.* 91 (5), 1240–1247. doi:10.3382/ps.2011-01947

Kuttappan, V. A., Hargis, B. M., and Owens, C. M. (2016). White striping and woody breast myopathies in the modern poultry industry: a review. *Poult. Sci.* 95 (11), 2724–2733. doi:10.3382/ps/pew216

Kuttappan, V. A., Bottje, W., Ramnathan, R., Hartson, S. D., Coon, C. N., Kong, B. W., et al. (2017a). Proteomic analysis reveals changes in carbohydrate and protein metabolism associated with broiler breast myopathy. *Poult. Sci.* 96 (8), 2992–2999. doi:10.3382/ps/pex069

Kuttappan, V. A., Owens, C. M., Coon, C., Hargis, B. M., and Vazquez-Anon, M. (2017b). Incidence of broiler breast myopathies at 2 different ages and its impact on selected raw meat quality parameters. *Poult. Sci.* 96 (8), 3005–3009. doi:10.3382/ps/pex072

Li, B., Dong, X., Puolanne, E., and Ertbjerg, P. (2022). Effect of wooden breast degree on lipid and protein oxidation and citrate synthase activity of chicken pectoralis major muscle. *LWT* 154, 112884. doi:10.1016/j.lwt.2021.112884

Li, B., Linden, J., Puolanne, E., and Ertbjerg, P. (2023). Effects of wooden breast syndrome in broiler chicken on sarcoplasmic, myofibrillar, and connective tissue proteins and their association with muscle fiber area. *Foods* 12 (18), 3360. doi:10.3390/foods12183360

Li, B., Kalmu, N., Dong, X., Zhang, Y., Puolanne, E., and Ertbjerg, P. (2024). Relationship between wooden breast severity in broiler chicken, antioxidant

enzyme activity and markers of energy metabolism. *Poult. Sci.* 103 (8), 103877. doi:10.1016/j.psj.2024.103877

Liu, Y., Hu, Y., and Li, S. (2022). Protein O-GlcNAcylation in metabolic modulation of skeletal muscle: a bright but long way to go. *Metabolites* 12 (10), 888. doi:10.3390/metabo12100888

Ma, J., and Hart, G. W. (2014). O-GlcNAc profiling: from proteins to proteomes. *Clin. Proteomics* 11 (1), 8. doi:10.1186/1559-0275-11-8

Malila, Y., Thanatsang, K., Arayamethakorn, S., Uengwetwanit, T., Srimarut, Y., Petracci, M., et al. (2019). Absolute expressions of hypoxia-inducible factor-1 alpha (HIF1A) transcript and the associated genes in chicken skeletal muscle with white striping and wooden breast myopathies. *PLoS One* 14 (8), e0220904. doi:10.1371/journal.pone.0220904

Mammucari, C., Gherardi, G., Zamparo, I., Raffaello, A., Boncompagni, S., Chemello, F., et al. (2015). The mitochondrial calcium uniporter controls skeletal muscle trophism *in vivo*. *Cell Rep.* 10 (8), 1269–1279. doi:10.1016/j.celrep.2015.01.056

Marshall, S., Bacote, V., and Traxinger, R. R. (1991). Discovery of a metabolic pathway mediating glucose-induced desensitization of the glucose transport system. Role of hexosamine biosynthesis in the induction of insulin resistance. *J. Biol. Chem.* 266 (8), 4706–4712. doi:10.1016/s0021-9258(19)67706-9

Matarneh, S. K., Beline, M., de Luz, E. S. S., Shi, H., and Gerrard, D. E. (2018a). Mitochondrial F(1)-ATPase extends glycolysis and pH decline in an *in vitro* model. *Meat Sci.* 137, 85–91. doi:10.1016/j.meatsci.2017.11.009

Matarneh, S. K., Yen, C. N., Elgin, J. M., Beline, M., da Luz, E. S. S., Wicks, J. C., et al. (2018b). Phosphofructokinase and mitochondria partially explain the high ultimate pH of broiler pectoralis major muscle. *Poult. Sci.* 97 (5), 1808–1817. doi:10.3382/ps/pex455

Matarneh, S. K., Yen, C. N., Bodmer, J., El-Kadi, S. W., and Gerrard, D. E. (2021). Mitochondria influence glycolytic and tricarboxylic acid cycle metabolism under postmortem simulating conditions. *Meat Sci.* 172, 108316. doi:10.1016/j.meatsci.2020.108316

McCormack, J. G., and Denton, R. M. (1981). A comparative study of the regulation of Ca2+ of the activities of the 2-oxoglutarate dehydrogenase complex and NAD+-isocitrate dehydrogenase from a variety of sources. *Biochem. J.* 196 (2), 619–624. doi:10.1042/bj1960619

Meloche, K. J., Fancher, B. I., Emmerson, D. A., Bilgili, S. F., and Dozier, W. A. (2018a). Effects of quantitative nutrient allocation on myopathies of the Pectoralis major muscles in broiler chickens at 32, 43, and 50 days of age. *Poult. Sci.* 97 (5), 1786–1793. doi:10.3382/ps/pex453

Meloche, K. J., Fancher, B. I., Emmerson, D. A., Bilgili, S. F., and Dozier, W. A. (2018b). Effects of reduced dietary energy and amino acid density on Pectoralis major myopathies in broiler chickens at 36 and 49 days of age1. *Poult. Sci.* 97 (5), 1794–1807. doi:10.3382/ps/pex454

Miller, M., Gerval, A., Hansen, J., and Grossen, G. (2022). *Poultry expected to continue leading global meat imports as demand rises*. OCE-2022-1. Washington, DC: U.S. Department of Agriculture.

Minchenko, A., Leshchinsky, I., Opentanova, I., Sang, N., Srinivas, V., Armstead, V., et al. (2002). Hypoxia-inducible factor-1-mediated expression of the 6-phosphofructo-2-kinase/fructose-2,6-bisphosphatase-3 (PFKFB3) gene. Its possible role in the Warburg effect. *J. Biol. Chem.* 277 (8), 6183–6187. doi:10.1074/jbc.M110978200

Mudalal, S., Lorenzi, M., Soglia, F., Cavani, C., and Petracci, M. (2015). Implications of white striping and wooden breast abnormalities on quality traits of raw and marinated chicken meat. *Animal* 9 (4), 728–734. doi:10.1017/S175173111400295X

Mutryn, M. F., Brannick, E. M., Fu, W., Lee, W. R., and Abasht, B. (2015). Characterization of a novel chicken muscle disorder through differential gene expression and pathway analysis using RNA-sequencing. *BMC Genomics* 16 (1), 399. doi:10.1186/s12864-015-1623-0

National Chicken Council (2022). U.S. Broiler performance national chicken Council. Washington, DC: National Chicken Council. Available at: https://www.nationalchickencouncil.org/about-the-industry/statistics/u-s-broilerperformance/

Papah, M. B., Brannick, E. M., Schmidt, C. J., and Abasht, B. (2017). Evidence and role of phlebitis and lipid infiltration in the onset and pathogenesis of Wooden Breast Disease in modern broiler chickens. *Avian Pathol.* 46 (6), 623–643. doi:10.1080/03079457.2017.1339346

Papah, M. B., Brannick, E. M., Schmidt, C. J., and Abasht, B. (2018). Gene expression profiling of the early pathogenesis of wooden breast disease in commercial broiler chickens using RNA-sequencing. *PLoS One* 13 (12), e0207346. doi:10.1371/journal.pone.0207346

Pesce, A., McKay, R. H., Stolzenbach, F., Cahn, R. D., and Kaplan, N. O. (1964). The comparative enzymology of lactic dehydrogenases. *J. Biol. Chem.* 239, 1753–1761. doi:10.1016/s0021-9258(18)91253-6

Petracci, M., Mudalal, S., Bonfiglio, A., and Cavani, C. (2013). Occurrence of white striping under commercial conditions and its impact on breast meat quality in broiler chickens. *Poult. Sci.* 92 (6), 1670–1675. doi:10.3382/ps.2012-03001

Plaitakis, A., Kalef-Ezra, E., Kotzamani, D., Zaganas, I., and Spanaki, C. (2017). The glutamate dehydrogenase pathway and its roles in cell and tissue biology in health and disease. *Biol. (Basel)* 6 (1), 11. doi:10.3390/biology6010011

Puolanne, T. J., Ertbjerg, P., and Costandache, C. G. (2021). Influence of woody breast myopathy on sarcomere length and tensile strength in commercial broiler pectoralis major muscle. *Meat Muscle Biol.* 5 (1), 1–11. doi:10.22175/mmb.11564

Rao, X., Duan, X., Mao, W., Li, X., Li, Z., Li, Q., et al. (2015). O-GlcNAcylation of G6PD promotes the pentose phosphate pathway and tumor growth. *Nat. Commun.* 6, 8468. doi:10.1038/ncomms9468

Roy, B. C., Oshima, I., Miyachi, H., Shiba, N., Nishimura, S., Tabata, S., et al. (2006). Effects of nutritional level on muscle development, histochemical properties of myofibre and collagen architecture in the pectoralis muscle of male broilers. *Br. Poult. Sci.* 47 (4), 433–442. doi:10.1080/00071660600828334

Scheffler, T. L., Scheffler, J. M., Park, S., Kasten, S. C., Wu, Y., McMillan, R. P., et al. (2014). Fiber hypertrophy and increased oxidative capacity can occur simultaneously in pig glycolytic skeletal muscle. *Am. J. Physiol. Cell Physiol.* 306 (4), C354–C363. doi:10.1152/ajpcell.00002.2013

Scheffler, T. L., Matarneh, S. K., England, E. M., and Gerrard, D. E. (2015). Mitochondria influence postmortem metabolism and pH in an *in vitro* model. *Meat Sci.* 110, 118–125. doi:10.1016/j.meatsci.2015.07.007

Sheng, G., Gao, Y., Wu, H., Liu, Y., and Yang, Y. (2023). Functional heterogeneity of MCT1 and MCT4 in metabolic reprogramming affects osteosarcoma growth and metastasis. *J. Orthop. Surg. Res.* 18 (1), 131. doi:10.1186/s13018-023-03623-w

Sihvo, H. K., Immonen, K., and Puolanne, E. (2014). Myodegeneration with fibrosis and regeneration in the pectoralis major muscle of broilers. *Vet. Pathol.* 51 (3), 619–623. doi:10.1177/0300985813497488

Sihvo, H. K., Linden, J., Airas, N., Immonen, K., Valaja, J., and Puolanne, E. (2017). Wooden breast myodegeneration of pectoralis major muscle over the growth period in broilers. *Vet. Pathol.* 54 (1), 119–128. doi:10.1177/0300985816658099

Simoes, C. T., Vieira, S. L., Stefanello, C., Kindlein, L., Ferreira, T., Favero, A., et al. (2020). An *in vivo* evaluation of the effects of feed restriction regimens on wooden breast using ultrasound images as a predictive tool. *Br. Poult. Sci.* 61 (5), 583–589. doi:10.1080/00071668.2020.1764909

Smith, D. P., and Fletcher, D. L. (1988). Chicken breast muscle fiber type and diameter as influenced by age and intramuscular location. *Poult. Sci.* 67 (6), 908–913. doi:10.3382/ps.0670908

Soglia, F., Mudalal, S., Babini, E., Di Nunzio, M., Mazzoni, M., Sirri, F., et al. (2016). Histology, composition, and quality traits of chicken Pectoralis major muscle affected by wooden breast abnormality. *Poult. Sci.* 95 (3), 651–659. doi:10.3382/ps/pev353

Soglia, F., Gao, J., Mazzoni, M., Puolanne, E., Cavani, C., Petracci, M., et al. (2017). Superficial and deep changes of histology, texture and particle size distribution in broiler wooden breast muscle during refrigerated storage. *Poult. Sci.* 96 (9), 3465–3472. doi:10.3382/ps/pex115

Soglia, F., Zeng, Z., Gao, J., Puolanne, E., Cavani, C., Petracci, M., et al. (2018). Evolution of proteolytic indicators during storage of broiler wooden breast meat. *Poult. Sci.* 97 (4), 1448–1455. doi:10.3382/ps/pex398

Spires, M. D., Bodmer, J. S., Beline, M., Wicks, J. C., Zumbaugh, M. D., Shi, T. H., et al. (2023). Postmortem metabolism and pork quality development are affected by electrical stimulation across three genetic lines. *Anim. (Basel)* 13 (16), 2599. doi:10.3390/ani13162599

Stincone, A., Prigione, A., Cramer, T., Wamelink, M. M., Campbell, K., Cheung, E., et al. (2015). The return of metabolism: biochemistry and physiology of the pentose phosphate pathway. *Biol. Rev. Camb Philos. Soc.* 90 (3), 927–963. doi:10.1111/brv.12140

Talbot, J., and Maves, L. (2016). Skeletal muscle fiber type: using insights from muscle developmental biology to dissect targets for susceptibility and resistance to muscle disease. *Wiley Interdiscip. Rev. Dev. Biol.* 5 (4), 518–534. doi:10.1002/wdev.230

Tasoniero, G., Bowker, B., Stelzleni, A., Zhuang, H., Rigdon, M., and Thippareddi, H. (2019). Use of blade tenderization to improve wooden breast meat texture. *Poult. Sci.* 98 (9), 4204–4211. doi:10.3382/ps/pez163

Thanatsang, K. V., Malila, Y., Arayamethakorn, S., Srimarut, Y., Tatiyaborworntham, N., Uengwetwanit, T., et al. (2020). Nutritional properties and oxidative indices of broiler breast meat affected by wooden breast abnormality. *Anim. (Basel)* 10 (12), 2272. doi:10.3390/ani10122272

Trocino, A., Piccirillo, A., Birolo, M., Radaelli, G., Bertotto, D., Filiou, E., et al. (2015). Effect of genotype, gender and feed restriction on growth, meat quality and the occurrence of white striping and wooden breast in broiler chickens. *Poult. Sci.* 94 (12), 2996–3004. doi:10.3382/ps/pev296

Verdiglione, R., and Cassandro, M. (2013a). Characterization of muscle fiber type in the pectoralis major muscle of slow-growing local and commercial chicken strains. *Poult. Sci.* 92 (9), 2433–2437. doi:10.3382/ps.2013-03013

Verdiglione, R., and Cassandro, M. (2013b). Characterization of muscle fiber type in the pectoralis major muscle of slow-growing local and commercial chicken strains. *Poult. Sci.* 92 (9), 2433–2437. doi:10.3382/ps.2013-03013

Vieira, S. L., Simoes, C. T., Kindlein, L., Ferreira, T. Z., Soster, P., and Stefanello, C. (2021). Progressive *in vivo* detection of wooden breast in broilers as affected by dietary energy and protein. *Poult. Sci.* 100 (6), 101120. doi:10.1016/j.psj.2021.101120

Wang, Z., Brannick, E., and Abasht, B. (2023). Integrative transcriptomic and metabolomic analysis reveals alterations in energy metabolism and mitochondrial

functionality in broiler chickens with wooden breast. *Sci. Rep.* 13 (1), 4747. doi:10.1038/s41598-023-31429-7

Welter, A. A., Wu, W. J., Maurer, R., O'Quinn, T. G., Chao, M. D., Boyle, D. L., et al. (2022). An investigation of the altered textural property in woody breast myopathy using an integrative omics approach. *Front. Physiol.* 13, 860868. doi:10.3389/fphys.2022.860868

Wheeler, T., Crouse, J., and Koohmaraie, M. (1992). The effect of postmortem time of injection and freezing on the effectiveness of calcium chloride for improving beef tenderness. *J. Animal Sci.* 70 (11), 3451–3457. doi:10.2527/1992.70113451x

Xing, T., Zhao, X., Zhang, L., Li, J. L., Zhou, G. H., Xu, X. L., et al. (2020). Characteristics and incidence of broiler chicken wooden breast meat under commercial conditions in China. *Poult. Sci.* 99 (1), 620–628. doi:10.3382/ps/pez560

Zhang, X., Xing, T., Li, J., Zhang, L., and Gao, F. (2023). Mitochondrial dysfunction and calcium dyshomeostasis in the pectoralis major muscle of broiler chickens with wooden breast myopathy. *Poult. Sci.* 102 (9), 102872. doi:10.1016/j.psj.2023.102872

Zhao, D., Kogut, M. H., Genovese, K. J., Hsu, C. Y., Lee, J. T., and Farnell, Y. Z. (2020). Altered expression of lactate dehydrogenase and monocarboxylate transporter involved in lactate metabolism in broiler wooden breast. *Poult. Sci.* 99 (1), 11–20. doi:10.3382/ps/pez572

Ziemkiewicz, N., Hilliard, G., Pullen, N. A., and Garg, K. (2021). The role of innate and adaptive immune cells in skeletal muscle regeneration. *Int. J. Mol. Sci.* 22 (6), 3265. doi:10.3390/ijms22063265

frontiers | Frontiers in Physiology

TYPE Original Research
PUBLISHED 23 December 2024
DOI 10.3389/fphys.2024.1513311

OPEN ACCESS

EDITED BY
Sandra G. Velleman,
The Ohio State University, United States

REVIEWED BY
Guglielmo Sorci,
University of Perugia, Italy
Colin Guy Scanes,
University of Wisconsin–Milwaukee,
United States

*CORRESPONDENCE
Lucie Pejšková,
lucie.pejskova@nofima.no

RECEIVED 18 October 2024
ACCEPTED 25 November 2024
PUBLISHED 23 December 2024

CITATION
Pejšková L, Pisconti A, Lunde M, Ho KY, Solberg NT, Koga S, Tengstrand E, Carlson CR, Pedersen ME and Rønning SB (2024) Wooden breast myopathy is characterized by satellite cell dysfunction and syndecan-4 shedding. *Front. Physiol.* 15:1513311. doi: 10.3389/fphys.2024.1513311

Wooden breast myopathy is characterized by satellite cell dysfunction and syndecan-4 shedding

Lucie Pejšková[1]*, Addolorata Pisconti[2], Marianne Lunde[3], Ka Yi Ho[2], Nina Therese Solberg[1], Shiori Koga[1], Erik Tengstrand[1], Cathrine Rein Carlson[3], Mona Elisabeth Pedersen[1] and Sissel Beate Rønning[1]

[1]Raw Materials and Optimalization, Nofima AS, Ås, Norway, [2]Department of Biochemistry and Cell Biology, SUNY Stony Brook, Stony Brook, NY, United States, [3]Institute for Experimental Medical Research, Oslo University Hospital and University of Oslo, Oslo, Norway

Introduction: Skeletal muscle satellite cells (MuSCs or stem cells) play a crucial role in muscle development, maintenance, and regeneration, supporting both hypertrophy and regenerative myogenesis. Syndecans (SDCs) act as communication bridges within the muscle microenvironment, regulating interactions with extracellular matrix components and contributing significantly to tissue repair and inflammation. Specifically, syndecan-4 (SDC4) is involved in muscle regeneration at multiple stages.

Methods: This study delves into the emerging challenge of wooden breast (WB) myopathy and its connection with SDC4. Our hypothesis proposes that disruptions in MuSC dynamics through SDC4 contribute to the increased incidence of breast myopathies observed in growing broilers. To test our hypothesis, non-affected and affected broilers were systematically selected, and the characteristics of WB myopathy were studied both *in vitro* and *in vivo*. SDC4 overexpression in MuSCs and blocking peptides (BPs) corresponding to the SDC4 ectodomain were used for investigating the role of SDC4 in muscle development and its shedding levels.

Results and discussion: *In vivo* examination of affected muscles revealed smaller fibers and changes in metabolic pathways. *In vitro* studies unveiled disrupted proliferation of MuSCs in WB myopathy, accompanied by the downregulation of several muscle markers. Investigation of the potential role of SDC4 in the pathogenesis of WB myopathy revealed a decreased tendency in SDC4 gene expression and increased shedding of its ectodomain. Moreover, we showed that SDC4 overexpression is linked to reduced proliferation in MuSCs and affected myogenesis. We detected an impaired proliferation of WB-affected MuSCs, revealing critical insights into the dysfunctional state of these cells in myopathy. Additionally, by treating MuSCs with blocking peptides derived from the SDC4 ectodomain, we identified altered proliferation. Taken

together, this work contributes with valuable knowledge on the molecular mechanisms underlying WB myopathy and the role of SDC4 in this chicken myopathy.

KEYWORDS

wooden breast, syndecan-4, myopathy, syndecans, broiler chicken, skeletal muscle satellite cells

1 Introduction

Commercial broiler chickens have undergone genetic selection for effective growth and higher breast muscle yield in response to increasing demand for poultry meat (Petracci and Cavani, 2012; Zuidhof et al., 2014; Petracci et al., 2015). However, this intensified selective breeding has led to an increase in production-related diseases, particularly wooden breast (WB) myopathy (Sihvo et al., 2014; Petracci et al., 2019). This condition predominantly affects the *pectoralis major* muscle in broiler chickens. WB myopathy results in firm, woody-like breast muscles, negatively affecting meat quality, animal welfare, and economic viability (Sihvo et al., 2014; Mudalal et al., 2015; Velleman, 2015; Velleman et al., 2019; Sanden et al., 2021).

Wooden breast is characterized by skeletal muscle fibrosis, necrosis, and multifocal degeneration of muscle tissue previously demonstrated both by us (Wold et al., 2017; Sanden et al., 2021; Pejšková et al., 2023) and others (Sihvo et al., 2014; Velleman and Clark, 2015; Soglia et al., 2016). Furthermore, the infiltration of inflammatory cells, muscle fiber myodegeneration with partial regeneration, reduced angiogenesis, and adipose infiltrations have also been demonstrated (Mutryn et al., 2015; Papah et al., 2017; Hosotani et al., 2020). The etiology of WB is still not completely identified, but hypoxia and oxidative stress are suggested as two major contributors to its onset (Hosotani et al., 2020; Bordini et al., 2024). Other mechanisms relevant to the onset and progression of WB include dysregulation of energy metabolism, mitochondrial, dysfunction, and a profound change in extracellular matrix composition (Hosotani et al., 2020; Young and Rasmussen, 2020).

Skeletal muscle satellite cells (MuSCs), also known as muscle stem cells, located between the basement membrane and the myofiber plasma membrane, are the primary contributors to postnatal growth, maintenance, and skeletal muscle regeneration (Ganassi et al., 2022; Careccia et al., 2024). MuSCs remain quiescent under normal conditions, interacting closely with myofibers and potentially with endothelial cells (Christov et al., 2007; Chakkalakal et al., 2012; Yin et al., 2013). In response to various stimuli and injuries, MuSCs become activated, proliferate, and differentiate, thus contributing to muscle tissue formation (Motohashi and Asakura, 2014; Mashinchian et al., 2018). The typical process of muscle fiber regeneration involves several sequential steps: initial inflammation accompanied by the removal of necrotic tissue, subsequent angiogenesis to re-establish blood flow, activation of MuSCs, migration and proliferation to the injured area, maturation of myotubes, and eventually innervation, leading to the formation of fully functional new muscle fibers (Tidball, 2011).

Myogenesis is regulated by a series of transcription factors, including Paired box 7 (*PAX7*), which is expressed in quiescent, activated, and proliferating MuSCs; myogenic factor 5 (*MYF5*), whose expression overlaps with PAX7 at the mRNA levels; and myogenic determination protein 1 homolog (*MYOD1*), which is expressed immediately after activation and continues through myotube formation (Zammit et al., 2006; Careccia et al., 2024). Once the cells progress through differentiation, other myogenic transcription factors, such as myogenin (*MYOG*) and different isoforms of skeletal muscle-specific myosin heavy chain 1B (*MyH1B*), are upregulated (Olguín and Pisconti, 2012; Careccia et al., 2024).

Regenerative mechanisms have been suggested to be impaired in chickens affected by WB syndrome (Velleman, 2015; Velleman, 2023), and modern commercial chickens experience decreased regeneration of damaged myofibers due to reduced MuSC myogenic activity in the *pectoralis major* muscle (Xu and Velleman, 2023). We have recently shown that the affected WB phenotype is characterized by more than 4,000 upregulated genes compared with the non-affected phenotype, as well as extensive extracellular matrix (ECM) remodeling, increased matrix metalloproteinase (MMP) activity, and altered expression and shedding levels of the syndecan protein family of four members (SDC1–4) (Pejšková et al., 2023).

SDCs are type I transmembrane proteins modified with glycosaminoglycan (GAG) chains, predominantly heparan sulfate, which play a pivotal role in mediating cell–cell and cell–matrix interactions (Couchman, 2010). Their cytoplasmic domains activate signaling pathways that regulate various cellular and transcriptional functions. As co-receptors, SDCs collaborate with integrins, growth factors, and other signaling molecules, influencing diverse biological processes such as cell adhesion, proliferation, differentiation, and ECM assembly (Afratis et al., 2017).

Moreover, SDCs are regulators of skeletal muscle growth and tissue repair (Pisconti et al., 2012; Rønning et al., 2015; Pisconti et al., 2016; Rønning et al., 2020; Jones et al., 2022; Sztretye et al., 2023), inflammation, and tumor progression, emphasizing their multifaceted roles in cellular processes (Xian et al., 2009; Gopal, 2020). All SDCs are expressed in MuSCs, and it has been shown that the activation of MuSCs occurs in an SDC-dependent manner in mice (Pisconti et al., 2012; Pisconti et al., 2016; De Micheli et al., 2020). This finding is also in accordance with studies in chickens addressing SDC4 (Velleman and Song, 2017). In the context of WB, a noteworthy aspect of SDCs lies in their regulatory mechanisms, involving the shedding of their ectodomains through various sheddases, including MMP2 and MMP9 (Manon-Jensen et al., 2013; Pejšková et al., 2023). We have recently identified the shedding of SDCs and increased SDC4 gene expression *in vivo* to be involved in WB pathogenesis (Pejšková et al., 2023).

The present study aimed to characterize metabolic changes and muscle fibers in WB-affected chickens compared with non-affected chickens. Furthermore, we investigated the proliferation and

differentiation potential of MuSCs isolated from normal and WB-affected chickens and their connection with SDC4 and its shedding.

2 Materials and methods

2.1 Animal handling and sampling

A total of 60 samples of breast muscle *(Pectoralis major)* were acquired from male Ross 308 broiler chickens (*Gallus Gallus*) at 36 days post-hatching (Pejšková et al., 2023). These chickens were raised with *ad libitum* access to a pelleted wheat/maize diet from the 10th day of age, housed in pens of dimensions 2.4 × 0.95 m with wood shavings, exposed to a lighting regimen of 6 h of light and 18 h of darkness, and subjected to a gradually decreasing temperature from 28°C to 21°C. The sampling procedure involved initial palpation-based sorting, followed by classification using histological methods and near-infrared (NIR) spectroscopy in combination with RNA-seq analysis. In our previous investigation (Pejšková et al., 2023), the samples showed a clear separation between birds with pronounced signs of fibrosis and collagen infiltration (hereafter termed "affected") those with fewer signs (hereafter termed "non-affected").

Muscle tissue specimens were obtained post-mortem from the breed chickens at NMBU, Norway. Given their conformity to established regulatory norms in food production, obtaining approval from the Regional Ethics Committee (REC) or the Norwegian Centre for Research Data (NSD) was deemed unnecessary. In accordance with Norwegian legislation governing the experimental use of animals (FOR-2015-06-18-761 §2a), ethical clearance is not obligatory for sample collection from animals slaughtered or utilized in non-experimental agricultural and aquacultural activities. This exemption was corroborated through direct correspondence with the Norwegian food safety authority, Mattilsynet.

2.2 *In vivo* tissue sample preparation and *in vitro* satellite cell isolation

In vivo tissue samples were prepared as described previously by Pejšková et al., 2023. Samples for RT-qPCR, RNA-seq, and proteomics were collected immediately after slaughter, snap-frozen in liquid nitrogen, and stored at −80°C until further analysis. For the microscopy immunofluorescence analysis, pieces of approximately 8 mm × 8 mm × 2 mm were cut from the outer layer in the upper part of the *pectoralis major* for all the animals after slaughtering, fixed in IHC Zinc Fixative (#550523, BD Pharmingen, New Jersey, USA) for 24 h before dehydrating and paraffin embedding. All animals were first sorted by palpation and then classified by histology and NIR spectroscopy (Pejšková et al., 2023) (hereafter termed NA (non-affected) and A (affected)).

Chicken primary muscle satellite cells (hereafter termed MuSCs) were isolated from biopsies collected from breast muscle (*pectoralis major*) obtained from the chicken sample groups described above or from breast fillet samples with or without WB from Ross 308 of the same age collected at the industrial abattoir and classified as non-affected or affected by NIR and histology (Nortura AS, Hærland, Norway). Tissue samples (2–5 g) were kept in PBS with 0.5% penicillin/streptomycin (10,000 units/mL) and 0.5% Fungizone before being minced using a knife on Petri dishes, and the resulting minced pieces of meat were transferred to tubes containing 10 mL collagenase (#C2674, Sigma-Aldrich) solution, followed by a 1-h incubation at 37°C with agitation at 70 rpm in a water bath. After a brief centrifugation at 550 RCF for 10 s, the supernatant was filtered using a 100-µm strainer and transferred to a new tube containing 10% fetal bovine serum (FBS). The tissue was further digested using 0.05% trypsin/EDTA for 1 h/70 rpm in a 37°C water bath, followed by 10% FBS addition for enzyme inactivation. The cell suspension was centrifuged, and the supernatant was again filtered using the strainer. Cells from both pellets were pooled and re-suspended in 3 mL of cell growth medium (DMEM 1X (#41965-047, Thermo Fisher Scientific, MA, USA), 20% chicken serum, 2% chicken embryo extract (#ICNA092850145, MP Biomedicals, CA, United States), 2% Ultroser™ G serum substitute (#15950-017, Sartorius AG, Germany), 0.5% penicillin/streptomycin (10,000 units/mL), and 0.5% Fungizone) and plated on uncoated 25-cm^2 flasks. For the removal of the fast-adhering fibroblast cells from the primary muscle cells, the cells were placed in uncoated cell flasks for 1 h at 37°C. The non-adhering MuSCs were then collected and further seeded in 25-cm^2 flasks coated with 3 µL/cm^2 entactin-collagen IV-laminin (ECL, 1 mg/mL, Millipore, Billerica, MA, USA). Cell culture media was changed every 48 h during the cell culture process. The isolated cells were proliferated, split into 75 cm^2 or 175 cm^2 coated culture flasks, and then stored in liquid nitrogen in a growth medium containing DMSO until further use. All experiments were performed at the 3rd, 4th, or 5th passage.

Following the isolation of primary chicken cell lines, the growth medium was transitioned from DMEM 1x supplemented with 20% chicken serum, 2% chicken embryo extract, 2% Ultroser™ G serum substitute, 0.5% penicillin/streptomycin (10,000 units/mL), and 0.5% Fungizone to DMEM 1x containing 10% FBS, 2% Ultroser™ G serum substitute, 0.5% penicillin/streptomycin (10,000 units/mL), and 0.5% Fungizone for experimental purposes. Cell counting was performed using the automated cell counter NucleoCounter® NC-202™ (ChemoMetec A/S, Lillerød, Denmark). The cells were seeded on ECL-coated 96-well plates with a concentration of 2000 cells/well for the proliferation assay and 25,000 cells/well for the differentiation assay. Using Incucyte SX3/SX1 (Sartorius AG, Germany), the cells were monitored for 7 days in the case of proliferation in the incubator at 37°C and 5% CO_2. The differentiation experiment was induced by a complete medium without FBS serum and Ultroser G in 85%–100% confluence after 1 day of proliferation and monitored for another 2 days.

2.3 Inhibition and transfection of MuSCs

MuSCs from both affected and non-affected groups (n = 3 each) were seeded at a density of 2000 cells per well in 96-well plates or 48,000 cells per well in 6-well plates. For the inhibition experiments, cells at 50% confluence were treated with inhibitors targeting the MEK/ERK pathway (#PD0325901, N-[(2R)-2,3-dihydroxypropoxy]-3,4-difluoro-2-[(2-fluoro-4-iodophenyl) amino]-benzamide, STEMCELL Technologies) and p38 MAPK pathway (#SB202190, 4-[4-(4-

TABLE 1 Custom-made blocking peptides and their solvents.

Name	Sequence	Solvent
BP1	MPLPRAAFLLGLLLAAAAAESVRETETMDA	3% NH_3
BP2	ETETMDARWLDNVGSGDLPDDEDIGEFTPH	H_2O
BP3	FTPHLTSDEFDIDDTSGSGDYSDY	DMSO
BP4	YSDYDDAIYLTTVDTPAISDNYIPGDTERK	H_2O
BP5	PGDTERKMEGEKKNTMLDNEIIPDKASPVE	H_2O

fluorophenyl)-5-(4-pyridinyl)-1H-imidazol-2-yl]-phenol, STEMCELL Technologies). Each inhibitor was dissolved in DMSO and administered to the well to reach a concentration of 25 µM.

MuSCs were transfected with chicken SDC4 (in pCEP4, UniProt #P49416, custom-made by GenScript Corp.) at 50% confluence using the Lipofectamine 3000 Transfection Kit (#L3000-008, Thermo Fisher Scientific) following the manufacturer's protocol. To assess transfection efficiency, pEGFP-N1 (GenScript Corp.) was used as a readout, with 2.5 µg of DNA used per well. MuSCs were transfected for 24 h before lysis or treatment with blocking peptides. Blocking peptide (BP) sequences, corresponding to the ectodomain of chicken SDC4 protein (custom-made by GenScript Corp.), with underlined overlapping sequences and different solvents are provided in Table 1. BPs were used at a concentration of 2.5 µM for 2 h during the treatment of proliferating MuSCs.

2.4 Reverse transcription-quantitative PCR and RNA sequencing

RT-qPCR: the total RNA for RT-qPCR was isolated from tissue lysate (n = 8 in each group) or proliferating MuSCs (n = 8 in each group) using the RNeasy Mini Kit (#74104, QIAGEN, Germany) according to the manufacturer's instructions.

The total RNA from tissue was prepared from approximately 100 mg of tissue by homogenization in the RLT buffer containing 2 mM DTT using the Precellys Lysing Kit (#P000911-LYSKO-A.0, Bertin Technologies, France), 4 × 20 at 6000 rpm with 10 break between shakes, followed by a 10-min spin at 5000 g. Samples were incubated with Proteinase K (#19131, QIAGEN, Germany) according to the manufacturer's instructions. cDNA was generated from 2 µg of total RNA using TaqMan Reverse Transcription Reagents (#N8080234, Thermo Fisher Scientific, MA, United States) in a 40 µL reaction volume with random hexamers according to the manufacturer's protocol.

Proliferating MuSCs (n = 8 in each group) were seeded in a 6-well plate at 12,000 cells/well and allowed to proliferate for 3 days; after washing twice, 350 µL of the RLT buffer containing 2 mM DTT was added. cDNA was generated from 290 ng of total RNA using the LunaScript RT SuperMix Kit (#E3010L, New England Biolabs, MA, USA) in a 30 µL reaction volume with random hexamers according to the manufacturer's protocol. RT-qPCR analysis was carried out using the Luna Universal probe RT-qPCR Master Mix (#M3004X, New England Biolabs, MA, USA) and QuantStudio 5 (Applied Biosystems, Foster City, CA, USA) PCR System. The amplification protocol was initiated at 95°C for 1 min by initial denaturation, followed 40 cycles of denaturation at 95°C for 15 s and then extension at 60°C for 30 s.

TABLE 2 Gene target and TaqMan® primer/probe assays.

Gene target	TaqMan® primer/probe assays
EEF2	Gg03339740_m1
Mki67	Gg07186598_s1
CDKN2A	Gg07157676_m1
CDKN1A	Gg03814244_s1
MYOG	Gg03363788_m1
MYOD1	Gg03363970_m1
SDC1	Gg07175697_s1
SDC2	Gg03345644_m1
SDC3	Gg03339851_m1
SDC4	Gg03370419_m1
PAX7	Gg03348488_m1

RT-qPCR analyses were performed with three technical replicates from each sample. The relative gene expression was calculated using the comparative $2^{-\Delta Ct}$ (Schmittgen and Livak, 2008; Bustin et al., 2010) method for the tissue and cell culture experiments comparing non-affected vs. affected samples. Non-affected MuSCs transfected with SDC4 were additionally analyzed and compared to the control using the $2^{-\Delta\Delta Ct}$ method. In short, the values are generated by subtracting reference gene EEF2 values for each sample to obtain ΔCt values, and for ΔΔCt values, the values were related to the average gene expression of the untransfected control (Lipofectamine, MuSCs) for each gene. The relative gene expression is then calculated using formula $2^{-\Delta Ct}$ or $2^{-\Delta\Delta Ct}$ in the case of non-affected MuSC transfection. All TaqMan® primers and probes are listed in Table 2.

RNAseq: total RNA was extracted from muscle tissue samples stored at −80°C using the RNAdvance Tissue Kit (Beckman Coulter, IN, USA) following the manufacturer's guidelines. A NanoDrop Spectrophotometer (Thermo Fisher Scientific, MA, United States) was utilized to assess RNA purity and concentration of all samples, while the integrity of nine randomly selected samples was evaluated using a 4150 TapeStation RNA Screen Tape (Agilent, CA, United States). Extracted RNA (1.5–4.5 µg) was subsequently dispatched to a commercial sequencing provider (Novogene, United Kingdom), where quality reassessment confirmed the lowest RNA Integrity Number (RIN) to be 9.1. Sequencing libraries were prepared using NEBNext Ultra Directional RNA Library Prep Kits (NEB, MA, United States) and subjected to PE150 sequencing on NovoSeq 6000 instruments with S4 flow cells (Illumina, CA, United States). Quality control of reads was performed using FastQC (Andrews, 2010), and raw reads underwent trimming with fastp (Chen et al., 2018) to eliminate adapter sequences. Gene expression levels were determined by quantifying transcript expression with Salmon (Patro et al., 2017) using the GRCg7b reference genome from NCBI, and the data were summarized at the gene level. DESeq2 (Love et al., 2014) facilitated the analysis of differentially expressed genes between affected and

normal groups. The R package clusterProfiler (Yu et al., 2012; Wu et al., 2021) was employed to estimate Gene Ontology (GO) and Kyoto Encyclopedia of Genes and Genomes (KEGG) pathway enrichment for upregulated and downregulated gene sets separately.

For RNAseq of MuSCs (n = 19), RNA was extracted using the RNeasy Mini Kit and sent to Novogene for library preparation and sequencing. At Novogene, messenger RNA was purified from total RNA using poly-T oligo-attached magnetic beads. After fragmentation, the first-strand cDNA was synthesized using random hexamer primers, followed by the second-strand cDNA synthesis. The library was ready after the end repair, A-tailing, adapter ligation, size selection, amplification, and purification. The library was quantified using Qubit and real-time PCR, and size distribution was detected using a bioanalyzer . The quantified libraries were pooled and sequenced on an Illumina NovoSeq 6000 instrument. Sequencing QC was performed using FastQC v0.12.1 (Andrews, 2023), Trim Galore v0.6.7 (Krueger et al., 2021), and Cutadapt v3.4 (Martin, 2011). Reads were mapped to the GRCg7b version of the *Gallus* reference genome using STAR v2.7.9a (Dobin et al., 2013). Alignments were converted to BAM format and sorted using SAMtools v1.17 (Li et al., 2009). Transcript expression was then quantified with Salmon v1.10.1 (Patro et al., 2017) and converted to gene-level counts with Tximport v1.12.0 (Soneson et al., 2015). Differential expression analysis comparing the affected and not affected groups was next performed using the nf-core differential abundance pipeline v1.4.0 (Cristina Tuñí i Domínguez et al., 2023), with read count normalization and statistical analysis performed using DESeq2 v1.34.0 (Love et al., 2014). Initial exploratory analysis showed that two samples from the "not affected" group were statistical outliers based on the median absolute deviation of their normalized read counts, and these samples were excluded from further analysis. This left nine remaining samples in the not affected group and 10 samples in the affected group. The results of the differential expression analysis were visualized using the Enhanced Volcano R package v1.20.0 (Blighe and Lun, 2018).

Gene Set Enrichment Analysis (GSEA) was performed with the ClusterProfiler R package v4.10.1 (Yu et al., 2012; Wu et al., 2021) using the FGSEA algorithm (Korotkevich et al., 2016). Log2 fold-change scores were used to rank genes, and the results were visualized using the enrichplot package v1.22.0 (Wu et al., 2021). Network analysis was performed to find genes with correlated expression levels with WGCNA v.1.72.5 (Langfelder and Horvath, 2008) using normalized and variance-stabilized read counts and a soft-thresholding power value of 10. The genes present in selected modules were then subject to functional overrepresentation analysis (ORA) using ClusterProfiler v4.10.1. For the ORA, the background gene list was defined as the set of genes used in the differential expression analysis that also possessed relevant functional annotations.

2.5 Western blotting

Proliferating MuSCs were seeded at a concentration of 30,000 cells per well in a 6-well plate and allowed to proliferate for 3 days; after washing twice with PBS, the cells were lysed with 100 µL of RIPA buffer containing a phosphatase inhibitor cocktail 2 (#P5726, Sigma-Aldrich, Merck) and AEBSF protease inhibitor (#78431, Thermo Scientific, United States) for 30 min on ice. Samples were centrifuged at 13.000× g for 30 min at 4°C. The supernatant, containing soluble proteins, was collected and stored at −80°C until analysis. The protein concentration was determined using the Micro BCA Protein Assay Kit (#PIER23235, Thermo Fisher Scientific, Waltham, MA, USA).

Samples were prepared by mixing with 4x sample buffer, consisting of 5 g sucrose (#16104, Sigma Merck, Darmstadt, Germany), 3.75 mL 20% SDS (L3771, Sigma Merck), 1.25 mL 0.5 M Tris-HCl (pH 6.8) (T5941, Sigma Merck), 310 mg DTT (D9779, Sigma Merck), 1 mL of 0.1% bromophenol blue (B5525, Sigma Merck), and 10 mL of MQ H_2O and boiling for 5 min at 95°C. In addition, 10 µg/µL of proteins were loaded onto a 4%–15% Criterion TGX Precast Gel (#5671084, Bio-Rad, Hercules, CA, United States). Precision Plus Protein All Blue Standards (#1610373, Bio-Rad) and Precision Plus Protein Dual Color Standards (#1610374, Bio-Rad) were used as standard molecular weights. The gels were blotted onto PVDF Western blotting membranes (#03010040001, Sigma Merck) with extra thick blot filter paper, precut (#1703967, Bio-Rad), using the Trans-Blot Turbo system (Bio-Rad). After transfer to membranes, the membranes were rinsed in ddH_2O, and the water was discarded. The membranes were then incubated in 10 mL of Revert 700 Total Protein Stain solution (cat# 926-11021, LI-COR, Lincoln, NE, United States) for 5 min with gentle shaking. The Total Protein Stain Solution was then decanted completely, and the membranes were rinsed two times for 30 s with 10 mL of wash solution (6.7% glacial acetic acid and 30% methanol in water). The membranes were imaged immediately in the 700 nm (IR700) channel with Azure 600 (Azure Biosystems, Redmond, WA, United States). After imaging, the membranes were washed for 15 min in 1x TBS-T to remove the turquoise color from the stain. The PVDF membranes were blocked in 1% casein (Western Blocking Reagent, #11921681001, Sigma Merck) and TBS-T for 60 min at room temperature (RT), followed by incubation with primary antibodies such as SDC1–4 (1:1,000, custom-made, GenScript, Piscataway, NN, United States), p38 (M138) (1:1,000, #ab31828, Abcam, United Kingdom), Phospho-p38 MAPK(Thr180/Tyr182) (1:1,000, #9211, Cell Signaling, MA, USA), p44/42 MAPK (Erk1/2) (1:1,000, #4695, Cell Signaling), or Phospho-p44/42 MAPK (Erk1/2) (Thr202/Tyr204) (1:1,000, #9101, Cell Signaling) overnight at 4°C. Membranes were washed three times for 10 min each in TBS-T before being incubated with horseradish-peroxidase-conjugated secondary antibodies (anti-mouse IgG, NA931V, or anti-rabbit, NA934V, both from Cytiva, Marlborough, MA, USA) diluted 1:3,000 in TBS-T, goat anti-rabbit IgG and goat anti-mouse IgG secondary antibodies, HRP-conjugated (1:5000, #31460, #31430, Invitrogen), followed by three additional times 10-min washes in TBS-T. Blots were developed using ECL Prime (#RPN2236, GE Healthcare, IL, United States) or SuperSignal West Pico PLUS Chemiluminescent Substrate (#34577, Thermo Fisher Scientific, MA, United States) for chemiluminescence signal detection. The chemiluminescence signals were detected using Azure 600 (CA, United States) or iBright™ CL1500 Imaging System (Invitrogen). The membranes were reprobed with reference protein anti-GAPDH (#sc-47724, Santa Cruz, CA, United States) after stripping using the Restore Western blot Stripping buffer for 5 min at RT (#21063,

Thermo Fisher Scientific, MA, United States) and washed 3 × 15 min in TBS-T before blocking. Quantification of Western bands was conducted using ImageQuant 10.2.499 (Cytiva).

2.6 Label-free quantitative mass spectrometry-based proteomics

Twelve biological replicates of each group, affected and non-affected samples, were included in the analysis. Salt-soluble proteins were extracted from approximately 100 mg chicken breast fillet using 1,000 µL of extraction buffer [10 mM Tris, pH 7.6; 1 mM EDTA; 0.25 M sucrose]. Samples were homogenized twice for 20 s at 6,000 rpm speed with a 5s pause between the homogenization steps using Precellys®24 (Bertin Technologies) and centrifuged at 16000 *g* for 15 min. The protein concentration was determined using the RC DC™ Protein Assay (#5000121, Bio-Rad Laboratories, Inc, United States). A measure of 60 µg of proteins was reduced with 0.1 M DTT, alkylated with 55 mM 2-iodoacetamide, and digested with trypsin/Lys-C (#V5071, Promega, United States) at a 1:30 (w/w) enzyme-to-protein ratio on a Microcon-10 YM (Merck Millipore, United States) centrifugal filter unit at 37°C overnight. The peptide concentration was measured using the NanoDrop One at 205 nm, and 10 µg of peptides were purified and concentrated using a StageTip following the protocols (Rappsilber et al., 2007; Yu et al., 2014). Peptides were resolved with a loading buffer [2% (v/v) ACN; 0.05% (v/v) trifluoroacetic acid], and 1 µg of peptides was analyzed using a nano-UHPLC coupled with a Q Exactive Quadrupole-Orbitrap Mass Spectrometer (Thermo Fisher Scientific, United States) at the MS/Proteomics Core Facility at Campus Ås. Detailed liquid chromatography-tandem mass spectrometry (LC-MS/MS) settings can be found in Koga et al. (2019). Peptides from the 12 most intense peaks obtained during the 120-min elution were fragmented, and the mass-to-charge ratios of these fragmented ions were measured (MS/MS). Mass spectral data were processed using MaxQuant version 2.3.1.0 (Cox and Mann, 2008). The parameters for protein identification included trypsin/Lys-C specificity with reference to the proteome database for broiler chicken, *Gallus gallus* (Entry nr. UP000000539), downloaded from UniProt (43710 entries). Other parameters were maintained as defaults, and the label-free quantification (LFQ) algorithm was employed for protein quantification. LFQ intensity values from MaxQuant were imported into Perseus software version 2.0.6.0 (Tyanova et al., 2016) for statistical analysis and visualization of the data. Prior to analysis, proteins identified only by site, reverse sequence, and potential contaminant proteins were excluded. LFQ intensities were log2-transformed, and proteins possessing valid LFQ intensity values in more than 70% of biological replicates for at least one of the groups (non-affected and affected) were retained for further analyses. Welch's T-tests, with a 95% confidence limit taking the false discovery rate (FDR) into account, were carried out for all identified proteins between non-affected and affected chicken groups. GO enrichment analyses were carried out for the significantly differentially expressed proteins with g:GOSt on the online g:Profiler platform (Kolberg et al., 2023) with the following data sources: GO terms biological processes (GO: BP), KEGG, and Human Phenotype Ontology (HPO). Gene names for the four proteins were unknown, and therefore, they were omitted from the GO enrichment analysis. Ensemble IDs with the most GO annotations were selected for three proteins (gene names: *RBP4*, *TTR*, and *ACTG1*). Moreover, missing values for LFQ intensities were imputed from a normal distribution (default setting of width 0.3 and downshift 1.8) in Perseus, and principal component analyses were carried out using MATLAB 2022b (The MathWorks, Inc, Natick, MA, USA).

2.7 Immunohistochemistry and immunofluorescence

The histology scoring of the samples used in this research was performed by staining with hematoxylin and eosin (H&E) according to standard procedures and previously described in Pejšková et al., 2023. To perform immunofluorescence analyses, tissue sections of affected and non-affected WB samples (N = 8–11 for each group) were deparaffinized, rehydrated with xylene, followed by gradually decreasing ethanol concentration (100%, 95%, 70%, and 50%) and ddH_2O (Milli-Q), and then washed once with PBS pH 7.4 for 3 min. Sections were permeabilized at RT with 0.5% Triton X-100 (#X100, Sigma-Aldrich, Merck) in PBS (PBS-T) for 10 min and then washed twice in PBS-T pH 7.4 for 5 min each. For muscle morphometry, sections were incubated with DAPI (4′,6-diamidino-2-phenylindole dihydrochloride) (#D1306, 2 mg/mL, Invitrogen, MA, USA), wheat germ agglutinin, and Alexa Fluor™ 555 Conjugated (#W32464, 1:1000, Thermo Fisher Scientific, MA, United States), diluted in PBS for 10 min, and washed with PBS for 5 min. For immunostaining, antigen retrieval was performed with sodium citrate buffer (10 mM sodium citrate, 0.05% Tween 20, and pH 6.0), prepared fresh on the day of use. Sections were incubated in pre-warmed sodium citrate buffer at 65°C for 10 min using a water bath (Fisher Scientific, Isotemp®, GPD 10, MA, United States) and plastic Coplin jars. Next, the coplin jars containing the slides were allowed to cool down to RT on the bench for at least 20 min. Sections were then briefly rinsed with ddH_2O, then washed three times with PBS for 5 min each, blocked in 5% BSA in PBS at RT for 1 h, and then incubated in AffiniPure Fab Fragment goat anti-mouse IgG (H + L) (#115-007-003, 1:100, Jackson ImmunoResearch, PA, USA) diluted in PBS at RT for 30 min. Sections were then incubated overnight at 4°C in a humidified chamber with anti-PAX7 mouse antibody (PAX7-b, AB 528428, 1:100, DSHB, IA, USA) and anti-PCNA rabbit antibody (CPTC-PCNA-3, AB 2888965, 1:25, DSHB, IA, USA) and diluted in 5% BSA in PBS. The following day, the sections were washed with 0.1% Triton-X-100 in PBS for 5 min and washed once with PBS for 5 min before incubation with Alexa Fluor™ 488 goat anti-mouse IgG1 (#A-21121, #A-10667, 1:400, Invitrogen, MA, United States) and Alexa Fluor™ 555 donkey anti-rabbit IgG (H + L) (#A-31572, 1:400, Invitrogen, MA, United States) or Alexa Fluor™ 555 donkey anti-mouse IgG (H + L) (#A-21426 1:400, Invitrogen, MA, United States) diluted in 5% BSA or 0.1% blocking buffer in PBS at RT for 1 h. Sections were then washed with 0.1% Triton-X-100 in PBS for 5 min before being stained with DAPI (4′,6-diamidino-2-phenylindole dihydrochloride) (#D1306, 2 µM, Invitrogen, MA, United States) or NucBlue Live Cell Stain Ready Probe (Hoechst 33342, Invitrogen, MA, United States) diluted in PBS for 10 min, then washed two more times in PBS for 5 min, before incubating with TrueBlack® Plus to quench autofluorescence (#23014, 1:40,

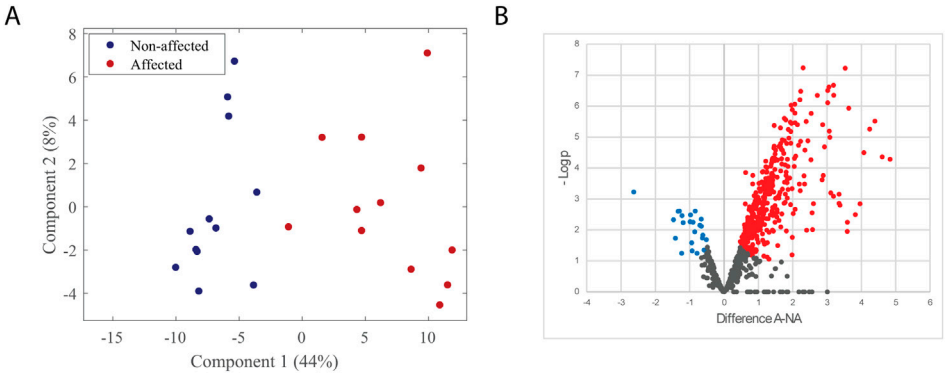

C

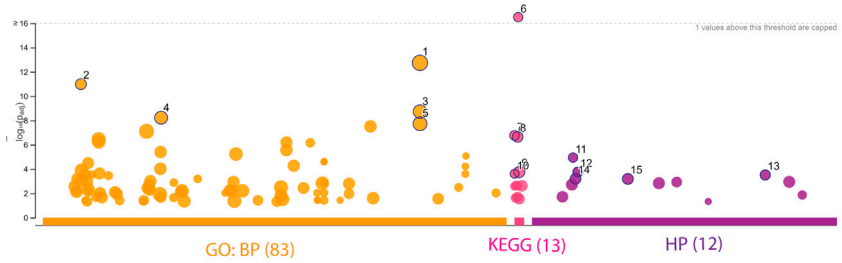

ID	Sour...	Term ...	Term Na...	p_{adj} (query...
1	GO:BP	GO:1901564	organonitrogen compound metabolic process	1.818×10^{-13}
2	GO:BP	GO:0006457	protein folding	1.032×10^{-11}
3	GO:BP	GO:1901565	organonitrogen compound catabolic process	1.877×10^{-9}
4	GO:BP	GO:0030163	protein catabolic process	5.983×10^{-9}
5	GO:BP	GO:1901575	organic substance catabolic process	1.856×10^{-8}
6	KEGG	KEGG:03050	Proteasome	5.692×10^{-23}
7	KEGG	KEGG:00010	Glycolysis / Gluconeogenesis	1.716×10^{-7}
8	KEGG	KEGG:01200	Carbon metabolism	2.248×10^{-7}
9	KEGG	KEGG:04141	Protein processing in endoplasmic reticulum	1.768×10^{-4}
10	KEGG	KEGG:00030	Pentose phosphate pathway	2.446×10^{-4}
11	HP	HP:0003327	Axial muscle weakness	1.144×10^{-5}
12	HP	HP:0003803	Type 1 muscle fiber predominance	1.742×10^{-4}
13	HP	HP:0033684	Abnormal muscle fiber-type distribution	3.075×10^{-4}
14	HP	HP:0003557	Increased variability in muscle fiber diameter	6.352×10^{-4}
15	HP	HP:0009027	Foot dorsiflexor weakness	6.511×10^{-4}

D

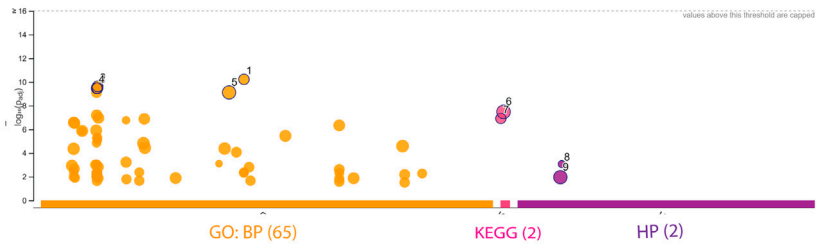

ID	Sour...	Term ...	Term Na...	p_{adj} (query...
1	GO:BP	GO:0046034	ATP metabolic process	6.016×10^{-11}
2	GO:BP	GO:0009205	purine ribonucleoside triphosphate metabolic pro...	2.376×10^{-10}
3	GO:BP	GO:0009199	ribonucleoside triphosphate metabolic process	3.359×10^{-10}
4	GO:BP	GO:0009144	purine nucleoside triphosphate metabolic process	3.359×10^{-10}
5	GO:BP	GO:0044281	small molecule metabolic process	7.660×10^{-10}
6	KEGG	KEGG:01100	Metabolic pathways	3.359×10^{-8}
7	KEGG	KEGG:00190	Oxidative phosphorylation	1.218×10^{-7}
8	HP	HP:0003756	Skeletal myopathy	8.604×10^{-4}
9	HP	HP:0003593	Infantile onset	1.093×10^{-2}

FIGURE 1
Mass spectrometry-based proteomic analysis of salt-soluble proteins. **(A)** Score plot from the PCA analysis of affected (red; A) and non-affected (blue; NA) samples. **(B)** Volcano plot of fold change (LFQ intensity) in 12 biological replicates for significantly regulated proteins. The plot is represented as a function of statistical significance (Welch's *t*-test) between affected (A) and non-affected (NA) samples. *X*- and *Y*-axes show protein ratio (log2 change) in A and NA samples and *p*-value (–log10), respectively. Each dot represents one protein. Significantly upregulated and downregulated proteins in A samples were colored red and blue, respectively. The false discovery rate and S0 parameters were set to 0.05 and 0.1, respectively. g: GOSt Manhattan plot of upregulated **(C)** and downregulated **(D)** proteins. The *x*-axis shows the GO functional terms colored by data source (Gene Ontology: biological
(*Continued*)

FIGURE 1 (Continued)
process, GO: BP; Kyoto Encyclopedia of Genes and Genomes, KEGG; Human Phenotype Ontology, HPO). Each colored dot presents a GO term. The *y*-axis is the adjusted −log10 *p*-values. The GO terms with the five lowest *p*-values were highlighted with a circle and listed in the table below the Manhattan plot. *p*-values in the table are color-coded according to significant levels, light green (less insignificant) to blue (highly significant).

Biotium, CA, United States) for 1 h, and washed again in PBS for 5 min. Finally, sections were mounted with VECTASHIELD® PLUS Antifade Mounting Medium (H-1900, Vector Laboratories, CA, United States) or fluorescent mounting medium (#S3023, DAKO, Denmark) and imaged on a fluorescence digital microscope (EVOS M5000, Invitrogen, MA, United States) or fluorescence microscope (ZEISS Axio Observer Z1 microscope, Jena, Germany). Quantification of Pax7+ and PCNA + cells was conducted manually. Quantification of myofiber morphological parameters (size and central nucleation) was conducted using software SMASH (Smith and Barton, 2014).

Proliferating MuSCs were seeded at 18,000–20,000 cells/well in 12-well plates and grown on coverslips (12 mm) for 3 days. MuSC for immunostaining of differentiation experiment (n = 5 in each group) were grown on 96-well plates with seeding 10,000 cells/well, and differentiation was induced after 24 h by medium without serum and allowed to differentiate for another 2 days. MuSCs were fixed with 4% PFA for 10 min and washed 3x with PBS-tween (PBS-T), followed by permeabilization with 0.1% Triton-X-100 for 10 min. Samples were blocked in 1x blocking buffer (#ab126587, Abcam, United Kingdom) in PBS-T for 30 min. Proliferation cells were stained with primary antibodies PAX7 (1:10, PAX7-b, AB 528428, 1:100, DSHB, IA, USA), SDC4 (1:1000, GenScript), or, in the case of differentiated MuSCs, desmin (#ab8592, 1:80, Abcam, United Kingdom) prepared in 0.1% blocking buffer (#ab126587, Abcam, United Kingdom) and incubated overnight at 4°C. The next day, cells were washed twice with PBS-T and incubated with goat anti-mouse IgG, IgM, and IgA (H + L) secondary antibodies conjugated with Alexa Fluor™ 488 (1:400, #A-10667, Invitrogen, MA, United States), Alexa Fluor™ 555 donkey anti-mouse IgG (H + L) (#A-21426, 1:400, Invitrogen, MA, United States), and goat anti-rabbit IgG (H + L) cross-adsorbed secondary antibody conjugated with Alexa Fluor™ 546 (1:400, #A-10667, Invitrogen, MA, USA) and NucBlue Live Cell stain ready probe (Hoechst 33342, Invitrogen, MA, United States) for 2 h at RT. The samples were washed with PBS-T before being transferred onto a microscope slide and mounted using the fluorescent mounting medium (#S3023, DAKO, Denmark) in the case of coverslip glass samples. The slides or wells were examined by fluorescence microscopy analysis (ZEISS Axio Observer Z1 microscope, Jena, Germany), and images were contrast-adjusted using ImageJ (NIH, MD, United States).

2.8 Statistical analysis and software

For quantification of Western blots, ImageQuant TL 10.2–499 (Cytiva, GE Healthcare Life Sciences, MA, US) was used, with the background method of rolling ball (radius 2). All quantifications of the bands generated from the Western blots were displayed as the mean ± SEM (standard error of mean, n = 4–5). The statistical analyses of RT-qPCR (n = 7–8) and Western blots (n = 4–5) were performed in Graph Pad Prism version 10.4.0 (GraphPad Software, La Jolla, CA, USA), using nested *t*-test with Welch correction for RT-qPCR and *t*-test with Welch correction for Western blots. Statistical significance was considered *p*-values <0.05, as indicated in each figure. Explorative multivariate analysis by principal component analysis (PCA) was performed on proteomics data, both with and without normalization, using MATLAB 2022b (The MathWorks, Inc, Natick, MA, USA). In addition, explorative univariate analysis was conducted using Welch's *t*-test for all detected proteins.

3 Results

3.1 Characterization of metabolic changes and myogenesis in WB *in vivo*

3.1.1 WB myopathic birds show metabolic changes

Previous studies have linked the importance of energy metabolism to the onset of WB development. We, therefore, investigated the salt-soluble proteins (proteins involved in metabolism and cellular processes) of the *pectoralis major* muscle from affected (N = 12) and non-affected (N = 12) animals by label-free quantitative MS-based proteomic analysis.

In addition, 819 proteins were identified, and PCA analysis showed a clear separation between the two groups along principal component 1 according to the expression of proteins (Figure 1A). Welch's *t*-test indicated that 414 proteins were differentially expressed between groups, with 23 proteins significantly downregulated and 391 proteins significantly upregulated in the affected samples (Figure 1B). GO enrichment analyses revealed changes in proteins related to metabolic changes. The five enriched GO terms with the lowest *p*-value for upregulated and downregulated proteins are highlighted in the Manhattan plots and listed in the table (Figures 1C, D, respectively). In upregulated terms such as glycolysis, abnormal muscle fiber-type distribution, and increased variability in muscle fiber diameter. On the other hand, downregulated terms highlighted oxidative phosphorylation, skeletal myopathy, or metabolic pathways. All significantly enriched GO terms from upregulated and downregulated proteins are shown in Supplementary Tables S1, S2, respectively.

3.1.2 Muscle fibers and myogenic markers are altered in WB myopathy

Further characterization of the skeletal muscle using WGA staining confirmed extensive fibrosis in WB-affected chickens and widespread central nucleation of myofibers (Figure 2A). Interestingly, the vast majority of fibers were centrally nucleated (80%), which did not differ between groups (Figures 2A, B), indicative of active degeneration/regeneration regardless of the extent of WB pathology. In affected individuals, the muscle fibers

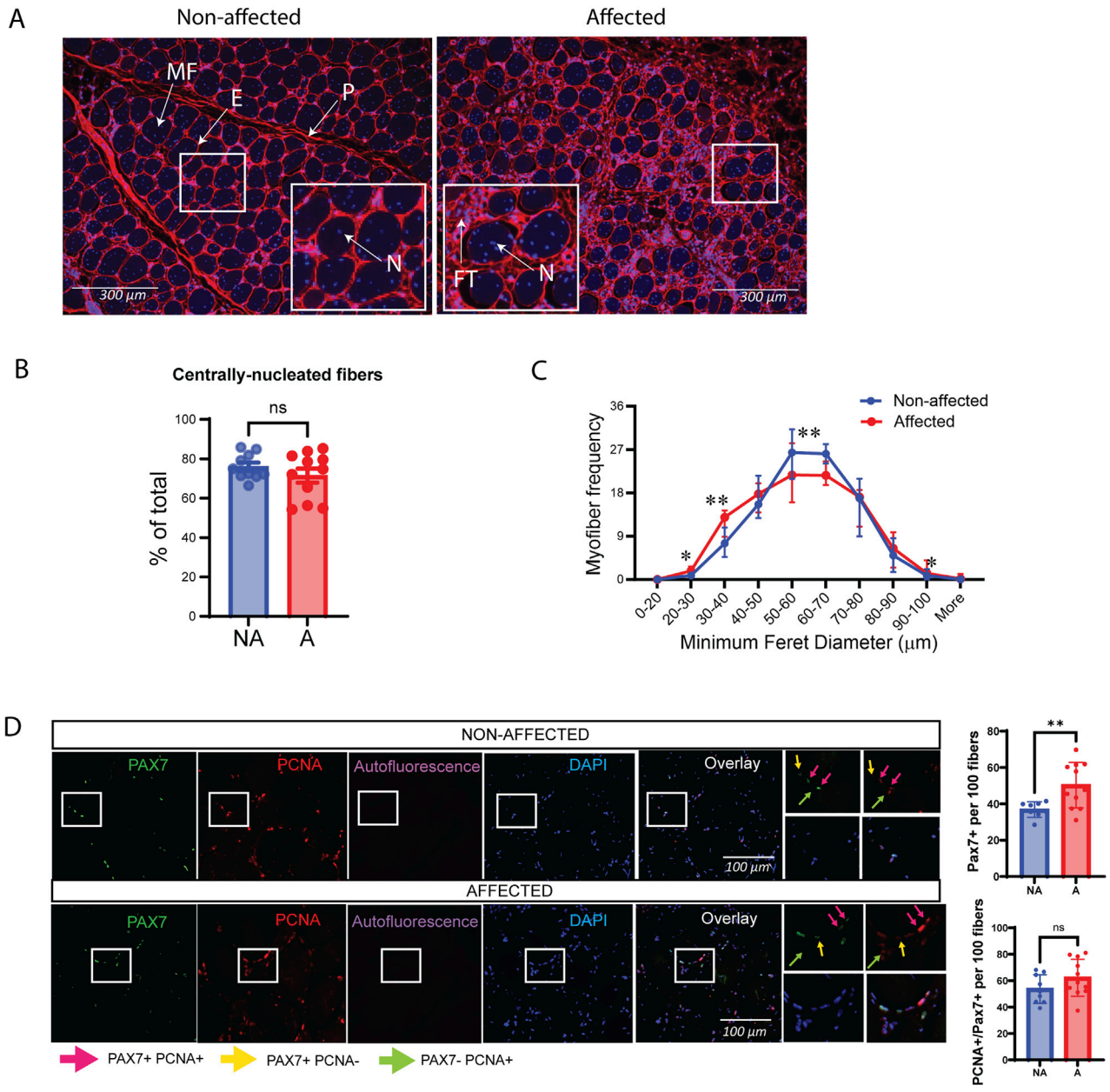

FIGURE 2
Altered muscle fiber sizes in affected chicken muscle sections and PAX7. **(A)** Representative images of DAPI (blue)/WGA (red) counterstaining of nuclei and muscle fibers in chicken muscle sections. A marked increase in WGA staining (fibrosis) is observed in affected muscle sections. Smaller fibers can also be observed in affected muscle sections by visual inspection. Magnification: ×10 with a fluorescent microscope. P, perimysium; E, endomysium; MF, muscle fiber; FT, fibrotic tissue; N, nuclei. **(B)** Bars represent quantification of centrally nucleated myofibers of affected and non-affected samples images presented in **(A)**. **(C)** Quantification of images in **(A)** show minimum Feret diameter distribution in affected and non-affected samples. **(D)** Representative images of PAX7/PCNA co-immunostaining in chicken muscle sections (left). Quantification of images shows that total PAX7 expressing satellite cells per 100 fibers are significantly increased in animals affected by WB; however, the fraction of proliferating PAX7+ cells are unchanged. A total of 10 random fields were quantified per image/animal. Pink arrows indicate PAX7+PCNA+, proliferating myoblasts. Yellow arrows indicate PAX7+PCNA-, non-proliferating myoblasts, and green arrows indicate proliferating cells that are not myoblasts (Pax7-PCNA+). Scale used was 100 µm. Significance was marked as ns > 0.05; *$p \leq 0.05$; **$p \leq 0.01$ with N = 10 affected and 11 non-affected. A; affected, NA; non-affected.

were generally smaller, as shown by a shift toward smaller minimum Feret diameters (20–40 µm). However, there was also an increase in very large fibers (90–100 µm) compared to non-affected individuals (Figure 2C).

Skeletal muscle regeneration relies on a population of locally resident MuSCs, which express the paired box transcription factor family member Paired box 7 (PAX7) (Olguín and Pisconti, 2012; Yin et al., 2013). Co-immunostaining with the proliferation marker proliferating cell nuclear antigen (PCNA) showed that, although the number of PAX7-positive satellite cells was higher in affected samples, the ratio of those that were actively proliferating (PAX7+PCNA+) was the same between affected and non-affected

10.3389/fphys.2024.1513311

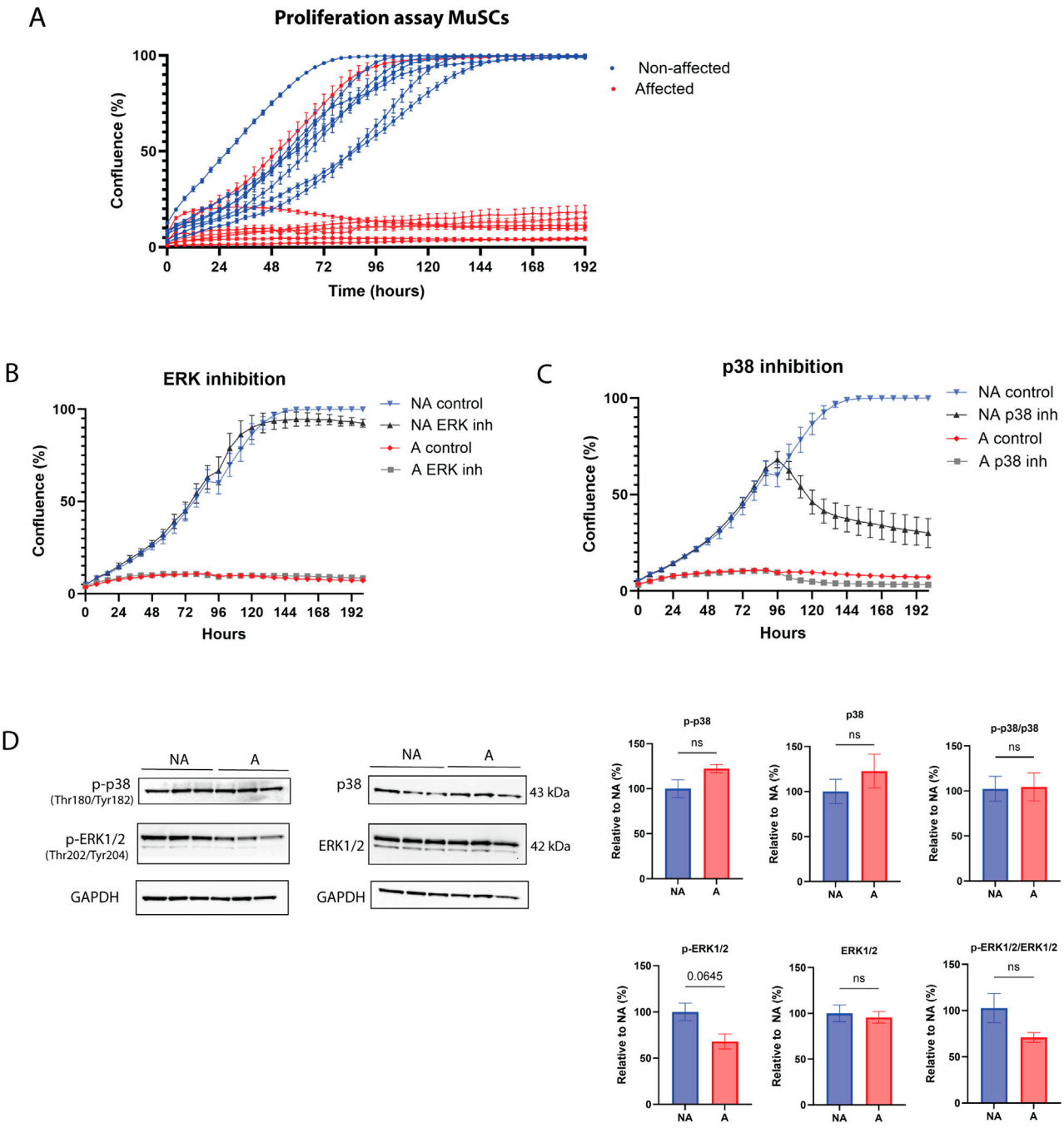

FIGURE 3
Proliferation disruption and MAPK signaling of WB MuSCs. **(A)** Incucyte S3 live cell proliferation assay (10x) of primary MuSCs isolated from affected and non-affected animals. Compared to affected cell lines (except one outlier SC cell line), all non-affected cell lines reached 100% confluence. **(B)** MuSCs treated with MEK/ERK inhibitor and **(C)** p38 inhibitor, **(D)** protein p38, ERK1/2, their phosphorylated forms, phospho (Thr180/Tyr182)-p38 and phospho (Thr202/Tyr204)-ERK1/2, and their ratios show no difference between WB affected (A) and non-affected (NA) group. Raw data for each condition (N = 3) were normalized to reference protein GAPDH and present it as a relative value to the non-affected group. Significance level was calculated by unpaired *t*-test with Welsh correction (ns, $p > 0.5$).

samples, suggesting a mild defect in MuSC proliferation *in vivo* (Figure 2D).

Consistently, RNA sequencing gene expression analysis of muscle tissue samples showed significant differences in several factors important for myogenesis in affected vs. non-affected chicken breast samples. MuSC markers Paired box3 (*PAX3*), *PAX7*, and myogenic factor 5 (*MYF5*), as well as the early myogenic differentiation marker myogenin (*MYOG*), were all upregulated in affected muscles compared with non-affected ones (Supplementary Figure S1A). Although not significant, we observed

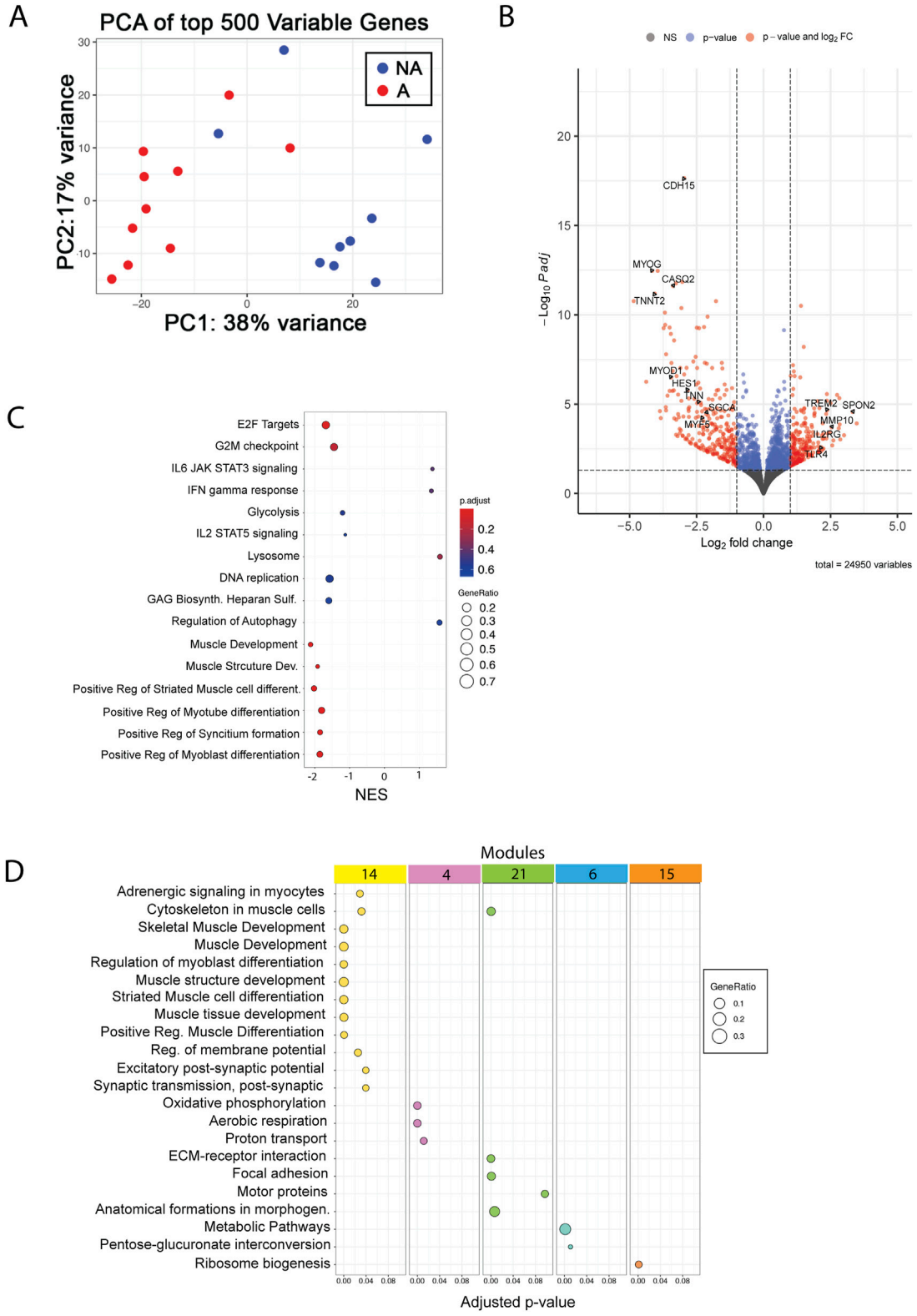

FIGURE 4
RNA-seq analysis of MuSCs. **(A)** PCA plot of top 500 variables genes between affected and non-affected chickens. A, affected; NA, non-affected **(B)** Volcano plot with selected genes showing the adjusted p-values and the log2 fold change (FC) values of genes. DEGs, indicated by the red dots, were identified as genes with an adjusted p-value of ≤ 0.05 and |log2 FC| between −1 and 1, and blue dots indicate only p-value. X-axis shows downregulation in the negative range of axis, and genes in the positive range are upregulated. **(C)** GSEA shows the top 16 pathways sorted by the normalized enrichment score, adjusted p-value (p-adjust), and gene ratio. **(D)** Functional enrichment analysis of the top five modules identified by network analysis.

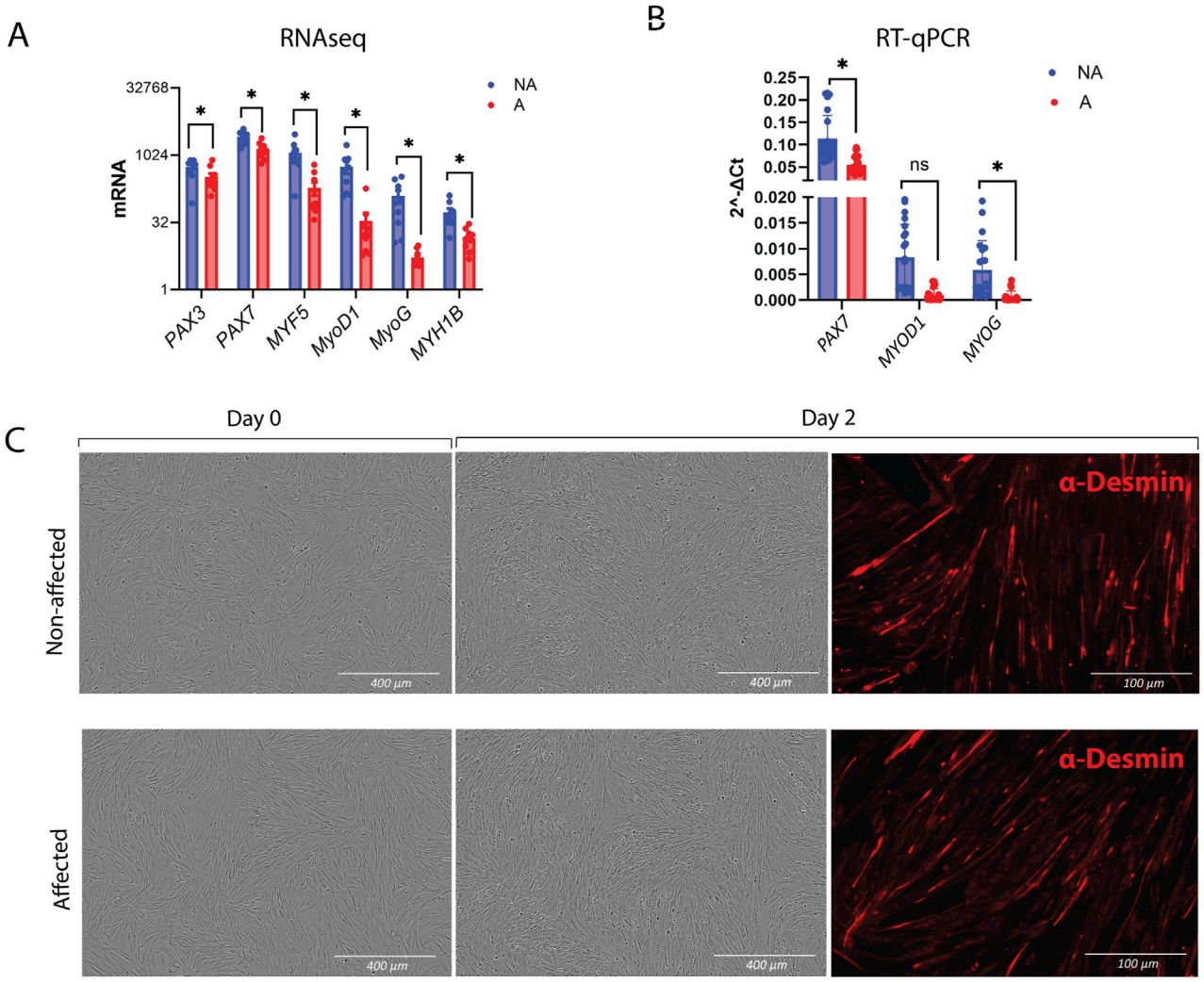

FIGURE 5
Myogenesis and differentiation in MuSCs. **(A)** Gene expression of myogenesis markers obtained by RNA-seq and **(B)** verification of *PAX7*, *MYOD1*, and *MYOG* by RT-qPCR. The data are presented as the fold change average relative to the mean of non-affected WB ± SEM. Comparisons between the groups were analyzed using the *t*-test with Brown–Forsythe and Welsh correction; $*p \leq 0.05$ **(C)** Differentiation assay showing intact differentiation in affected MuSCs after 2 days. Chicken NA and A MuSCs were seeded in roughly 80% confluency. Differentiated MuSCs were immunostained after 2 days with Desmin and secondary antibody Alexa Fluor™ 555 donkey anti-mouse IgG (Right panel). A, affected; NA, non-affected.

the same trend for PAX7 and MYOG using RT-qPCR (Supplementary Figures S1B–D).

3.2 Exploration of SC proliferation and differentiation

3.2.1 MuSC proliferation is impaired

The data described so far suggests that a defect in myogenesis may be associated with tissue degeneration in the *pectoralis major* of chickens affected by WB. To further investigate a potential cell-autonomous role for MuSCs in the pathogenesis of WB, we isolated primary MuSCs from the *pectoralis major* of affected and non-affected individuals and expanded them in culture using established isolation and culture conditions (Yoshioka et al., 2020). Upon observing cell proliferation (Figure 3A), it became evident that the cells sourced from WB-affected muscles demonstrated impaired proliferation. Most of these cells failed to achieve more than 50% confluency before the cessation of cell growth. Two key signaling pathways regulating cell proliferation are the ERK and p38 pathways (Zhang and Liu, 2002). When these signaling pathways were inhibited (Figures 3B, C), the response was similar in both non-affected and affected chickens, suggesting these pathways were not impaired. Interestingly, inhibiting the ERK pathway did not impact cell proliferation in MuSCs (Figure 3B), while inhibiting p38 dramatically stopped proliferation in non-affected MuSCs (Figure 3C). Protein expression of p38 and ERK1/2 and their phosphorylated forms showed no statistical difference between groups; however, phosphorylated ERK1/2 showed a tendency to be downregulated in affected chickens (Figure 3D). These observations suggest that although the p38 MAPK signaling pathway is important for cell proliferation in chickens, this signaling pathway does not appear to be fully impaired in WB-affected cells.

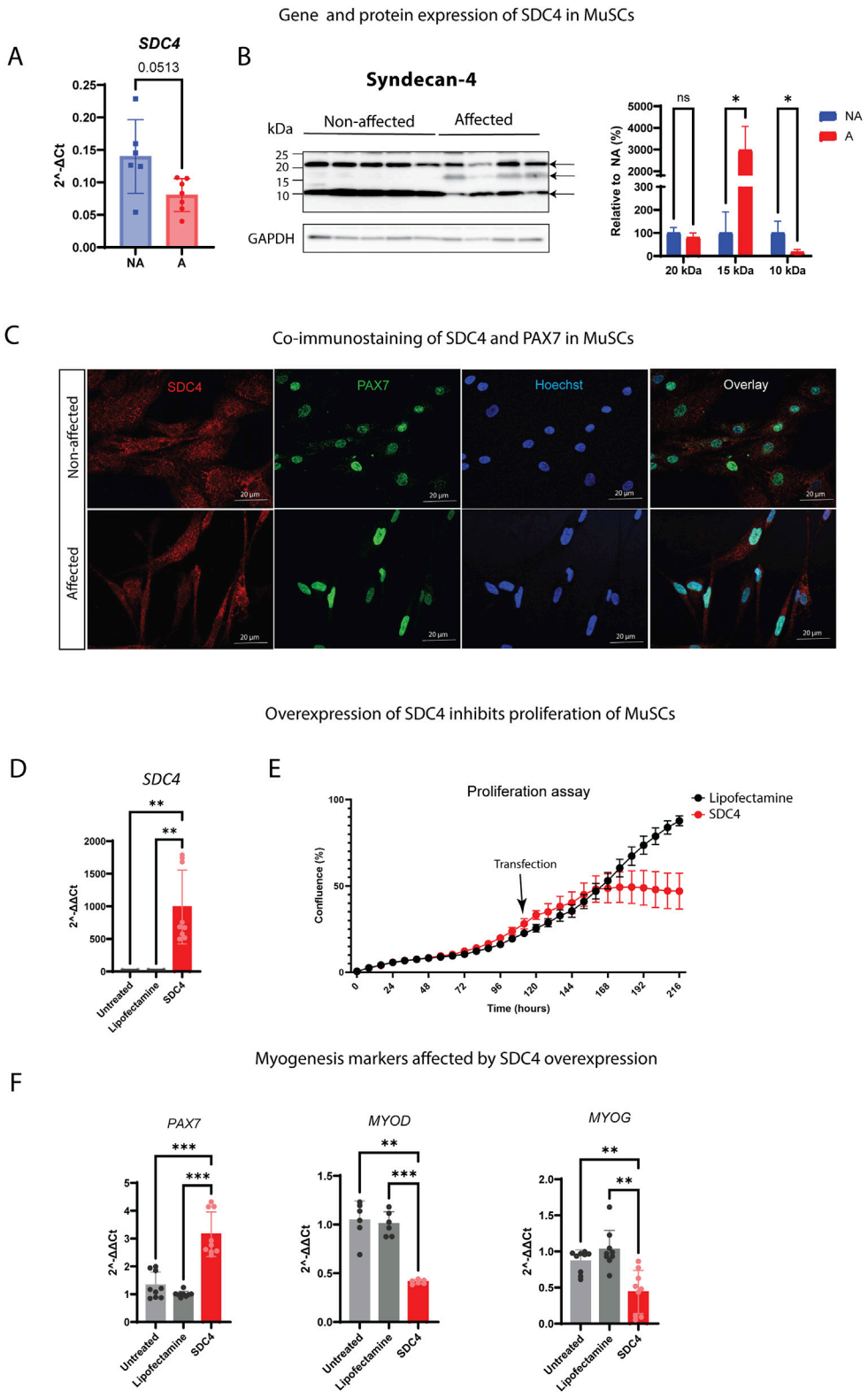

FIGURE 6
Expression and overexpression of SDC4 in chicken MuSCs. **(A)** Bars show the relative gene expression of SDC4 in non-affected (NA) and affected (A) chicken MuSCs (n = 8 chickens in each group) assessed by RT-qPCR. The data are presented as an average of eight chickens in triplicates. The two groups were compared using an unpaired *t*-test with Welch's correction. **(B)** Levels of the syndecan-4 core protein (22 kDa) and two remaining syndecan-4 fragments after shedding (10 and 15 kDa) in non-affected (n = 5) and affected (n = 4) MuSCs were quantitated using ImageQuant TL and normalized to the loading control (GAPDH) and the average of NA group. Data were analyzed using an unpaired *t*-test with Welch's correction and presented as a relative percentage to NA. Arrows indicate the three specific syndecan-4 bands (10, 15, and 20 kDa) confirmed by blocking experiments of the SDC4 antibody (data not shown) (ns $p > 0.05$; *$p \leq 0.05$). **(C)** Co-immunostaining of SDC4 (red) and PAX7 (green) in proliferating affected and non-
(*Continued*)

FIGURE 6 (Continued)
affected chicken MuSCs. Additionally, the panel shows staining of nuclei (blue) and overlay of the channels. **(D)** Gene expression levels of SDC4 in SDC4-transfected MuSCs vs. lipofectamine-treated and non-transfected/untreated MuSCs (controls). **(E)** Proliferation assay showing decreased proliferation of SDC4 overexpressing MuSCs. The black arrow indicates the time point of transfection (4 days of proliferation). Lipofectamine was used as a control. N = 3 individual WB non-affected chickens. **(F)** Gene expression levels of the myogenic markers *PAX7*, *MYOD1*, and *MYOG* in SDC4 overexpressing MuSCs. Untreated and lipofectamine-treated MuSCs were used as controls. Three individual animals measured in technical triplicates. Significant differences were detected using one-way ANOVA with Brown–Forsythe and Welsh correction (**$p \leq 0.01$; ***$p \leq 0.001$).

To gather further insights into the underlying molecular causes of the striking differences observed in MuSC proliferation *in vitro* between affected and non-affected animals, we carried out transcriptomic analysis using RNA extracted from proliferating MuSCs. Surprisingly, the number of differentially expressed genes was relatively small, with 232 upregulated and 278 downregulated genes (Figure 4A) in the affected *versus* non-affected samples. Consistently, PCA analysis showed partial overlap between groups (Figure 4B); however, GSEA identified several terms that were differentially expressed between affected and non-affected MuSCs. The most highly significant function, with a negative normalized enrichment score (NES), downregulated in affected *versus* non-affected MuSCs samples, was related to proliferation (E2F targets and G2/M checkpoint, Figure 4C), as well as terms related to myogenesis (muscle structure development, cell, myotube, and myotube differentiation) (Figure 4C). In contrast, functions related to metabolisms appeared both upregulated (e.g., regulation of autophagy and lysosome) and downregulated (glycolysis), albeit overall pointing toward an anabolic trend. Finally, among the most significant trends were also those related to a pro-inflammatory response, which were mostly upregulated (e.g., interferon-gamma response and IL-6 signaling) (Figure 4C).

Investigation of senescence signs and markers of WB-affected MuSCs showed that apart from CDKN1a (p21), neither the genes of the senescence-associated secretory program (Supplementary Figure S2A) nor other cell cycle arrest markers (Supplementary Figures S2C–E) were differentially expressed in cells from affected chickens compared with cells from non-affected chickens. On the other hand, downregulation of *TP53* (Supplementary Figures S2B, C), *LMNB2* (Supplementary Figure S2B), and *Ki67* (Supplementary Figure S2F) was observed in affected proliferating MuSCs. Inspection of nuclei morphology revealed a decreased perimeter of nuclei and increased area and circularity of nuclei in the affected cells (Supplementary Figure S2G).

Finally, network analysis identified five gene modules that were differentially enriched in affected vs. non-affected MuSCs. These modules again mapped to functions related to muscle development (Figure 4D, module 14), metabolisms (Figure 4D, modules 4, 6, and 15), and cell adhesion (Figure 4D, module 21), further supporting the findings previously described in the pathogenesis of WB.

3.2.2 Myogenesis in WB MuSCs is reduced, but differentiation remains intact

Since the downregulation of myogenesis was the most striking transcriptomic signature displayed by MuSCs isolated from affected chickens compared with those from non-affected chickens, we carried out RT-qPCR-based validation of genes that play a key role in myogenesis. As already observed in RNAseq (Figure 5A), *PAX3* and *PAX7* showed a modest, although statistically significant, decrease in affected samples, while *MYF5*, *MYOD*, and *MYOG* showed a trend toward a greater decrease, which was validated by RT-qPCR *MYOG* and *PAX7* by RT-qPCR (Figure 5B).

Since the gene expression data suggested a differentiation defect, we sought to test whether cells from WB-affected chickens were inherently differentiation-defective. The differentiation assay was performed by seeding the cells at high density and immediately inducing them to differentiate without prior expansion. Surprisingly, MuSCs from both affected and non-affected chickens were able to form myotubes, as visualized by desmin staining (Figure 5C).

3.2.3 Syndecan-4 decreases the proliferation rate, and its shedding increased during WB

We have previously shown that SDC4 is a crucial regulator of MuSC homeostasis and function (Pisconti et al., 2012; Rønning et al., 2015; Velleman and Song, 2017; Keller-Pinter et al., 2018). When analyzing the relative gene expression of SDC4 in isolated MuSCs, we observed a slight, although not statistically significant, downregulation in the affected cells compared to the non-affected ones (Figure 6A). We have previously developed specific antibodies targeting the cytoplasmic part of the chicken SDCs (Pejšková et al., 2023). Interestingly, the band representing the core protein (20 kDa) and the remaining 10–17 kDa fragments, left after shedding, differed greatly between the groups. We observed that the 17 kDa fragment increased in the affected cells, while the 10 kDa band decreased, indicating a different shedding pattern (Figure 6B, full-length immunoblot is shown in Supplementary Figure S3A). We could not detect a difference in the intracellular localization pattern of SDC4 when we co-stained cells with PAX7 (Figure 6C).

To further study the mechanism of SDC4 *in vitro*, we overexpressed SDC4 in non-affected chicken MuSCs (Figure 6D), which confirmed the involvement of SDC4 in cell proliferation since we observed a reduced cell growth of transfected cells compared to non-transfected controls (Figure 5E). However, this reduction was not linked to p38 MAPK or its phosphorylation (Supplementary Figure S4). Likewise, the overexpression of SDC4 influenced gene expression levels of *PAX7*, *MYOD*, and *MYOG* (Figure 6F).

Finally, we analyzed the gene expression levels of the other SDCs and observed that the gene expression of SDC1–3 was upregulated although not significantly for SDC1 and SDC3 (Supplementary Figure S3B). When we examined their protein levels, the SDC1–3 band pattern differed greatly between the groups, showing increased shedding in affected animals compared to non-affected ones (Supplementary Figure S3B), similar to what we observed for SDC4 (Figure 6B). Additionally, SDC4 overexpression in non-affected MuSCs led to increased gene expression of SDC1 and SDC2, whereas SDC3 remained unchanged, suggesting that SDC4 is able to modulate levels of other SDC family members in MuSCs (Supplementary Figure S3C).

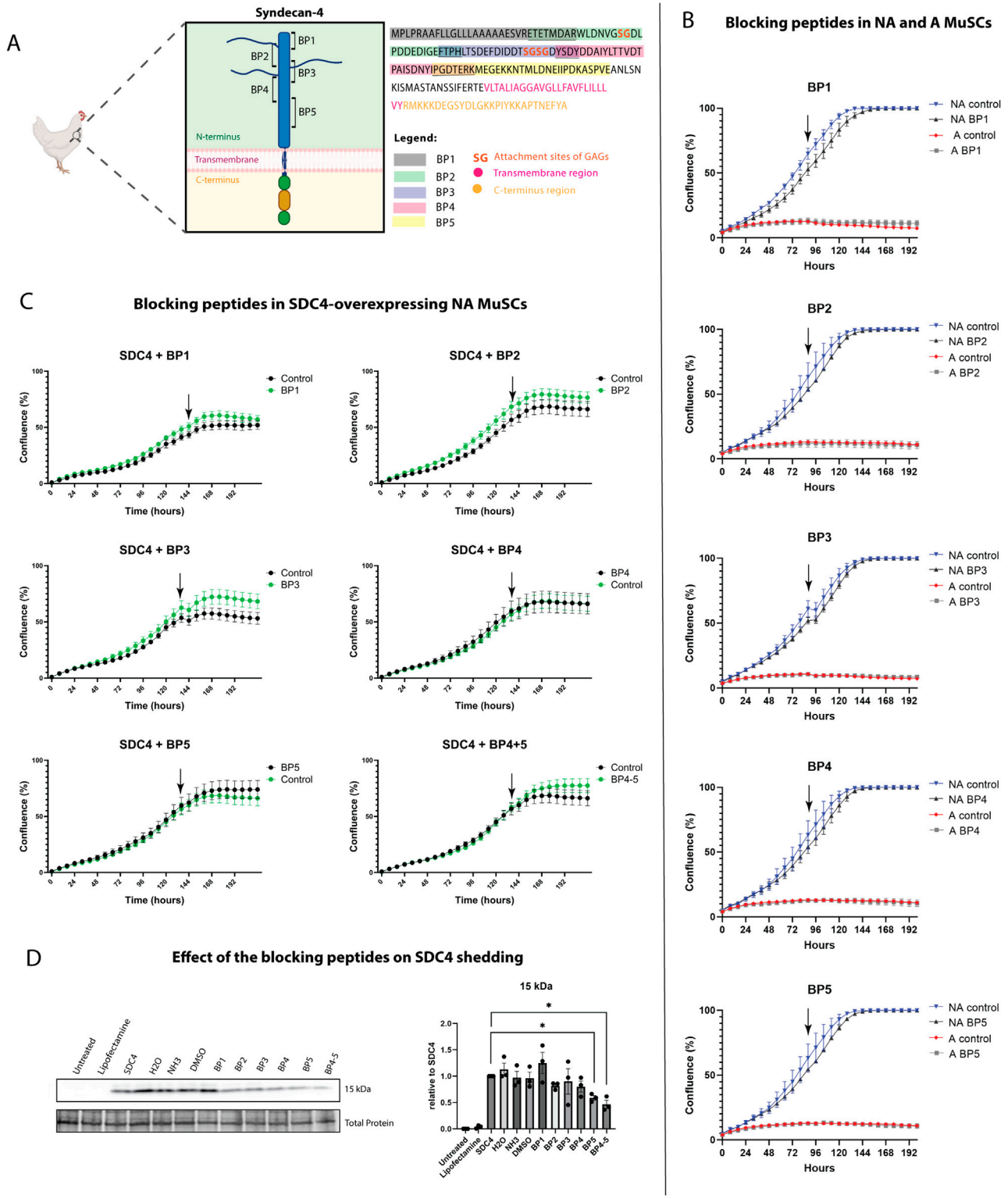

FIGURE 7
Effect of syndecan-4 derived blocking peptides on MuSC proliferation and shedding. **(A)** Schematic illustration of chicken SDC4 with its extracellular domain showing overlapping blocking peptides. Full sequence of chicken SDC4 showing exact amino acids of each blocking peptide and their overlap (underlined). The sequence also features SDC4 transmembrane domain (pink), C-terminus (light orange), and GAG attachment sites (dark orange). Illustration used partially image source from Biorender.com. **(B)** Effect of syndecan-4-derived blocking peptides on the proliferation of affected and non-affected MuSCs. **(C)** Effect of syndecan-4 derived blocking peptides on the proliferation of SDC4-overexpressing MuSCs. Black arrows indicate the time point of treatment with the respective blocking peptides. Lipofectamine was used as a control at the same final concentration. **(D)** Immunoblot of the 15 kDa shed SDC4 fragment in MuSCs treated with or without the respective blocking peptides. The levels were quantified using ImageQuant TL, and
(*Continued*)

FIGURE 7 (Continued)
values were normalized to total protein LI-COR staining (loading control) and SDC4-overexpressing MuSCs without any peptide treatment (set to 1). For comparison, untreated MuSCs and the lipofectamine control are presented. Significant differences were detected using an unpaired *t*-test with Welch's correction. N = 3 for individual non-affected chickens (*$p \leq 0.05$).

3.3 Blocking peptides derived from SDC4 ectodomain reduced shedding

To investigate whether SDC4 shedding is involved in the regulation of MuSC proliferation *in vitro*, we developed five overlapping blocking peptides representing the extracellular part of chicken SDC4 (Figure 7A). When incubated with the MuSCs, the SDC4-derived blocking peptides (BP1-5) did not show any significant effect on proliferation, neither on non-affected nor affected cells (Figure 7B). However, when the peptides were incubated with non-affected MuSCs overexpressing SDC4, an increase in the growth rate was observed, particularly in the presence of BP3 or the combination of BP4+5 (Figure 7C). Furthermore, immunoblot analysis showed that at least BP5 appeared to reduce SDC4 shedding (Figure 7D). Notably, SDC4 overexpression could not be achieved in affected MuSCs due to their low proliferation rate.

4 Discussion

4.1 Skeletal muscle regeneration in WB chickens *in vivo*

This study aimed to investigate the underlying causes of the pathological changes in skeletal muscle in chickens with WB, specifically focusing on the role of SDC function. We have previously identified altered SDC expression and function associated with the extensive ECM remodeling in chicken WB myopathy (Pejšková et al., 2023). The chicken breed Ross 308 investigated in this study developed WB myopathy at relatively high rates and showed signs of degenerative pathologies, such as central nucleation, regardless of the disease severity. Interestingly, even the group classified as 'non-affected' in our study, despite lacking extensive fibrosis, includes birds whose breast muscle shows centrally nucleated myofibers and, occasionally, necrotic myofibers and regions of inflammation. There were no differences in the number of centrally nucleated fibers between affected and non-affected WB birds. Although the percentage of centrally nucleated fibers in our study was similar between groups, other studies have shown that these fibers, defined by nuclei positioned at the center of the cytoplasm, are markers of muscle regeneration (Gutpell et al., 2015). They are commonly observed in patients with muscular dystrophies and their animal models (Folker and Baylies, 2013; Sihvo et al., 2014; Roman and Gomes, 2018), suggesting a potential genetic predisposition to myopathy in all Ross 308 chickens.

A hallmark of several muscular disorders, including wooden breast myopathy, is myofiber size heterogeneity, often resulting from continuous cycles of degeneration/regeneration (Soglia et al., 2016). Our histological analysis revealed a significant increase in small and large muscle fibers in affected chickens compared to medium muscle fiber sizes of non-affected chickens. This observation is partially consistent with previous research, showing an increase in small myofibers in WB (Meloche et al., 2018). Von Maltzahn et al. (2013) demonstrated that muscles of *Pax7*$^{-/-}$ mice showed myofibers with approximately 50% fewer nuclei and significantly smaller fiber diameters. However, in our case, we observed increased *PAX7* gene expression, as well as a higher number of total PAX7 expressing satellite cells per 100 fibers. Additionally, *PAX3*, *MYF5*, *MYOG*, and *MYH1B* were upregulated, indicating an expansion of the MuSC pool and maintained differentiation potential. This contrasts with previous findings by Daughtry et al. (2017), who showed that greater muscle hypertrophy correlates with a decrease in MuSCs and their impaired function.

Fibrosis and metabolic alterations are deeply interconnected with the progression and severity of muscle disorders (Lake and Abasht, 2020; Lake et al., 2022; Chen et al., 2023). Our proteomic data highlighted metabolic changes in affected samples linked to muscle abnormalities and significant disruptions in glycolysis, lipid, and amino acid metabolism. Mitochondrial processes play a crucial role in maintaining cellular homeostasis and skeletal muscle health, and their dysfunction is a key feature of muscle disorders such as muscular dystrophy, sarcopenia, and cachexia—all marked by muscle mass loss, reduced fiber size, decreased strength, and fibrosis (Hasegawa et al., 2021). We observed downregulation of proteins related to respiration and mitochondrial function, and GO terms of interest included proteins related to muscle fiber type, distribution, diameter variability, oxidative phosphorylation, and skeletal myopathies, suggesting mitochondrial dysfunction and oxidative stress involved in our affected chickens (Supplementary Table S2) and aligning with previous metabolomic analysis in WB chickens (Wang et al., 2023). Similar findings have been highlighted in other proteomics studies on white striping myopathy (Kong et al., 2024) and oxidative stress (Carvalho et al., 2023).

4.2 Involvement of syndecan-4 in impaired MuSC proliferation

Muscle regeneration involves several stages: necrosis of the injured muscle cells, activation and proliferation of muscle stem cells, differentiation into muscle fibers, remodeling of the muscle tissue, and, finally, maturation of the regenerated fibers. To examine the regenerative capabilities of primary chicken MuSCs, MuSCs were extracted from both affected and non-affected chicken pectoral muscles, and their proliferation was

assessed in real time. Primary MuSCs from WB-affected chickens exhibited impaired proliferation but were still able to differentiate and form myotubes, in contrast to previous reports of reduced proliferation accompanied by a loss of differentiation capability (Daughtry et al., 2017; Xu and Velleman, 2023). RNA-seq analysis of the MuSCs identified several functions associated with impaired proliferation (E2F targets and G2/M checkpoint) and DNA replication, supporting our findings of decreased proliferation *in vitro*. Moreover, we also observed the downregulation of development and differentiation markers, such as *PAX7*, *PAX3*, *MYF5*, and *MYOG*. The seemingly conflicting results between our RNA-seq data, which suggest a differentiation defect, and the differentiation assay results, which show that MuSCs from affected animals retain their differentiation potential *in vitro*, can be explained by the fact that delayed proliferation may lead to delayed initiation of the differentiation program due to the community effect (Arnold et al., 2020).

Cellular senescence in skeletal muscle serves multiple functions, and it has been proposed that senescence in MuSCs delays muscle regeneration (Saito and Chikenji, 2021). Furthermore, signs of senescence have been observed in other myopathies in chickens (Wright, 1985; Malila et al., 2020). To investigate whether the impaired proliferation in chicken MuSCs was due to senescence, we examined multiple senescence markers. Senescent cells exhibit characteristic morphological and biochemical changes, including hypertrophy, flattened morphology, incomplete nuclear envelope, and increased activity of biomarkers such as *CDKN2A*, *CDKN1A*, *Ki67*, γH2AX, and SA-β-gal, markers of the senescence-associated secretory phenotype (SASP), such as IL6 and LAMB1, several insulin-like growth factor binding proteins, and MMPs and their inhibitors such asTIMP (Gorgoulis et al., 2019; Hansel et al., 2020; Saito and Chikenji, 2021). Our data showed only partial morphological changes in the proliferating MuSCs, along with an increase in *CDKN1A* mRNA, without any alterations in SASP gene expression. This suggests that the impairment in MuSC proliferation is unlikely to be solely caused by senescence.

Subsequently, we explored whether an impaired response to mitogenic signals might contribute to the reduced proliferation of primary MuSCs from WB-affected chickens. It has been earlier postulated that a possible mechanism for senescence-induced impairment of muscle regeneration is the premature senescence triggered by sustained p38 MAPK activity, leading to stem cell exhaustion (Bernet et al., 2014; Cosgrove et al., 2014; Blau et al., 2015; Saito and Chikenji, 2021), although the involvement of signaling pathways in WB myopathy remains not fully explained. To test this hypothesis, we inhibited the P38 MAPK and MEK/ERK signaling pathways, which are recognized as crucial regulators of cell proliferation, differentiation, and survival (Jones et al., 2001; Jones et al., 2005; Perdiguero et al., 2007). While the inhibition of ERK did not affect the proliferation rate in either of the samples, the inhibition of p38 led to a decrease in proliferation in both affected and non-affected cells, suggesting that neither ERK nor p38 is likely involved in the mechanisms that lead to WB-associated defect in MuSC proliferation. Observation of their protein expression and phosphorylation during WB myopathy showed that p38 remains without changes between affected and non-affected group, and ERK1/2 showed a tendency to decrease phosphorylation in WB-affected MuSCs. However, in our earlier *in vivo* investigation of WB myopathy, we observed the upregulation of the ERK1/2 MAPK signaling pathway (Pejšková et al., 2023), which supports the involvement of the ERK pathway in WB, although not necessarily through its role in myogenesis.

In mammals, all four SDCs are expressed during muscle development (Cornelison et al., 2001; Olguin and Brandan, 2001; Do et al., 2015) and contribute to the regulation of myogenesis and MuSC activity, as supported by multiple studies (Cornelison et al., 2001; Cornelison et al., 2004; Velleman et al., 2004; Pisconti et al., 2012; Rønning et al., 2015; Pisconti et al., 2016). Our RNA-seq from MuSCs isolated from WB-affected chickens revealed the downregulation of several gene terms associated with ECM-receptor interactions, focal adhesion, and GAG heparan biosynthesis, pointing toward the involvement of SDCs. Interestingly, the loss of MAPK signaling in SDC4 knockout mice prevented MuSC activation and proliferation (Jones et al., 2001; Jones et al., 2005; Perdiguero et al., 2007; Karimian et al., 2016), showing SDC4 to be required for satellite cell activation. On the other hand, other studies have shown that silencing or knockdown of *SDC4* resulted in decreased progression of cell cycle (Keller-Pinter et al., 2018) and decreased proliferation (Yan et al., 2014; Velleman et al., 2018; Pham et al., 2023). Interestingly, SDC1 expression is shown to be downregulating SDC4 via ERK1/2 and p38 (Hara et al., 2021). Due to the decreased tendency of the mRNA level of *SDC4* in WB-affected MuSCs and their reduced proliferation rate, we tested whether overexpression of SDC4 would impact proliferation or alter myogenesis. Our results demonstrated a reduction in *MYOD* and *MYOG* gene expression following SDC4 overexpression in NA MuSCs, mirroring the findings observed in the cells isolated from chickens with WB. This suggests that SDC4 overexpression may mimic the impaired myogenesis observed in WB. In contrast, the overexpression of SDC4 led to an increase in *PAX7* mRNA and a reduction in MuSC proliferation, suggesting a role for SDC4 in promoting MuSC self-renewal at the expense of myogenesis. Consistent with our findings, the overexpression of SDC4 in turkey satellite cells has been shown to reduce proliferation after 72 h, and it has been proposed that increased SDC4 expression may lead to the formation of more focal adhesions, thereby reducing cell migration (Song et al., 2011).

4.3 Shedding of the SDC4 ectodomain contributes to wooden breast

Although we did not observe any significant changes in the relative gene expression of *SDC4* in proliferating MuSCs, we detected alterations in protein expression, specifically the various SDC4 fragments that remained after shedding. This was also the case for the other SDCs, highlighting the complexity and significance of these molecules in WB myopathy *in vitro*. These findings complement our earlier *in vivo* study,

indicating that all SDCs are present during WB and exhibit significant shedding (Pejšková et al., 2023). Although SDC1 has been extensively studied for its shedding and use as a biomarker for several diseases (Bertrand and Bollmann, 2019; Rangarajan et al., 2020), shedding of SDC4 has been previously shown as an important regulator in pathologies such as cardiac dysfunctions (Strand et al., 2013; Strand et al., 2023), diabetes mellitus (Li et al., 2016), osteoarthritis (Bollmann et al., 2021), and cancer (Choi et al., 2010).

The SDC4 ectodomain is critical in interactions with the extracellular matrix, growth factors, and cytokines (Tkachenko et al., 2005). Shedding of this ectodomain affects cell behavior, such as cell migration during tissue repair (Manon-Jensen et al., 2010), although the complete impact of this process is not yet fully understood. We tried to elucidate the function of SDC4 ectodomain shedding by adding custom-made blocking peptides to proliferating non-affected and WB-affected MuSCs, representing specific areas of the SDC4 ectodomain. We could not observe any change in cell proliferation when adding the peptides. However, when adding the BPs to SDC4-transfected MuSCs, we were able to restore some of the proliferation capability, especially using the blocking peptide BP3. BP3 consists of the chicken protein sequence FTPHLTSDEFDIDDT**SGSG**DYSDY. Interestingly, this sequence corresponds to the SDC4 ectodomain, containing two consecutive Ser-Gly (SG) sites reported to be GAG chain regions (Kokenyesi and Bernfield, 1994). Compared to SDC1 and SDC3, SDC4 exhibits only heparan sulfate GAG chains. Heparan sulfates on proteoglycans regulate growth factor signaling by acting as co-receptors, reservoirs, or transporters; therefore, adding BP hindering shedding activity might alter the biological function of syndecan directly or indirectly (Keller-Pinter et al., 2018). It has been shown that several growth factors bind to the SDC4 heparan sulfates, which then act as co-receptors for tyrosine kinase activity (Sarrazin et al., 2011). However, it is important to point out that our BP3 is most likely not able to bind to ligands that are dependent on heparan sulfates/GAGs as BP3 only is a short protein sequence with identical amino acids to a smaller stretch of the SDC4 ectodomain. It is possible that BP3 is competing with other ligands containing similar protein sequences, preventing the cells from undergoing differentiation, which might explain our increase in cell proliferation. Still, we cannot rule out the possibility of peptide uptake into the cell, with GAG chains of other molecules potentially playing a role in this process (Favretto et al., 2014), or effect on other cellular functions, such as signaling pathways, adhesion dynamics, or differentiation. Interestingly, shedding of the core SDC4 protein was significantly reduced by BP5 or a combination of BP4 and BP5, which indicates that at least BP5 contains an MMP-binding (cleavage) site, allowing it to outcompete MMP binding to the SDC4 ectodomain, thereby inhibit shedding of SDC4. This observation corresponds with previously detected cleavage by MMP2 and MMP9 in the human SDC4 ectodomain in lysine 105 (Manon-Jensen et al., 2013) situated in our BP5 region. However, current knowledge about the specific cleavage sites on the chicken SDC4 core protein remains limited. Our findings offer new insights into the cleavage and shedding of SDC4 in chickens. Considering the pivotal role of SDC4 in cellular regulation and disease, additional research is essential to unravel the mechanisms driving myogenesis.

5 Conclusion

This study aimed to elucidate the molecular basis of WB myopathy. Our research revealed significant molecular and cellular alterations associated with WB myopathy and indicated a role of SDC4 in its pathogenesis. We showed different shedding patterns of SDC4 in affected and non-affected primary MuSCs and observed reduced growth in non-affected MuSCs during SDC4 overexpression. Using specific blocking peptides, each representing a specific part of the chicken SDC4 ectodomain, we demonstrated increased proliferation and decreased shedding of SDC4 in MuSCs. The increased shedding identified across all members of the syndecan family suggests an involvement of SDCs in the pathogenesis of WB; further investigation into their regulatory mechanisms could provide valuable insights for the development of targeted therapeutic interventions.

Data availability statement

The proteomic data presented in the study are deposited in the UCSD/CCMS - MassIVE Datasets - Mass Spectrometry Repository Dataset List repository, accession number MSV000096414. The RNA seq data presented in the study are deposited in the GEO Accession viewer repository, accession number GSE279699.

Ethics statement

Ethical approval was not required for the study involving animals in accordance with the local legislation and institutional requirements because the muscle tissues used are extracted from already slaughtered chickens (Ross 308 breed, NMBU, Norway). These chickens are in line with common regulatory roles of food production and, therefore, do not require REC or NSD approval. In compliance with Norwegian law regulations concerning the experimental use of animals (FOR-2015-06-18- 761 §2a), ethical approval is not necessary when samples are collected from slaughtered animals/non-experimental agriculture and aquaculture. This is also confirmed by direct communication with the Norwegian Food Safety Authority (Mattilsynet).

Author contributions

LP: data curation, formal analysis, investigation, methodology, visualization, writing–original draft, and writing–review and editing. AP: data curation, formal analysis, methodology, and writing–review and editing. ML: data curation, formal analysis, methodology, and writing–review and editing. KH: data curation, formal analysis, methodology, and writing–review and editing. NS: data curation, formal analysis, methodology, and writing–review and editing. SK: data curation, formal analysis, methodology, and

writing–review and editing. ET: writing–review and editing, data curation, and validation. CC: conceptualization, funding acquisition, project administration, supervision, and writing–review and editing. MP: conceptualization, funding acquisition, supervision, writing–review and editing, and project administration. SR: writing–review and editing, conceptualization, funding acquisition, methodology, and supervision.

Funding

The author(s) declare that financial support was received for the research, authorship, and/or publication of this article. Funding from the Norwegian Research Council ("ChickenHealth", no.323939) is acknowledged. The authors also thank the Norwegian Fund for Research Fees for Agricultural Products (FFL) for additional support through the projects "SusHealth" (project number 314599) and "Precision" (project number 314111).

Acknowledgments

The authors would like to acknowledge Birger Svihus at the Norwegian University of Life Sciences for assistance in planning the chicken feeding trial and the Livestock Production Research Center for technical assistance. The authors would also like to thank Atle Løvland from Nortura for assistance in planning and sampling and Karen Sanden and Lene Øverby from Nofima for technical assistance during sampling. The authors would like to thank Jens-Petter Wold for NIR spectroscopy initial grading and Vibeke Høst for the histology and scoring of affected/non-affected chickens, as well as for technical assistance during the proteomics experiments, and Matthew Peter Kent and Thu-Hien To for contribution on *in vivo* RNAseq and scientific discussions. Finally, the author's acknowledges David Carlson, Genomics Core Facility, Stony Brook University, who performed statistics on RNA sequencing dataset from MuSCs. ChatGPT (GPT-4 model) was used for polishing and improving the clarity, coherence, and overall readability of the scientific paper. The tool was used in a manner that does not conflict with APS ethical policies, and the authors take full responsibility for the content. The authors thank the Norwegian Fund for Research Fees for Agricultural Products (FFL) for supporting the study through the projects "SusHealth" (project number 314599) and "Precision" (project number 314111).

Conflict of interest

The authors declare that the research was conducted in the absence of any commercial or financial relationships that could be construed as a potential conflict of interest.

Generative AI statement

The author(s) declare that Generative AI was used in the creation of this manuscript. The author(s) verify and take full responsibility for the use of generative AI in the preparation of this manuscript. Generative AI, ChatGPT (GPT-4 model), was used to polish and improve the clarity, coherence, and overall readability of the scientific paper. The tool was used in a manner that does not conflict with APS ethical policies, and the authors take full responsibility for the content.

Publisher's note

Supplementary material

The Supplementary Material for this article can be found online at: https://www.frontiersin.org/articles/10.3389/fphys.2024.1513311/full#supplementary-material

References

Afratis, N. A., Nikitovic, D., Multhaupt, H. A., Theocharis, A. D., Couchman, J. R., and Karamanos, N. K. (2017). Syndecans–key regulators of cell signaling and biological functions. *Febs J.* 284 (1), 27–41. doi:10.1111/febs.13940

Andrews, S. (2010). "FastQC: a quality control tool for high throughput sequence data," in *Babraham bioinformatics*. Cambridge, United Kingdom: Babraham Institute.

Andrews, S. (2023). FastQC version 0.12.1. *Babraham Bioinforma.* Available at: https://www.bioinformatics.babraham.ac.uk/projects/fastqc/.

Arnold, L. L., Cecchini, A., Stark, D. A., Ihnat, J., Craigg, R. N., Carter, A., et al. (2020). EphA7 promotes myogenic differentiation via cell-cell contact. *Elife* 9, e53689. doi:10.7554/eLife.53689

Bernet, J. D., Doles, J. D., Hall, J. K., Kelly Tanaka, K., Carter, T. A., and Olwin, B. B. (2014). p38 MAPK signaling underlies a cell-autonomous loss of stem cell self-renewal in skeletal muscle of aged mice. *Nat. Med.* 20 (3), 265–271. doi:10.1038/nm.3465

Bertrand, J., and Bollmann, M. (2019). Soluble syndecans: biomarkers for diseases and therapeutic options. *Br. J. Pharmacol.* 176 (1), 67–81. doi:10.1111/bph.14397

Blau, H. M., Cosgrove, B. D., and Ho, A. T. V. (2015). The central role of muscle stem cells in regenerative failure with aging. *Nat. Med.* 21 (8), 854–862. doi:10.1038/nm.3918

Blighe, K., and Lun, A. (2018). PCAtools: everything principal components analysis. *R. Package Version*. Available at: https://github.com/kevinblighe.PCAtools.

Bollmann, M., Pinno, K., Ehnold, L. I., Märtens, N., Märtson, A., Pap, T., et al. (2021). MMP-9 mediated Syndecan-4 shedding correlates with osteoarthritis severity. *Osteoarthr. Cartil.* 29 (2), 280–289. doi:10.1016/j.joca.2020.10.009

Bordini, M., Wang, Z., Soglia, F., Petracci, M., Schmidt, C. J., and Abasht, B. (2024). RNA-sequencing revisited data shed new light on wooden breast myopathy. *Poult. Sci.* 103, 103902. doi:10.1016/j.psj.2024.103902

Bustin, S. A., Beaulieu, J.-F., Huggett, J., Jaggi, R., Kibenge, F. S. B., Olsvik, P. A., et al. (2010). MIQE précis: practical implementation of minimum standard guidelines for fluorescence-based quantitative real-time PCR experiments. *BMC Mol. Biol.* 11 (1), 74. doi:10.1186/1471-2199-11-74

Careccia, G., Mangiavini, L., and Cirillo, F. (2024). Regulation of satellite cells functions during skeletal muscle regeneration: a critical step in physiological and pathological conditions. *Int. J. Mol. Sci.* 25 (1), 512. doi:10.3390/ijms25010512

Carvalho, L. M., Rocha, T. C., Delgado, J., Díaz-Velasco, S., Madruga, M. S., and Estévez, M. (2023). Deciphering the underlying mechanisms of the oxidative perturbations and impaired meat quality in Wooden breast myopathy by label-free

quantitative MS-based proteomics. *Food Chem.* 423, 136314. doi:10.1016/j.foodchem.2023.136314

Chakkalakal, J. V., Jones, K. M., Basson, M. A., and Brack, A. S. (2012). The aged niche disrupts muscle stem cell quiescence. *Nature* 490 (7420), 355–360. doi:10.1038/nature11438

Chen, S., Zhou, Y., Chen, Y., and Gu, J. (2018). fastp: an ultra-fast all-in-one FASTQ preprocessor. *Bioinformatics* 34 (17), i884–i890. doi:10.1093/bioinformatics/bty560

Chen, W., Zhao, H., and Li, Y. (2023). Mitochondrial dynamics in health and disease: mechanisms and potential targets. *Signal Transduct. Target. Ther.* 8 (1), 333. doi:10.1038/s41392-023-01547-9

Choi, S.-J., Lee, H.-W., Choi, J.-R., and Oh, E.-S. (2010). Shedding; towards a new paradigm of syndecan function in cancer. *BMB Rep.* 43 (5), 305–310. doi:10.5483/bmbrep.2010.43.5.305

Christov, C., Chrétien, F., Abou-Khalil, R., Bassez, G., Vallet, G., Authier, F. J., et al. (2007). Muscle satellite cells and endothelial cells: close neighbors and privileged partners. *Mol. Biol. Cell* 18 (4), 1397–1409. doi:10.1091/mbc.e06-08-0693

Cornelison, D. D., Wilcox-Adelman, S. A., Goetinck, P. F., Rauvala, H., Rapraeger, A. C., and Olwin, B. B. (2004). Essential and separable roles for Syndecan-3 and Syndecan-4 in skeletal muscle development and regeneration. *Genes Dev.* 18 (18), 2231–2236. doi:10.1101/gad.1214204

Cornelison, D. D. W., Filla, M. S., Stanley, H. M., Rapraeger, A. C., and Olwin, B. B. (2001). Syndecan-3 and syndecan-4 specifically mark skeletal muscle satellite cells and are implicated in satellite cell maintenance and muscle regeneration. *Dev. Biol.* 239 (1), 79–94. doi:10.1006/dbio.2001.0416

Cosgrove, B. D., Gilbert, P. M., Porpiglia, E., Mourkioti, F., Lee, S. P., Corbel, S. Y., et al. (2014). Rejuvenation of the muscle stem cell population restores strength to injured aged muscles. *Nat. Med.* 20 (3), 255–264. doi:10.1038/nm.3464

Couchman, J. R. (2010). Transmembrane signaling proteoglycans. *Annu. Rev. Cell Dev. Biol.* 26, 89–114. doi:10.1146/annurev-cellbio-100109-104126

Cox, J., and Mann, M. (2008). MaxQuant enables high peptide identification rates, individualized p.p.b.-range mass accuracies and proteome-wide protein quantification. *Nat. Biotechnol.* 26 (12), 1367–1372. doi:10.1038/nbt.1511

Daughtry, M. R., Berio, E., Shen, Z., Suess, E. J. R., Shah, N., Geiger, A. E., et al. (2017). Satellite cell-mediated breast muscle regeneration decreases with broiler size. *Poult. Sci.* 96 (9), 3457–3464. doi:10.3382/ps/pex068

De Micheli, A. J., Laurilliard, E. J., Heinke, C. L., Ravichandran, H., Fraczek, P., Soueid-Baumgarten, S., et al. (2020). Single-cell analysis of the muscle stem cell hierarchy identifies heterotypic communication signals involved in skeletal muscle regeneration. *Cell Rep.* 30 (10), 3583–3595.e5. doi:10.1016/j.celrep.2020.02.067

Do, M. K. Q., Shimizu, N., Suzuki, T., Ohtsubo, H., Mizunoya, W., Nakamura, M., et al. (2015). Transmembrane proteoglycans syndecan-2, 4, receptor candidates for the impact of HGF and FGF 2 on semaphorin 3A expression in early-differentiated myoblasts. *Physiol. Rep.* 3 (9), e12553. doi:10.14814/phy2.12553

Dobin, A., Davis, C. A., Schlesinger, F., Drenkow, J., Zaleski, C., Jha, S., et al. (2013). STAR: ultrafast universal RNA-seq aligner. *Bioinformatics* 29 (1), 15–21. doi:10.1093/bioinformatics/bts635

Favretto, M. E., Wallbrecher, R., Schmidt, S., van de Putte, R., and Brock, R. (2014). Glycosaminoglycans in the cellular uptake of drug delivery vectors – bystanders or active players? *J. Control. Release* 180, 81–90. doi:10.1016/j.jconrel.2014.02.011

Folker, E., and Baylies, M. (2013). Nuclear positioning in muscle development and disease. *Front. Physiology* 4, 363. doi:10.3389/fphys.2013.00363

Ganassi, M., Muntoni, F., and Zammit, P. S. (2022). Defining and identifying satellite cell-opathies within muscular dystrophies and myopathies. *Exp. cell Res.* 411 (1), 112906. doi:10.1016/j.yexcr.2021.112906

Gopal, S. (2020). Syndecans in inflammation at a glance. *Front. Immunol.* 11, 227. doi:10.3389/fimmu.2020.00227

Gorgoulis, V., Adams, P. D., Alimonti, A., Bennett, D. C., Bischof, O., Bishop, C., et al. (2019). Cellular senescence: defining a path forward. *Cell* 179 (4), 813–827. doi:10.1016/j.cell.2019.10.005

Gutpell, K. M., Hrinivich, W. T., and Hoffman, L. M. (2015). Skeletal muscle fibrosis in the mdx/utrn+/- mouse validates its suitability as a murine model of duchenne muscular dystrophy. *PLOS ONE* 10 (1), e0117306. doi:10.1371/journal.pone.0117306

Hansel, C., Jendrossek, V., and Klein, D. (2020). Cellular senescence in the lung: the central role of senescent epithelial cells. *Int. J. Mol. Sci.* 21 (9), 3279. [Online]. doi:10.3390/ijms21093279

Hara, T., Sato, A., Yamamoto, C., and Kaji, T. (2021). Syndecan-1 downregulates syndecan-4 expression by suppressing the ERK1/2 and p38 MAPK signaling pathways in cultured vascular endothelial cells. *Biochem. Biophys. Rep.* 26, 101001. doi:10.1016/j.bbrep.2021.101001

Hasegawa, Y., Kawasaki, T., Maeda, N., Yamada, M., Takahashi, N., Watanabe, T., et al. (2021). Accumulation of lipofuscin in broiler chicken with wooden breast. *Anim. Sci. J.* 92 (1), e13517. doi:10.1111/asj.13517

Hosotani, M., Kawasaki, T., Hasegawa, Y., Wakasa, Y., Hoshino, M., Takahashi, N., et al. (2020). Physiological and pathological mitochondrial clearance is related to pectoralis major muscle pathogenesis in broilers with wooden breast syndrome. *Front. Physiol.* 11, 579. doi:10.3389/fphys.2020.00579

Jones, F. K., Phillips, A. M., Jones, A. R., and Pisconti, A. (2022). The INSR/AKT/mTOR pathway regulates the pace of myogenesis in a syndecan-3-dependent manner. *Matrix Biol.* 113, 61–82. doi:10.1016/j.matbio.2022.09.004

Jones, N. C., Fedorov, Y. V., Rosenthal, R. S., and Olwin, B. B. (2001). ERK1/2 is required for myoblast proliferation but is dispensable for muscle gene expression and cell fusion. *J. Cell Physiol.* 186 (1), 104–115. doi:10.1002/1097-4652(200101)186:1<104::Aid-jcp1015>3.0.Co;2-0

Jones, N. C., Tyner, K. J., Nibarger, L., Stanley, H. M., Cornelison, D. D., Fedorov, Y. V., et al. (2005). The p38alpha/beta MAPK functions as a molecular switch to activate the quiescent satellite cell. *J. Cell Biol.* 169 (1), 105–116. doi:10.1083/jcb.200408066

Karimian, A., Ahmadi, Y., and Yousefi, B. (2016). Multiple functions of p21 in cell cycle, apoptosis and transcriptional regulation after DNA damage. *DNA Repair* 42, 63–71. doi:10.1016/j.dnarep.2016.04.008

Keller-Pinter, A., Szabo, K., Kocsis, T., Deak, F., Ocsovszki, I., Zvara, A., et al. (2018). Syndecan-4 influences mammalian myoblast proliferation by modulating myostatin signalling and G1/S transition. *FEBS Lett.* 592 (18), 3139–3151. doi:10.1002/1873-3468.13227

Koga, S., Rieder, A., Ballance, S., Uhlen, A. K., and Veiseth-Kent, E. (2019). Gluten-degrading proteases in wheat infected by Fusarium graminearum—protease identification and effects on gluten and dough properties. *J. Agric. Food Chem.* 67 (40), 11025–11034. doi:10.1021/acs.jafc.9b03869

Kokenyesi, R., and Bernfield, M. (1994). Core protein structure and sequence determine the site and presence of heparan sulfate and chondroitin sulfate on syndecan-1. *J. Biol. Chem.* 269 (16), 12304–12309. doi:10.1016/S0021-9258(17)32716-3

Kolberg, L., Raudvere, U., Kuzmin, I., Adler, P., Vilo, J., and Peterson, H. (2023). g:Profiler—interoperable web service for functional enrichment analysis and gene identifier mapping (2023 update). *Nucleic Acids Res.* 51 (W1), W207–W212. doi:10.1093/nar/gkad347

Kong, B., Owens, C., Bottje, W., Shakeri, M., Choi, J., Zhuang, H., et al. (2024). Proteomic analyses on chicken breast meat with white striping myopathy. *Poult. Sci.* 103 (6), 103682. doi:10.1016/j.psj.2024.103682

Korotkevich, G., Sukhov, V., Budin, N., Shpak, B., Artyomov, M. N., and Sergushichev, A. (2016). Fast gene set enrichment analysis. *biorxiv*, 060012. doi:10.1101/060012

Krueger, F., James, F., Ewels, P., Afyounian, E., and Schuster-Boeckler, B. (2021). *FelixKrueger/TrimGalore: v0.6.7 - DOI via zenodo*. Zenodo. doi:10.5281/zenodo.5127899

Lake, J. A., and Abasht, B. (2020). Glucolipotoxicity: a proposed etiology for wooden breast and related myopathies in commercial broiler chickens. *Front. Physiology* 11, 169. doi:10.3389/fphys.2020.00169

Lake, J. A., Yan, Y., Dekkers, J. C. M., Qiu, J., Brannick, E. M., and Abasht, B. (2022). Identification of circulating metabolites associated with wooden breast and white striping. *PLoS One* 17 (9), e0274208. doi:10.1371/journal.pone.0274208

Langfelder, P., and Horvath, S. (2008). WGCNA: an R package for weighted correlation network analysis. *BMC Bioinforma.* 9, 559. doi:10.1186/1471-2105-9-559

Li, H., Handsaker, B., Wysoker, A., Fennell, T., Ruan, J., Homer, N., et al. (2009). The sequence alignment/map format and SAMtools. *Bioinformatics* 25 (16), 2078–2079. doi:10.1093/bioinformatics/btp352

Li, R., Xie, J., Wu, H., Li, G., Chen, J., Chen, Q., et al. (2016). Syndecan-4 shedding impairs macrovascular angiogenesis in diabetes mellitus. *Biochem. Biophysical Res. Commun.* 474 (1), 15–21. doi:10.1016/j.bbrc.2016.03.112

Love, M. I., Huber, W., and Anders, S. (2014). Moderated estimation of fold change and dispersion for RNA-seq data with DESeq2. *Genome Biol.* 15 (12), 550. doi:10.1186/s13059-014-0550-8

Malila, Y., Uengwetwanit, T., Arayamethakorn, S., Srimarut, Y., Thanatsang, K. V., Soglia, F., et al. (2020). Transcriptional profiles of skeletal muscle associated with increasing severity of white striping in commercial broilers. *Front. Physiology* 11, 580. doi:10.3389/fphys.2020.00580

Manon-Jensen, T., Itoh, Y., and Couchman, J. R. (2010). Proteoglycans in health and disease: the multiple roles of syndecan shedding. *FEBS J.* 277 (19), 3876–3889. doi:10.1111/j.1742-4658.2010.07798.x

Manon-Jensen, T., Multhaupt, H. A. B., and Couchman, J. R. (2013). Mapping of matrix metalloproteinase cleavage sites on syndecan-1 and syndecan-4 ectodomains. *FEBS J.* 280 (10), 2320–2331. doi:10.1111/febs.12174

Martin, M. (2011). Cutadapt removes adapter sequences from high-throughput sequencing reads. *EMBnet. J.* 17 (1), 10–12. doi:10.14806/ej.17.1.200

Mashinchian, O., Pisconti, A., Le Moal, E., and Bentzinger, C. F. (2018). The muscle stem cell niche in health and disease. *Curr. Top. Dev. Biol.* 126, 23–65. doi:10.1016/bs.ctdb.2017.08.003

Meloche, K. J., Dozier, W. A., Brandebourg, T. D., and Starkey, J. D. (2018). Skeletal muscle growth characteristics and myogenic stem cell activity in broiler chickens affected by wooden breast. *Poult. Sci.* 97 (12), 4401–4414. doi:10.3382/ps/pey287

Motohashi, N., and Asakura, A. (2014). Muscle satellite cell heterogeneity and self-renewal. *Front. Cell Dev. Biol.* 2, 1. doi:10.3389/fcell.2014.00001

Mudalal, S., Lorenzi, M., Soglia, F., Cavani, C., and Petracci, M. (2015). Implications of white striping and wooden breast abnormalities on quality traits of raw and marinated chicken meat. *Animal* 9 (4), 728–734. doi:10.1017/S175173111400295X

Mutryn, M. F., Brannick, E. M., Fu, W., Lee, W. R., and Abasht, B. (2015). Characterization of a novel chicken muscle disorder through differential gene expression and pathway analysis using RNA-sequencing. *BMC Genomics* 16 (1), 399. doi:10.1186/s12864-015-1623-0

Olguin, H., and Brandan, E. (2001). Expression and localization of proteoglycans during limb myogenic activation. *Dev. Dyn. official Publ. Am. Assoc. Anatomists* 221 (1), 106–115. doi:10.1002/dvdy.1129

Olguín, H. C., and Pisconti, A. (2012). Marking the tempo for myogenesis: Pax7 and the regulation of muscle stem cell fate decisions. *J. Cell Mol. Med.* 16 (5), 1013–1025. doi:10.1111/j.1582-4934.2011.01348.x

Papah, M. B., Brannick, E. M., Schmidt, C. J., and Abasht, B. (2017). Evidence and role of phlebitis and lipid infiltration in the onset and pathogenesis of Wooden Breast Disease in modern broiler chickens. *Avian Pathol.* 46 (6), 623–643. doi:10.1080/03079457.2017.1339346

Patro, R., Duggal, G., Love, M. I., Irizarry, R. A., and Kingsford, C. (2017). Salmon provides fast and bias-aware quantification of transcript expression. *Nat. Methods* 14 (4), 417–419. doi:10.1038/nmeth.4197

Pejšková, L., Rønning, S. B., Kent, M. P., Solberg, N. T., Høst, V., Thu-Hien, T., et al. (2023). Characterization of wooden breast myopathy: a focus on syndecans and ECM remodeling. *Front. Physiology* 14, 1301804. doi:10.3389/fphys.2023.1301804

Perdiguero, E., Ruiz-Bonilla, V., Serrano, A. L., and Muñoz-Cánoves, P. (2007). Genetic deficiency of p38alpha reveals its critical role in myoblast cell cycle exit: the p38alpha-JNK connection. *Cell Cycle* 6 (11), 1298–1303. doi:10.4161/cc.6.11.4315

Petracci, M., and Cavani, C. (2012). Muscle growth and poultry meat quality issues. *Nutrients* 4 (1), 1–12. doi:10.3390/nu4010001

Petracci, M., Mudalal, S., Soglia, F., and Cavani, C. (2015). Meat quality in fast-growing broiler chickens. *World's Poult. Sci. J.* 71 (2), 363–374. doi:10.1017/S0043933915000367

Petracci, M., Soglia, F., Madruga, M., Carvalho, L., Ida, E., and Estevez, M. (2019). Wooden-breast, white striping, and spaghetti meat: causes, consequences and consumer perception of emerging broiler meat abnormalities. *Compr. Rev. Food Sci. Food Saf.* 18 (2), 565–583. doi:10.1111/1541-4337.12431

Pham, S. H., Vuorinen, S. I., Arif, K. M. T., Griffiths, L. R., Okolicsanyi, R. K., and Haupt, L. M. (2023). Syndecan-4 regulates the HER2-positive breast cancer cell proliferation cells via CK19/AKT signalling. *Biochimie* 207, 49–61. doi:10.1016/j.biochi.2022.11.010

Pisconti, A., Banks, G. B., Babaeijandaghi, F., Betta, N. D., Rossi, F. M., Chamberlain, J. S., et al. (2016). Loss of niche-satellite cell interactions in syndecan-3 null mice alters muscle progenitor cell homeostasis improving muscle regeneration. *Skelet. Muscle* 6, 34. doi:10.1186/s13395-016-0104-8

Pisconti, A., Bernet, J. D., and Olwin, B. B. (2012). Syndecans in skeletal muscle development, regeneration and homeostasis. *Muscles, ligaments tendons J.* 2 (1), 1–9.

Rangarajan, S., Richter, J. R., Richter, R. P., Bandari, S. K., Tripathi, K., Vlodavsky, I., et al. (2020). Heparanase-enhanced shedding of syndecan-1 and its role in driving disease pathogenesis and progression. *J. Histochem. and Cytochem.* 68 (12), 823–840. doi:10.1369/0022155420937087

Rappsilber, J., Mann, M., and Ishihama, Y. (2007). Protocol for micro-purification, enrichment, pre-fractionation and storage of peptides for proteomics using StageTips. *Nat. Protoc.* 2 (8), 1896–1906. doi:10.1038/nprot.2007.261

Roman, W., and Gomes, E. R. (2018). Nuclear positioning in skeletal muscle. *Seminars Cell and Dev. Biol.* 82, 51–56. doi:10.1016/j.semcdb.2017.11.005

Rønning, S. B., Carlson, C. R., Aronsen, J. M., Pisconti, A., Høst, V., Lunde, M., et al. (2020). Syndecan-4(-/-) mice have smaller muscle fibers, increased akt/mTOR/S6K1 and notch/HES-1 pathways, and alterations in extracellular matrix components. *Front. Cell Dev. Biol.* 8, 730. doi:10.3389/fcell.2020.00730

Rønning, S. B., Carlson, C. R., Stang, E., Kolset, S. O., Hollung, K., and Pedersen, M. E. (2015). Syndecan-4 regulates muscle differentiation and is internalized from the plasma membrane during myogenesis. *PloS one* 10 (6), e0129288. doi:10.1371/journal.pone.0129288

Saito, Y., and Chikenji, T. S. (2021). Diverse roles of cellular senescence in skeletal muscle inflammation, regeneration, and therapeutics. *Front. Pharmacol.* 12, 739510. doi:10.3389/fphar.2021.739510

Sanden, K. W., Böcker, U., Ofstad, R., Pedersen, M. E., Høst, V., Afseth, N. K., et al. (2021). Characterization of collagen structure in normal, wooden breast and spaghetti meat chicken fillets by FTIR microspectroscopy and histology. *Foods* 10 (3), 548. doi:10.3390/foods10030548

Sarrazin, S., Lamanna, W. C., and Esko, J. D. (2011). Heparan sulfate proteoglycans. *Cold Spring Harb. Perspect. Biol.* 3 (7), a004952. doi:10.1101/cshperspect.a004952

Schmittgen, T. D., and Livak, K. J. (2008). Analyzing real-time PCR data by the comparative CT method. *Nat. Protoc.* 3 (6), 1101–1108. doi:10.1038/nprot.2008.73

Sihvo, H. K., Immonen, K., and Puolanne, E. (2014). Myodegeneration with fibrosis and regeneration in the pectoralis major muscle of broilers. *Vet. Pathol.* 51 (3), 619–623. doi:10.1177/0300985813497488

Smith, L. R., and Barton, E. R. (2014). SMASH - semi-automatic muscle analysis using segmentation of histology: a MATLAB application. *Skelet. Muscle* 4, 21. doi:10.1186/2044-5040-4-21

Soglia, F., Mudalal, S., Babini, E., Di Nunzio, M., Mazzoni, M., Sirri, F., et al. (2016). Histology, composition, and quality traits of chicken Pectoralis major muscle affected by wooden breast abnormality. *Poult. Sci.* 95 (3), 651–659. doi:10.3382/ps/pev353

Soneson, C., Love, M. I., and Robinson, M. D. (2015). Differential analyses for RNA-seq: transcript-level estimates improve gene-level inferences. *F1000Res* 4, 1521. doi:10.12688/f1000research.7563.2

Song, Y., McFarland, D. C., and Velleman, S. G. (2011). Role of syndecan-4 side chains in Turkey satellite cell growth and development. *Dev. Growth Differ.* 53 (1), 97–109. doi:10.1111/j.1440-169X.2010.01230.x

Strand, M. E., Herum, K. M., Rana, Z. A., Skrbic, B., Askevold, E. T., Dahl, C. P., et al. (2013). Innate immune signaling induces expression and shedding of the heparan sulfate proteoglycan syndecan-4 in cardiac fibroblasts and myocytes, affecting inflammation in the pressure-overloaded heart. *FEBS J.* 280 (10), 2228–2247. doi:10.1111/febs.12161

Strand, M. E., Vanhaverbeke, M., Henkens, M. T. H. M., Sikking, M. A., Rypdal, K. B., Braathen, B., et al. (2023). Inflammation and syndecan-4 shedding from cardiac cells in ischemic and non-ischemic heart disease. *Biomedicines* 11 (4), 1066. [Online]. doi:10.3390/biomedicines11041066

Sztretye, M., Singlár, Z., Ganbat, N., Al-Gaadi, D., Szabó, K., Köhler, Z. M., et al. (2023). Unravelling the effects of syndecan-4 knockdown on skeletal muscle functions. *Int. J. Mol. Sci.* 24 (8), 6933. doi:10.3390/ijms24086933

Tidball, J. G. (2011). Mechanisms of muscle injury, repair, and regeneration. *Compr. Physiol.* 1 (4), 2029–2062. doi:10.1002/cphy.c100092

Tkachenko, E., Rhodes, J. M., and Simons, M. (2005). Syndecans: new kids on the signaling block. *Circulation Res.* 96 (5), 488–500. doi:10.1161/01.RES.0000159708.71142.c8

Tyanova, S., Temu, T., Sinitcyn, P., Carlson, A., Hein, M. Y., Geiger, T., et al. (2016). The Perseus computational platform for comprehensive analysis of (prote)omics data. *Nat. Methods* 13 (9), 731–740. doi:10.1038/nmeth.3901

Velleman, S. G. (2015). Relationship of skeletal muscle development and growth to breast muscle myopathies: a review. *Avian Dis.* 59 (4), 525–531. doi:10.1637/11223-063015-Review.1

Velleman, S. G. (2023). Broiler breast muscle myopathies: association with satellite cells. *Poult. Sci.* 102 (10), 102917. doi:10.1016/j.psj.2023.102917

Velleman, S. G., and Clark, D. L. (2015). Histopathologic and myogenic gene expression changes associated with wooden breast in broiler breast muscles. *Avian Dis.* 59 (3), 410–418. doi:10.1637/11097-042015-Reg.1

Velleman, S. G., Clark, D. L., and Tonniges, J. R. (2018). The effect of syndecan-4 and glypican-1 knockdown on the proliferation and differentiation of Turkey satellite cells differing in age and growth rates. *Comp. Biochem. Physiology Part A Mol. and Integr. Physiology* 223, 33–41. doi:10.1016/j.cbpa.2018.05.014

Velleman, S. G., Clark, D. L., and Tonniges, J. R. (2019). The effect of nutrient restriction on the proliferation and differentiation of Turkey pectoralis major satellite cells differing in age and growth rate. *Poult. Sci.* 98 (4), 1893–1902. doi:10.3382/ps/pey509

Velleman, S. G., Liu, X., Coy, C. S., and McFarland, D. C. (2004). Effects of syndecan-1 and glypican on muscle cell proliferation and differentiation: implications for possible functions during myogenesis. *Poult. Sci.* 83 (6), 1020–1027. doi:10.1093/ps/83.6.1020

Velleman, S. G., and Song, Y. (2017). Development and growth of the avian pectoralis major (breast) muscle: function of syndecan-4 and glypican-1 in adult myoblast proliferation and differentiation. *Front. physiology* 8, 577. doi:10.3389/fphys.2017.00577

von Maltzahn, J., Jones, A. E., Parks, R. J., and Rudnicki, M. A. (2013). Pax7 is critical for the normal function of satellite cells in adult skeletal muscle. *Proc. Natl. Acad. Sci.* 110 (41), 16474–16479. doi:10.1073/pnas.1307680110

Wacker, O., Manning, J., Zoufir, A., nf-core bot, Alexander, P., Domínguez, C. T., et al. (2023). nf-core/differentialabundance: v1.4.0 - 2023-11-27.

Wang, Z., Brannick, E., and Abasht, B. (2023). Integrative transcriptomic and metabolomic analysis reveals alterations in energy metabolism and mitochondrial functionality in broiler chickens with wooden breast. *Sci. Rep.* 13 (1), 4747. doi:10.1038/s41598-023-31429-7

Wold, J. P., Veiseth-Kent, E., Høst, V., and Løvland, A. (2017). Rapid on-line detection and grading of wooden breast myopathy in chicken fillets by near-infrared spectroscopy. *PLOS ONE* 12 (3), e0173384. doi:10.1371/journal.pone.0173384

Wright, W. E. (1985). Myoblast senescence in muscular dystrophy. *Exp. Cell Res.* 157 (2), 343–354. doi:10.1016/0014-4827(85)90119-3

Wu, T., Hu, E., Xu, S., Chen, M., Guo, P., Dai, Z., et al. (2021). clusterProfiler 4.0: a universal enrichment tool for interpreting omics data. *Innov. (Camb)* 2 (3), 100141. doi:10.1016/j.xinn.2021.100141

Xian, X., Gopal, S., and Couchman, J. R. (2009). Syndecans as receptors and organizers of the extracellular matrix. *Cell Tissue Res.* 339 (1), 31–46. doi:10.1007/s00441-009-0829-3

Xu, J., and Velleman, S. G. (2023). Effects of thermal stress and mechanistic target of rapamycin and wingless-type mouse mammary tumor virus integration site family pathways on the proliferation and differentiation of satellite cells derived from the breast muscle of different chicken lines. *Poult. Sci.* 102 (5), 102608. doi:10.1016/j.psj.2023.102608

Yan, Z., Chen, G., Yang, Y., Sun, L., Jiang, Z., Feng, L., et al. (2014). Expression and roles of syndecan-4 in dental epithelial cell differentiation. *Int. J. Mol. Med.* 34, 1301–1308. doi:10.3892/ijmm.2014.1910

Yin, H., Price, F., and Rudnicki, M. A. (2013). Satellite cells and the muscle stem cell niche. *Physiol. Rev.* 93 (1), 23–67. doi:10.1152/physrev.00043.2011

Yoshioka, K., Kitajima, Y., Okazaki, N., Chiba, K., Yonekura, A., and Ono, Y. (2020). A modified pre-plating method for high-yield and high-purity muscle stem cell isolation from human/mouse skeletal muscle tissues. *Front. Cell Dev. Biol.* 8, 793. doi:10.3389/fcell.2020.00793

Young, J. F., and Rasmussen, M. K. (2020). Differentially expressed marker genes and glycogen levels in pectoralis major of Ross308 broilers with wooden breast syndrome indicates stress, inflammation and hypoxic conditions. *Food Chem. (Oxf)* 1, 100001. doi:10.1016/j.fochms.2020.100001

Yu, G., Wang, L.-G., Han, Y., and He, Q.-Y. (2012). clusterProfiler: an R Package for comparing biological themes among gene clusters. *OMICS A J. Integr. Biol.* 16 (5), 284–287. doi:10.1089/omi.2011.0118

Yu, Y., Smith, M., and Pieper, R. (2014). A spinnable and automatable StageTip for high throughput peptide desalting and proteomics. *Protoc. Exch.* doi:10.1038/protex.2014.033

Zammit, P. S., Relaix, F., Nagata, Y., Ruiz, A. P., Collins, C. A., Partridge, T. A., et al. (2006). Pax7 and myogenic progression in skeletal muscle satellite cells. *J. Cell Sci.* 119 (Pt 9), 1824–1832. doi:10.1242/jcs.02908

Zhang, W., and Liu, H. T. (2002). MAPK signal pathways in the regulation of cell proliferation in mammalian cells. *Cell Res.* 12 (1), 9–18. doi:10.1038/sj.cr.7290105

Zuidhof, M. J., Schneider, B. L., Carney, V. L., Korver, D. R., and Robinson, F. E. (2014). Growth, efficiency, and yield of commercial broilers from 1957, 1978, and 2005. *Poult. Sci.* 93 (12), 2970–2982. doi:10.3382/ps.2014-04291

frontiers | Frontiers in Physiology

TYPE Opinion
PUBLISHED 20 January 2025
DOI 10.3389/fphys.2024.1520196

OPEN ACCESS

EDITED BY
Monika Proszkowiec-Weglarz,
United States Department of Agriculture,
United States

REVIEWED BY
Sami Dridi,
University of Arkansas, United States
Elisabeth Duval,
Institut National de recherche pour l'agriculture, l'alimentation et l'environnement (INRAE), France

*CORRESPONDENCE
Gale M. Strasburg,
stragale@msu.edu

RECEIVED 30 October 2024
ACCEPTED 30 December 2024
PUBLISHED 20 January 2025

CITATION
Guo W, Velleman SG and Strasburg GM (2025) From discovery to application: merging modern omics with traditional hypothesis-driven approaches in muscle myopathy studies. *Front. Physiol.* 15:1520196. doi: 10.3389/fphys.2024.1520196

From discovery to application: merging modern omics with traditional hypothesis-driven approaches in muscle myopathy studies

Wei Guo[1], Sandra G. Velleman[2] and Gale M. Strasburg[3]*

[1]Department of Animal and Dairy Sciences, University of Wisconsin-Madison, Madison, WI, United States, [2]Department of Animal Sciences, The Ohio State University, Wooster, OH, United States, [3]Department of Food Science and Human Nutrition, Michigan State University, East Lansing, MI, United States

KEYWORDS

hypothesis-testing approach, hypothesis-generating approach, omics, meat quality, muscle myopathy

Introduction–A historical perspective

The conventional wisdom within the scientific community dictates that a complete understanding of the factors that determine the quality of muscle as a food requires that we define the molecular mechanisms of muscle growth and development, of the function of muscle as an organ, and ultimately of *postmortem* conversion of muscle tissue to meat. As a corollary, understanding the mechanistic underpinnings that lead to myopathies such as wooden breast, white striping, or pale, soft, exudative meat would–ideally–be applied by breeders, producers, and processors to prevent or mitigate meat quality problems. However, the growing gap between knowledge accumulation and its application suggests that we pause and reconsider our approach to addressing scientific questions.

Interestingly, the gap between knowledge accumulation and application has deep roots in our field. In 1965 and 1969, the University of Wisconsin-Madison hosted two international, ground-breaking symposia on "The Physiology and Biochemistry of Muscle as a Food." Attendees of this interdisciplinary conference included medical scientists, physiologists, biochemists, pathologists, nutritional scientists, and meat scientists, all sharing the goal of better understanding the relationship between the biology of living muscle and the quality of muscle tissue as a food.

In the first chapter of the proceedings of the second meeting (Marsh et al., 1970), published in 1970, Dr. B. Bruce Marsh quoted from a paper by Prof. E. C. Bate-Smith published in 1948 in the first Volume of *Advances in Food Research*:

> "In the past two decades . . . fundamental knowledge of the physiological and biochemical properties and behavior of muscle has increased out of all recognition. Perhaps because of the bewildering rate of growth of this fundamental knowledge and the constantly changing conception of muscle which has resulted, there has not been . . . any striking application of the principles of modern biochemistry to the technology of handling of meat animals and meat."

Marsh goes on to observe:

> "... one's attention is drawn ... to [Bate-Smith's] thoughts on the bewildering growth of fundamental knowledge, on 'the constantly changing conception of muscle,' and on the absence of 'any striking application of these principles' to meat technology. These views are even more relevant today than they were in 1948; for although our knowledge of meat and its qualities has grown enormously in the intervening years, knowledge of muscle and its behavior has increased even more. The gap between discovery and application is still widening. The output of new information, the development of new concepts, the postulation of new theories --- these are accelerating at such a rate that we may liken muscle biology to an expanding universe and ourselves to the particles within it, fast receding from each other and suffering the inevitable consequence of greater and greater isolation. Compounding the problem, new branches of science splinter from the old, and studies which a few years ago were clearly together within one particular discipline are now so altered that they are scarcely recognizable as relatives."

Since those words were published over five decades ago, we have witnessed an exponential growth of these "new branches of science" and a shift in our approach to doing science. In the following sections, we contrast the historical approach to addressing scientific questions with that which is increasingly dominant in today's culture. We then illustrate with examples the importance of using hypothesis-generating (data-driven) science to generate hypotheses that address mechanistic questions. Finally, we propose a framework for integrating the two approaches and application of knowledge.

Present-day challenges: hypothesis-based vs. hypothesis-generating research

Historically, science made incremental advances by asking a question based on observations, formulating a hypothesis, explaining the observations, and testing that hypothesis with an appropriate experimental design. The results of the experiment(s) would be analyzed and interpreted, and the conclusions drawn would lead to a new hypothesis.

Contrast this hypothesis-based approach with that used today by many muscle biologists (including ourselves) as we routinely employ techniques from these "new branches of science" such as nucleic acid sequencing, transcriptomics, proteomics, lipidomics, metabolomics to address broad-based biological questions. For example, how do the muscles of the meat animal respond to heat or cold stress, and what are the implications for meat quality?

Applying transcriptome analysis, for example, may provide information on genes that are up- or downregulated in response to a biological perturbation or stress. These genes may be organized into clusters that are associated with specific biological pathways and functions, and in turn, may suggest a hypothesis to be tested that would not only define a mechanism by which muscle responds to the stress, but also, in so doing, may suggest a dietary or other management intervention that may result in reduced incidence of myopathy due to a stress, and improvement in meat quality.

We contend that collectively, we all too frequently conduct and publish our studies that conclude with pious words such as "these results provide new information that may be useful for breeders and producers for improvement of avian health and meat quality." If that is our endpoint, we have missed the opportunity to generate hypotheses that could lead to discovery of mechanisms that indeed lead to strategies that can be applied at the level of breeder and producer.

This shift in research paradigms introduces both opportunities and challenges. On one hand, hypothesis-generating research allows the discovery of new mechanisms that may otherwise remain uncovered. On the other hand, it can lead to data overload, making it difficult to pinpoint the most significant findings. To fully utilize the power of -omics research, scientists must integrate these exploratory methods with traditional hypothesis-driven research. Although exploratory data alone may provide new insights, it is critical that researchers develop testable hypotheses from these findings, ensuring that molecular discoveries lead to practical, mechanistic insights. By integrating these approaches, we can narrow the gap between data collection and actionable applications. In the following section, we offer examples of work that illustrate this approach.

Examples of -omics research as hypothesis-generating research

Example 1: Sporer et al. (2011) investigated temporal changes in breast muscle gene expression in two lines of turkeys at three stages of muscle development: 18d embryo (when the breast muscle is undergoing hyperplasia), 1-day post-hatch (when muscle is undergoing hypertrophy), and 16 weeks (market age of the turkey). Of the >3,000 differentially expressed genes (FDR <0.0001), three were selected for further investigation for their role in muscle growth and development: versican (*VCAN*), matrix Gla protein (*MGP*), and death-associated protein (*DAP*). These selections were based on the magnitude of expression changes with developmental stage coupled with lack of information on their roles in myogenesis (Velleman et al., 2012). Velleman et al. then used small interfering RNA (siRNA) in cultured satellite cells to characterize the roles of these genes in proliferation and differentiation (Velleman et al., 2012). Subsequent studies further documented the critical role of DAP in satellite cell proliferation and differentiation (Shin et al., 2013; Horton et al., 2020). Although the significance of these genes is now evident, the next steps should extend this work to define the specific functions of these gene products.

Example 2: Lake et al. (2021) used genome-wide association and transcriptome studies to identify genes associated with the wooden breast myopathy in broilers. Velleman and colleagues then selected the top differentially expressed genes in Wooden Breast that are not typically associated with the growth or regeneration of skeletal muscle for further study in a cell culture system examining their effect on satellite cell activity (Velleman et al., 2022; Velleman et al., 2024). Of the genes studied, Calponin 1 (CNN1) and PHD and RING finger domain-containing protein 1 (PHRF1) were the most promising targets, as they were the top genes affected by Wooden Breast determined by Genome Wide Association studies. The

follow-up studies on these genes examined these novel genes for their effects on satellite cells. CNN1 is a smooth muscle protein that binds F-actin and tropomyosin. In Wooden Breast myopathy-affected muscle, sarcomere integrity is lost, and CNN 1 may be involved in the maintenance of actin filament integrity. Like CNN1, PHRF1 was not previously reported in skeletal muscle until the study by Lake and colleagues (Lake et al., 2021). PHRF1 stabilizes genomic integrity with DNA damage and in tumorigenesis (Chang et al., 2015). Wooden Breast results in DNA damage; PHRF1 may localize in Wooden-Breast-affected muscle to areas of genomic damage and be involved in the stabilization of these lesions. Like Example 1, the next steps should target the specific mechanisms by which these proteins function.

A call for deeper mechanistic understanding

A balanced research approach that integrates both strategies would be ideal for translating molecular discoveries into meaningful biological insights and practical applications. One of the greatest challenges researchers face when transitioning from hypothesis-generating to hypothesis-driven research is selecting the right target gene(s) from the vast -omics dataset. Although most researchers focus on the greatest -fold changes (highest or lowest), this approach can lead to false starts. Genes that show dramatic changes in expression may not be the most important contributors to the observed phenotype, while some key regulatory genes or non-coding RNAs, which act as "fine-tuners," may exhibit only modest expression changes. The overwhelming amount of data generated by -omics research often makes it difficult to discern which gene(s) are truly driving a particular phenotype.

To overcome this issue, a more systematic and integrative approach to gene selection is needed. We offer the following thoughts as a possible strategy for breeders to consider in the selection of genes for further investigation:

1. Network and Pathway Analysis: Rather than focusing solely on the highest or lowest expressed genes, integrating systems biology approaches—such as gene regulatory network or pathway analysis—can help prioritize genes that play central roles in biological processes. By understanding how genes interact within networks, researchers can identify key nodes that may have outsized influence on phenotype, even if their expression levels are not extreme.
2. Functional Annotation and Validation: Combining -omics data with existing knowledge of gene function can guide researchers toward more promising candidates. Databases that annotate gene function, evolutionary conservation, or known involvement in specific biological processes can provide context for selecting target genes. Furthermore, targeted functional studies (e.g., RNAi, CRISPR/Cas9) can quickly validate the role of key genes.
3. Integration of Multiple Layers: Cross-referencing data from multiple -omics layers (e.g., transcriptomics, proteomics, and metabolomics) can improve gene selection accuracy. For example, if a gene shows differential expression at the RNA level and corresponding changes at the protein or metabolite level, this strengthens the case for its functional relevance.
4. Phenotype-Gene Correlation Models: Developing computational models that link gene expression patterns to specific phenotypic traits can aid in the identification of causal genes. Machine learning techniques, in particular, can be used to predict which genes are most likely responsible for observed phenotypes, helping to narrow down targets for experimental validation.

Due to space limitations of an opinion paper, a comprehensive discussion of strategies to extend experimental results to applications for use by breeders and producers is beyond the scope of this article. However, researchers may refer to previous studies that have proposed detailed strategies aimed at improving traits and achieving desired phenotypes, such as enhanced meat quality characteristics (Te Pas et al., 2017; Rexroad et al., 2019).

Conclusion

In the 54 years since Marsh noted the widening gap between discovery and application, this separation has exponentially intensified. Despite the remarkable advances in our understanding of muscle biology, driven largely by the explosion of omics technologies, the challenges remain the same: translating new discoveries into tangible solutions for animal agriculture and biomedical science. The vast increase in data from -omics has illuminated new biological pathways and mechanisms; however, the practical integration and application of these findings into meat production, animal health, and disease prevention has lagged. Modern molecular biology tools have provided us unprecedented access to the vast and intricate networks regulating muscle growth and function; grabbing this opportunity to integrate the hypothesis-generating -omics data with traditional, hypothesis-driven research lies in the potential to address economically costly myopathies, such as Wooden Breast disease in poultry.

In conclusion, integration of a traditional hypothesis-driven research with modern -omics approaches represent a unique and powerful opportunity to close the gap that has persisted for decades. By embracing both strategies, we can advance our understanding of muscle biology and deliver the practical benefits envisioned over 50 years ago. Therefore, the challenges are clear: ensuring that the wealth of data generated by -omics technologies does not remain disconnected from practical applications but instead leads to developing innovative and actionable solutions that improve animal health, meat quality, and beyond.

Author contributions

WG: Writing–original draft, Writing–review and editing. SV: Writing–review and editing. GS: Conceptualization, Writing–original draft, Writing–review and editing.

Funding

The author(s) declare that no financial support was received for the research, authorship, and/or publication of this article.

Conflict of interest

The authors declare that the research was conducted in the absence of any commercial or financial relationships that could be construed as a potential conflict of interest.

The author(s) declared that they were an editorial board member of Frontiers, at the time of submission. This had no impact on the peer review process and the final decision.

Generative AI statement

The author(s) declare that no Generative AI was used in the creation of this manuscript.

Publisher's note

References

Chang, C. F., Chu, P. C., Wu, P. Y., Yu, M. Y., Lee, J. Y., Tsai, M. D., et al. (2015). PHRF1 promotes genome integrity by modulating non-homologous end-joining. *Cell Death Dis.* 6 (4), e1716. doi:10.1038/cddis.2015.81

Horton, K. A., Sporer, K. R. B., Tempelman, R. J., Malila, Y., Reed, K. M., Velleman, S. G., et al. (2020). Knockdown of death-associated protein expression induces global transcriptome changes in proliferating and differentiating muscle satellite cells. *Front. Physiol.* 11, 1036. doi:10.3389/fphys.2020.01036

Lake, J. A., Dekkers, J. C. M., and Abasht, B. (2021). Genetic basis and identification of candidate genes for wooden breast and white striping in commercial broiler chickens. *Sci. Rep.* 11 (1), 6785. doi:10.1038/s41598-021-86176-4

Marsh, B. B. (1970). "Muscle as a food," in *The Physiology and biochemistry of muscle as food*. Editors E. J. Briskey, R. G. Cassens, and B. B. Marsh (Madison, Wis: University of Wisconsin Press), 2, 3–10.

Rexroad, C., Vallet, J., Matukumalli, L. K., Reecy, J., Bickhart, D., Blackburn, H., et al. (2019). Genome to phenome: improving animal health, production, and well-being - a new usda blueprint for animal genome research 2018-2027. *Front. Genet.* 10, 327. doi:10.3389/fgene.2019.00327

Shin, J., McFarland, D. C., Strasburg, G. M., and Velleman, S. G. (2013). Function of death-associated protein 1 in proliferation, differentiation, and apoptosis of chicken satellite cells. *Muscle Nerve* 48 (5), 777–790. doi:10.1002/mus.23832

Sporer, K. R., Tempelman, R. J., Ernst, C. W., Reed, K. M., Velleman, S. G., and Strasburg, G. M. (2011). Transcriptional profiling identifies differentially expressed genes in developing Turkey skeletal muscle. *BMC Genomics* 12, 143. doi:10.1186/1471-2164-12-143

Te Pas, M. F., Madsen, O., Calus, M. P., and Smits, M. A. (2017). The importance of endophenotypes to evaluate the relationship between genotype and external phenotype. *Int. J. Mol. Sci.* 18 (2), 472. doi:10.3390/ijms18020472

Velleman, S. G., Coy, C. S., and Abasht, B. (2022). Effect of expression of PPARG, DNM2L, RRAD, and LINGO1 on broiler chicken breast muscle satellite cell function. *Comp. Biochem. Physiol. A Mol. Integr. Physiol.* 268, 111186. doi:10.1016/j.cbpa.2022.111186

Velleman, S. G., Coy, C. S., and Abasht, B. (2024). Research Note: chicken breast muscle satellite cell function: effect of expression of CNN1 and PHRF1. *Poult. Sci.* 103 (7), 103781. doi:10.1016/j.psj.2024.103781

Velleman, S. G., Sporer, K. R., Ernst, C. W., Reed, K. M., and Strasburg, G. M. (2012). Versican, matrix Gla protein, and death-associated protein expression affect muscle satellite cell proliferation and differentiation. *Poult. Sci.* 91 (8), 1964–1973. doi:10.3382/ps.2012-02147

frontiers | Frontiers in Physiology

TYPE Original Research
PUBLISHED 17 February 2025
DOI 10.3389/fphys.2025.1543788

OPEN ACCESS

EDITED BY
Krystyna Pierzchała-Koziec,
University of Agriculture in Krakow, Poland

REVIEWED BY
Prasanna Katti,
Indian Institute of Science Education and Research, India
Chidozie Okoye,
University of Nigeria, Nigeria

*CORRESPONDENCE
Sami Dridi,
dridi@uark.edu

RECEIVED 11 December 2024
ACCEPTED 27 January 2025
PUBLISHED 17 February 2025

CITATION
Greene ES, Chen PR, Walk C, Bedford M and Dridi S (2025) Mitochondrial dysfunction is a hallmark of woody breast myopathy in broiler chickens.
Front. Physiol. 16:1543788.
doi: 10.3389/fphys.2025.1543788

Mitochondrial dysfunction is a hallmark of woody breast myopathy in broiler chickens

Elizabeth S. Greene[1], Paula R. Chen[2], Carrie Walk[3], Mike Bedford[3] and Sami Dridi[1]*

[1]Center of Excellence for Poultry Science, Division of Agriculture, University of Arkansas, Fayetteville, AR, United States, [2]USDA-ARS, Plant Genetics Research Unit, Columbia, MO, United States, [3]AB Vista, Marlborough, United Kingdom

The woody breast (WB) myopathy poses significant economic and welfare concerns to the poultry industry, however, there is no effective strategy to mitigate this pathology due to its unknown etiology. After showing previously that hypoxia is a key factor in WB progression, we used here various techniques demonstrating dysregulated mitochondria (morphology, biogenesis, tethering, function, and bioenergetics) in WB-affected muscles and in hypoxic myoblasts compared to healthy tissues and normoxic cells, respectively. The increased levels of calcium (Ca^{2+}) in both WB-affected tissues and hypoxic myoblasts suggested that mitochondrial Ca^{2+} overload is likely a leading cause for mitochondrial dysfunction that merits further in-depth investigation. These findings are the first, to the best of our knowledge, to provide fundamental insights into the underlying molecular mechanisms of WB and open new vistas for understanding the interplay between calcium, mitochondrial (dys)function, and avian muscle health for subsequent development of effective preventative/corrective strategies.

KEYWORDS

woody breast, broiler, mitochondrial dysfunction, hypoxia, bioenergetics

1 Introduction

Concurrent with an increasing global population, demand for poultry, and specifically chicken meat, is projected to increase over the coming decades (Dohlman et al., 2024). Though selection for increased growth, efficiency, and meat yields has made incredible progress to date, this trajectory must be maintained and improved. One challenge, however, has been the parallel rise in growth-related abnormalities that impact production, welfare, and sustainability. The woody breast (WB) myopathy in chicken breast meat was initially described over 10 years ago (Sihvo et al., 2014), and its occurrence is surging at global scale, already present in many world regions (de Brot et al., 2016; Cemin et al., 2018; Kawasaki et al., 2018). It is deleteriously impacting global chicken meat production and quality, leading to downgraded value, meat condemnation, and increased processing charges, all together results in heavy economic losses (Soglia et al., 2016).

A plethora of research since its initial identification has sought to define causes and potential preventive-corrective measures. Characterized by a noticeable hardness of the *Pectoralis major* muscle (Sihvo et al., 2014), with muscle fiber degeneration, necrosis, lipidosis, and fibrosis evident upon histological examination (Sihvo et al., 2014; Velleman and Clark, 2015), WB presents also a significant wellbeing concern to the poultry industry. Although the underlying mechanisms of this myopathy yet to be fully characterized, work

by our group (Greene et al., 2019; Emami et al., 2021) and others (Zhang et al., 2024) indicates a hypoxic state in WB muscles, associated with increased muscle fiber size, decreased capillary density, and therefore, decreased oxygen supply and clearance of metabolic waste products from the tissue. Additionally, in skeletal muscle, it has been established that chronic hypoxic conditions lead to the production of mitochondrial reactive oxygen species (ROS) and subsequent oxidative stress (Clanton, 2007), all factors likely contributing to the WB myopathy.

A major function of mitochondria is the generation of adenosine triphosphate (ATP) for energy through oxidative phosphorylation (OXPHOS). The mitochondria of skeletal muscle are also a primary source of ROS, as well as the major target of oxidative damage and the intracellular redox buffering system (Murphy, 2009), and mitochondrial dysfunction has been identified as an underlying factor in multiple muscular diseases (Chen et al., 2022). This dysfunction can be caused by defective OXPHOS (Fernandez-Vizarra and Zeviani, 2021), mitochondrial DNA (mtDNA) mutations (Rossignol et al., 2003), Ca^{2+} imbalances (Garbincius and Elrod, 2022), and structural defects (Vincent et al., 2016; Jenkins et al., 2024). In addition, an imbalance between mitochondrial fusion and fission (Sprenger and Langer, 2019), lysosomal dysfunction (de la Mata et al., 2016), and defects in mitophagy (Gottlieb et al., 2011) can lead to mitochondrial damage. However, most of this in-depth relationship between mitochondrial (dys) function and muscle health has been elucidated in human myopathies and murine models. We hypothesized that mitochondrial dysfunction is also a key contributor to the WB condition, which is a distinct myopathy peculiar and unique to poultry. By using *in vivo*-derived samples and a highly relevant *in vitro* primary cell culture model (Greene et al., 2023), we showed a disproportional mitochondrial morphology along with dysregulated function, bioenergetics, and dynamics in WB-affected muscle and hypoxic primary myotubes.

2 Materials and methods

2.1 Care and use of animals

This study was conducted in accordance with the National Institutes of Health recommendations guide for laboratory animal use and care. All the procedures in this study were approved by the University of Arkansas Animal Care and Use Committee under protocol #21050. Day-old male Cobb 500 broiler chicks (n = 720) were reared in floor pens covered with clean pine wood shavings and equipped with separate feeders and water lines in a controlled environment. Ambient temperature was gradually reduced from 32°C to 25°C by day 21. A 23 h light/1 h dark cycle and a ~30–40% relative humidity was maintained throughout the experiment. Birds were fed a nutrient adequate diet, recommended by the poultry industry and formulated to meet Cobb 500 nutrition requirements, with starter, grower, and finisher phases.

2.2 Processing and WB myopathy scoring

Birds (n = 512) were processed on day 56 at the University of Arkansas Pilot Processing Plant (Fayetteville, AR) using a commercial inline system. Feed was removed 10 h prior to processing, while *ad libitum* access to water was maintained. Birds were electrically stunned, exsanguinated, soft scalded, de-feathered, and eviscerated, then chilled for 4 h prior to deboning. Breast fillets were hand scored by a well-trained person for WB on a scale of 0–3, with 0 showing no signs of WB, 1 was mild, 2 was considered moderate, and score 3 being severe WB (Kuttappan et al., 2016; Dalgaard et al., 2018; Greene et al., 2019). Breast muscle samples taken from the cranial region of score 0 (normal) and 3 (severe WB) were either snap-frozen in liquid nitrogen and stored at −80 °C for RNA and protein analysis or fixed for electron microscopy.

2.3 Chicken primary myoblast culture

Chicken primary myoblasts were isolated from E18 embryos as previously described (Greene et al., 2023). Cells were cultured at 37°C in a humidified atmosphere in complete media for the indicated times. Hypoxia was induced by placing the cultures into a gas-tight hypoxic chamber (1% O_2/5% CO_2/94% N_2; The Baker Company, Inc., Sanford, ME) for 24 h. The control cells were maintained at normoxic conditions (5% CO_2/95% O_2).

2.4 Transmission electron microscopy

Unless otherwise stated, all reagents were purchased from Electron Microscopy Sciences and all specimen preparation was performed at the Electron Microscopy Core Facility, University of Missouri. Samples were fixed in 2% paraformaldehyde, 2% glutaraldehyde in 100 mM sodium cacodylate buffer, pH 7.35. Tissues were rinsed with 100 mM sodium cacodylate buffer, pH 7.35 (Sigma Aldrich, St. Louis, MO) and 130 mM sucrose. Secondary fixation was performed using 1% osmium tetroxide (Ted Pella, Inc. Redding, California) in cacodylate buffer. Specimens were incubated at 4°C for 1 h, then rinsed with cacodylate buffer and further with distilled water. *En bloc* staining was performed using 1% aqueous uranyl acetate and incubated at 4°C overnight, then rinsed with distilled water. A graded dehydration series was performed using ethanol, transitioned into acetone, and dehydrated tissues were then infiltrated with EMbed 812 resin and polymerized at 60°C overnight. Semithin sections were at a thickness of 1 µm and stained with Toluidine blue to locate the region of interest. The block face was additionally trimmed for the region of interest and sections were cut to a thickness of 75 nm using an ultramicrotome (Ultracut UCT, Leica Microsystems, Germany) and a diamond knife (Diatome, Hatfield PA). Images were acquired with a JEOL JEM 1400 transmission electron microscope (JEOL, Peabody, MA) at 80 kV on a Gatan Rio CMOS camera (Gatan, Inc., Pleasanton, CA).

2.5 Mitochondrial isolation from breast tissue

Mitochondria were isolated from chicken breast tissue as previously described (Frezza et al., 2007), with modifications. Briefly, ~800 mg of chicken breast muscle was thawed in ice-cold PBS/10 mM EDTA. The tissue was then finely minced with ice-cold scissors and washed 2x with PBS/10 mM EDTA. The minced muscle tissues were incubated on ice for 30 min in PBS/10 mM EDTA/0.05% Trypsin. Samples were then centrifuged (10 min, 200 g, 4°C) and supernatant was discarded. The pellet was resuspended in 67 mM sucrose/50 mM Tris-HCl/50 mM KCl/10 mM EDTA/0.2% BSA, pH 7.4 then homogenized via Dounce homogenizer for 10 passes. Samples were then centrifuged (5 min, 200 g, 4°C). The supernatant was transferred to a clean tube, and the process was repeated twice. The supernatant was again transferred to a new tube and centrifuged (10 min, 700 g, 4°C). Supernatant was transferred to a clean tube and centrifuged (10 min, 8,000 g, 4°C). The pellet was resuspended in ice-cold 250mM sucrose/3mM Tris-EGTA/10 mM Tris-HCl, pH 7.4, then centrifuged (10 min, 8,000 g, 4°C). The supernatant was removed by decanting, and the mitochondrial pellet was resuspended in the remaining buffer.

2.6 Mitochondrial respiration

Primary myotubes were subject to hypoxia as described above and mitochondrial respiration was measured using the Seahorse XF flux analyzer (Agilent, Santa Clara, CA), as previously described (Dhamad et al., 2021). Basal respiration, ATP production, proton leak, non-mitochondrial oxygen consumption, maximal respiration, and spare respiratory capacity were calculated as previously described (Lassiter et al., 2014; Lassiter et al., 2015). The respiratory capacity of complex I, II, and IV was measured in isolated mitochondria from normal and WB muscle using the protocol of Osto et al. (2020), with 5 µg of mitochondria per well. Mitochondrial respiratory capacity through complex I, II, and IV was calculated as follows:

$$\text{Complex I: } OCR_{NADH} - OCR_{antimycin}$$

$$\text{Complex II: } OCR_{succinate+rotenone} - OCR_{antimycin}$$

$$\text{Complex IV: } OCR_{TPMD+ascorbate} - OCR_{azide}$$

2.7 RNA extraction and RT-qPCR

Total RNA was extracted using Trizol reagent (Life Technologies, Carlsbad, CA) according to the manufacturer's protocol, and concentration and quality were determined using the Take3 microvolume plate of the Synergy HTX multimode microplate reader (BioTek, Winooski, VT). cDNA synthesis and qPCR were performed as previously described (Lassiter et al., 2015). Briefly, RNA was reverse transcribed using qScript cDNA Synthesis Supermix (Quanta Biosciences, Gaithersburg, MD), and amplified by qPCR (Applied Biosystems 7,500 Real Time System) with Power-Up Sybr green master mix (Life Technologies, Carlsbad, CA). Relative expression of the target genes was determined using the $2^{-\Delta\Delta CT}$ method, with normalization to ribosomal 18s gene expression (Schmittgen and Livak, 2008). Oligonucleotide primer sequences specific to chicken are presented in Table 1.

2.8 Western blot

Western blot was performed as previously described (Lassiter et al., 2015). Briefly, muscle tissue, isolated mitochondria, and primary cells were homogenized in lysis buffer containing protease- and phosphatase-inhibitors. Protein concentrations were determined via Bradford assay kit (Bio-Rad, Hercules, CA) and the Synergy HTX multimode microplate reader (BioTek, Winooski, VT). Proteins were separated on 4%–12% gradient Bis-Tris gels (Life Technologies, Carlsbad, CA), and transferred to PVDF membranes. Membranes were blocked with 5% non-fat milk in TBS-T for 1 h at room temperature, then incubated with primary antibodies overnight at 4°C. Primary antibodies used were rabbit anti-ANT1 (1:1,000, PA1-85116, ThermoFisher Scientific, Waltham, MA), rabbit anti-INF2 (1:1,000, A303-427A, Bethyl Laboratories, Montgomery, TX), rabbit anti-ITPR2 (1:1,000, A19320, ABClonal, Woburn, MA), rabbit anti-MFN1 (1:1,000, ab104274, Abcam, Boston. MA), rabbit anti-MFN2 (1:1,000, 12186-1-AP, Proteintech, Rosemont, IL), rabbit anti-OMA1 (1:1,000, ab104316, Abcam, Boston, MA), rabbit anti-OPA1 (1:1,000, A9833, ABClonal, Woburn, MA), rabbit anti VDAC1 (1:1,000, 4,866, Cell Signalling, Danvers, MA), and OXPHOS antibody cocktail (1:1,000, ab110413, Abcam, Boston. MA). Rabbit anti-GAPDH (1:1,000, NB300-327, Novus Biologicals, Centennial, CO) was used as a loading control, with representative blots shown. HRP-conjugated secondary antibodies (goat anti-rabbit IgG #7074 and rabbit anti-mouse IgG #7076, Cell Signaling, Danvers, MA) were used at 1:5,000 dilution for 1 h at room temperature. The signal was visualized by chemiluminescence (Super ECL, ABP Biosciences, North Potomac, MD) and captured by FluorChem M MultiFluor System (ProteinSimple, Santa Clara, CA). Image acquisition and analysis were performed with AlphaView software (version 3.4.0.0, ProteinSimple, Santa Clara, CA).

2.9 Calcium assay

Total calcium concentration in muscle tissue and primary myotubes was measured by a Calcium Assay Kit (#701220, Cayman Chemical, Ann Arbor, MI) according to manufacturer's recommendations.

2.10 ATP synthase enzyme activity and ATP assay

ATP Synthase Enzyme activity was measured in isolated mitochondria from normal and WB tissues and primary myotubes using the ATP synthase Enzyme Activity Microplate Assay Kit (ab109714, Abcam, Boston, MA) according to manufacturer's recommendations. Briefly, 5ug of protein was plated in duplicate into a 96 well plate. The activity of the ATP

10.3389/fphys.2025.1543788

TABLE 1 Oligonucleotide qPCR primers.

Gene[a]	Accession number[b]	Primer sequence (5′-3′)	Orientation	Product size, bp
ANT1	NM_204231	GCAGCTGATGTCGGCAAA	For	56
		CAGTCCCCGAGACCAGAGAA	Rev	
UCP	NM_204107	TGGCAGCGAAGCGTCAT	For	59
		TGGGATGCTGCGTCCTATG	Rev	
NFE2L2	NM_205117	AAACGACAACCTGGCTGAAGTAA	For	59
		TCTCCGCTGGCTTGGTTTC	Rev	
SKI	NM_001039318	GGCCCTGCTGCTTTCTCA	For	75
		AGGTTCCGCTGGGTCTTTG	Rev	
DNM1	XM_015279546	GAACTTTCGCCCCGATGA	For	57
		TGGACCATCTGAAGCAGAGCTT	Rev	
MFN1	NM_001012931	CGGTGGTTTTGAGCCCATT	For	57
		GAAGCCTGGCACCCAAATC	Rev	
MFN2	XM_040689232	ATGTGCCTGTGACACGTTCAC	For	63
		TCGAGTGTCAGGCAGCTTCTT	Rev	
OMA1	XM_422503	TCACTATGATTTGGGCCATCTG	For	59
		GATCCGCTGGCCAACAAC	Rev	
OPA1	NM_001039309	CCCAAGCAGGATCCAACAA	For	73
		AACAACTGCAAAGTAACCCAAAGC	Rev	
mtDNA	X52392	ACACCTGCGTTGCGTCCTA	For	58
		ACGCAAACCGTCTCATCGA	Rev	
PGC1α	NM_001006457	GAGGATGGATTGCCTTCATTTG	For	62
		GCGTCATGTTCATTGGTCACA	Rev	
PGC1β	XM_040647119	TTGCCGGCATTGGTTTCT	For	66
		CACGGGAAGCCACAGGAA	Rev	
SSBP1	NM_001278007	CACAGACAGGTGATATCAGTCAGAAG	For	65
		GAGGCCTGGTCTGAAGACAGA	Rev	
PPARα	NM_001001464	CAAACCAACCATCCTGACGAT	For	64
		GGAGGTCAGCCATTTTTTGGA	Rev	
PPARγ	NM_001001460	CACTGCAGGAACAGAACAAAGAA	For	67
		TCCACAGAGCGAAACTGACATC	Rev	
ITPR1	XM_046925976	TCCGTGTACGTTTAGTTCATCTTGTAA	For	116
		CGGCGTGTGCAAACAGT	Rev	
ITPR2	XM_040657966	GGAAGTTTTGGATGTGGTCATTACT	For	90
		ACTCCGAATATCTGAGCCAAAAT	Rev	
ITPR3	XM_040691640	TGCACGCCAGCAACTATGAG	For	87
		GGTTGATTTTCCAGCTGGTGTT	Rev	
INF2	XM_040672115	AAACCTTGCCTGCGGAGAT	For	61
		TGCGGATCCTTAATGCTCTTC	Rev	

(Continued on following page)

TABLE 1 (*Continued*) Oligonucleotide qPCR primers.

Gene[a]	Accession number[b]	Primer sequence (5′-3′)	Orientation	Product size, bp
FUNDC1	NM_001276363	CGCACCGCCCCAGAA	For	61
		ATTCCGTTAGGTCCAACACTTCA	Rev	
TOMM20	XM_423972	TCGGCTACTGCATCTACTTCGA	For	62
		CAGCCGGTTCTTGAAATTCG	Rev	
VDAC1	NM_001033869	GGCTGCGACATGGATTTTG	For	55
		GCACCAGGGCTCCACGTAT	Rev	
SPIRE1	XM_040664833	AAGTGATCGGGGATTTACGAA	For	60
		TGTATTGACGCTCTTGGACTTTCT	Rev	
18s	AF173612	TCCCCTCCCGTTACTTGGAT	For	60
		GCGCTCGTCGGCATGTA	Rev	

[a]ANT1, adenine nucleotide translocator 1; UCP, uncoupling protein; NFE2L2, nuclear factor erythroid 2-related factor 2; SKI, nuclear sarcoma viral oncogene homolog; DNM1, dynamin-related protein 1; MFN1, mitofusin 1; MFN2, mitofusin 2; OMA1, OMA1 zinc metallopeptidase; OPA1, OPA1 mitochondrial dynamin like GTPase; mtDNA, mitochondrial DNA; PGC1α, peroxisome proliferator-activated receptor gamma coactivator 1-alpha; PGC1β, peroxisome proliferator-activated receptor gamma coactivator 1-beta; SSBP1, single stranded DNA binding protein 1; PPARα, peroxisome proliferator activated receptor alpha; PPARγ, peroxisome proliferator activated receptor gamma; ITPR1, inositol 1,4,5-trisphosphate receptor type 1; ITPR2, inositol 1,4,5-trisphosphate receptor type 2; ITPR3, inositol 1,4,5-trisphosphate receptor type 3; INF2, inverted formin 2; FUNDC1, FUN14 domain-containing protein 1; TOMM20, translocase of outer mitochondrial membrane 20; VDAC1, voltage dependent anion channel 1; SPIRE1, spire type actin nucleation factor 1.
[b]Accession number refers to GenBank (National Center for Biotechnology Information – NCBI).

synthase enzyme is coupled to the molar conversion of NADH to NAD^+ and is measured as a decrease in absorbance at OD 340 nm. The activity rate is expressed as the change in absorbance at 340 nm/min/amount of sample. The rate was calculated over the linear phase of incubation.

ATP levels were measured using the ATP Assay Kit (ab83355, Abcam, Waltham, MA). Muscle tissues from normal and WB-affected birds were homogenized in ice cold 2 N perchloric acid and kept on ice for 30 min. Tissue samples were centrifuged at 13,000 g for 2 min, and supernatant collected. Supernatant was diluted 1:5 with ATP assay buffer, and excess perchloric acid precipitated with 2 M KOH. Samples were again centrifuged at 13,000 g for 2 min, and the supernatant used for the ATP assay, according to manufacturer's protocol.

2.11 Statistical analyses

Data were analyzed by Student "t" test using Graph Pad Prism software (version 9.03 for Windows, Graph Pad Software, La Jolla California, United States). All data are expressed as the mean ± SEM and were considered statistically significant at a P value ≤0.05.

3 Results

3.1 Calcium concentration is higher in WB muscle and hypoxic primary myoblasts

Total calcium concentration in WB tissue extracts was significantly higher (P = 0.0079) than normal controls (Figure 1A). Similarly, chicken primary myotubes exposed to hypoxic conditions had higher calcium than their normoxic controls (P < 0.0001, Figure 1B).

3.2 Mitochondrial morphology is altered in WB muscle

As compared to normal tissue, WB muscle showed distorted myofiber structure (Figures 2A–D). The linearity of the myofibrils was disrupted and formed wave-like patterns in WB (Figures 2C, D, asterisk). Although myofiber separation was evident in both normal and WB muscle, the degree of separation was much higher in WB. In addition, Z line streaming was evident (Figures 2F, H, red arrows). Swollen and/or elongated mitochondria (0.72 ± 0.1 vs. 0.3 ± 0.03 in WB and normal muscle, respectively, P < 0.05) with indistinct cristae structure were observed in WB-affected muscle (Figures 2F, H, yellow arrows) as compared to normal muscle (Figures 2E, G).

3.3 Disruption of mitochondrial network genes in WB muscle and hypoxic primary myoblasts

3.3.1 Mitochondrial function

Among the genes involved in mitochondrial function, adenine nucleotide translocase 1 (ANT1) expression was significantly increased in both WB muscle (P = 0.0264, Figure 3A) and hypoxic primary myoblasts (P = 0.0128, Figure 4A) compared to normal breast muscle and normoxic cells, respectively. Sloan-Kettering Institute (SKI) proto-oncogene (Ski) mRNA abundance was upregulated in WB (P = 0.0238, Figure 3A) compared to normal breast muscle, but remained unchanged in both normoxic and hypoxic myoblasts (Figure 4A). Avian uncoupling protein (av-UCP) gene expression was significantly downregulated in both WB tissue and hypoxic myoblast compared to normal breast muscle and normoxic cells, respectively (Figures 3A, 4A). Nuclear factor erythroid-derived 2-like 2 (NFE2L2) mRNA

10.3389/fphys.2025.1543788

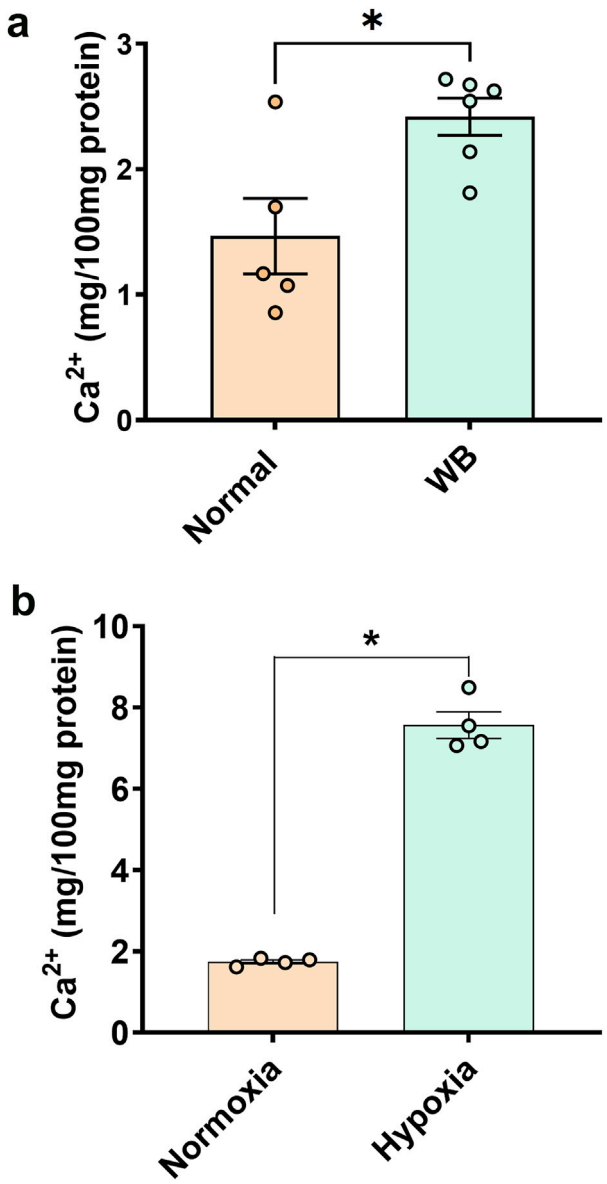

FIGURE 1
Total calcium concentration in chicken muscle **(A)** and primary myoblasts **(B)**. Data are expressed as means ± SEM (n = 4–6/group). *Significantly different at $P < 0.05$.

abundances and ANT1 protein levels did not change between all tissues and cells (Figures 3A, E).

3.3.2 Mitochondrial dynamics

Dynamin-related protein 1 (*DNM1*, $P = 0.0056$) and optic atrophy type 1 (*OPA1*, $P = 0.0318$) gene expressions were significantly upregulated in WB as compared to normal muscle (Figure 3B), and OMA1 zinc metallopeptidase (OMA1) mRNA levels were significantly increased in hypoxic compared to normoxic cells (Figure 4B). The other mitochondrial dynamics-related genes were not affected (Figures 3B, 4B). At the protein level, only mitofusin 1 (MFN1) was significantly decreased in WB compared to normal muscle, however both MFN1 and MFN2 proteins were significantly reduced in hypoxic compared to normoxic cells (Figures 3E, H, 4E, H). The expression of OMA1 protein was significantly increased in WB compared to normal muscle (Figures 3E, H), but it was significantly decreased in hypoxic compared to normoxic cells (Figures 4E, H). Protein levels of l-OPA1 were significantly diminished and that of s-OPA1 were significantly induced only in WB compared to normal muscle (Figures 3E, H), but not in hypoxic cells (Figures 4E, H).

3.3.3 Mitochondrial biogenesis

Mitochondrial DNA (mtDNA)-D loop and peroxisome proliferator activated receptor gamma (*PPARγ*) gene expression were both significantly upregulated in WB (Figure 3C) and hypoxic cells (Figure 4C) as compared to normal muscles and normoxic cells, respectively. Peroxisome proliferator-activated receptor gamma coactivator 1 alpha (*PGC1α*, $P = 0.0129$) and peroxisome proliferator-activated receptor alpha (*PPARα*, $P = 0.0491$) gene expressions were downregulated in the hypoxic compared to normoxic cells (Figure 4C) but not in WB muscles (Figure 3C). The expression of PGC1β and single stranded DNA binding protein 1 (SSBP1) genes did not differ between all tissue and cell groups (Figures 3C, 4C).

3.3.4 Mitochondrial-endoplasmic reticulum tethering

The expression of inositol 1,4,5-trisphosphate receptor type 1 and 2 (*ITPR1 and ITPR2*) and inverted formin 2 (IFN 2) genes was significantly upregulated in both WB and hypoxic cells compared to normal breast tissue and normoxic cells, respectively (Figures 3D, 4D). The expression of spire type actin nucleation factor 1 (SPIRE1) was significantly upregulated only in hypoxic cells compared to normoxic ones (Figure 4D), but not in WB muscles (Figure 3D). The expression of voltage dependent anion channel 1 (*VDAC1*), FUN14 domain containing 1 (FUNDC1), and translocase of outer mitochondrial membrane 20 (TOMM20) genes was not affected neither by the WB myopathy nor by the hypoxia exposure of primary myoblasts (Figures 3D, 4D). At the protein levels, VDAC1, ITPR2, and INF2 were all significantly increased in hypoxic compared to normoxic cells (Figures 4E, G), however only INF2 protein levels were significantly induced in WB compared to normal breast tissues (Figures 3E, G).

3.3.5 Altered mitochondrial bioenergetics in WB muscle and hypoxic primary myoblasts

A schematic illustration of mitochondrial complexes is presented in Figure 5A. Gene expression of components of Complex I was altered in WB-affected muscles. The expression of the NADH-ubiquinone oxidoreductase core subunit V2 (NDUFV2), belonging to N-module, and NADH dehydrogenase 4 (mtND4), belonging to P-module, was downregulated in WB-affected muscles (Figure 5G) and in hypoxic myoblasts (Figure 6A) compared to normal muscles and normoxic cells, respectively. The expression of NADH-ubiquinone oxidoreductase MLRQ subunit (NDUFA4), NADH dehydrogenase [Ubiquinone] iron-sulfur protein (NDUFS2), NADH dehydrogenase [Ubiquinone] flavoprotein (NDUFV1), and beta-transducin repeat containing E3 ubiquitin protein ligase (BTRC) genes remained unchanged between WB-affected and healthy muscles (Figure 5G).

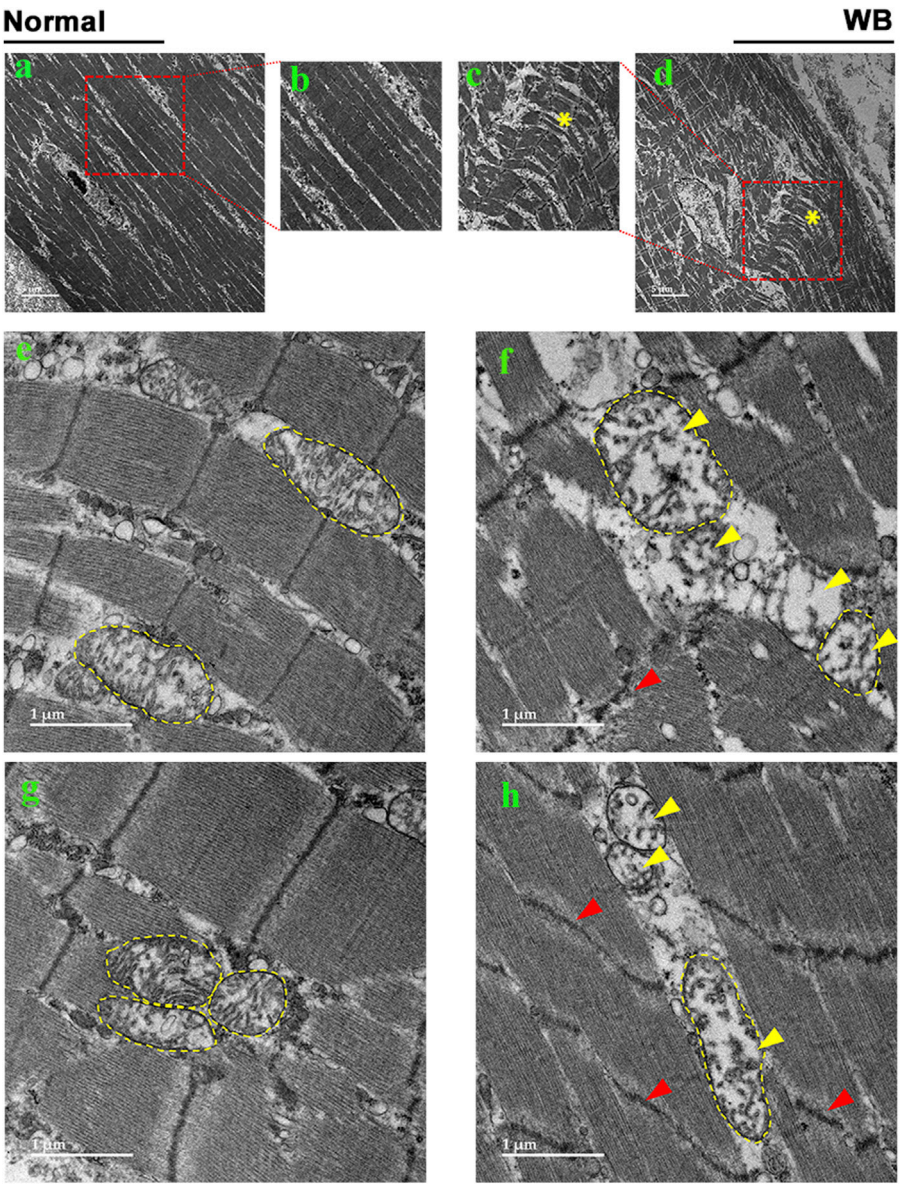

FIGURE 2
Electron microscopy images of normal **(A, B, E, G)** and woody breast **(C, D, F, H)**. Yellow arrows - mitochondria with degraded cristae. Red arrows - Z-line streaming. "*" – wave-like pattern in myofibers.

In the mitochondrial complex II, only succinate dehydrogenase complex subunit C (SDHC) gene expression was upregulated, but not that of succinate dehydrogenase complex flavoprotein subunit A (SDHA), succinate dehydrogenase complex iron sulfur subunit B (SDHB), and succinate dehydrogenase complex subunit D (SDHD), in WB-affected and hypoxic cells compared to normal muscles and normoxic cells, respectively (Figures 5H, 6B).

The expression of the complex III-associated genes, rieske iron-sulfur protein (RISP) and ubiquinol-cytochrome C reductase core protein 2 (UQCRC2) was significantly downregulated in WB compared to healthy muscles (Figure 5I), however only UQCRC2 gene expression was downregulated in hypoxic compared to normoxic cells (Figure 6C). The expression of cytochrome B subunit (CytB) remained unchanged between all muscle and cell groups (Figures 5I, 6C).

In complex IV, cytochrome C oxidase subunit I (MT-CO1) mRNA abundances, but not that of cytochrome C oxidase subunit 4 isoform 1 (COX4I1) and cytochrome C oxidase subunit 5 A (COX5a), were significantly decreased in WB and hypoxic myoblasts compared to healthy muscles and normoxic cells, respectively (Figures 5J, 6D).

Although the expression of complex V-associated genes, ATP synthase 8 (ATP8) and ATP synthase F1 subunit alpha Z chromosome (ATP5F1AZ), was not affected (Figure 5K). Although ATP synthase activity was significantly increased (Figure 5L), ATP levels were significantly decreased in WB compared to healthy muscles (Figure 5M). Neither ATP8, ATP5F1AZ nor ATP synthase activity was affected in hypoxic cells (Figures 6E, F).

Immunoblot measurements of OXPHOS proteins indicated that NDUFB (complex I) and MT-CO1 (complex IV) protein levels were

10.3389/fphys.2025.1543788

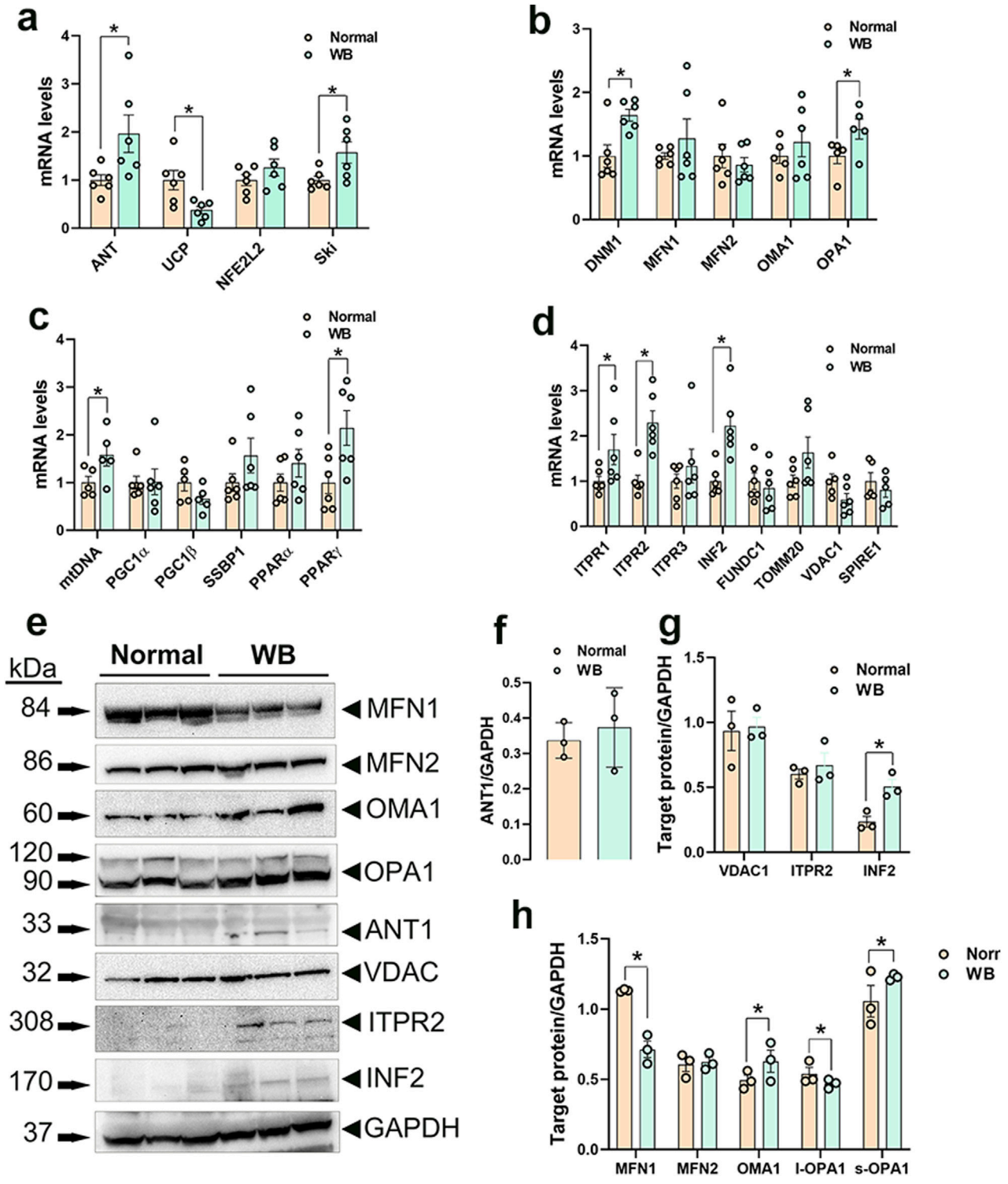

FIGURE 3
Mitochondrial network-related gene and protein expression in chicken breast muscle. Gene expression for mitochondrial function **(A)**, dynamics **(B)**, biogenesis **(C)**, and tethering **(D)** was determined by qPCR. Protein levels were determined by Western blot **(E–H)**. Data are expressed as means ± SEM (n = 6/group). *Significantly different at $P < 0.05$. ANT1, adenine nucleotide translocase; DNM1, dynamin-related protein 1; FUNDC1, FUN14 domain containing 1; INF2, inverted formin 2; ITPR1, inositol 1,4,5-trisphosphate receptor type 1; ITPR2, inositol 1,4,5-trisphosphate receptor type 2; ITPR3, inositol 1,4,5-trisphosphate receptor type 3; MFN1, mitofusin 1; MFN2, mitofusin 2; mtDNA, mitochondrial DNA; NFE2L2, nuclear factor erythroid 2-related factor 2; PGC1α, peroxisome proliferator-activated receptor gamma coactivator 1 alpha; PGC1β, peroxisome proliferator-activated receptor gamma coactivator 1 beta; PPARα, peroxisome proliferator activated receptor alpha; PPARγ, peroxisome proliferator activated receptor gamma; OMA1, OMA1 zinc metallopeptidase; OPA1, OPA1 mitochondrial dynamin like GTPase; SKI, nuclear sarcoma viral oncogene homolog; SPIRE1, spire type actin nucleation factor 1; SSBP1, mitochondrial single-stranded DNA binding protein 1; TOMM20, translocase of outer mitochondrial membrane 20; VDAC1, voltage dependent anion channel 1; UCP, uncoupling protein.

10.3389/fphys.2025.1543788

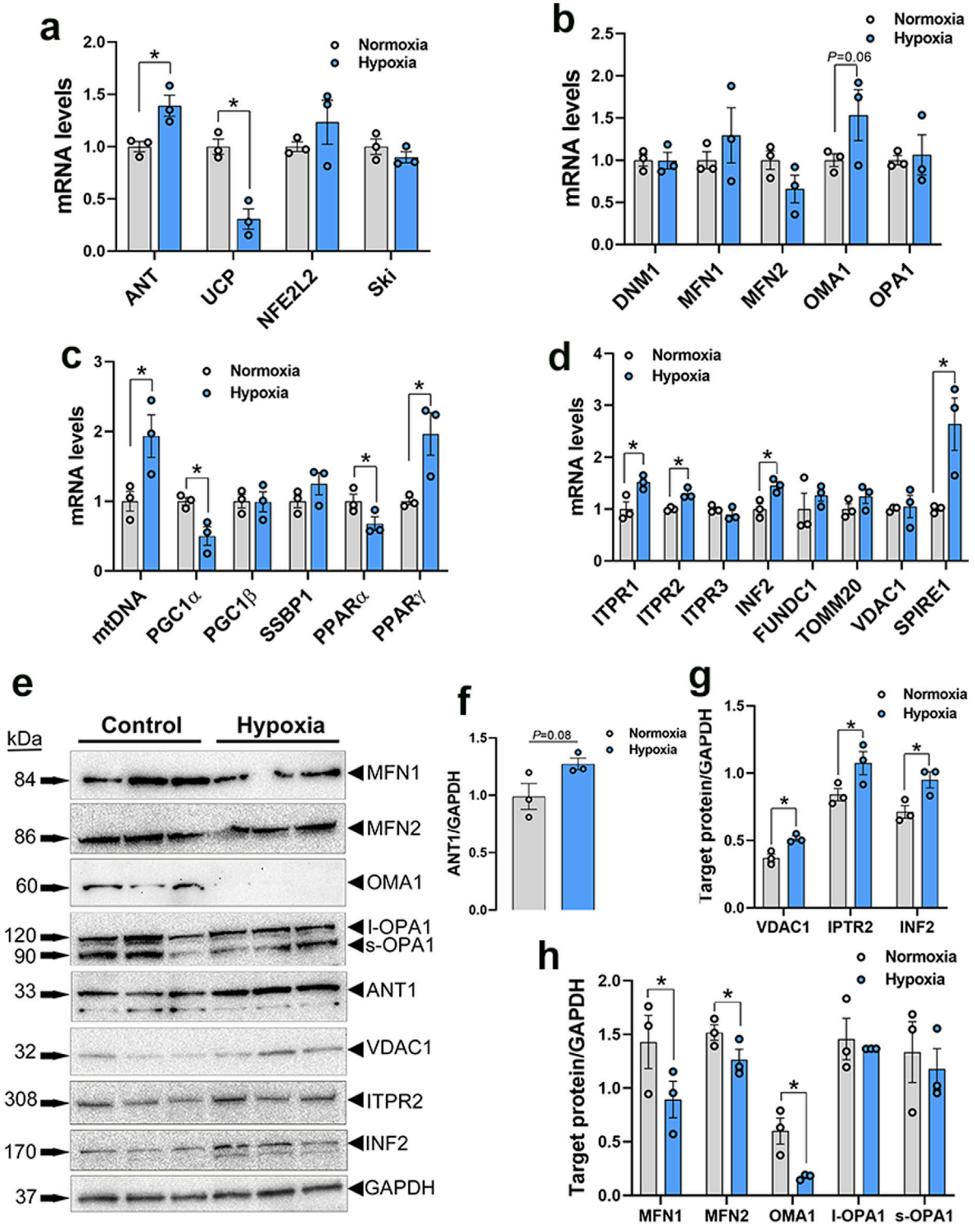

FIGURE 4
Mitochondrial network-related gene and protein expression in primary myoblasts. Gene expression for mitochondrial function **(A)**, dynamics **(B)**, biogenesis **(C)**, and tethering **(D)** was determined by qPCR. Protein levels were determined by Western blot **(E–H)**. Data are expressed as means ± SEM (n = 6/group), representative blots are shown. *Significantly different at $P < 0.05$. ANT1, adenine nucleotide translocase; DNM1, dynamin-related protein 1; FUNDC1, FUN14 domain containing 1; INF2, inverted formin 2; ITPR1, inositol 1,4,5-trisphosphate receptor type 1; ITPR2, inositol 1,4,5-trisphosphate receptor type 2; ITPR3, inositol 1,4,5-trisphosphate receptor type 3; MFN1, mitofusin 1; MFN2, mitofusin 2; mtDNA, mitochondrial DNA; NFE2L2, nuclear factor erythroid 2-related factor 2; PGC1α, peroxisome proliferator-activated receptor gamma coactivator 1 alpha; PGC1β, peroxisome proliferator-activated receptor gamma coactivator 1 beta; PPARα, peroxisome proliferator activated receptor alpha; PPARγ, peroxisome proliferator activated receptor gamma; OMA1, OMA1 zinc metallopeptidase; OPA1, OPA1 mitochondrial dynamin like GTPase; SKI, nuclear sarcoma viral oncogene homolog; SPIRE1, spire type actin nucleation factor 1; SSBP1, mitochondrial single-stranded DNA binding protein 1; TOMM20, translocase of outer mitochondrial membrane 20; VDAC1, voltage dependent anion channel 1; UCP, uncoupling protein.

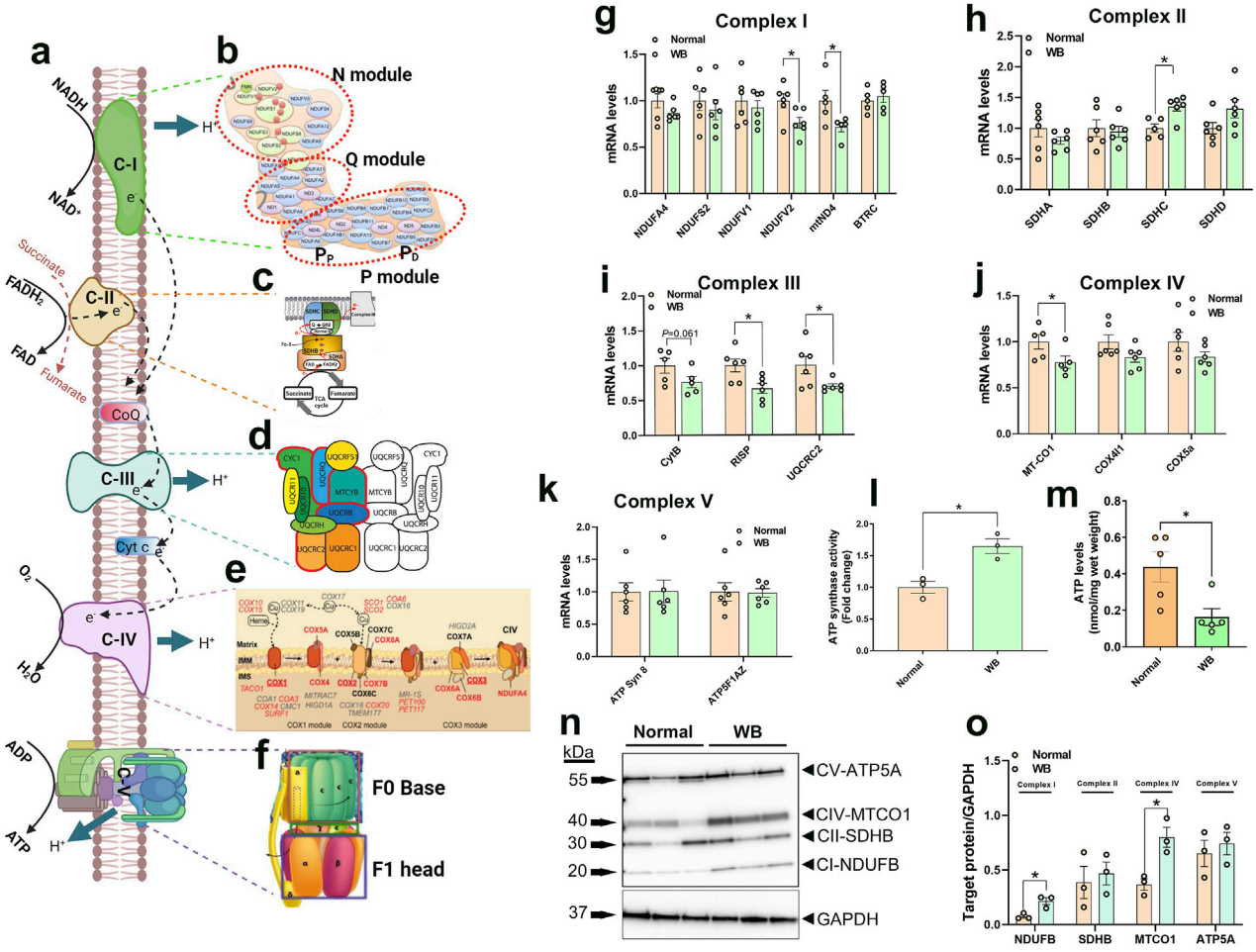

FIGURE 5
Expression profile of genes associated with mitochondrial ETC in chicken breast muscle. A schematic illustration of ETC and its complexes [I to V, **(A–F)**] (not for scale). Gene expression for complex I **(G)**, II **(H)**, III **(I)**, IV **(J)**, and V **(K)** was determined by qPCR. ATP synthase activity was determined in muscle isolated mitochondria by Enzyme Activity Microplate Assay Kit **(L)** and ATP levels were measured by ATP assay kit **(M)**. Protein levels were determined by immunoblot **(N, O)** and representative blots are shown. Data are expressed as means ± SEM (n = 6/group). *Significantly different at $P < 0.05$. ATP5FAZ, ATP synthase F1 subunit alpha Z chromosome; ATPSyn8, ATP Synthase F0 subunit 8; COX4I1, cytochrome C oxidase subunit 4I1; COX5A, cytochrome C oxidase subunit 5A; CytB, mitochondrially encoded cytochrome B; MT-CO1, mitochondrially encoded cytochrome C oxidase I; NDUFA4, NADH dehydrogenase (Ubiquinone) 1 alpha subcomplex subunit 4; NDUFS2, NADH:ubiquinone oxidoreductase core subunit S2; NDUFV1, NADH:ubiquinone oxidoreductase core subunit V1; NDUFV1, NADH:ubiquinone oxidoreductase core subunit V2; mtND4, mitochondrially encoded NADH:ubiquinone oxidoreductase core subunit 4; RISP, ubiquinol-cytochrome C reductase, Rieske iron-sulfur polypeptide 1; SDHA, succinate dehydrogenase complex flavoprotein subunit A; SDHB, succinate dehydrogenase complex iron sulfur subunit B; SDHC, succinate dehydrogenase complex subunit C; SDHD, succinate dehydrogenase complex subunit D; UQCRC2, ubiquinol-cytochrome C reductase core protein 2. Figures 5B–F were modified from (Saada, 2013) **(B)** (Moosavi et al., 2019) **(C)** (Tucker et al., 2013) **(D)** (Hock et al., 2020) **(E)**, and (Ahern and Rajagopal, 2024) **(F)**, with permission from Springer Nature license (#5915970048082 and 5916040393036).

significantly increased in WB compared to normal muscles (Figures 5N, O), and SDHB (complex II) and ATP5A (complex V) protein levels were increased in hypoxic compared to normoxic cells (Figures 6G, H). In mitochondria isolated from breast muscle, complex I activity tended to be lower in WB as compared to normal muscles ($P = 0.081$, Figures 7A, B). There were no significant differences in complex II or complex IV ($P > 0.05$, Figures 7C, D).

Seahorse XF analyzer showed that hypoxic primary myotubes had significantly lower basal respiration ($P = 0.0057$, Figures 8A–D) and ATP production ($P = 0.0033$, Figure 8E) as compared to normoxic cells. There were no significant differences in proton leak, maximal respiration, spare capacity, or non-mitochondrial respiration (Figures 8F–I).

4 Discussion

Woody breast is a muscle myopathy that adversely impacts the poultry industry through decreased meat quality and increased condemnations, resulting in significant welfare concerns and heavy economic losses (Kuttappan et al., 2016). Several lines of research have indicated local hypoxia as a concurrent condition (Greene et al., 2019; Emami et al., 2021; Zhang et al., 2024), however the cellular and molecular mechanisms by which hypoxia causes the myopathy are still not completely understood. As mitochondria are the primary consumers of oxygen within the cell and the powerhouse providing the necessary energy for cellular homeostasis and functions, we sought to assess mitochondrial

10.3389/fphys.2025.1543788

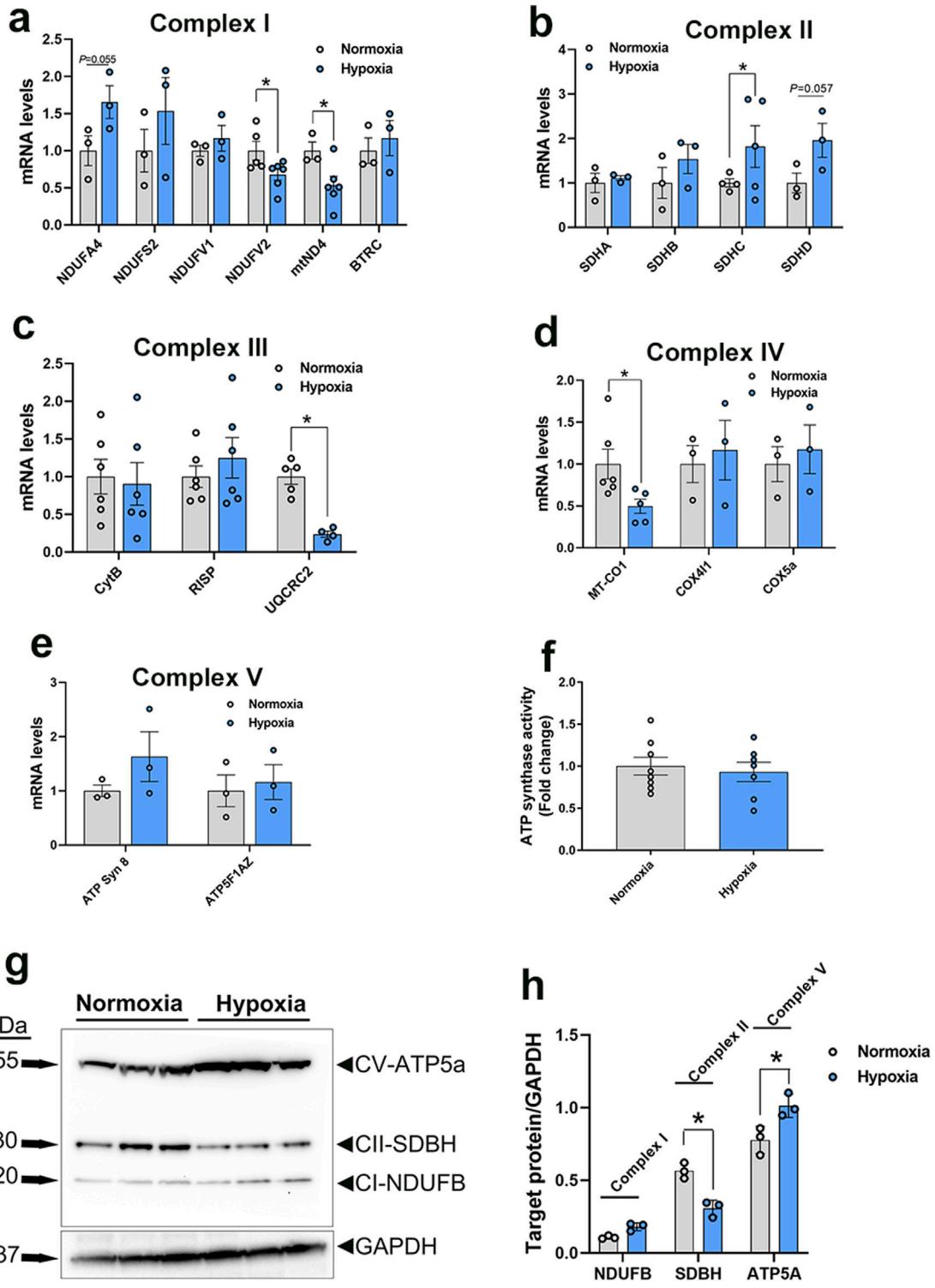

FIGURE 6
Expression profile of genes associated with mitochondrial ETC in primary myoblasts. Gene expression for complex I **(A)**, II **(B)**, III **(C)**, IV **(D)**, and V **(E)** was determined by qPCR. ATP synthase activity was determined in cells by Enzyme Activity Microplate Assay Kit **(F)**. Protein levels were determined by immunoblot **(G, H)** and representative blots are shown. Data are expressed as means ± SEM (n = 6/group). *Significantly different at $P < 0.05$. ATP5FAZ, ATP synthase F1 subunit alpha Z chromosome; ATPSyn8, ATP Synthase F0 subunit 8; COX4I1, cytochrome C oxidase subunit 4I1; COX5A, cytochrome C oxidase subunit 5A; CytB, mitochondrially encoded cytochrome B; MT-CO1, mitochondrially encoded cytochrome C oxidase I; NDUFA4, NADH dehydrogenase (Ubiquinone) 1 alpha subcomplex subunit 4; NDUFS2, NADH:ubiquinone oxidoreductase core subunit S2; NDUFV1, NADH: ubiquinone oxidoreductase core subunit V1; NDUFV1, NADH:ubiquinone oxidoreductase core subunit V2; mtND4, mitochondrially encoded NADH: ubiquinone oxidoreductase core subunit 4; RISP, ubiquinol-cytochrome C reductase, Rieske iron-sulfur polypeptide 1; SDHA, succinate dehydrogenase complex flavoprotein subunit A; SDHB, succinate dehydrogenase complex iron sulfur subunit B; SDHC, succinate dehydrogenase complex subunit C; SDHD, succinate dehydrogenase complex subunit D; UQCRC2, ubiquinol-cytochrome C reductase core protein 2.

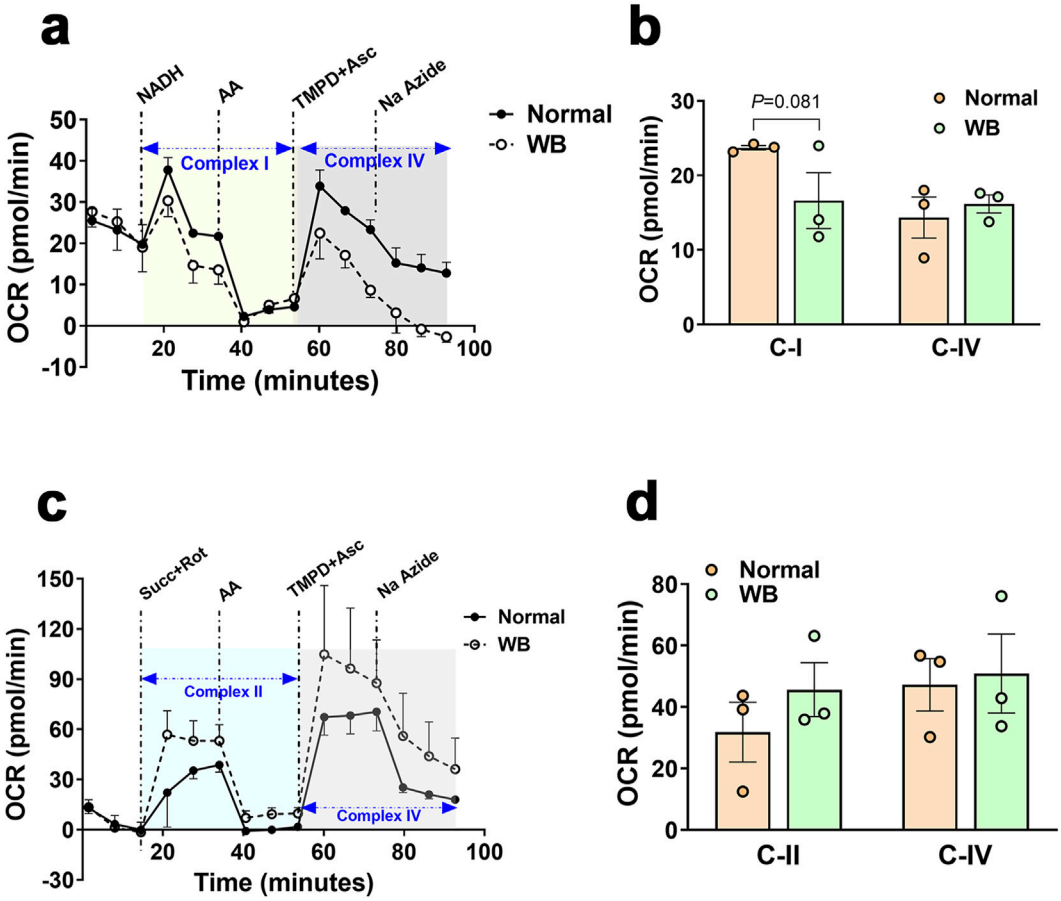

FIGURE 7
Respirometry measurement of mitochondrial complex I, II, and IV in chicken breast muscle. The oxygen consumption rate (OCR) was measured in mitochondria isolated from breast muscles treated with various selective (un)coupler reagents using seahorse XF analyzer following the protocol of (Osto et al., 2020). Complex I and IV **(A, B)** and complex II and IV **(C, D)**. Data are mean ± SEM (n = 6). AA, antimycin; Asc, ascorbic acid; Na azide, sodium azide; NADH, Rot, rotenone; Succ, succinate; TMPD, N1,N1,N1,N1-tetramethyl-1,4-phenylene diamine; WB, woody breast.

function, biogenesis, dynamics, and bioenergetics within the WB-affected muscles and hypoxic primary myoblasts.

As a hallmark of many muscle disorders, mitochondrial dysfunction presents in multiple ways, including defective OXPHOS, Ca^{2+} imbalances, mtDNA mutations, and structural defects, leading to altered ATP production, decreased mitochondrial respiration, and increased ROS (Chen et al., 2022).

Here, transmission electron microscopy analysis of WB-affected tissues revealed an extremely disordered muscle structure with multiple defects in myofibers and organellar architecture. The wave-like shape of myofibers observed in WB muscle resembles that of human working muscle during exercise and restricted blood flow (Wilburn et al., 2021). The distortion observed in the human working muscle was postulated to be due to the inhibition of venous return during muscle contraction and represented the result of increased pressure, leading to disruption of myofiber integrity. This is also true for broilers that are characterized by rapid growth and breast muscle hypertrophy with compromised blood supply. Noticeably, heavy broilers spend much of their time lying down, which may increase pressure and breast muscle contraction. Furthermore, swollen and elongated mitochondria with indistinct cristae structure were spotted in WB-affected muscles. This observation was not surprising because hypoxia has been shown to induce mitochondrial swelling (Niquet et al., 2003) and elongation (Khacho et al., 2014), and consequently leads to apoptosis/necrosis through caspase-3 activation, which has also been previously delineated in WB-affected muscles and in hypoxic myoblasts (Greene et al., 2023).

Although warranting further functional studies, the increased level of Ca^{2+} in both WB-affected muscles and hypoxic myoblasts suggests that calcium overload is likely a leading cause for the mitochondrial dysfunction. The first supporting argument for the abovementioned hypothesis is that mitochondria can uptake Ca^{2+} through at least two routes, a uniporter (Gunter et al., 1998; Rizzuto et al., 1998; Kirichok et al., 2004) and a rapid uptake pathway (Sparagna et al., 1995), whose molecular nature and mechanisms still elude us. The second rationalization is that hypoxia has been shown to induce Ca^{2+} accumulation in mitochondria through the reversal of the Na^{+}-Ca^{2+} exchanger (Haigney et al., 1992; Griffiths and Halestrap, 1993; Chacon et al., 1994; Miyamae et al., 1996; Griffiths et al., 1998; Kushwaha et al., 2023). The third assertion is that mitochondrial Ca^{2+} overloading triggers the opening of the mitochondrial permeability transition pore (Giorgio et al., 2017), a non-specific pore in the mitochondria inner membrane, allowing

10.3389/fphys.2025.1543788

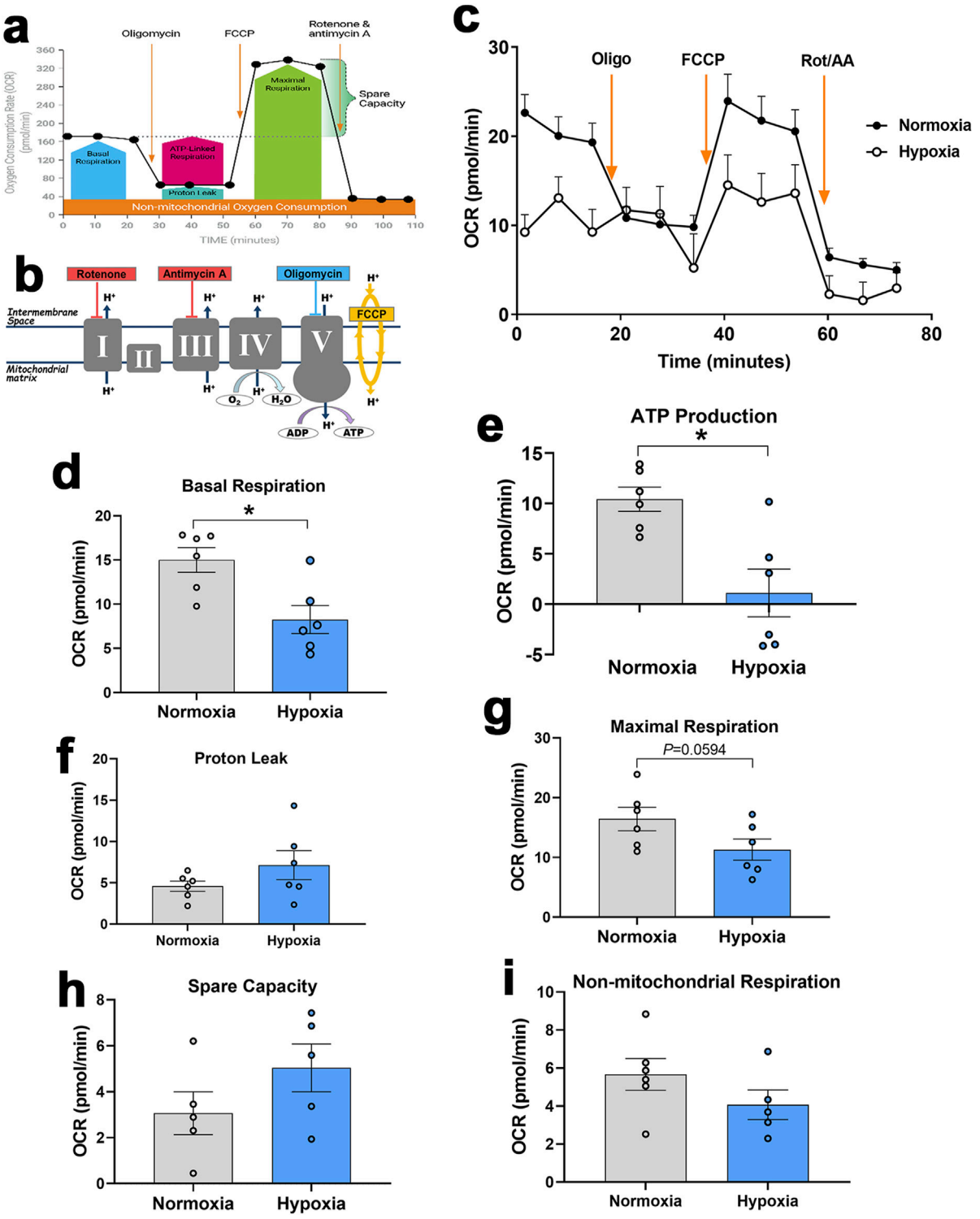

FIGURE 8
Measurement of mitochondrial respiration in primary myoblasts using Seahorse XF analyzer. Respirometry and OCR were measured in primary myoblasts exposed to normoxia or hypoxia followed by consecutive injections of various selective (un)couplers. Typical OCR patterns from Agilent **(A, B)**, OCR in primary myoblasts **(C)**, basal respiration **(D)**, ATP production **(E)**, proton leak **(F)**, Maximal respiration **(G)**, spare capacity **(H)**, and non-mitochondrial respiration **(I)**. **(A, B)** were obtained from Agilent user guide (kit 103015-100) with permission from Agilent Technologies, Inc. AA, antimycin; FCCP, carbonyl cyanide-4-(trifluoromethoxy)phenylhydrazone; OCR, oxygen consumption rate; Oligo, oligomycin; Rot, rotenone.

the entry of water and solutes into the mitochondrial matrix, and thereby resulting in mitochondrial swelling and disruption of cristae and outer membrane.

Of vested interest, Ca^{2+} and ROS are considered the main transduction signals linking the ER and mitochondria and help them to adapt their response to hypoxia in a tightly regulated manner (Yan et al., 2008). In a previous study, using primary myoblasts, we have shown that hypoxia induced ER stress, which was also evident in WB-affected muscle (Greene et al., 2023), suggesting that ER-mitochondria tethering could be dysregulated. The significant decline of MFN1 protein levels in both WB-affected muscles and hypoxic myoblasts supports the abovesaid hypothesis. In addition to its key role in mitochondrial dynamics, MFN1/2 were found to be located on both the ER and mitochondrial membranes (Chen et al., 2012; Liu and Zhu, 2017), where it interacts with other proteins and mediates ER-mitochondria tethering (Filadi et al., 2015; Kirshenbaum et al., 2024). Genetic manipulation studies demonstrated critical roles for MFNs in maintaining a physical juxtaposition of the ER and mitochondria and a normal inter-organelle Ca^{2+} signaling (Han et al., 2021; Chen et al., 2024). In addition, the upregulated expression of the calcium channels, ITPR1/2, supports the notion of increased transfer of Ca^{2+} from the ER to the mitochondria and its mitochondrial accumulation (Wiel et al., 2014). Inositol 1,4,5-trisphosphate receptor (ITPRs) are parts of contact sites between mitochondria and ER, which are known as mitochondria-ER contacts (MERCs) or mitochondria-associated ER membranes (MAMs) (Pinton, 2018). In fact, ITPRs interact with VDAC of the outer mitochondrial membrane through the molecular chaperone glucose-regulated protein, GRP75, to form a tripartite complex that is critical for mitochondria-ER coupling, crosstalk, and tethering (Lee et al., 2019; Ziegler et al., 2021).

The close contacts between the ER and mitochondria became widely appreciated as important dynamic platforms that provide an excellent scaffold for communication and crosstalk between the two organelles and play key roles in different signaling pathways. This allows rapid exchanges of biological molecules, such as Ca^{2+} transfer, to maintain cellular homeostasis and organelle function. It has been shown that ER-mitochondria contact also stimulates mitochondrial division (Friedman et al., 2011), which is required for many cellular processes, including metabolic adaptation (Mishra and Chan, 2016), and any defect in this contact may affect mitochondrial dynamics and leads to pathologies (Nunnari and Suomalainen, 2012). Here, we showed that INF2 expression was significantly upregulated in both WB-affected muscles and hypoxic myoblasts, indicating an alteration of mitochondrial division. Inverted formin 2 (INF2) polymerizes actin at the ER, enhances ER-mitochondria contact, and recruits DNM1 (which was also upregulated in WB-affected muscles), leading to a ring formation and subsequent mitochondrial outer membrane (OMM) contraction (Korobova et al., 2013; Fung et al., 2023). Mitochondrial division also requires the division of the inner mitochondrial membrane (IMM) (Chakrabarti et al., 2018). The concomitant increase of the IMM mitochondrial gatekeepers OMA1 and s-OPA1 proteins, at least in WB-affected muscles, suggested a mitochondrial fission status, which is supported by mitochondrial fragmentations observed by the EM analysis. However, the elongated mitochondria also observed in our experimental conditions by EM indicated two potential scenarios: 1) these elongated mitochondria were protected from being degraded by mitophagy (Gomes and Scorrano, 2011), or 2) they were elongated to be ready for division (Scott and Youle, 2010). Overall, it is known that when the transmembrane potential across the IMM is lost, long L-OPA1 is cleaved to short fusion-inactive s-OPA1 isoforms by the mitochondrial stress-sensitive protease OMA1, causing mitochondria fission and fragmentation (Zhang et al., 2014; Gilkerson et al., 2021). Although OPA1 protein expression did not change in hypoxic myoblasts, the upregulation of SPIRE supported mitochondrial fission status (Manor et al., 2015) and suggested differential fission pathways between *in vivo* and *in vitro* models, with the same outcome and endpoint as hypoxia has been shown to induce mitochondrial fission (Nishimura et al., 2018; Yuan et al., 2021; Gillmore et al., 2022).

It is well known that in high-energy demanding tissues, like muscle, calcium homeostasis is intrinsically associated to ATP production both via the Krebs cycle and OXPHOS to regulate cellular bioenergetics (Glancy and Balaban, 2012). It is, therefore, expected that hypoxia, mitochondrial Ca^{2+} overload, and defects in mitochondrial dynamics and tethering would affect mitochondrial biogenesis, function, and bioenergetics. The upregulation of mtDNA D-loop and PPARγ expression on one hand (in WB muscle and hypoxic myoblasts), and the downregulation of PGC-1α (in hypoxic myoblasts) on other hand, indicated that mitochondrial biogenesis was altered. PGC-1 is considered as the master regulator of mitochondrial biogenesis by virtue of its ability to control the expression of several critical transcription factors, and its inhibition has been reported to alter mitochondrial biogenesis (Gureev et al., 2019; Jamwal et al., 2021). The increased expression of mtDNA D-loop is intriguing, but it was probably associated with increased number of mitochondria due to fission and/or release of mtDNA following mitochondrial fragmentation (Bao et al., 2019).

Similarly, the dysregulation of av-UCP, ANT1, and Ski genes indicated that mitochondrial function was affected. In contrast to mammals where at least 5 UCPs have been discovered, only one av-UCP has been characterized in avian species (Raimbault et al., 2001). Although its physiological roles are still largely unknown, av-UCP, a member of the mitochondrial anion carrier family, was postulated to be involved in thermogenesis, redox balance, and ROS (Dridi et al., 2004; Davoodi et al., 2023). Among the four ANT paralogous, ANT1, located in the IMM, acts as a gated pore that allows ADP to enter the mitochondria and ATP to exit (Chen et al., 2023). Ski has been found to enhance the activity of cytochrome C oxidase and citrate synthase and stimulates mitochondrial biogenesis and fatty acid beta oxidation (Ye et al., 2011). Mammalian and rodent studies showed that UCPs (UCP2/3) are key uniport mechanisms for mitochondrial Ca^{2+} uptake (Trenker et al., 2007), as well as major promoters for mitochondrial proton leak and inefficient OXPHOS (Parker et al., 2008). Approximately two-thirds of the basal proton conductance is correlated to ANT abundance, which has been reported to stimulate mitochondrial proton leak (Bertholet et al., 2019). While direct evidence is limited, research suggested that Ski, through the TGFβ signaling pathway, might alter mitochondrial function and increase proton leak (Tecalco-Cruz et al., 2018).

Together, all the abovementioned mitochondrial abnormalities (morphology, structure, tethering, biogenesis, etc.) point to a defect

in OXPHOS and ATP production. The dysregulated expression of genes and proteins associated with mitochondrial complexes I to IV support this hypothesis. Abundances of complex I components, NDUFV2 (N module, hydrophilic arm) and mtND4 (P module, hydrophobic arm) mRNA were significantly decreased in both WB-affected muscle and hypoxic myoblasts, suggesting a decreased activity of complex I, which oxidizes NADH and transfers electrons to ubiquinone in a reaction coupled with proton pumping (Gutiérrez-Fernández et al., 2020). Complex I is pivotal in maintaining metabolic homeostasis by sensing O_2 and initiating response to mitochondrial stress, such as hypoxia (Fernández-Agüera et al., 2015). Previous studies have reported that hypoxia decreased complex I activity, which was also associated with increased mitochondrial ROS (Keeney et al., 2006; Grivennikova and Vinogradov, 2013; Papa and De Rasmo, 2013). The increased expression of the complex II component, SDHA, suggested an activation of complex II due to complex I deficiency. In that regard, it has been reported that compensatory complex II activity remodel and rescue mitochondrial respiration by shifting cellular fuel sources from NADH to FADH2 (Acín-Pérez et al., 2014). The downregulation of its subunit expression (CytB, RISP, and UQCRC2 in WB-affected muscle and UQCRC2 in hypoxic myoblasts) indicated lower activity of complex III, which is the central collector delivering electrons through cytochrome c to complex IV. It has been shown that cells with defects in complex III have decreased activity of complex I (Acín-Pérez et al., 2004). Furthermore, it has been reported in a human cellular model that a small frame deletion in CytB was associated with a severe impairment of respirasome (complexes III, I and IV) assembly and ROS production (Tropeano et al., 2020). Complex IV is the terminal complex in the ETC, transferring electrons from ferro-cytochrome c to molecular oxygen, converting the latter to water (Li et al., 2006). MT-CO1 is encoded by the mitochondrial genome and serves as the main integral membrane catalytic subunit of complex IV. Its downregulation in our experimental conditions in both WB-affected muscles and hypoxic myoblasts indicated a decreased activity of complex IV that likely leads to increased oxidative stress (Shen et al., 2018) and altered ATP production (Belevich et al., 2007). Reduced MT-CO1 was found to be associated with dysregulation of mitochondrial biogenesis and lower expression of PGC-1, which have also been seen in this study.

The mitochondrial complex V or ATP synthase is the fifth multi subunit OXPHOS complex that synthesizes ATP from ADP (Nijtmans et al., 1995). It is a dual motor that is composed of two molecular units, the cytoplasmic catalytic F1 and the membrane-embedded F0 that allows proton channeling (Forgac, 2007). Although the low basal and maximal respiration and ATP production were expected in hypoxic cells (Heerlein et al., 2005; Flood et al., 2023) and WB-affected tissue (Zhang et al., 2024), the increased ATP synthase activity in isolated mitochondria from WB-affected was puzzling. While principles and mechanisms of intracellular energy distribution as well as interaction of ATP-producing systems remain poorly understood particularly in avian species, it is probable that the observed increase in ATP synthase activity was associated with high levels of AMP/ADP and/or Ca^{2+}. It is well accepted that ATP synthase can allosterically be activated by AMP, which is also known to activate AMPK and both AMP content and phosphorylated AMPK have been reported to be higher in WB-affected tissues (Zhang et al., 2020; Zhang et al., 2024). Despite the fact that no molecular mechanism has yet been described, intramitochondrial Ca^{2+} has been reported to directly activate F1-F0-ATPase (Harris, 1993; Scholz and Balaban, 1994; Territo et al., 2000). Several studies have demonstrated that Ca^{2+}-dependent mitochondrial dehydrogenases (PDH, ICDH, and KDH) are potential routes for Ca^{2+}-dependent ATP synthase activation (Denton et al., 1972; Kerbey et al., 1976; Denton et al., 1978; McCormack and Denton, 1979; Lawlis and Roche, 1980; Rutter and Denton, 1989; McCormack et al., 1990).

In summary, regardless of some differences in gene/protein expression (SPIRE, OMA1, OPA1, etc.) between *in vivo* (WB muscles) and *in vitro* (hypoxic cells) studies, overall, it is clear that mitochondrial morphology, biogenesis, dynamics, tethering, function, and bioenergetics were all affected. Our study is the first, to the best of our knowledge, providing fundamental insights related to mitochondrial dysfunction in relatively new muscle myopathy with unknown etiology, and suggesting that Ca^{2+} signaling might play a key role that needs further in-depth investigations. It is also worth noting that several mRNA abundances and protein levels, such as OMA1 and MTCO1, were not perfectly correlated, which is not surprising, and this might due to RNA decay and stability, protein half-life and stability, translation efficiency, and/or likely other complex regulatory pathways (post-translational modifications) that can decrease protein production even when the mRNA levels are high (Maier et al., 2009).

Data availability statement

The data that support the findings of this study are available from the corresponding author upon reasonable request.

Ethics statement

The animal study was approved by University of Arkansas Animal Care and Use Committee. The study was conducted in accordance with the local legislation and institutional requirements.

Author contributions

EG: Data curation, Formal Analysis, Writing–original draft. PC: Data curation, Methodology, Writing–original draft. CW: Writing–original draft. MB: Writing–original draft. SD: Conceptualization, Funding acquisition, Supervision, Writing–original draft, Writing–review and editing.

Funding

The author(s) declare that financial support was received for the research, authorship, and/or publication of this article. This study was supported by a grant from USDA-AFRI Sustainable

Agriculture Systems (2020-69012-31823 to SD) and ABV (to SD). USDA-AFRI and ABV had no role in conducting the research, generating the data, interpreting the results or writing the manuscript.

Acknowledgments

Authors would like to thank DeAna Grant and Rowan Fink of the Electron Microscopy Core Facility at the University of Missouri for assistance in transmission electron microscopy.

Conflict of interest

Authors CW and MB were employed by AB Vista.

The remaining authors declare that the research was conducted in the absence of any commercial or financial relationships that could be construed as a potential conflict of interest.

The author(s) declared that they were an editorial board member of Frontiers, at the time of submission. This had no impact on the peer review process and the final decision.

Generative AI statement

The author(s) declare that no Generative AI was used in the creation of this manuscript.

Publisher's note

All claims expressed in this article are solely those of the authors and do not necessarily represent those of their affiliated organizations, or those of the publisher, the editors and the reviewers. Any product that may be evaluated in this article, or claim that may be made by its manufacturer, is not guaranteed or endorsed by the publisher.

References

Acín-Pérez, R., Bayona-Bafaluy, M. P., Fernández-Silva, P., Moreno-Loshuertos, R., Pérez-Martos, A., Bruno, C., et al. (2004). Respiratory complex III is required to maintain complex I in mammalian mitochondria. *Mol. Cell* 13 (6), 805–815. doi:10.1016/s1097-2765(04)00124-8

Acín-Pérez, R., Carrascoso, I., Baixauli, F., Roche-Molina, M., Latorre-Pellicer, A., Fernández-Silva, P., et al. (2014). ROS-triggered phosphorylation of complex II by Fgr kinase regulates cellular adaptation to fuel use. *Cell Metab.* 19 (6), 1020–1033. doi:10.1016/j.cmet.2014.04.015

Ahern, K., and Rajagopal, I. (2024). "Cellular phosphorylations," in *Biochemistry free and easy*. (LibreTexts).

Bao, D., Zhao, J., Zhou, X., Yang, Q., Chen, Y., Zhu, J., et al. (2019). Mitochondrial fission-induced mtDNA stress promotes tumor-associated macrophage infiltration and HCC progression. *Oncogene* 38 (25), 5007–5020. doi:10.1038/s41388-019-0772-z

Belevich, I., Bloch, D. A., Belevich, N., Wikström, M., and Verkhovsky, M. I. (2007). Exploring the proton pump mechanism of cytochrome c oxidase in real time. *Proc. Nat. Acad. Sci.* 104(8), 2685–2690. doi:10.1073/pnas.0608794104

Bertholet, A. M., Chouchani, E. T., Kazak, L., Angelin, A., Fedorenko, A., Long, J. Z., et al. (2019). H(+) transport is an integral function of the mitochondrial ADP/ATP carrier. *Nature* 571 (7766), 515–520. doi:10.1038/s41586-019-1400-3

Cemin, H. S., Vieira, S. L., Stefanello, C., Kindlein, L., Ferreira, T. Z., and Fireman, A. K. (2018). Broiler responses to increasing selenium supplementation using Zn-L-selenomethionine with special attention to breast myopathies. *Poult. Sci.* 97 (5), 1832–1840. doi:10.3382/ps/pey001

Chacon, E., Reece, J. M., Nieminen, A.-L., Zahrebelski, G., Herman, B., and Lemasters, J. J. (1994). Distribution of electrical potential, pH, free Ca2+, and volume inside cultured adult rabbit cardiac myocytes during chemical hypoxia: a multiparameter digitized confocal microscopic study. *Biophys. J.* 66 (4), 942–952. doi:10.1016/S0006-3495(94)80904-X

Chakrabarti, R., Ji, W. K., Stan, R. V., de Juan Sanz, J., Ryan, T. A., and Higgs, H. N. (2018). INF2-mediated actin polymerization at the ER stimulates mitochondrial calcium uptake, inner membrane constriction, and division. *J. Cell Biol.* 217 (1), 251–268. doi:10.1083/jcb.201709111

Chen, S., Sun, Y., Qin, Y., Yang, L., Hao, Z., Xu, Z., et al. (2024). Dynamic interaction of REEP5–MFN1/2 enables mitochondrial hitchhiking on tubular ER. *J. Cell Biol.* 223 (10), e202304031. doi:10.1083/jcb.202304031

Chen, T. H., Koh, K. Y., Lin, K. M., and Chou, C. K. (2022). Mitochondrial dysfunction as an underlying cause of skeletal muscle disorders. *Int. J. Mol. Sci.* 23 (21), 12926. doi:10.3390/ijms232112926

Chen, Y., Csordás, G., Jowdy, C., Schneider, T. G., Csordás, N., Wang, W., et al. (2012). Mitofusin 2-containing mitochondrial-reticular microdomains direct rapid cardiomyocyte bioenergetic responses via interorganelle Ca2+ crosstalk. *Circ. Res.* 111 (7), 863–875. doi:10.1161/CIRCRESAHA.112.266585

Chen, Y., Wu, L., Liu, J., Ma, L., and Zhang, W. (2023). Adenine nucleotide translocase: current knowledge in post-translational modifications, regulations and pathological implications for human diseases. *FASEB J.* 37 (6), e22953. doi:10.1096/fj.202201855RR

Clanton, T. L. (2007). Hypoxia-induced reactive oxygen species formation in skeletal muscle. *J. Appl. Physiol.* 102 (6), 2379–2388. doi:10.1152/japplphysiol.01298.2006

Dalgaard, L. B., Rasmussen, M. K., Bertram, H. C., Jensen, J. A., Møller, H. S., Aaslyng, M. D., et al. (2018). Classification of wooden breast myopathy in chicken pectoralis major by a standardised method and association with conventional quality assessments. *Int. J. Food Sci. Technol.* 53 (7), 1744–1752. doi:10.1111/ijfs.13759

Davoodi, P., Ghaderi-Zefrehei, M., Dolatabady, M. M., Razmkabir, M., Kianpour, S., Esfahani, E. N., et al. (2023). *In silico* investigation of uncoupling protein function in avian genomes. *Front. Vet. Sci.* 9, 1085112. doi:10.3389/fvets.2022.1085112

de Brot, S., Perez, S., Shivaprasad, H., Baiker, K., Polledo, L., Clark, M., et al. (2016). Wooden breast lesions in broiler chickens in the UK. *Vet. Rec.* 178 (6), 141. doi:10.1136/vr.103561

de la Mata, M., Cotán, D., Villanueva-Paz, M., de Lavera, I., Álvarez-Córdoba, M., Luzón-Hidalgo, R., et al. (2016). Mitochondrial dysfunction in lysosomal storage disorders. *Diseases* 4 (4), 31. doi:10.3390/diseases4040031

Denton, R. M., Randle, P. J., and Martin, B. R. (1972). Stimulation by calcium ions of pyruvate dehydrogenase phosphate phosphatase. *Biochem. J.* 128 (1), 161–163. doi:10.1042/bj1280161

Denton, R. M., Richards, D. A., and Chin, J. G. (1978). Calcium ions and the regulation of NAD+-linked isocitrate dehydrogenase from the mitochondria of rat heart and other tissues. *Biochem. J.* 176 (3), 899–906. doi:10.1042/bj1760899

Dhamad, A., Zampiga, M., Greene, E. S., Sirri, F., and Dridi, S. (2021). Neuropeptide Y and its receptors are expressed in chicken skeletal muscle and regulate mitochondrial function. *Gen. Comp. Endocrinol.* 310, 113798. doi:10.1016/j.ygcen.2021.113798

Dohlman, E., Hansen, J., and Chambers, W. (2024). *USDA agricultural projections to 2033*.

Dridi, S., Onagbesan, O., Swennen, Q., Buyse, J., Decuypere, E., and Taouis, M. (2004). Gene expression, tissue distribution and potential physiological role of uncoupling protein in avian species. *Comp. Biochem.Physiol. Mol. Integr. Physiol.* 139 (3), 273–283. doi:10.1016/j.cbpb.2004.09.010

Emami, N. K., Cauble, R. N., Dhamad, A. E., Greene, E. S., Coy, C. S., Velleman, S. G., et al. (2021). Hypoxia further exacerbates woody breast myopathy in broilers via alteration of satellite cell fate. *Poult. Sci.* 100, 101167. doi:10.1016/j.psj.2021.101167

Fernández-Agüera, M. C., Gao, L., González-Rodríguez, P., Pintado, C. O., Arias-Mayenco, I., García-Flores, P., et al. (2015). Oxygen sensing by arterial chemoreceptors depends on mitochondrial complex I signaling. *Cell. Metab.* 22 (5), 825–837. doi:10.1016/j.cmet.2015.09.004

Fernandez-Vizarra, E., and Zeviani, M. (2021). Mitochondrial disorders of the OXPHOS system. *FEBS Lett.* 595 (8), 1062–1106. doi:10.1002/1873-3468.13995

Filadi, R., Greotti, E., Turacchio, G., Luini, A., Pozzan, T., and Pizzo, P. (2015). Mitofusin 2 ablation increases endoplasmic reticulum–mitochondria coupling. *Proc. Nat. Acad. Sci.* 112 (17), E2174–E2181. doi:10.1073/pnas.1504880112

Flood, D., Lee, E. S., and Taylor, C. T. (2023). Intracellular energy production and distribution in hypoxia. *J. Biol. Chem.* 299 (9), 105103. doi:10.1016/j.jbc.2023.105103

Forgac, M. (2007). Vacuolar ATPases: rotary proton pumps in physiology and pathophysiology. *Nat. Rev. Mol. Cell. Biol.* 8 (11), 917–929. doi:10.1038/nrm2272

Frezza, C., Cipolat, S., and Scorrano, L. (2007). Organelle isolation: functional mitochondria from mouse liver, muscle and cultured fibroblasts. *Nat. Protoc.* 2 (2), 287–295. doi:10.1038/nprot.2006.478

Friedman, J. R., Lackner, L. L., West, M., DiBenedetto, J. R., Nunnari, J., and Voeltz, G. K. (2011). ER tubules mark sites of mitochondrial division. *Science* 334 (6054), 358–362. doi:10.1126/science.1207385

Fung, T. S., Chakrabarti, R., and Higgs, H. N. (2023). The multiple links between actin and mitochondria. *Nat. Rev. Mol. Cell. Biol.* 24 (9), 651–667. doi:10.1038/s41580-023-00613-y

Garbincius, J. F., and Elrod, J. W. (2022). Mitochondrial calcium exchange in physiology and disease. *Physiol. Rev.* 102 (2), 893–992. doi:10.1152/physrev.00041.2020

Gilkerson, R., De La Torre, P., and St. Vallier, S. (2021). Mitochondrial OMA1 and OPA1 as gatekeepers of organellar structure/function and cellular stress response. *Front.Cell Dev. Biol.* 9, 626117. doi:10.3389/fcell.2021.626117

Gillmore, T., Farrell, A., Alahari, S., Sallais, J., Kurt, M., Park, C., et al. (2022). Dichotomy in hypoxia-induced mitochondrial fission in placental mesenchymal cells during development and preeclampsia: consequences for trophoblast mitochondrial homeostasis. *Cell Death Dis.* 13 (2), 191. doi:10.1038/s41419-022-04641-y

Giorgio, V., Burchell, V., Schiavone, M., Bassot, C., Minervini, G., Petronilli, V., et al. (2017). Ca2+ binding to F-ATP synthase β subunit triggers the mitochondrial permeability transition. *EMBO Rep.* 18 (7), 1065–1076. doi:10.15252/embr.201643354

Glancy, B., and Balaban, R. S. (2012). Role of mitochondrial Ca2+ in the regulation of cellular energetics. *Biochemistry* 51 (14), 2959–2973. doi:10.1021/bi2018909

Gomes, L. C., and Scorrano, L. (2011). Mitochondrial elongation during autophagy: a stereotypical response to survive in difficult times. *Autophagy* 7 (10), 1251–1253. doi:10.4161/auto.7.10.16771

Gottlieb, R. A., Mentzer, R. M., Jr., and Linton, P. J. (2011). Impaired mitophagy at the heart of injury. *Autophagy* 7 (12), 1573–1574. doi:10.4161/auto.7.12.18175

Greene, E., Flees, J., Dadgar, S., Mallmann, B., Orlowski, S., Dhamad, A., et al. (2019). Quantum Blue reduces the severity of woody breast myopathy via modulation of oxygen homeostasis-related genes in broiler chickens. *Front. Physiol.* 10, 1251. doi:10.3389/fphys.2019.01251

Greene, E. S., Maynard, C., Mullenix, G., Bedford, M., and Dridi, S. (2023). Potential role of endoplasmic reticulum stress in broiler woody breast myopathy. *Am. J. Physiol. Cell Physiol.* 324 (3), C679–C693. doi:10.1152/ajpcell.00275.2022

Griffiths, E. J., and Halestrap, A. P. (1993). Protection by Cyclosporin A of ischemia/reperfusion-induced damage in isolated rat hearts. *J. Mol. Cell. Cardiol.* 25 (12), 1461–1469. doi:10.1006/jmcc.1993.1162

Griffiths, E. J., Ocampo, C. J., Savage, J. S., Rutter, G. A., Hansford, R. G., Stern, M. D., et al. (1998). Mitochondrial calcium transporting pathways during hypoxia and reoxygenation in single rat cardiomyocytes. *Cardiovasc. Res.* 39 (2), 423–433. doi:10.1016/s0008-6363(98)00104-7

Grivennikova, V. G., and Vinogradov, A. D. (2013). Partitioning of superoxide and hydrogen peroxide production by mitochondrial respiratory complex I. *Biochim. Biophys. Acta* 1827 (3), 446–454. doi:10.1016/j.bbabio.2013.01.002

Gunter, T. E., Buntinas, L., Sparagna, G. C., and Gunter, K. K. (1998). The Ca2+ transport mechanisms of mitochondria and Ca2+ uptake from physiological-type Ca2+ transients. *Biochim. Biophys. Acta* 1366 (1-2), 5–15. doi:10.1016/s0005-2728(98)00117-0

Gureev, A. P., Shaforostova, E. A., and Popov, V. N. (2019). Regulation of mitochondrial biogenesis as a way for active longevity: interaction between the Nrf2 and PGC-1α signaling pathways. *Front. Genet.* 10, 435. doi:10.3389/fgene.2019.00435

Gutiérrez-Fernández, J., Kaszuba, K., Minhas, G. S., Baradaran, R., Tambalo, M., Gallagher, D. T., et al. (2020). Key role of quinone in the mechanism of respiratory complex I. *Nat. Commun.* 11 (1), 4135. doi:10.1038/s41467-020-17957-0

Haigney, M., Miyata, H., Lakatta, E. G., Stern, M. D., and Silverman, H. S. (1992). Dependence of hypoxic cellular calcium loading on Na (+)-Ca2+ exchange. *Circ. Res.* 71 (3), 547–557. doi:10.1161/01.res.71.3.547

Han, S., Zhao, F., Hsia, J., Ma, X., Liu, Y., Torres, S., et al. (2021). The role of Mfn2 in the structure and function of endoplasmic reticulum-mitochondrial tethering *in vivo*. *J. Cell Sci.* 134 (13), jcs253443. doi:10.1242/jcs.253443

Harris, D. A. (1993). Regulation of the mitochondrial ATP synthase in rat heart. *Biochem. Soc. T.* 21 (3), 778–781. doi:10.1042/bst0210778

Heerlein, K., Schulze, A., Hotz, L., Bärtsch, P., and Mairbäurl, H. (2005). Hypoxia decreases cellular ATP demand and inhibits mitochondrial respiration of a549 cells. *Am. J. Respir. Cell. Mol. Biol.* 32 (1), 44–51. doi:10.1165/rcmb.2004-0202OC

Hock, D. H., Robinson, D. R. L., and Stroud, D. A. (2020). Blackout in the powerhouse: clinical phenotypes associated with defects in the assembly of OXPHOS complexes and the mitoribosome. *Biochem. J.* 477 (21), 4085–4132. doi:10.1042/bcj20190767

Jamwal, S., Blackburn, J. K., and Elsworth, J. D. (2021). PPARγ/PGC1α signaling as a potential therapeutic target for mitochondrial biogenesis in neurodegenerative disorders. *Pharmacol. Ther.* 219, 107705. doi:10.1016/j.pharmthera.2020.107705

Jenkins, B. C., Neikirk, K., Katti, P., Claypool, S. M., Kirabo, A., McReynolds, M. R., et al. (2024). Mitochondria in disease: changes in shapes and dynamics. *Trends biochem. Sci.* 49 (4), 346–360. doi:10.1016/j.tibs.2024.01.011

Kawasaki, T., Iwasaki, T., Yamada, M., Yoshida, T., and Watanabe, T. (2018). Rapid growth rate results in remarkably hardened breast in broilers during the middle stage of rearing: a biochemical and histopathological study. *PLOS ONE* 13 (2), e0193307. doi:10.1371/journal.pone.0193307

Keeney, P. M., Xie, J., Capaldi, R. A., and Bennett, J. P., Jr. (2006). Parkinson's disease brain mitochondrial complex I has oxidatively damaged subunits and is functionally impaired and misassembled. *J. Neurosci.* 26 (19), 5256–5264. doi:10.1523/jneurosci.0984-06.2006

Kerbey, A. L., Randle, P. J., Cooper, R. H., Whitehouse, S., Pask, H. T., and Denton, R. M. (1976). Regulation of pyruvate dehydrogenase in rat heart. Mechanism of regulation of proportions of dephosphorylated and phosphorylated enzyme by oxidation of fatty acids and ketone bodies and of effects of diabetes: role of coenzyme A, acetyl-coenzyme A and reduced and oxidized nicotinamide-adenine dinucleotide. *Biochem. J.* 154 (2), 327–348. doi:10.1042/bj1540327

Khacho, M., Tarabay, M., Patten, D., Khacho, P., MacLaurin, J. G., Guadagno, J., et al. (2014). Acidosis overrides oxygen deprivation to maintain mitochondrial function and cell survival. *Nat. Commun.* 5 (1), 3550. doi:10.1038/ncomms4550

Kirichok, Y., Krapivinsky, G., and Clapham, D. E. (2004). The mitochondrial calcium uniporter is a highly selective ion channel. *Nature* 427 (6972), 360–364. doi:10.1038/nature02246

Kirshenbaum, L. A., Dhingra, R., Bravo-Sagua, R., and Lavandero, S. (2024). DIAPH1-MFN2 interaction decreases the endoplasmic reticulum-mitochondrial distance and promotes cardiac injury following myocardial ischemia. *Nat. Commun.* 15 (1), 1469. doi:10.1038/s41467-024-45560-0

Korobova, F., Ramabhadran, V., and Higgs, H. N. (2013). An actin-dependent step in mitochondrial fission mediated by the ER-associated formin INF2. *Science* 339 (6118), 464–467. doi:10.1126/science.1228360

Kushwaha, A. D., Kalra, N., Varshney, R., and Saraswat, D. (2023). Mitochondrial Ca^{2+} overload due to altered proteostasis amplifies apoptosis in C2C12 myoblasts under hypoxia: protective role of nanocurcumin formulation. *IUBMB Life* 75 (8), 673–687. doi:10.1002/iub.2720

Kuttappan, V. A., Hargis, B. M., and Owens, C. M. (2016). White striping and woody breast myopathies in the modern poultry industry: a review. *Poult. Sci.* 95 (11), 2724–2733. doi:10.3382/ps/pew216

Lassiter, K., Dridi, S., Piekarski, A., Greene, E., Hargis, B., Kong, B.-W., et al. (2014). Bioenergetics in chicken embryo fibroblast cells: evidence of lower proton leak in spontaneously immortalized chicken embryo fibroblasts compared to young and senescent primary chicken embryo fibroblast cells. *Comp. Biochem. Physiol. Mol. Integr. Physiol.* 175, 115–123. doi:10.1016/j.cbpa.2014.06.003

Lassiter, K., Greene, E., Piekarski, A., Faulkner, O. B., Hargis, B. M., Bottje, W., et al. (2015). Orexin system is expressed in avian muscle cells and regulates mitochondrial dynamics. *Am. J. Physiol. Regul. Integr. Comp. Physiol.* 308 (3), R173–R187. doi:10.1152/ajpregu.00394.2014

Lawlis, V. B., and Roche, T. E. (1980). Effect of micromolar Ca2+ on NADH inhibition of bovine kidney alpha-ketoglutarate dehydrogenase complex and possible role of Ca2+ in signal amplification. *Mol. Cell. Biochem.* 32 (3), 147–152. doi:10.1007/BF00227441

Lee, S., Wang, W., Hwang, J., Namgung, U., and Min, K.-T. (2019). Increased ER–mitochondria tethering promotes axon regeneration. *Proc. Nat. Acad. Sci.* 116(32), 16074–16079. doi:10.1073/pnas.1818830116

Li, Y., Park, J.-S., Deng, J.-H., and Bai, Y. (2006). Cytochrome c oxidase subunit IV is essential for assembly and respiratory function of the enzyme complex. *J. Bioenerg. Biomembr.* 38 (5), 283–291. doi:10.1007/s10863-006-9052-z

Liu, Y., and Zhu, X. (2017). Endoplasmic reticulum-mitochondria tethering in neurodegenerative diseases. *Transl. Neurodegener.* 6 (1), 21. doi:10.1186/s40035-017-0092-6

Maier, T., Güell, M., and Serrano, L. (2009). Correlation of mRNA and protein in complex biological samples. *FEBS Lett.* 583 (24), 3966–3973. doi:10.1016/j.febslet.2009.10.036

Manor, U., Bartholomew, S., Golani, G., Christenson, E., Kozlov, M., Higgs, H., et al. (2015). A mitochondria-anchored isoform of the actin-nucleating spire protein regulates mitochondrial division. *elife* 4, e08828. doi:10.7554/eLife.08828

McCormack, J. G., and Denton, R. M. (1979). The effects of calcium ions and adenine nucleotides on the activity of pig heart 2-oxoglutarate dehydrogenase complex. *Biochem. J.* 180 (3), 533–544. doi:10.1042/bj1800533

McCormack, J. G., Halestrap, A. P., and Denton, R. M. (1990). Role of calcium ions in regulation of mammalian intramitochondrial metabolism. *Physiol. Rev.* 70 (2), 391–425. doi:10.1152/physrev.1990.70.2.391

Mishra, P., and Chan, D. C. (2016). Metabolic regulation of mitochondrial dynamics. *J. Cell. Biol.* 212 (4), 379–387. doi:10.1083/jcb.201511036

Miyamae, M., Camacho, S. A., Weiner, M. W., and Figueredo, V. M. (1996). Attenuation of postischemic reperfusion injury is related to prevention of [Ca2+] m

overload in rat hearts. *Am. J. Physiol. Heart Circ. Physiol.* 271 (5), H2145–H2153. doi:10.1152/ajpheart.1996.271.5.H2145

Moosavi, B., Berry, E. A., Zhu, X. L., Yang, W. C., and Yang, G. F. (2019). The assembly of succinate dehydrogenase: a key enzyme in bioenergetics. *Cell. Mol. Life Sci.* 76 (20), 4023–4042. doi:10.1007/s00018-019-03200-7

Murphy, M. P. (2009). How mitochondria produce reactive oxygen species. *Biochem. J.* 417 (1), 1–13. doi:10.1042/bj20081386

Nijtmans, L. G. J., Klement, P., Houštěk, J., and van den Bogert, C. (1995). Assembly of mitochondrial ATP synthase in cultured human cells: implications for mitochondrial diseases. *Biochim. Biophy. Acta* 1272 (3), 190–198. doi:10.1016/0925-4439(95)00087-9

Niquet, J., Baldwin, R. A., Allen, S. G., Fujikawa, D. G., and Wasterlain, C. G. (2003). Hypoxic neuronal necrosis: protein synthesis-independent activation of a cell death program. *Proc. Nat. Acad. Sci.* 100(5), 2825–2830. doi:10.1073/pnas.0530113100

Nishimura, A., Shimauchi, T., Tanaka, T., Shimoda, K., Toyama, T., Kitajima, N., et al. (2018). Hypoxia-induced interaction of filamin with Drp1 causes mitochondrial hyperfission–associated myocardial senescence. *Sci. Signal.* 11(556), eaat5185. doi:10.1126/scisignal.aat5185

Nunnari, J., and Suomalainen, A. (2012). Mitochondria: in sickness and in health. *Cell* 148 (6), 1145–1159. doi:10.1016/j.cell.2012.02.035

Osto, C., Benador, I. Y., Ngo, J., Liesa, M., Stiles, L., Acin-Perez, R., et al. (2020). Measuring mitochondrial respiration in previously frozen biological samples. *Curr. Protoc. Cell Biol.* 89 (1), e116. doi:10.1002/cpcb.116

Papa, S., and De Rasmo, D. (2013). Complex I deficiencies in neurological disorders. *Trends Mol. Med.* 19 (1), 61–69. doi:10.1016/j.molmed.2012.11.005

Parker, N., Vidal-Puig, A., and Brand, M. D. (2008). Stimulation of mitochondrial proton conductance by hydroxynonenal requires a high membrane potential. *Biosci. Rep.* 28 (2), 83–88. doi:10.1042/bsr20080002

Pinton, P. (2018). Mitochondria-associated membranes (MAMs) and pathologies. *Cell Death Dis.* 9 (4), 413. doi:10.1038/s41419-018-0424-1

Raimbault, S., Dridi, S., Denjean, F., Lachuer, J., Couplan, E., Bouillaud, F., et al. (2001). An uncoupling protein homologue putatively involved in facultative muscle thermogenesis in birds. *Biochem. J.* 353 (Pt 3), 441–444. doi:10.1042/0264-6021:3530441

Rizzuto, R., Pinton, P., Carrington, W., Fay, F. S., Fogarty, K. E., Lifshitz, L. M., et al. (1998). Close contacts with the endoplasmic reticulum as determinants of mitochondrial Ca2+ responses. *Science* 280 (5370), 1763–1766. doi:10.1126/science.280.5370.1763

Rossignol, R., Faustin, B., Rocher, C., Malgat, M., Mazat, J.-P., and Letellier, T. (2003). Mitochondrial threshold effects. *Biochem. J.* 370 (3), 751–762. doi:10.1042/bj20021594

Rutter, G. A., and Denton, R. M. (1989). The binding of Ca2+ ions to pig heart NAD+-isocitrate dehydrogenase and the 2-oxoglutarate dehydrogenase complex. *Biochem. J.* 263 (2), 453–462. doi:10.1042/bj2630453

Saada, A. (2013). "Complex subunits and assembly genes: complex I," in *Mitochondrial disorders caused by nuclear genes*. Editor L.-J. C. Wong (New York, NY: Springer), 185–202.

Schmittgen, T. D., and Livak, K. J. (2008). Analyzing real-time PCR data by the comparative CT method. *Nat. Protoc.* 3, 1101–1108. doi:10.1038/nprot.2008.73

Scholz, T. D., and Balaban, R. S. (1994). Mitochondrial F1-ATPase activity of canine myocardium: effects of hypoxia and stimulation. *Am. J. Physiol. Heart Circ. Physiol.* 266 (6), H2396–H2403. doi:10.1152/ajpheart.1994.266.6.H2396

Scott, I., and Youle, R. J. (2010). Mitochondrial fission and fusion. *Essays Biochem.* 47, 85–98. doi:10.1042/bse0470085

Shen, X., Han, G., Li, S., Song, Y., Shen, H., Zhai, Y., et al. (2018). Association between the T6459C point mutation of the mitochondrial MT-CO1 gene and susceptibility to sepsis among Chinese Han people. *J. Cell. Mol. Med.* 22 (11), 5257–5264. doi:10.1111/jcmm.13746

Sihvo, H. K., Immonen, K., and Puolanne, E. (2014). Myodegeneration with fibrosis and regeneration in the pectoralis major muscle of broilers. *Vet. Pathol.* 51 (3), 619–623. doi:10.1177/0300985813497488

Soglia, F., Laghi, L., Canonico, L., Cavani, C., and Petracci, M. (2016). Functional property issues in broiler breast meat related to emerging muscle abnormalities. *Food Res. Int.* 89, 1071–1076. doi:10.1016/j.foodres.2016.04.042

Sparagna, G. C., Gunter, K. K., Sheu, S. S., and Gunter, T. E. (1995). Mitochondrial calcium uptake from physiological-type pulses of calcium. A description of the rapid uptake mode. *J. Biol. Chem.* 270 (46), 27510–27515. doi:10.1074/jbc.270.46.27510

Sprenger, H.-G., and Langer, T. (2019). The good and the bad of mitochondrial breakups. *Trends Cell Biol.* 29 (11), 888–900. doi:10.1016/j.tcb.2019.08.003

Tecalco-Cruz, A. C., Ríos-López, D. G., Vázquez-Victorio, G., Rosales-Alvarez, R. E., and Macías-Silva, M. (2018). Transcriptional cofactors Ski and SnoN are major regulators of the TGF-β/Smad signaling pathway in health and disease. *Signal Transduct. Target. Ther.* 3 (1), 15. doi:10.1038/s41392-018-0015-8

Territo, P. R., Mootha, V. K., French, S. A., and Balaban, R. S. (2000). Ca(2+) activation of heart mitochondrial oxidative phosphorylation: role of the F(0)/F(1)-ATPase. *Am. J. Physiol. Cell Physiol.* 278 (2), C423–C435. doi:10.1152/ajpcell.2000.278.2.C423

Trenker, M., Malli, R., Fertschai, I., Levak-Frank, S., and Graier, W. F. (2007). Uncoupling proteins 2 and 3 are fundamental for mitochondrial Ca2+ uniport. *Nat. Cell. Biol.* 9 (4), 445–452. doi:10.1038/ncb1556

Tropeano, C. V., Aleo, S. J., Zanna, C., Roberti, M., Scandiffio, L., Loguercio Polosa, P., et al. (2020). Fine-tuning of the respiratory complexes stability and supercomplexes assembly in cells defective of complex III. *Biochim. Biophys. Acta Bioenerg.* 1861 (2), 148133. doi:10.1016/j.bbabio.2019.148133

Tucker, E. J., Wanschers, B. F., Szklarczyk, R., Mountford, H. S., Wijeyeratne, X. W., van den Brand, M. A., et al. (2013). Mutations in the UQCC1-interacting protein, UQCC2, cause human complex III deficiency associated with perturbed cytochrome b protein expression. *PLoS Genet.* 9 (12), e1004034. doi:10.1371/journal.pgen.1004034

Velleman, S. G., and Clark, D. L. (2015). Histopathologic and myogenic gene expression changes associated with wooden breast in broiler breast muscles. *Avian Dis.* 59 (3), 410–418. doi:10.1637/11097-042015-Reg.1

Vincent, A. E., Ng, Y. S., White, K., Davey, T., Mannella, C., Falkous, G., et al. (2016). The spectrum of mitochondrial ultrastructural defects in mitochondrial myopathy. *Sci. Rep.* 6 (1), 30610. doi:10.1038/srep30610

Wiel, C., Lallet-Daher, H., Gitenay, D., Gras, B., Le Calvé, B., Augert, A., et al. (2014). Endoplasmic reticulum calcium release through ITPR2 channels leads to mitochondrial calcium accumulation and senescence. *Nat. Commun.* 5 (1), 3792. doi:10.1038/ncomms4792

Wilburn, D. T., Machek, S. B., Zechmann, B., and Willoughby, D. S. (2021). Comparison of skeletal muscle ultrastructural changes between normal and blood flow-restricted resistance exercise: a case report. *Exp. Physiol.* 106 (11), 2177–2184. doi:10.1113/EP089858

Yan, Y., Liu, J., Wei, C., Li, K., Xie, W., Wang, Y., et al. (2008). Bidirectional regulation of Ca2+ sparks by mitochondria-derived reactive oxygen species in cardiac myocytes. *Cardiovasc. Res.* 77 (2), 432–441. doi:10.1093/cvr/cvm047

Ye, F., Lemieux, H., Hoppel, C. L., Hanson, R. W., Hakimi, P., Croniger, C. M., et al. (2011). Peroxisome proliferator-activated receptor γ (PPARγ) mediates a Ski oncogene-induced shift from glycolysis to oxidative energy metabolism. *J. Biol. Chem.* 286 (46), 40013–40024. doi:10.1074/jbc.M111.292029

Yuan, Y., Chen, J., Ge, X., Deng, J., Xu, X., Zhao, Y., et al. (2021). Activation of ERK–Drp1 signaling promotes hypoxia-induced Aβ accumulation by upregulating mitochondrial fission and BACE1 activity. *FEBS Open Bio* 11 (10), 2740–2755. doi:10.1002/2211-5463.13273

Zhang, K., Li, H., and Song, Z. (2014). Membrane depolarization activates the mitochondrial protease OMA1 by stimulating self-cleavage. *EMBO Rep.* 15 (5), 576–585. doi:10.1002/embr.201338240

Zhang, X., Antonelo, D., Hendrix, J., To, V., Campbell, Y., Von Staden, M., et al. (2020). Proteomic characterization of normal and woody breast meat from broilers of five genetic strains. *Meat Muscle Biol.* 4. doi:10.22175/mmb.8759

Zhang, X., Xing, T., Zhang, L., Zhao, L., and Gao, F. (2024). Hypoxia-mediated programmed cell death is involved in the formation of wooden breast in broilers. *J. Anim. Sci. Biotechnol.* 15 (1), 77. doi:10.1186/s40104-024-01036-1

Ziegler, D. V., Vindrieux, D., Goehrig, D., Jaber, S., Collin, G., Griveau, A., et al. (2021). Calcium channel ITPR2 and mitochondria–ER contacts promote cellular senescence and aging. *Nat. Commun.* 12 (1), 720. doi:10.1038/s41467-021-20993-z

frontiers | Frontiers in Physiology

TYPE Original Research
PUBLISHED 02 April 2025
DOI 10.3389/fphys.2025.1520826

OPEN ACCESS

EDITED BY
Sandra G. Velleman,
The Ohio State University, United States

REVIEWED BY
Paul Siegel,
Virginia Tech, United States
Colin Guy Scanes,
University of Wisconsin–Milwaukee, United States

*CORRESPONDENCE
Yi Ding,
dingyi.umd@gmail.com
Jiuzhou Song,
songj88@umd.edu

RECEIVED 31 October 2024
ACCEPTED 06 January 2025
PUBLISHED 02 April 2025

CITATION
Ding Y, Dunn J, Zhang H, Zhao K and Song J (2025) Comparative transcriptomic analysis of chicken immune organs affected by Marek's disease virus infection at latency phases. *Front. Physiol.* 16:1520826. doi: 10.3389/fphys.2025.1520826

Comparative transcriptomic analysis of chicken immune organs affected by Marek's disease virus infection at latency phases

Yi Ding[1]*, John Dunn[2], Huanmin Zhang[2], Keji Zhao[3] and Jiuzhou Song[4]*

[1]Allen Institute for Brian Science, Seattle, WA, United States, [2]U.S. Department of Agriculture, U.S. National Poultry Research Center, Agricultural Research Service, Athens, GA, United States, [3]Laboratory of Epigenome Biology, Systems Biology Center, National Heart, Lung and Blood Institute, NIH, Bethesda, MD, United States, [4]Department of Animal and Avian Sciences, University of Maryland, College Park, MD, United States

Over the past decades, MDV has dramatically evolved towards more virulent strains and remains a persistent threat to the world's poultry industry. We performed genome-wide gene expression analysis in the spleen, thymus, and bursa tissues from MD-resistant line and susceptible line to explore the mechanism of MD resistance and susceptibility. We identified genes and pathways associated with the transcriptional response to MDV infection using the robust RNA sequencing approach. The transcriptome analysis revealed a tissue-specific expression pattern among immune organs when confronting MDV. At pathway and network levels, MDV infections influenced cytokine-cytokine receptor interaction and cellular development in resistant and susceptible chicken lines. Meanwhile, we also observed different genetic responses between the two chicken lines: some pathways like herpes simplex infection and influenza A were found in MD resistant line spleen tissues, whereas metabolic-related pathways and DNA replication could only be observed in MD susceptible line chickens. In summary, our research renders new perceptions of the MD progression mechanism and beckons further gene function studies into MD resistance.

KEYWORDS

Marek's disease, Marek's disease virus, poultry health, immune organs, gene exression

Introduction

Marek's disease (MD) is a highly contagious and neuropathic disease in chickens caused by Marek's disease virus (MDV), which is a cell-associated alphaherpesvirus that transforms T lymphocytes and triggers mononuclear tissue infiltration in tissues such as peripheral nerves, muscle, visceral organs, and skin (Bacon et al., 2000; Biggs, 2001; Witter et al., 2005). MDV infection involves the early cytolytic stage, latency phase, and late cytolytic phase; at each stage of infection, the virus targets immune components of the host system (Tian et al., 2012). MDV confronts primary target cells (B lymphocytes and activated $CD4^+$ T lymphocytes) and reaches replication peak from three to 7 days post-infection (Shek et al., 1983; Baigent and Davison, 1999; Baigent et al., 1998). 7–8 days after infection, MDV progression switches from cytolytic phase to latency without producing infectious progeny

in activated CD4+ T cells and infected B cells. Reactivation from latency to late cytolytic infection occurs around 2–3 weeks post-infection in susceptible chickens (Osterrieder et al., 2006). The reactivation period (late cytolytic phase) is usually companioned with tumor formation and other acute disease symptoms.

High-throughput gene expression analysis has been widely used to understand host-virus interactions. Before the RNA-Seq method, microarrays were helpful to detect host gene expression in chicken embryo fibroblasts (Morgan et al., 2001) and spleen tissue (Sarson et al., 2006; Heidari et al., 2010; Kano et al., 2009a) using MD-resistant and MD-susceptible chicken models (Sarson et al., 2008; Yu et al., 2011; Smith et al., 2011). *CD8A*, *IL8*, *USP1*, and *CTLA4* genes were considered as significant genes associated with MD-resistance or–susceptibility by testing temporal transcriptome changes using three representative chicken lines (Yu et al., 2011). By taking advantage of next-generation sequencing techniques, researchers have characterized differential expression of genes in the spleen of broiler and layer chickens, finding that TLR receptor and JAK/STAT signaling pathways were enriched following MDV infection (Perumbakkam et al., 2013).

Well-defined chicken models involve two highly inbred chicken lines 6_3 and 7_2, sub-lines of lines 6 and 7, which have been bred since 1939 and served as unique resources to explore the mechanistic difference towards MD response (Bacon et al., 2002). Availability of chicken genome sequence (Hillier et al., 2004) and next-generation sequencing techniques have altered our capability to identify more critical factors for MD resistance using these two chicken lines. Here we conducted genome-wide profiling of spleen, thymus, and bursa transcriptomes in MD-resistant line 6_3 and MD-susceptible line 7_2 using mRNA sequencing (RNA-Seq). Age-matched controls aiming at testing innate distinction among inbred chicken lines and those induced by MDV infection were implemented in our experimental design. Also, comparisons among immune organs would further uncover gene candidates related to different MD response.

Materials and methods

Animals and experimental design

Two inbred lines of White Leghorn (line 6_3 and line 7_2) were hatched, raised and maintained in USDA-ARS Avian Disease and Oncology Laboratory (Michigan, United States). Chickens from each line were separated into infected and non-infected groups respectively. Chickens from the infected group were injected intra-abdominally with a partially attenuated virulent plus strain of MDV (648A passage 40) at 5 days after hatching with a viral dosage of 500 plaque-forming units (PFU) (Chang et al., 2010). At 21 days post-infection, five chickens from each treatment and control group were sacrificed following standard animal ethics and usage guidelines. Samples from spleen, thymus, and bursa organs were gathered, frozen and stored at −20°C until RNA extraction.

RNA preparation and sequencing

Two replicates of spleen, bursa, and thymus samples were randomly selected from infected and control groups from MD-resistant line 6_3 and MD-susceptible line 7_2 chickens. Approximately 30~50 mg of the spleen, thymus, and bursa tissues were homogenized in TRizol Reagent (Qiagen, United States), and total RNA in infected and control groups was extracted by using RNeasy Mini Kit (Qiagen, United States). The mRNA isolation was performed using Oligotex mRNA Mini Kit (Qiagen United States) according to the manufacturer's instruction. Biological replicates were applied for further RNA-Seq library construction and analysis. About 300 ng of mRNA was used to synthesize the first and second strands of cDNA by SuperScriptTM III Reverse Transcriptase (Invitrogen, United States) and Second Strand cDNA Synthesis Kit (NEB, United States). After sonication, the dscDNA fragment ends were repaired by T4 and Klenow DNA polymerase and underwent library construction procedures following Illumina. Each library was identified by adding a 6-bp adaptor and sequenced at 50-bp read by an Illumina HiSeq 2,500 Sequencer.

Differential expression and pathway analysis

Raw sequencing data were checked for quality considering read counts, overall read quality, and read distribution, etc. The alignment to the reference genome (ICGSC Gallus_gallus-4.0/galGal4) downloaded from the UCSC Genome Brower (http://genome.ucsc.edu/) was performed by using an ultrafast memory-efficient short read aligner Bowtie (Langmead and Salzberg, 2012). First 15 bps from the original raw 50-bp reads were trimmed to control the mapping quality. The counting matrix was generated by the summarizeOverlaps function in R. R package edgeR (Robinson et al., 2010) and corresponding complementary functions GLM were executed to analyze count reads data and perform comparative analysis. The threshold of differentially expressed genes was set as 0.1 FDR. David (Huang et al., 2007) and Ingenuity Pathways Analysis (IPA) (Dessì et al., 2011) were utilized to analyze the biological process, molecular functions and pathways enriched for those differentially expressed genes.

Principal component analysis and Venn diagram construction

After alignment of sequencing reads and the generation of counting matrix by summarizeOverlaps function in R, an integrated, normalized data matrix for the spleen, bursa, and thymus was created using Bioconductor's DESeq (Anders and Huber, 2010) package. Principal components facilitate dimensionality reduction and noise filter, which identifies directions of maximum variance in the original data. The function *prcomp* in the R statistic package was used to perform PCA on the integrated, normalized data matrix. The top PCs were visualized using the factoextra package in R. The Venn diagram was constructed using Venn diagram function in R.

Quantitative real-time RT-PCR

Several significant genes based on RNA-Seq analysis were validated by real-time PCR using the synthesized dscDNA

described previously (Yu et al., 2011). Real-time reactions were conducted with an iQ SYBR Green PCR Kit (Bio-rad, United States) according to manufacturer's instructions. Primers were designed using Primer3 (http://fokker.wi.mit.edu/primer3/input.htm). The melting temperature was 60, and the length of amplicons was between 50 and 200bp. Ct values were calculated based on normalization of the housekeeping gene GAPDH, and three technical replicates were performed.

Results

Gene expression profiles of immune organs in MDV challenge experiments

To discover genes involved in MDV response, we performed transcriptome analysis on the spleen, thymus, and bursa of Fabricius of two chicken lines at 21 days post-MDV infection. An integrated gene expression dataset of three immune organs was created as described in Materials and Methods—the data matrix contained normalized gene expression measurements of 24 samples for 17,108 genes (Supplementary Table S1). To explore whether the samples would form distinct groups based on their gene expression profiles, we used principal component analysis (PCA) on the data matrix, and the results were visualized by scatter plots (Figures 1A, B). The preliminary PCA plot indicated the chicken samples tended to cluster by organs regardless of MDV infection when we examined the first two principal components, indicating tissue-specific gene expression patterns after MDV infection. Also, the similarity of gene expression patterns between the spleen and thymus was higher compared to other combinations when we plotted PC2 and PC3 as shown in Figure 1B.

Genome-wide profiling of the spleen transcriptome at the late cytolytic phase

For the spleen tissue, more than 211 million sequence reads were generated and mapped to the chicken genome (galGal4). Read counts associated with annotated Ensembl genes (Flicek et al., 2014) the statistical package edgeR profiled was calculated, and differential gene expression (Robinson et al., 2010). Comparisons were carried out between infected and control birds within each line, and birds underwent non-infection status from two lines to indicate disease response and baseline transcription differences.

The behavior discrepancy between the two chicken lines (MD-resistant and MD-susceptible) is remarkable when challenged by MDV infection. We witnessed a significantly larger number of differentially expressed (DE) genes in the comparison between MDV-infected and non-infected line 7_2 chickens (susceptible chicken line) than that between MD-resistant chickens. In general, the analysis detected 817 differentially expressed (DE) genes between infected and control MD-resistant line 6_3 chickens, and 4584 DE genes in MD-susceptible $L7_2$ chickens using a threshold of FDR<0.1 (Figure 2). Two chicken lines share 522 DE genes regardless of the changing direction. The direction of changes in these two lines is similar: most of the DE transcripts in the resistant line 6_3 (563 out of 817, 68.91%) and the susceptible line 7_2 (2,959 out of 4,584, 64.55%) were downregulated. In those shared 522 DE genes, 136 genes were upregulated both in MD-resistant line 6_3 and MD-susceptible line 7_2 infected birds, and 365 genes were downregulated, while the remaining 21 genes displayed opposite alteration trends in resistant and susceptible chicken lines.

When comparing the innate difference between two chicken lines, most DE genes (801 out of 1,118, 71.64%) exhibited higher expression levels in MD-resistant line 6_3. Almost half (49%) of these genes were also differentially expressed in susceptible line 7_2 in response to MDV infection (84.49% downregulated). Those distinctions between the two inbred chicken lines might reflect the baseline transcription that could be the possible contribution of varying MD-resistant phenotypes.

Thymus and bursa transcriptome profiling at late cytolytic phase

Following a similar experimental design and analysis methodology, we examined the genome-wide transcription levels in the thymus and bursa organs at the late cytolytic phase for the above chicken lines. Similarly, considerably larger DE genes were observed in MD-susceptible line 7_2 birds for both tissues. In thymus tissues, we discovered 734 DE genes in susceptible chicken lines while only 14 DE genes in resistant chicken lines using a threshold of FDR < 0.1 (Figure 3). In the bursa organ, 259 and 5387 DE genes were detected in resistant and susceptible chickens, respectively with FDR < 0.1 (Figure 4). Interestingly, most DE genes were upregulated in response to MDV infection in the bursa and thymus tissues except for MD-resistant line 6_3 chicken thymus.

Comparisons between control birds in thymus and bursa organs revealed the intrinsic difference between chicken lines. Approximately 57% (266 out of 465) DE genes showed higher expression levels in the thymus of resistant line 6_3 chickens and 54.74% (1,542 out of 2,817) in the bursa of resistant line 6_3 chickens. In summary, by conducting two sets of comparisons in different immune organs, we were able to uncover the innate and MDV-induced variation in two inbred chicken lines. A slightly larger proportion of genes exhibited higher baseline expression levels in the resistant line. However, more significant DE genes were detected in the susceptible chickens than in the resistant chickens at the late stage of infection, probably due to transcriptional activation during the late cytolytic phase in MDV-susceptible chickens.

Witnessing the distinct features of these chicken lines, we attempted to characterize genes associated with MD resistance and–susceptibility to pair-wise comparisons. We made the following hypothesis: genes differentially expressed after MDV infection in all three immune organs are likely a reflection of the typical host response and an immune network to viral infection; genes that are differentially expressed merely in one immune tissue could be part of an organ-specific host response and function to viral infection. According to this rationale, we identified common responses and organ-specific functional genes after MDV challenges (Figure 5). Most DE genes were only present in one tissue, indicating the tissue-specific expression patterns of MDV infection. Based on the KEGG pathway, the significant pathway for those shared DE genes involved the cytokine-cytokine receptor interaction.

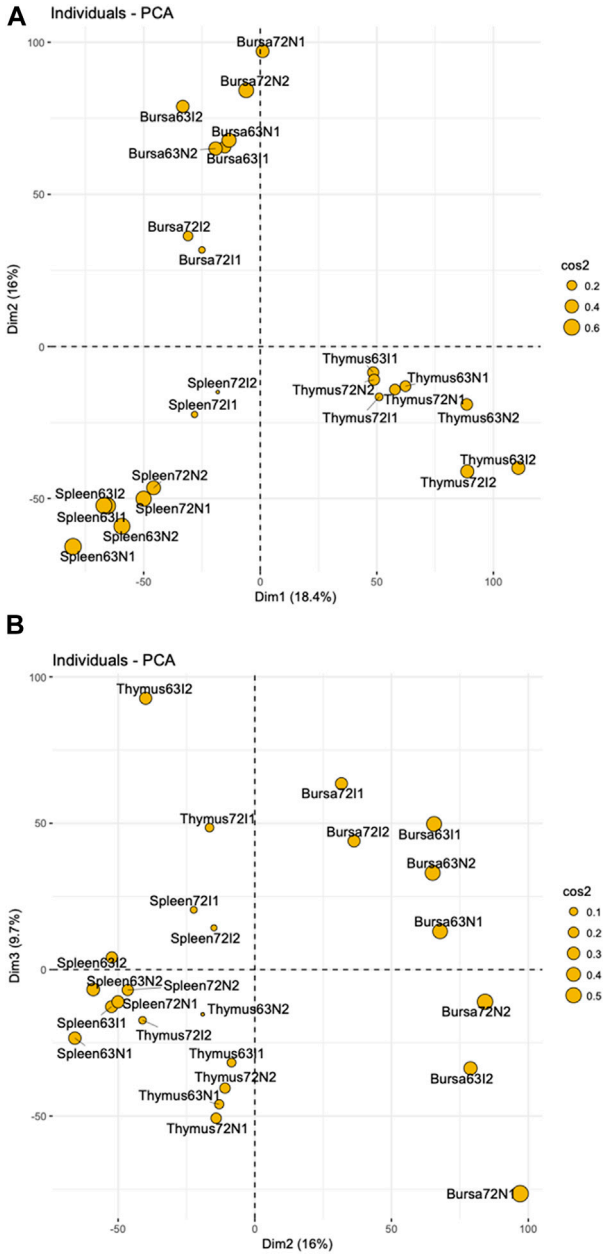

FIGURE 1
PCA Plots **(A)** a two-dimensional PCA plot showing principal component 1 (Dim1) and principal component (Dim2) of 24 individuals indicate tissue-specific gene expression patterns with a slight similarity between chicken spleen and thymus organs. **(B)** a two-dimensional PCA plot showing principal component 2 (Dim2) and principal component 3 (Dim3) across spleen, thymus, and bursa tissue. In both figures, the percentages represent the proportion of the total variance in the data that is captured by each principal component. Cos2 values indicate quality of the representation for individuals on the principal components. A higher cos2 represents a better representation of the individual on the principal component.

Pathway analysis to reveal networks and biofunctions involved in MDV infection

Previous studies have identified some well-known immune factors in the DE gene list. These include chemokine receptor 1 (Xcr1), chemokine receptor 2 (CCR2), interleukin 1 receptor, type II (IL1R2), type I (IFNA) interferon, and type II (IFNG) interferon. Additionally, several other innate immune function genes were influenced, such as FYN oncogene related to SRC, FGR, YES (FYN), and CD247 molecule (cd247), which are involved in natural killer cell-mediated cytotoxicity. Interestingly, some profoundly affected genes have no known function in innate immune responses, including collagen type II alpha 1 (COL2A1) and growth factor receptor-bound protein 2 (GRB2).

To identify enriched biological function and networks associated with the differentially expressed genes after MDV infection, we utilized the Ingenuity Pathway Analysis (IPA) and DAVID Bioinformatics Resources to analyze the gene sets

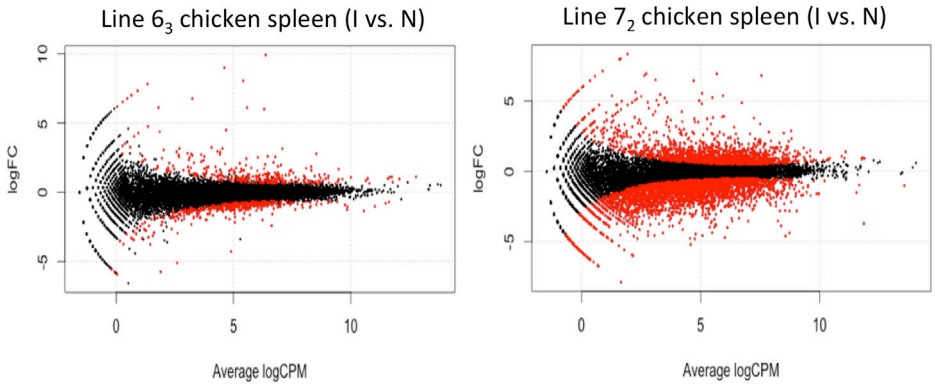

FIGURE 2
Differentially Expressed Genes in Chicken Spleen Tissues in the volcano plot In chicken spleen tissues, the analysis detected 817 differentially expressed genes between MDV-infected and non-infected L63 chickens (left panel) and 4,584 genes in L7$_2$ chickens (right panel) with FDR < 0.1. Each red dot represents the significant individual differentially expressed gene.

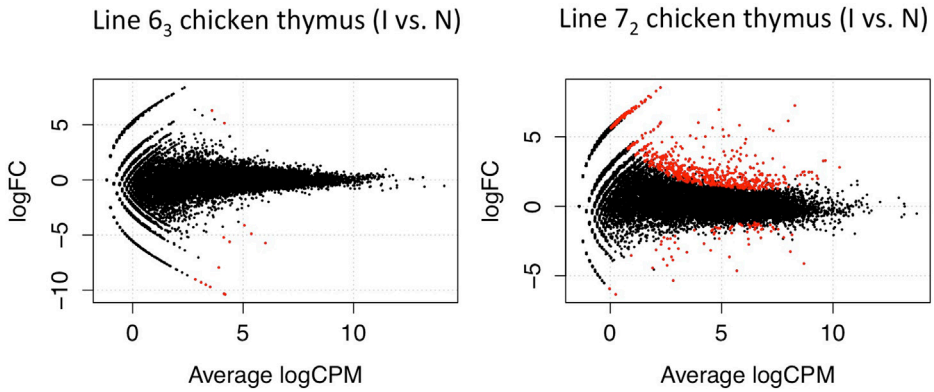

FIGURE 3
Differentially Expressed Genes in Thymus Tissue. The volcano plot shows the discovered 734 significant differentials expressed genes in susceptible line 7$_2$ chickens while 14 DE genes in resistant line 6$_3$ birds using a threshold of FDR < 0.1 in the thymus tissue (red dots).

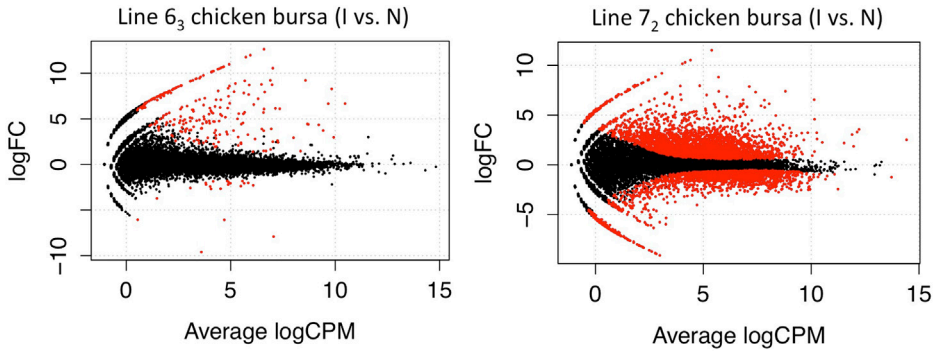

FIGURE 4
Differentially Expressed Genes in Bursa Tissue In the bursa organ, 259 and 5387 DE genes were detected in line 6$_3$ and line 7$_2$ chickens respectively with FDR < 0.1.

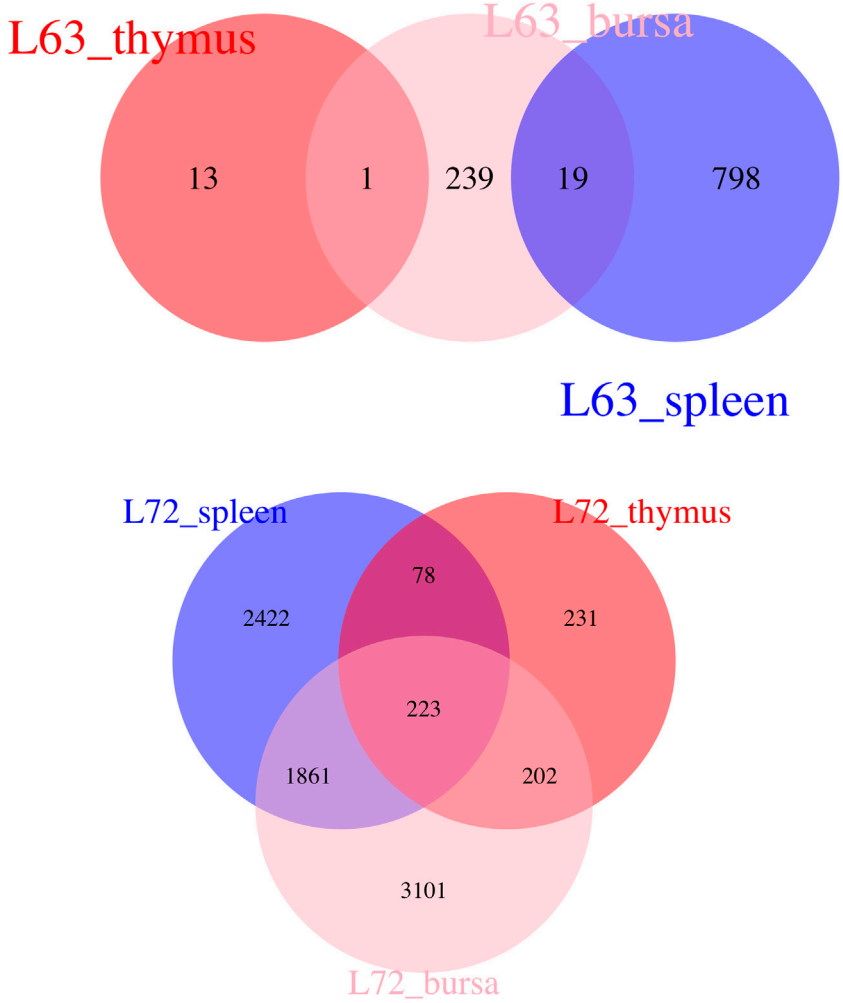

FIGURE 5
Venn Diagram Indicating Overlap Genes The Venn diagram indicates the overlap differentially expressed genes among different organs after Marek's disease virus infection.

obtained by comparing to age-matched uninfected controls. Top networks (from IPA) influenced by MDV infection in three organs are shown in Table 1. From these networks, we noticed that the virus has a broad impact on host gene expression in three immune organs of two chicken lines. Also, if we considered those genes associated with diseases and bio-functions, we discovered that many genes were influenced by MDV infection, including those involved in metabolism, tissue development, and immune-related disorders. Those genes indicated broad similarities in the host response to MDV infection. Nevertheless, some unique networks, such as digestive system development and function, gastrointestinal disease, and hepatic system development and function, were only shown in the spleen of MD-susceptible line 7_2 chickens after MDV infection (Table 1). To gain more insight into the bio-function associated with MDV infection, we utilized the IPA program to analyze disease and bio-function of those differentially expressed genes (Table 2). As might be expected, cancer and immunological illness were observed.

Complementary to the discoveries from IPA, DAVID displays biological pathways that were altered (compared to a relevant control) during the host response to MDV infection. Based on KEGG pathways (Kanehisa and Goto, 2000), immune-related pathways, such as cytokine-cytokine receptor interaction (Figure 6), phagosome, herpes simplex infection, and lysosome, were involved in MDV infection response. Also interestingly we could notice the changes in focal adhesion and tight junction pathways, and this might relate to the viral progression in host bodies since MDV requires cell-to-cell contact for dispersal (Smith et al., 2011). The virus might promote such communication by altering the expression of related tight junction formation genes.

The potential native dissimilarity between lines makes the resistance different

The underlying mechanism for the different responses to MDV infection between two lines might be complex since MD is a complex disease. One possible hypothesis is that before MDV infection, MD-resistant line 6_3 chickens could promote better

TABLE 1 Enriched networks in organs of chicken lines after MDV infection.

Lines	Organ	Enriched network functions
$L6_3$	Spleen	Cellular Development, Embryonic Development, Nervous System Development and Function
		Cancer, Respiratory Disease, Developmental Disorder
		Cell Death and Survival, Cellular Development, Cellular Function and Maintenance
		Developmental Disorder, Hereditary Disorder, Immunological Disease
		Cellular Function and Maintenance, Connective Tissue Development and Function
	Bursa	Cell-To-Cell Signaling and Interaction, Hematological System Development and Function, Immune Cell Trafficking
		Cardiac Hypertrophy, Cardiovascular Disease, Developmental Disorder
		Cellular Development, Embryonic Development, Organismal Development
		Cell-mediated Immune Response, Cellular Development, Cellular Function and Maintenance
	Thymus	Cardiac Arrythmia, Cardiovascular Disease, Organismal Injury and Abnormalities
		Cell Death and Survival, Cell Morphology, Cellular Compromise
$L7_2$	Spleen	Cell-To-Cell Signaling and Interaction, Cell Signaling, Cell Morphology
		Post-Translational Modification, Dermatological Diseases and Conditions, Developmental Disorder
		Digestive System Development and Function, Gastrointestinal Disease, Hepatic System Development and Function
		Hematological Disease, Metabolic Disease, Protein Synthesis
		Embryonic Development, Organismal Development, Cellular Movement
	Bursa	Cellular Development, Cellular Growth and Proliferation, Hematological System Development and Function
		Cell-mediated Immune Response, Cellular Function and Maintenance
		Carbohydrate Metabolism, Cell Death and Survival, Cellular Movement
		DNA Replication, Recombination, and Repair, Developmental Disorder
	Thymus	Infectious Disease, Connective Tissue Disorders, Dental Disease
		Metabolic Disease, Lipid Metabolism, Small Molecule Biochemistry
		Humoral Immune Response, Protein Synthesis, Inflammatory
		Response Cell-To-Cell Signaling and Interaction, Cell Signaling, Molecular Transport
		Cell Cycle, Cellular Development, Cellular Growth and Proliferation

immune system development and higher expression of innate immune-related genes compared to MD-susceptible line 7_2 chickens, while after MDV infection, MD-resistant line 6_3 chickens mount more robust induced immune responses by regulating adaptive immunity gene activities. As demonstrated previously, baseline transcription differences were discovered between two lines (1118 DE genes in the spleen, 465 DE genes in the thymus, and 2817 DE genes in the bursa) in tissues from the control (uninfected) birds. Among those genes, examples like Apoa4, C3, IL1RL1, LOC395914, Rag2, Smad5, CATHL2, TLR4, TNFRSF1A, Cxcl14, and IL1B are involved in immune system development and innate immune response.

Gene expression disparity was also witnessed between these two lines after MDV infection (3852 DE genes in the spleen, 222 DE genes in the thymus, and 1439 DE genes in the bursa). We could notice changes of adaptive immunity genes including IL18, il10, IRF7, TAP2, SWAP70, Fas, CD28, TNFSF13B, TNFRSF13C, B-MA1, CD40LG, ada, HSPD1, PRKCD, and IFNG. For example, if we focused on the DE genes that only existed in the spleen tissue of MD-resistant line 6_3 but were not seen in the spleen tissue of MD-susceptible line 7_2 chickens after MDV infection, we would detect two exciting pathways: toll-like receptor signaling pathway and herpes simplex infection pathway. Therefore, regardless of MDV infection, the inborn discrepancy between the two lines might contribute to the MD resistance mechanism.

Experimental validation of differentially expressed genes

We randomly selected several DE genes to confirm the RNA-Seq reliability and differential expression among contrasting treatment groups. We analyzed the sample using qPCR with dscDNA as the template from the sequencing samples. A reference gene with stable expression is necessary to avoid distortions in qPCR, so GAPDH was used as an internal reference (Sarson et al., 2008). Notably, eight genes were examined in the spleen organ in both MD-resistant $L6_3$ and MD-susceptible $L7_2$ chickens in response to MDV infection

TABLE 2 Top disease and bio-functions in chicken organs after MDV infection.

Lines	Organ	Diseases and disorders	Physiological system development and function
$L6_3$	Spleen	Metabolic Disease, Inflammatory Response, Immunological Disease, Cancer, Organismal Injury and Abnormalities	Cardiovascular System Development and Function, Hepatic System Development and Function, Tissue Development, Connective Tissue Development and Function, Embryonic Development
	Bursa	Cancer, Organismal Injury and Abnormalities, Inflammatory Response	Hematological System Development and Function, Cell-mediated Immune Response, Hematopoiesis, Lymphoid Tissue Structure and Development, Immune Cell Trafficking
	Thymus	Cardiovascular Disease, Organismal Injury and Abnormalities, Connective Tissue Disorders, Developmental Disorder, hereditary Disorder	Cardiovascular System Development and Function, Embryonic Development, Organ Morphology, Organismal Development, Skeletal and Muscular System Development and Function
$L7_2$	Spleen	Cancer, Gastrointestinal Disease, Organismal Injury and Abnormalities, Reproductive System Disease, Hepatic System Disease	Cardiovascular System Development and Function, Organismal Survival, Organismal Development, Tissue Morphology, Embryonic Development
	Bursa	Cancer, Organismal Injury and Abnormalities, Inflammatory Response, Hematological Response, Immunological Disease	Hematological System Development and Function, Tissue Morphology, Hematopoiesis, Cell-mediated Immune Response, Lymphoid Tissue Structure and Development
	Thymus	Cancer, Inflammatory Response, Infectious Disease, Cardiovascular Disease, Gastrointestinal Disease	Tissue Morphology, Organismal Development, Hematological System Development and Function, Immune Cell Trafficking, Humoral Immune Response

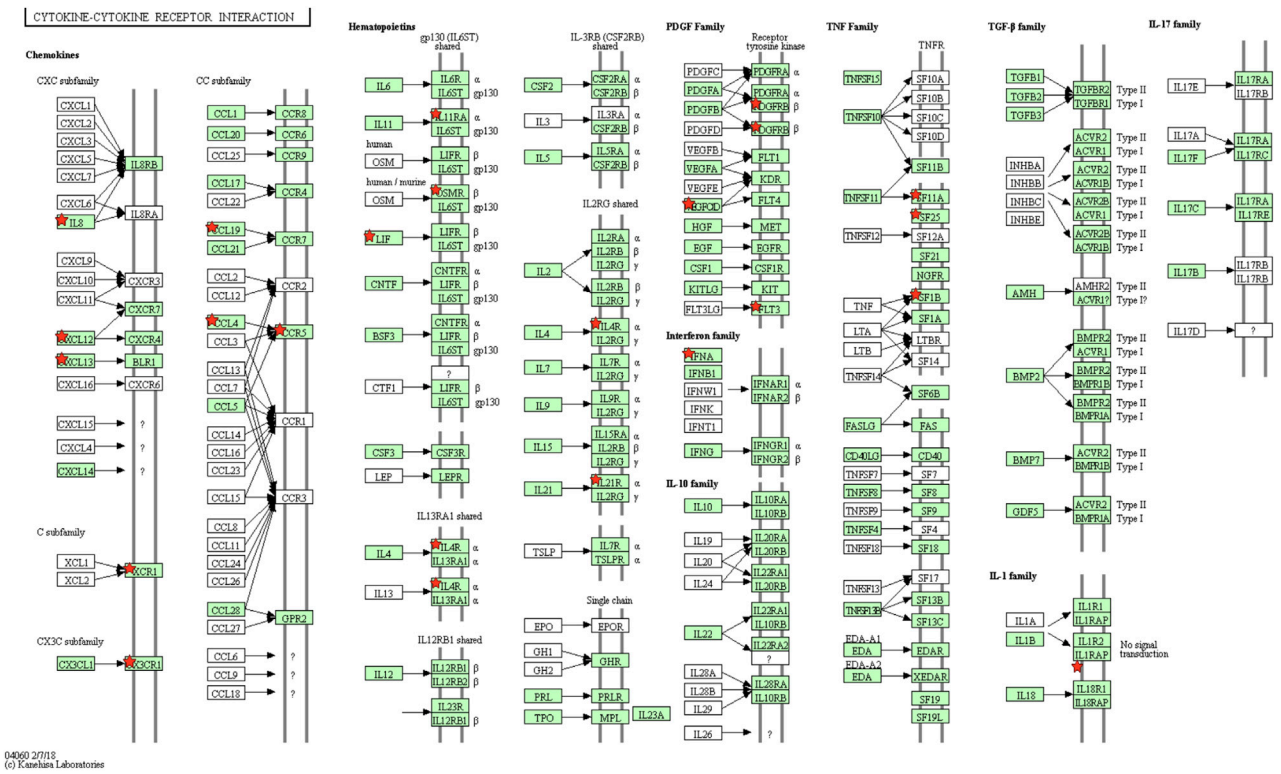

FIGURE 6
Cytokine-cytokine Receptor Interaction Pathway. One example of the enriched pathway induced by MDV infection in line 6_3 chickens. Several identified genes from this pathway display significant differential expression patterns, as indicated by red stars in the figure.

(Figure 7). These eight genes manifested a concordant change direction compared to the RNA-Seq analysis estimate, and the gene expression difference was verified. In general, the validation outcomes from the qPCR assay provide us with further confidence in our analysis.

Discussion

With extensive studies, cytokine production in response to MDV infection and their potential immune functions against MD have been described including IL4 (Heidari et al., 2008), IL6

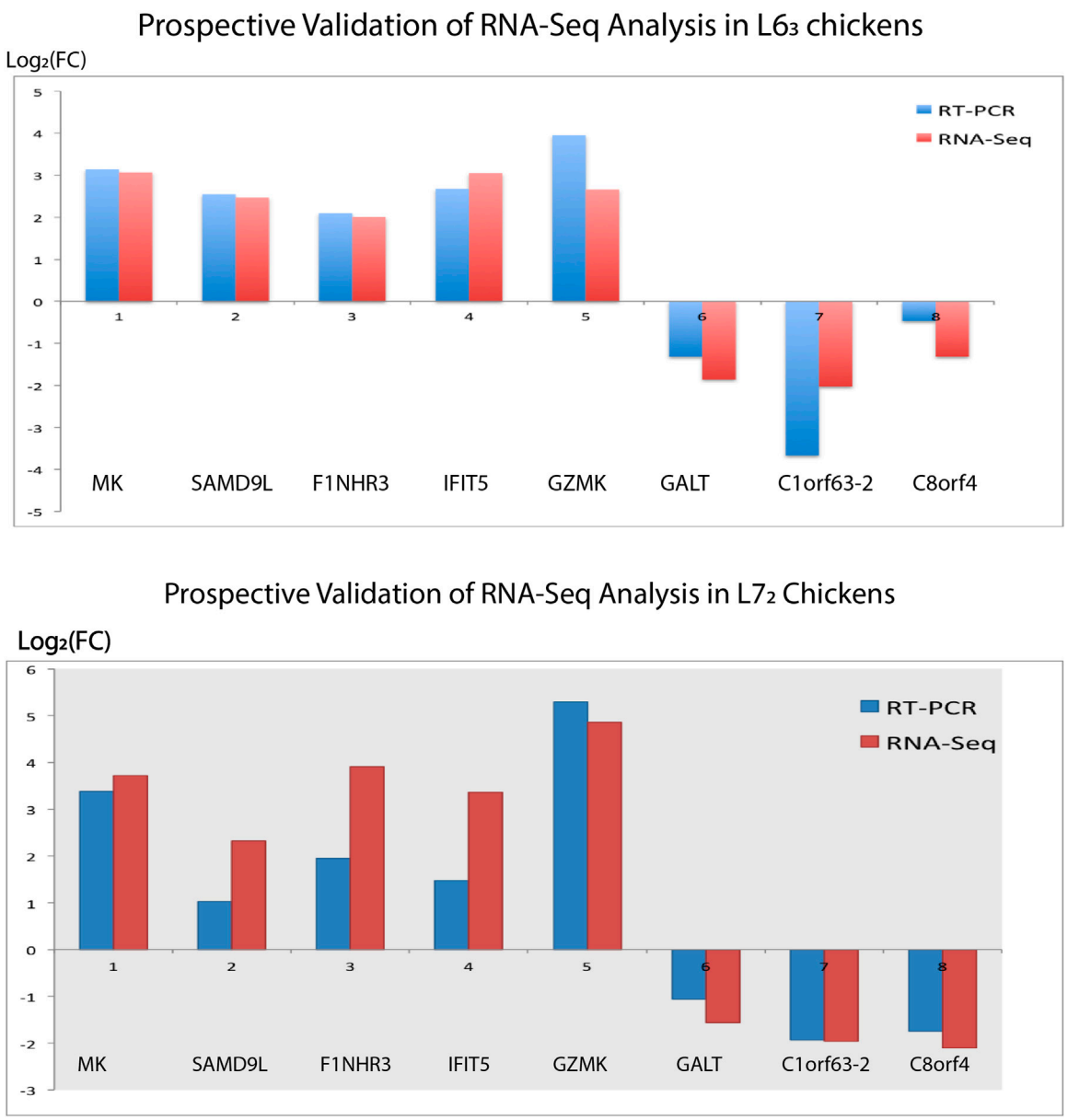

FIGURE 7
Real-time PCR Validation. Eight genes (five upregulated genes and three downregulated genes) identified in the spleen tissues of $L6_3$ and $L7_2$ chickens were selected for validation, respectively. The gene expression trend is confirmed if the expression fold change in qPCR analysis is concordant as measured by RNA-seq analysis.

(Kaiser et al., 2003; Abdul-Careem et al., 2007), IL10 (Lian et al., 2012), IL18 (Smith et al., 2011; Kaiser et al., 2003; Abdul-Careem et al., 2007), and IFN-© (Xing and Schat, 2000; Kano et al., 2009b). For instance, several studies together indicated the lacking association of IFN-© expression with resistance against MD (Abdul-Careem et al., 2007). Meanwhile, increased IL6 and IL18 expression levels were observed in splenocytes of susceptible chickens. However, those cytokines alone do not adequately manifest interactions among vital immunological mediators and their receptors.

We noticed several interesting DE genes including a set of chemokine receptors and interleukin receptors. For example, chemokine receptors XCR1, CCR2, and CX3CR1 were upregulated in the resistant line's spleen tissue at the late cytolytic phase, and interleukin receptors IL1R2, IL21R, IL4R, and IL11RA underwent dramatic expression changes. The XCL1-XCR1 axis is necessary for efficient cytotoxic immune response mediated by $CD8^+$ T cells (Lei and Takahama, 2012). Also, CCR2 is indispensable for macrophage-dependent inflammatory reactions and regulates monocyte and macrophage recruitment (Weisberg et al., 2006), and has been correlated with delayed AIDS progression in HIV infection (Faure et al., 2000; Arenzana-Seisdedos and Parmentier, 2006). The expression of CX3CR1 appears to induce both adhesion and migration of

leukocytes (Imai et al., 1997). Considering the potential roles of these chemokine receptors in innate immunity and adaptive immunity against HIV infection, etc., it's reasonable to infer that upregulation of these chemokine receptors in MDV-infected birds from the resistant line might suggest a stronger anti-viral response compared to the susceptible line. Meanwhile, the over-expressed interleukin receptor IL1R2 in the resistant chicken spleen indicates the regulation of inflammatory response; researchers have revealed IL1R2's function as a proinflammatory factor by activating several inflammatory cytokines' expression (Mar et al., 2013). Also, in the chicken spleen, the upregulated IL4R (ENSGALG00000006313) promotes differentiation of Th2 cells (Fernandez-Botran et al., 1988), and IL21R (ENSGALG00000006318) fosters T cells, B cells, and natural killer cells' proliferation and differentiation (Parrish-Novak et al., 2000).

Other interesting genes include signal transducer and activator of transcription 1 (STAT1) and leukemia inhibitory factor (LIF). STAT1 was discovered through its involvement in interferon (IFN) signaling and its function in regulating cell growth and differentiation, immune response, antiviral activity, and homeostasis (Ramana et al., 2000). Challenged with chemical carcinogens, mice lacking STAT1 showed more rapid and frequent tumor development (Lee et al., 2000). There was little or no STAT1 expression even after IFN treatment in some tumor cells and tumor-derived cell lines, and STAT1-depleted cells resisted apoptosis in response to TNF or IFN-gamma (Lee et al., 2000; Sun et al., 1998). ChIP-seq experiments using IFN-stimulated HeLa S3 cells indicated the genome-wide binding sites of STAT1 mainly fall into promoters and intronic regions, and suggested the high complexity of STAT1-mediated gene regulatory mechanism (Satoh and Tabunoki, 2013). Leukemia inhibitory factor (LIF) was observed to stimulate proliferation of breast, kidney, and prostate cancer cells (Kellokumpu-Lehtinen et al., 1996). LIF inhibited Th17 cells differentiation by exerting an opposite effect on STAT3 phosphorylation, which is required for Th17 cell differentiation, in experimental autoimmune encephalomyelitis mice (Cao et al., 2011). When examining STAT1 and LIF expression levels in spleen tissues from the resistant chickens, it is interesting to note that STAT1 was overexpressed (with a logFC of 1.43), and LIF was downregulated (with a logFC −3.33) compared to the non-infected control birds. In resistant chickens, the high level of STAT1 might promote the expression of immune-related genes to fight against MDV while the inhibition of LIF could activate T cell differentiation under the MDV challenge. Since these two genes were only differentially expressed in resistant rather than susceptible chicken lines, their biological functions may contribute to the phenotypic variations induced by MDV infection.

In the three immune organs, we discovered common pathways including cytokine-cytokine receptor interactions and cell adhesion molecules (CAMs) induced by MDV infection. The cytokines and cell adhesion molecules indicate the involvement of innate as well as adaptive inflammatory host defense against MDV infection and immune cell-cell interactions. In fact, most DE genes (as shown in Figure 5) and enriched pathways (Appendix I) identified in our study were tissue-specific. For instance, Herpes simplex infection and Influenza A pathways were mainly enriched in MD-resistant line 6_3 chicken spleen tissues, while tight junction and focal adhesion were enriched in MD-resistant line 6_3 chicken bursa tissues. In MD-susceptible line 7_2 chickens, pathways associated with metabolism, cell cycle, and DNA replication were highly enriched in three organs induced by MDV infection. This observation is in line with previous findings that networks related to cell-mediated immune response were specifically enriched in MD-resistant line 6_3 chickens (Yu et al., 2011; Mitra et al., 2015).

Although in recent years many studies examining gene expression changes related to MD have revealed the interaction between virus and hosts to some extent, the results from similar experiments vary significantly. Admittedly, the complex nature of Marek's disease introduces confounding sources of variations, such as virus strains, the genetic background of birds and experimental procedures. Hence, it is arbitrary to compare results from experiments performed under different circumstances simply.

In summary, we have carried out a comprehensive analysis of three immune organs' transcriptomes in inbred chicken lines, showing differential reactions to MD with a focus focusing on the spleen tissue because all stages of the MDV life cycle occur in the spleen (Baigent and Davison, 2004). We designed and performed a pair-wise experiment based on chicken lines and infection time to control the intrinsic transcriptional fluctuation and take full advantage of the similar genetic background of these inbred lines. This methodology enabled us to characterize genes highly associated with MD resistance and susceptibility and reveal a universal impact of MDV infection on the hosts. Using DAVID and IPA analysis, we observed remarkable distinctions between two lines in the natural state and in response to MDV infection. We discovered enriched networks in metabolism, tissue development, gene expression, and cell signaling. Although our data have provided candidate genes and pathways controlling the different physiological responses between two chicken lines, functional studies are necessary to validate the impacts of those intriguing genes/pathways and elucidate the underlying mechanism associated with MD resistance.

Data availability statement

The original contributions presented in the study are publicly available. This data can be found here: NCBI SRA Repository, accession numbers SRR32499841, SRR32499840, SRR32499829, SRR32499824, SRR32499823, SRR32499822, SRR32499821, SRR32499820, SRR32499819, SRR32499818, SRR32499839, SRR32499838, SRR32499837, SRR32499836, SRR32499835, SRR32499834, SRR32499833, SRR32499832, SRR32499828, SRR32499827, SRR32499826 and SRR32499825.

Ethics statement

The animal study was approved by ADOL (31320-008-00D) and University of Maryland (R-08-62). The study was conducted in accordance with the local legislation and institutional requirements.

Author contributions

YD: Data curation, Formal Analysis, Methodology, Validation, Writing–original draft, Writing–review and editing. JD: Data curation, Resources, Writing–review and editing. HZ: Methodology, Project administration, Resources, Writing–review and editing. KZ: Project administration, Resources, Validation, Methodology, Writing–review and editing. JS: Conceptualization, Data curation, Funding acquisition, Investigation, Methodology, Project administration, Resources, Supervision, Writing–original draft, Writing–review and editing.

Funding

The author(s) declare that financial support was received for the research and/or publication of this article. This project was supported by National Research Initiative Competitive Grants nos USDA-NRI/NIFA 2008-35204 04660 and USDA-NRI/NIFA 2010-65205-20588 from the USDA National Institute of Food and Agriculture.

Conflict of interest

The authors declare that the research was conducted in the absence of any commercial or financial relationships that could be construed as a potential conflict of interest.

The author(s) declared that they were an editorial board member of Frontiers, at the time of submission. This had no impact on the peer review process and the final decision.

Generative AI statement

The author(s) declare that no Generative AI was used in the creation of this manuscript.

Publisher's note

Supplementary material

The Supplementary Material for this article can be found online at: https://www.frontiersin.org/articles/10.3389/fphys.2025.1520826/full#supplementary-material

References

Abdul-Careem, M. F., Hunter, B. D., Parvizi, P., Haghighi, H. R., Thanthrige-Don, N., and Sharif, S. (2007). Cytokine gene expression patterns associated with immunization against Marek's disease in chickens. *Vaccine* 25 (3), 424–432. doi:10.1016/j.vaccine.2006.08.006

Anders, S., and Huber, W. (2010). Differential expression analysis for sequence count data. *Genome Biol.* 11 (10), R106. doi:10.1186/gb-2010-11-10-r106

Arenzana-Seisdedos, F., and Parmentier, M. (2006). "Genetics of resistance to HIV infection: role of co-receptors and co-receptor ligands," in *Seminars in immunology* (Elsevier), 387–403.

Bacon, L., Hunt, H., and Cheng, H. (2000). A review of the development of chicken lines to resolve genes determining resistance to diseases. *Poult. Sci.* 79 (8), 1082–1093. doi:10.1093/ps/79.8.1082

Bacon, L. D., Zajchowski, L., Clark, M. E., and Etches, R. J. (2002). Identification and evaluation of major histocompatibility complex antigens in chicken chimeras and their relationship to germline transmission. *Poult. Sci.* 81 (10), 1427–1438. doi:10.1093/ps/81.10.1427

Baigent, S. J., and Davison, F. (2004). "Marek's disease virus: biology and life cycle," in *Marek's disease, an evolving problem* (Elsevier Academic Press Great Britain), 62–77.

Baigent, S. J., and Davison, T. (1999). Development and composition of lymphoid lesions in the spleens of Marek's disease virus-infected chickens: association with virus spread and the pathogenesis of Marek's disease. *Avian Pathol.* 28 (3), 287–300. doi:10.1080/03079459994786

Baigent, S. J., Ross, L., and Davison, T. (1998). Differential susceptibility to Marek's disease is associated with differences in number, but not phenotype or location, of pp38+ lymphocytes. *J. general virology* 79 (11), 2795–2802. doi:10.1099/0022-1317-79-11-2795

Biggs, P. (2001). "The history and biology of Marek's disease virus," in *Marek's disease* (Springer), 1–24.

Cao, W., Yang, Y., Wang, Z., Liu, A., Fang, L., Wu, F., et al. (2011). Leukemia inhibitory factor inhibits T helper 17 cell differentiation and confers treatment effects of neural progenitor cell therapy in autoimmune disease. *Immunity* 35 (2), 273–284. doi:10.1016/j.immuni.2011.06.011

Chang, S., Dunn, J. R., Heidari, M., Lee, L. F., Song, J., Ernst, C. W., et al. (2010). Genetics and vaccine efficacy: host genetic variation affecting Marek's disease vaccine efficacy in White Leghorn chickens. *Poult. Sci.* 89 (10), 2083–2091. doi:10.3382/ps.2010-00740

Dessì, A., Atzori, L., Noto, A., Adriaan Visser, G. H., Gazzolo, D., Zanardo, V., et al. (2011). Metabolomics in newborns with intrauterine growth retardation (IUGR): urine reveals markers of metabolic syndrome. *J. Maternal-Fetal Neonatal Med.* 24 (S2), 35–39. doi:10.3109/14767058.2011.605868

Faure, S., Meyer, L., Costagliola, D., Vaneensberghe, C., Genin, E., Autran, B., et al. (2000). Rapid progression to AIDS in HIV+ individuals with a structural variant of the chemokine receptor CX3CR1. *Science* 287 (5461), 2274–2277. doi:10.1126/science.287.5461.2274

Fernandez-Botran, R., Sanders, V., Mosmann, T., and Vitetta, E. (1988). Lymphokine-mediated regulation of the proliferative response of clones of T helper 1 and T helper 2 cells. *J. Exp. Med.* 168 (2), 543–558. doi:10.1084/jem.168.2.543

Flicek, P., Amode, M. R., Barrell, D., Beal, K., Billis, K., Brent, S., et al. (2014). Ensembl 2014. *Nucleic acids Res.* 2013, gkt1196. doi:10.1093/nar/gkt1196

Heidari, M., Sarson, A. J., Huebner, M., Sharif, S., Kireev, D., and Zhou, H. (2010). Marek's disease virus–induced immunosuppression: array analysis of chicken immune response gene expression profiling. *Viral Immunol.* 23 (3), 309–319. doi:10.1089/vim.2009.0079

Heidari, M., Zhang, H. M., and Sharif, S. (2008). Marek's disease virus induces Th-2 activity during cytolytic infection. *Viral Immunol.* 21 (2), 203–214. doi:10.1089/vim.2007.0078

Hillier, L. W., Miller, W., Birney, E., Warren, W., Hardison, R. C., Ponting, C. P., et al. (2004). Sequence and comparative analysis of the chicken genome provide unique perspectives on vertebrate evolution. *Nature* 432 (7018), 695–716. doi:10.1038/nature03154

Huang, D. W., Sherman, B. T., Tan, Q., Kir, J., Liu, D., Bryant, D., et al. (2007). DAVID Bioinformatics Resources: expanded annotation database and novel algorithms to better extract biology from large gene lists. *Nucleic acids Res.* 35 (Suppl. 2), W169–W175. doi:10.1093/nar/gkm415

Imai, T., Hieshima, K., Haskell, C., Baba, M., Nagira, M., Nishimura, M., et al. (1997). Identification and molecular characterization of fractalkine receptor CX 3 CR1, which mediates both leukocyte migration and adhesion. *Cell* 91 (4), 521–530. doi:10.1016/s0092-8674(00)80438-9

Kaiser, P., Underwood, G., and Davison, F. (2003). Differential cytokine responses following Marek's disease virus infection of chickens differing in resistance to Marek's disease. *J. virology* 77 (1), 762–768. doi:10.1128/jvi.77.1.762-768.2003

Kanehisa, M., and Goto, S. (2000). KEGG: kyoto encyclopedia of genes and genomes. *Nucleic acids Res.* 28 (1), 27–30. doi:10.1093/nar/28.1.27

Kano, R., Konnai, S., Onuma, M., and Ohashi, K. (2009a). Microarray analysis of host immune responses to Marek's disease virus infection in vaccinated chickens. *J. Veterinary Med. Sci.* 71 (5), 603–610. doi:10.1292/jvms.71.603

Kano, R., Konnai, S., Onuma, M., and Ohashi, K. (2009b). Cytokine profiles in chickens infected with virulent and avirulent Marek's disease viruses: interferon-gamma is a key factor in the protection of Marek's disease by vaccination. *Microbiol. Immunol.* 53 (4), 224–232. doi:10.1111/j.1348-0421.2009.00109.x

Kellokumpu-Lehtinen, P., Talpaz, M., Harris, D., Van, Q., Kurzrock, R., and Estrov, Z. (1996). Leukemia-inhibitory factor stimulates breast, kidney and prostate cancer cell proliferation by paracrine and autocrine pathways. *Int. J. cancer* 66 (4), 515–519. doi:10.1002/(SICI)1097-0215(19960516)66:4<515::AID-IJC15>3.0.CO;2-6

Langmead, B., and Salzberg, S. L. (2012). Fast gapped-read alignment with Bowtie 2. *Nat. methods* 9 (4), 357–359. doi:10.1038/nmeth.1923

Lee, C.-K., Smith, E., Gimeno, R., Gertner, R., and Levy, D. E. (2000). STAT1 affects lymphocyte survival and proliferation partially independent of its role downstream of IFN-gamma. *J. Immunol.* 164 (3), 1286–1292. doi:10.4049/jimmunol.164.3.1286

Lei, Y., and Takahama, Y. (2012). XCL1 and XCR1 in the immune system. *Microbes Infect.* 14 (3), 262–267. doi:10.1016/j.micinf.2011.10.003

Lian, L., Qu, L., Sun, H., Chen, Y., Lamont, S., Liu, C., et al. (2012). Gene expression analysis of host spleen responses to Marek's disease virus infection at late tumor transformation phase. *Poult. Sci.* 91 (9), 2130–2138. doi:10.3382/ps.2012-02226

Mar, A.-C., Lee, H.-J., and Lee, T.-C. (2013). Abstract 1423: proinflammatory activity of type II interleukin 1 receptor, a decoy receptor. *Cancer Res.* 73 (8 Suppl. ment), 1423. doi:10.1158/1538-7445.am2013-1423

Mitra, A., Luo, J., He, Y., Gu, Y., Zhang, H., Zhao, K., et al. (2015). Histone modifications induced by MDV infection at early cytolytic and latency phases. *BMC Genomics* 16 (1), 311. doi:10.1186/s12864-015-1492-6

Morgan, R. W., Sofer, L., Anderson, A. S., Bernberg, E. L., Cui, J., and Burnside, J. (2001). Induction of host gene expression following infection of chicken embryo fibroblasts with oncogenic Marek's disease virus. *J. virology* 75 (1), 533–539. doi:10.1128/JVI.75.1.533-539.2001

Osterrieder, N., Kamil, J. P., Schumacher, D., Tischer, B. K., and Trapp, S. (2006). Marek's disease virus: from miasma to model. *Nat. Rev. Microbiol.* 4 (4), 283–294. doi:10.1038/nrmicro1382

Parrish-Novak, J., Dillon, S. R., Nelson, A., Hammond, A., Sprecher, C., Gross, J. A., et al. (2000). Interleukin 21 and its receptor are involved in NK cell expansion and regulation of lymphocyte function. *Nature* 408 (6808), 57–63. doi:10.1038/35040504

Perumbakkam, S., Muir, W. M., Black-Pyrkosz, A., Okimoto, R., and Cheng, H. H. (2013). Comparison and contrast of genes and biological pathways responding to Marek's disease virus infection using allele-specific expression and differential expression in broiler and layer chickens. *BMC genomics* 14 (1), 64. doi:10.1186/1471-2164-14-64

Ramana, C. V., Chatterjee-Kishore, M., Nguyen, H., and Stark, G. R. (2000). Complex roles of Stat1 in regulating gene expression. *Oncogene* 19 (21), 2619–2627. doi:10.1038/sj.onc.1203525

Robinson, M. D., McCarthy, D. J., and Smyth, G. K. (2010). edgeR: a Bioconductor package for differential expression analysis of digital gene expression data. *Bioinformatics* 26 (1), 139–140. doi:10.1093/bioinformatics/btp616

Sarson, A., Abdul-Careem, M., Zhou, H., and Sharif, S. (2006). Transcriptional analysis of host responses to Marek's disease viral infection. *Viral Immunol.* 19 (4), 747–758. doi:10.1089/vim.2006.19.747

Sarson, A., Parvizi, P., Lepp, D., Quinton, M., and Sharif, S. (2008). Transcriptional analysis of host responses to Marek's disease virus infection in genetically resistant and susceptible chickens. *Anim. Genet.* 39 (3), 232–240. doi:10.1111/j.1365-2052.2008.01710.x

Satoh, J.-i., and Tabunoki, H. (2013). A comprehensive profile of ChIP-Seq-based STAT1 target genes suggests the complexity of STAT1-mediated gene regulatory mechanisms. *Gene Regul. Syst. Biol.* 7, 41–56. doi:10.4137/GRSB.S11433

Shek, W., Calnek, B., Schat, K., and Chen, C. (1983). Characterization of Marek's disease virus-infected lymphocytes: discrimination between cytolytically and latently infected cells. *J. Natl. Cancer Inst.* 70 (3), 485–491.

Smith, J., Sadeyen, J.-R., Paton, I. R., Hocking, P. M., Salmon, N., Fife, M., et al. (2011). Systems analysis of immune responses in Marek's disease virus-infected chickens identifies a gene involved in susceptibility and highlights a possible novel pathogenicity mechanism. *J. virology* 85 (21), 11146–11158. doi:10.1128/JVI.05499-11

Sun, W. H., Pabon, C., Alsayed, Y., Huang, P. P., Jandeska, S., Uddin, S., et al. (1998). Rosen ST: interferon-α resistance in a cutaneous T-cell lymphoma cell line is associated with lack of STAT1 expression. *Blood* 91 (2), 570–576. doi:10.1182/blood.v91.2.570

Tian, F., Luo, J., Zhang, H., Chang, S., and Song, J. (2012). MiRNA expression signatures induced by Marek's disease virus infection in chickens. *Genomics* 99 (3), 152–159. doi:10.1016/j.ygeno.2011.11.004

Weisberg, S. P., Hunter, D., Huber, R., Lemieux, J., Slaymaker, S., Vaddi, K., et al. (2006). CCR2 modulates inflammatory and metabolic effects of high-fat feeding. *J. Clin. Investigation* 116 (1), 115–124. doi:10.1172/JCI24335

Witter, R., Calnek, B., Buscaglia, C., Gimeno, I., and Schat, K. (2005). Classification of Marek's disease viruses according to pathotype: philosophy and methodology. *Avian Pathol.* 34 (2), 75–90. doi:10.1080/03079450500059255

Xing, Z., and Schat, K. (2000). Expression of cytokine genes in Marek's disease virus-infected chickens and chicken embryo fibroblast cultures. *Immunology* 100 (1), 70–76. doi:10.1046/j.1365-2567.2000.00008.x

Yu, Y., Luo, J., Mitra, A., Chang, S., Tian, F., Zhang, H., et al. (2011). Temporal transcriptome changes induced by MDV in marek's disease-resistant and-susceptible inbred chickens. *BMC genomics* 12 (1), 501. doi:10.1186/1471-2164-12-501

Frontiers in Physiology

Understanding how an organism's components work together to maintain a healthy state

The second most-cited physiology journal, promoting a multidisciplinary approach to the physiology of living systems - from the subcellular and molecular domains to the intact organism and its interaction with the environment.

Discover the latest Research Topics

See more →

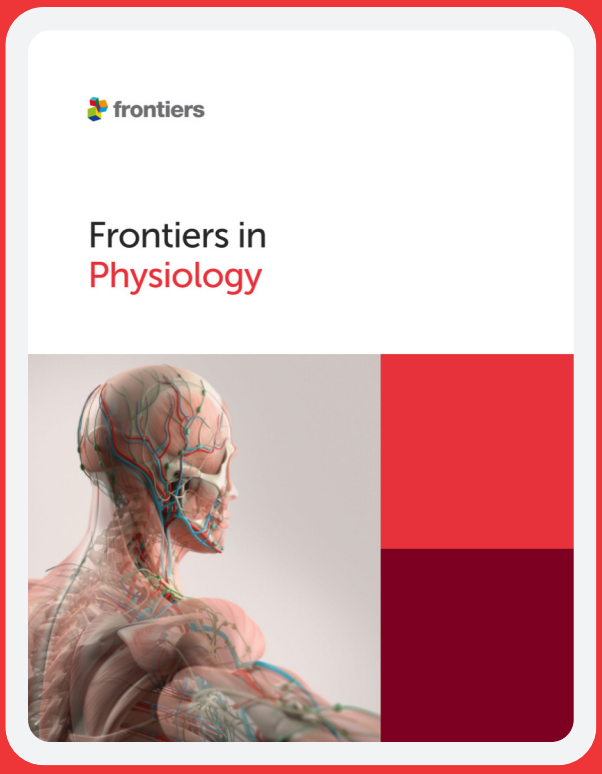

Frontiers

Avenue du Tribunal-Fédéral 34
1005 Lausanne, Switzerland
frontiersin.org

Contact us

+41 (0)21 510 17 00
frontiersin.org/about/contact